PROFILING MOLECULAR SIGNALS ASSOCIATED WITH PODOCYTE EFFACEMENT IN MINIMAL CHANGE NEPHROTIC SYNDROME FOLLOWING TH2 CYTOKINE STIMULATION

CHAN CHANG YIEN

B.Sc., Second Class Honours (Upper Division), NTU

A THESIS SUBMITTED FOR THE
PH.D. DEGREE OF SCHOOL OF MEDICINE
GRADUATE PROGRAMME

DEPARTMENT OF PAEDIATRICS
NATIONAL UNIVERSITY OF SINGAPORE

2013

DECLARATION PAGE

I hereby declare that this thesis is my original work and it has been written by me in its entirety. I have duly acknowledged all the sources of information which have been used in the thesis.

This thesis has also not been submitted for any degree in any university previously.

_____

Chan Chang Yien

5th August, 2013

ACKNOWLEDGEMENTS

I would like to extend my gratitude to:

My supervisor, Professor Yap Hui Kim, for her guidance and sharing of knowledge throughout these years;

Dr Lai Kin Wai, for his advice and guidance in histological staining;

Dr Henry Yang He and Dr Chen Jinmiao, for their guidance in microarray analysis;

Chin Hui Xian, Joni Chong, Liang Ai Wei, Lauretta Low, Ng Jun Li, Sun Zi Jin, Seah Ching Ching, Toh Xue Yun, and Zhang Yao Chun for their company and support;

My family members, for their continuous support and encouragement.

This work was supported by grants NMRC/1134/2007 from the National Medical Research Council, Singapore and BMRC/10/1/21/19/651 from the Biomedical Research Council, Singapore.

TABLE OF CONTENTS

SUMMARY

The pathogenesis of minimal change nephrotic syndrome (MCNS), the most common cause of significant morbidity amongst the childhood glomerulonephritides, is unknown. We have demonstrated that *IL-13* overexpression in the rat resulted in podocyte foot process (FP) effacement with B7-1 upregulation and concurrent downregulation of the slit diaphragm proteins inducing a minimal change-like nephropathy. We therefore hypothesized that IL-13 and/or other Th2 cytokines could act through the B7-1 danger signaling pathway, causing podocyte FP effacement and proteinuria (Figure 1). Our *IL-13* overexpression rat model of MCNS thus provided a platform to study the molecular signaling pathways that were differentially regulated, in order to better understand the pathogenesis of this intriguing disease. The aims of this study were firstly to delineate the glomerular "gene signature" related to our *IL-13* rat model of MCNS through microarray analysis of glomerular transcription profile in *IL-13* overexpression and control rats; secondly, to validate the *in vivo* microarray results in human podocyte cell culture system; and lastly to investigate the mechanism of IL-13-induced B7-1 danger signaling in causing podocyte injury.

RNA from glomeruli of six control and six *IL-13* overexpressed rats with MCNS were reverse transcribed and hybridized into Sentrix® BeadChip Array RatRef-12v1. Differentially expressed genes (DEGs) were selected based on the criteria of fold change greater than 1.6, coefficient of variance less than 0.7 and *t-test* $p<0.05$. Gene ontology analysis was done using DAVID and pathway analysis was carried out using Ingenuity Pathway Analysis and MetaCore™. Protein expression of vav1 on the glomeruli and podocytes were validated using immunohistochemical staining on rat kidney section as well as immunofluorescence staining and Western blotting on podocytes. Morphology of podocyte actin cytoskeleton was examined using phalloidin staining. RhoA/Rac1 activity in IL-13 stimulated podocytes was measured using ELISA. The role of vav1 in IL-13 induced podocyte injury was studied using podocytes transfected with siRNA specific for vav1. Gene and protein expression levels were studied using real-time PCR and Western blotting respectively.

Transcriptional profile of the glomeruli in *IL-13* overexpressed rats showed characteristic features of podocyte injury in which more than 87% of genes known to be related to podocytes were significantly downregulated. Gene expression of *vav1* was highly upregulated in the glomeruli of *IL-13* overexpressed rats and MetaCore^{TM} pathway analysis of the DEGs suggested a possible novel role of vav1 in podocyte cytoskeleton remodeling. Immunohistochemical staining confirmed the glomerular expression of vav1, which co-localized with synaptopodin in serial sections of the kidney. Moreover, the presence of vav1 in cultured podocytes was further confirmed by immunofluorescence staining and immunoblotting.

In vitro IL-13 stimulation in podocytes resulted in significant increased expression of IL-13Rα2, B7-1 and phosphorylated vav1 compared to controls. This was associated with actin cytoskeleton rearrangement and activation of Rac1. Additionally, podocytes with vav1 siRNA transfection were protected from IL-13 induced actin cytoskeleton changes and Rac1 activity.

In conclusion, we have shown that the direct action of IL-13 in inducing podocyte FP effacement in our rat model of MCNS was through activation of B7-1-vav1-Rac1 mediated actin cytoskeleton rearrangement in podocytes.

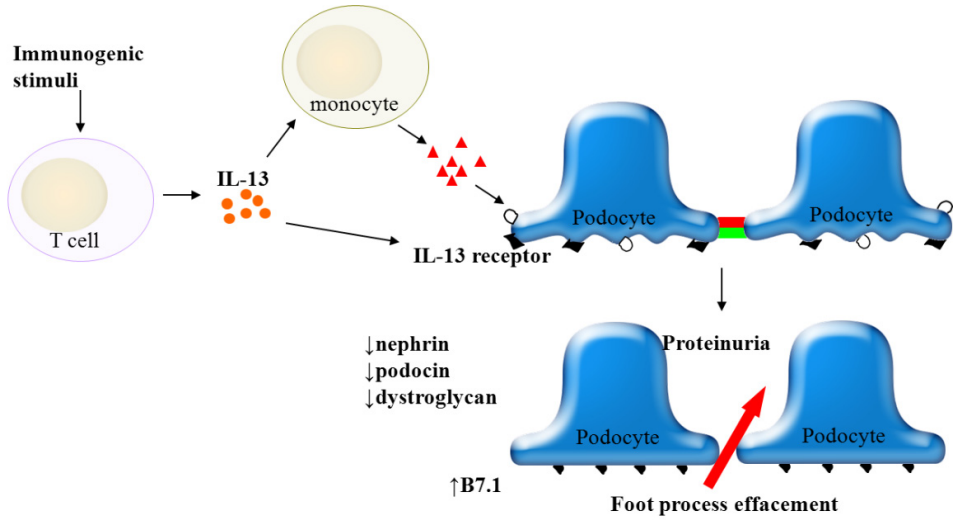

Figure 1: Proposed Th2 cytokine bias model of MCNS results from primary immune disturbance.
IL-13 and/or other immune mediators may directly or indirectly act on podocytes and cause podocyte FP effacement, resulting in proteinuria and the nephrotic syndrome.

LIST OF ABBREVIATIONS

Ac	Acidic
ACTN4	Alpha-actinin-4
AMD	Apical membrane domain
AP-1	Activator protein 1
aPKC	Atypical protein kinase C
Arp	Actin-related protein
AT1R	Angiotensin II Type I Receptors
ATF	Activating transcription factors
B7-1	CD80
BCG	Bromocresol green
BMD	Basal membrane domain
BSA	Bovine serum albumin
CapZ	Capping protein (actin filament) muscle Z-line
CAR	Coxsackievirus and adenovirus receptor
CASK	Calcium/calmodulin-dependent serine protein kinase
CD	Cluster of differentiation
CD2AP	CD2 associated protein
Cdc42	Cell division cycle 42
Cdh11	Cadherin 11
cDNA	Complementary DNA
c-fos	c-FBJ osteosarcoma oncogene
CH	Calponin homology
Cp	Crossing point
cRNA	Complementary RNA
Ct	Threshold cycle
CTLA-4	Cytotoxic T-lymphocyte-associated antigen-4
Ctnnal1	α-catenin
DAB	Diaminobenzine
DAPI	4’6-diamidino-2-phenylindole
ddH_2O	Double distilled water
DEGs	Differentially expressed genes

DEPC	Diethylpyrocarbonate
DH	Dbl homology
DIP	Diaphanous interacting protein
DNA	Deoxyribonucleic acid
dNTPs	Deoxynucleotide triphosphates
EDTA	Ethylenediaminetetraacetic acid
ELISA	Enzyme Linked Immuno Sorbent Assay
Ena	Enabled
Ezr	Ezrin
F-actin	Filamentous actin
FITC	Fluorescein isothiocyanate
FP	Foot processes
FRNS	Frequent relapsing nephrotic syndrome
FSGS	Focal segmental glomerulosclerosis
GAPDH	Glyceraldehyde-3-phosphate dehydrogenase
GBM	Glomerular basement membrane
GDP	Guanosine diphosphate
GECs	Glomerular endothelial cells
GEF	Guanine nucleotide exchange factor
GLEPP1	Glomerular epithelial protein 1
GM-CSF	Granulocyte-monocyte colony stimulating factor
GN	Glomerulonephritis
Grb2	Growth factor receptor-bound protein 2
GTP	Guanosine triphosphate
HBSS	Hank's balanced salt solution
HIV	Human immunodeficiency virus
hnRNP	Heterogeneous nuclear ribonucleoprotein
HO-1	Heme oxygenase 1
HRP	Horseradish peroxidase
IFN	Interferon
Ig	Immunoglobulin
IgAN	Immunoglobulin A Nephropathy
IHC	Immunohistochemistry

IL	Interleukin
IL-13Rα1	Interleukin-13 receptor alpha 1
IL-13Rα2	Interleukin-13 receptor alpha 2
IL-1RA	Interleukin 1 receptor antagonist
IL-4Rα	Interleukin-4 receptor alpha
ILK	Integrin-linked kinase
IQGAP1	IQ motif containing GTPase activating protein 1
ISKDC	International Study of Kidney Disease in Children
Itga3	α3 integrin
iTRAQ	Isobaric tags for relative and absolute quantitation
JAK	Janus tyrosine kinase
JAM4	Junctional adhesion molecule-4
JNK	c-Jun N-terminal kinases
Kirrel2	Kin of IRRE like 2
Ku-70	ATP-dependent DNA helicase 2 subunit KU70
LB	Luria-Bertani
LC	Liquid chromatography
LPS	Lipopolysaccharides
MAGI	Membrane associated guanylate kinase, WW and PDZ domain containing
MAGUK	Membrane-associated guanylate kinases
MCNS	Minimal change nephrotic syndrome
MEKK1	Mitogen-activated protein kinase kinase kinase 1
MHC	Major histocompatibility complex
MKK	MAP kinase kinase
MN	Membranous nephropathy
MPGN	Membranoproliferative glomerulonephritis
mRNA	Messenger Ribonucleic acid
MS	Mass spectrometry
ND	Not determined
Nef	Negative Regulatory Factor
Neph1	Nephrin homolog 1
NFATc1	Nuclear factor of activated T cells, cytoplasmic 1

NF-κB	Nuclear factor kappa-light-chain-enhancer of activated B cells
NHERF2	Na^+/H^+ exchanger regulatory factor 2
N-WASP	Neuronal Wiskott–Aldrich syndrome protein
OD	Optical density
OPD	o-Diphenylenediamine
Par	Partition defective
PBMC	Peripheral blood mononuclear cell
PBS	Phosphate buffered saline
P-cadherin	Proto-cadherin
PCR	Polymerase chain reaction
PH	pleckstrin homology
PI3K	Phosphoinositide 3-OH kinase
PINCH	Particularly interesting Cys-His-rich protein
PIP2	Phosphatidylinositol 4,5-bisphosphate
PIP3	Phosphatidylinositol 3,4,5-trisphosphate
Plaur	Plasminogen activator, urokinase receptor
PMT	Photomultiplier tube
Ptpro	Protein tyrosine phosphatase, receptor type, O
PVDF	Polyvinylidene fluoride
Rac1	Ras-related C3 botulinum toxin substrate 1
RBC	Red blood cell
RhoA	Ras homolog family member A
RIN	RNA integrity number
RNA	Ribonucleic acid
RNase	Ribonuclease
SD	Slit diaphragms
SDNS	Steroid-dependent nephrotic syndrome
SDS	Sodium dodecyl sulfate
SEM	Standard error of the mean
SH	Src Homology
siRNA	Small interference ribonucleic acids

SLP-76	Lymphocyte cytosolic protein 2 (SH2 domain containing leukocyte protein of 76kDa)
Smurf-1	SMAD specific E3 ubiquitin protein ligase 1
SRsNS	Steroid-resistant nephrotic syndrome
SSNS	Steroid-sensitive nephrotic syndrome
STAT	Signal transducer and activator of transcription
Syk	Spleen tyrosine kinase
TGF	Transforming growth factor
Th	T helper
TLR	Toll-like receptor
TNF-α	Tumor necrosis factor-alpha
TRPC	Transient receptor potential cation channels
Tyk	Tyrosine kinase
uPA	Urokinase-type plasminogen activator
uPAR	Urokinase plasminogen activator surface receptor
UTR	Untranslated region
VASP	Vasodilator-stimulated phosphoprotein
VE-cadherin	Vascular endothelial cadherin
VIK-1	Vav-interacting Kruppel-like protein
WT1	Wilms' tumor 1
X-Gal	5-bromo-4-chloro-3-indolyl-beta-D-galactopyranoside
ZAP70	Zeta-chain (TCR) associated protein kinase 70kDa
ZO-1	Zonula occludens-1

UNITS OF MEASUREMENT

bp	Base pair
^{o}C	Degree Celsius
G	Gauge
g	Gram
g/day/1.73m^2	Gram per day per 1.73 meter square
g/L	Gram per litre
g/mmol	Gram per millimole
g	Gravity
kDa	Kilo daltons
kDa	KiloDalton
w/v	Mass per volume
µg	Microgram
µg/24hr	Microgram per 24 hour
µg/ml	Microgram per millilitre
µl	Microlitre
µm	Micrometer
µmol/L	Micromole per litre
mg/m^2	Milligram per meter square
mg/m^2/day	Milligram per meter square per day
mg/ml	Milligram per millilitre
ml	Millilitre
mm	Millimeter
mM	Millimolar
mmol/L	Millimole per litre
mins	Minutes
M	Molar
ng	Nanogram
ng/µl	Nanogram per microlitre
ng/ml	Nanogram per millilitre
nm	Nanometer
N	Normality
%	Percent

pg/ml	Picogram per millilitre
pmole	Picomole
rcf	Relative Centrifugal Force
rpm	Revolutions per minute
s	Second
U	Unit
V	Volt
v/v	Volume per volume

LIST OF TABLES

LIST OF FIGURES

LIST OF APPENDICES

LIST OF CONFERENCE ABSTRACTS AND AWARDS

Poster presentation at 8th NHG Annual Scientific Congress 2009, Singapore 16.10.2009 – 17.10.2009. PI3K/Akt activated B7-1 Transcription in Regulation of Glomerular Podocyte Effacement in an *IL-13* Overexpression Rat Model of Minimal Change Nephrotic Syndrome (MCNS). CY Chan, TK Maheshwari, JM Chen, C Prakash, JH Lu, GL Lee, H Yang, HK Yap.

Poster presentation at 1st Singapore Health & Biomedical Congress 2010, Singapore 12.11.2010 – 13.11.2010. Endotoxin-tolerance Monocyte Profile in Nephrotic Syndrome. Chang Yien Chan, Wee Song Yeo, Jinmiao Chen, Tarun K Maheshwari, Subhra K Biswas, Henry Yang, and Hui Kim Yap. **(Bronze award)**

Poster presentation at ASN Renal Week 2010, Denver, Colorado, USA 16.11.2010 – 21.11.2010. Endotoxin-tolerance monocyte profile in minimal change nephritic syndrome (MCNS): Role in increased susceptibility to bacterial infections. Chang Yien Chan, Wee Song Yeo, Jinmiao Chen, Tarun K Maheshwari, Subhra K Biswas, Henry Yang, and Hui Kim Yap.

Poster presentation at ASN Renal Week 2010, Denver, Colorado, USA 16.11.2010 – 21.11.2010. B7-1 mediated danger signaling in podocyte injury in IL-13 overexpression rat model of minimal change like nephropathy (MCN). Chang Yien Chan, Tarun K Maheshwari, Jinmiao Chen, Caroline GL Lee, Subhra K Biswas, Henry Yang, and Hui Kim Yap.

Poster presentation at ASN Kidney Week 2011, Philadelphia, Pennsylvania, USA 8.11.2011 – 13.11.2011. Decreased Plasma RANTES Concentration in Children with Minimal Change Nephrotic Syndrome in Relapse is Associated with Th2 Cytokine Profile. Chang Yien Chan, Wee Song Yeo, Kar Hui Ng, Subhra K Biswas, and Hui Kim Yap.

Poster presentation at NKF 1st Scientific Meeting 2012, Singapore 4th February 2012. Endotoxin-tolerance monocyte profile in minimal change nephritic

syndrome (MCNS): Role in increased susceptibility to bacterial infections. Chang Yien Chan, Wee Song Yeo, Subhra K Biswas, and Hui Kim Yap.

Poster presentation at 9th International Podocyte Conference 2012, Miami Beach, Florida USA 22.4.2012 – 25.4.2012. Interleukin-13-induced B7-1 activation And Cytoskeleton Rearrangement In Podocytes. Chang Yien Chan, Jinmiao Chen, Subhra K Biswas, Henry Yang and Hui Kim Yap.

Oral presentation at the 8th Congress of Asian Society for Pediatric Research, Seoul, Korea, 17.5.2012 – 19.5.2012. Enhanced Th2 Cytokine Profile in Children with Relapse of Minimal Change Nephrotic Syndrome is Associated with Decreased Plasma RANTES Concentration. Chang Yien Chan, Ai Wei Liang, Wee Song Yeo, Kar Hui Ng, Subhra K Biswas, and Hui Kim Yap. **(Young Investigator Award)**

Poster presentation at ASN Kidney Week 2012, San Diego, California, USA 30.10.2012 – 4.11.2012. High suPAR Levels in FSGS Patients Is Associated with Decreased Treg Cells. Chang Yien Chan, Wee Song Yeo, Changli Wei, Subhra K. Biswas, and Hui Kim Yap.

Oral presentation at 3rd Annual Graduate Scientific Congress 2012, Singapore 30.1.2013. Circulating Soluble Urokinase-type Plasminogen Activator Receptor (suPAR) as a Prognostic Biomarker in Focal Segmental Glomerulosclerosis (FSGS). Chang Yien Chan, Lourdes Paula Resontoc, Wee Song Yeo, Changli Wei, Jochen Reiser, Subhra K. Biswas and Hui Kim Yap.

CHAPTER 1

INTRODUCTION

1.1. Nephrotic Syndrome

With the decline in acute post-infectious glomerulonephritis, idiopathic nephrotic syndrome, in particular minimal change nephrotic syndrome (MCNS) is now the most common cause of significant morbidity amongst the childhood glomerular diseases both in Singapore and worldwide [1]. Up to 70% of children with MCNS will have multiple relapses, of whom at least half will require long-term steroid therapy or courses of cytotoxic drugs, with their attendant adverse effects on growth and puberty, cataract formation, and risk of malignancy. Better therapeutic strategies based on a clearer understanding of the etiology of the disease are hence required.

1.1.1 Definition of nephrotic syndrome

Nephrotic syndrome is a kidney disease commonly seen in children. It is characterized by proteinuria, hypoalbuminemia, edema and hypercholesterolemia. Clinical diagnosis of nephrotic syndrome requires the presence of edema, nephrotic-range proteinuria (urinary protein excretion of ≥3 g/day/1.73m^2) and hypoalbuminemia (serum albumin level ≤25 g/L) [2]. Hypercholesterolemia associated with MCNS is usually much more severe with extremely high total serum cholesterol, typically 10-20 mmol/L [3, 4] (normal <5.1mmol/L) [5], primarily due to marked elevation of LDL-cholesterol, compared to other diseases with protein loss such as patients with chronic nephropathy or those on peritoneal dialysis whose protein losses can reach a similar range as nephrotic patients but serum total cholesterol levels rarely exceed 7 mmol/L [6]. Upon receiving corticosteroid therapy, the majority of children will respond to the treatment, entering remission, which is defined as resolution of edema and proteinuria (urine albumin reduced to <0.3 g/24hr/1.73m^2, or a urine protein/creatinine ratio of <0.02 g/mmol) and normalization of serum albumin level to at least ≥35 g/L [7, 8].

1.1.2 Classification of nephrotic syndrome

Nephrotic syndrome presenting in the first three months of life, that is, congenital nephrotic syndrome, are mainly due to mutations in genes such as *WT1*, *nephrin* and *podocin*. More than 90% of children with nephrotic syndrome have a primary cause, that is, a disease specific to the kidneys. However, secondary causes, such as systemic lupus erythematosus, Henoch-Schonlein purpura and viral etiologies (hepatitis B, hepatitis C, parvovirus, human immunodeficiency virus (HIV)) have to be excluded.

Primary nephrotic syndrome (also known as idiopathic nephrotic syndrome) can be classified histologically into MCNS, focal segmental glomerulosclerosis (FSGS), membranous nephropathy (MN), mesangial proliferative glomerulonephritis (GN) and membranoproliferative GN (MPGN). The most common histopathologic type in children is MCNS, accounting for more than 80% of all cases [9].

1.1.3 Treatment of Nephrotic Syndrome

Prednisolone is the mainstay of treatment for children with idiopathic nephrotic syndrome. The treatment regime is 60 mg/m^2/day of prednisone for four to six weeks, followed by 40 mg/m^2 on alternate days for a further six to twelve weeks. It is estimated that 70% of patients will respond to this treatment with complete resolution of proteinuria and edema, however, up to 40% may have frequent relapses or require long-term steroid treatment to maintain in remission.

Based on the responses to corticosteroid treatment, these patients can be classified as: i) steroid-sensitive nephrotic syndrome (SSNS); ii) steroid-resistant nephrotic syndrome (SRsNS); iii) steroid-dependent nephrotic syndrome (SDNS); or iv) frequent relapsing nephrotic syndrome (FRNS). Patients with SSNS are able to attain remission within eight weeks of treatment with corticosteroid treatment; patients with SRsNS fail to attain remission after eight weeks of corticosteroid treatment; patients with SDNS are able to respond to initial corticosteroid treatment but develop a relapse either while still on steroids or within two weeks of discontinuation of treatment following a steroid

taper, hence requiring the continued low-dose steroid treatment to prevent relapses; patients with FRNS enter complete remission in response to steroid treatment but develop four or more relapses in any 12-months period [2].

In addition to corticosteroid treatment, patients with SDNS and FRNS often require other immunosuppressive agents such as cyclophosphamide, levamisole, cyclosporine, tacrolimus, and mycophenolate mofetil. Similarly, patients with SRsNS require multiple immunosuppressive agents such as cyclosporine, tacrolimus, high dose intravenous methylprednisolone, mycophenolate mofetil, and rituximab to achieve remission.

Prolonged use of corticosteroids and immunosuppressive agents result in adverse side effects such as growth retardation, obesity, infections, hypertension, osteoporosis, cataracts, infertility and nephrotoxicity [10-13].

1.1.4 Epidemiology of Nephrotic Syndrome

The annual incidence of nephrotic syndrome in most countries in the Western countries ranges from 2 to 7 new cases per 100,000 children [8, 14-16]. Countries in Asia, however, reported a higher incidence of about 16 new cases per 100,000 children [17].

Renal biopsy is commonly recommended for patients who are steroid-resistant. Among the 103 biopsy proven cases in the International Study of Kidney Disease in Children (ISKDC) series, MCNS, FSGS and MPGN were the most common lesions in SRsNS, each accounting for approximately 25% of the histological findings [7]. In Singapore, however, MCNS and FSGS formed the main fraction of SRsNS cases, accounting for 30% and 49% of the cases respective in renal biopsies of 47 children with SRsNS [18] (Table 1).

Table 1: Distribution of children with SRsNS by glomerular histopathology in ISKDC and Singapore.

Histopathologic category	ISKDC	Singapore
Minimal change nephrotic syndrome	25	14
Focal segmental glomerulosclerosis	26	23
Membranoproliferative glomerulonephritis	27	5
Mesangial proliferative glomerulonephritis	9	3
Membranous glomerulonephritis	6	ND
Chronic glomerulonephritis	3	ND
Diffuse Mesangial Hypercellularity	4	ND
Focal Global Glomerulosclerosis	2	2
Unclassified	1	ND
Total	**103**	**47**

Adopted from reference [7] and [18]. ND: not determined.

1.2. Minimal change nephrotic syndrome

MCNS is the most common cause of childhood nephrotic syndrome. Although it is not limited to children, studies have reported a median age of onset of four years, where MCNS accounts for close to 85% of all cases of childhood nephrotic syndrome [9, 19]. Although more than 90% of children with MCNS respond to corticosteroid therapy, up to 70% will have multiple relapses requiring long-term steroid therapy or courses of cytotoxic drugs, with their attendant adverse effects on growth and puberty, cataract formation, and risk of malignancy.

In MCNS, the glomeruli appear normal by light microscopy or show a minimal increase in mesangial cells and matrix. Findings on immunofluorescence microscopy are typically negative, and electron microscopy reveals effacement of podocyte foot processes and absence of electron-dense immune deposits in the glomeruli [20].

The underlying mechanism in the majority of patients with nephrotic syndrome is a permeability defect in the glomerular filtration barrier that allows the loss of protein from the plasma into the urine. However, the fundamental cause and pathogenesis of MCNS is still largely unknown.

1.2.1 Minimal change nephrotic syndrome and the immune system

In 1974, Shalhoub postulated that lipoid nephrosis, an older term for MCNS, is produced by a systemic disorder of T-cell function [21]. He hypothesized that the domination of an abnormal clone of T cells results in the production of a circulating lymphokine toxic to the glomerular basement membrane (GBM), resulting in increased glomerular permeability to protein.

The onset of idiopathic nephrotic syndrome has been associated with prior respiratory tract infections or other immunogenic stimuli such as insect stings [22, 23], vaccinations [24, 25] or allergic reactions to inhaled allergens [26-29]. Clinical observations such as remission induced by measles, the occurrence of nephrotic syndrome in lymphoproliferative disease like Hodgkin's disease [30-32], leukemia [33], lymphoma [34] and thymoma [35-40], both of which modify cell-mediated immunity, and the therapeutic benefits of steroids and cyclophosphamide [41], which suppresses cell-mediated responses, all support Shalhoub's hypothesis that MCNS might be related to T-cell dysfunction, resulting in the production of a lymphocyte-derived permeability factor that induces proteinuria.

The association of interleukin (IL-) 13 (IL-13) with MCNS may also account for the relationship of MCNS with Hodgkin's disease. IL-13 expression is a characteristic feature of Hodgkin's disease. *In situ* hybridization of lymph node tissue from patients with Hodgkin's disease showed elevated levels of IL-13 and IL-13 receptor (IL-13Rα1) localized to Reed-Sternberg cells, a malignant cell population in Hodgkin's disease [42-44]. Constitutive phosphorylation of signal transducer and activator of transcription 6 (STAT6) in Reed-Sternberg cells [45] and inhibition of Hodgkin's lymphoma growth by IL-13Rα2 (decoy receptor of IL-13) [46] further implicate IL-13 as an important growth factor in Hodgkin's disease, and may account for the proteinuria in MCNS associated with this disease.

In addition, the lack of morphological changes in the kidney suggests that MCNS represents a generalized disorder of the immune system resulting in renal manifestations, rather than a specific disease of the kidney. A number of studies have shown immunologic abnormalities in this disease, including an increase in the $CD4^+CD25^+$ (IL-2 receptor-α chain) [47], $CD4^+CD45RO^+$ and $CD8^+CD45RO^+$ memory subsets [48] in patients with active relapse, selective recruitment of some νβ gene family in $CD8^+$ T cells from nephrotic patients with frequent relapses [49], increased NF-κB DNA binding activity in T-cells in MCNS patients during relapse [50], as well as abnormalities in serum immunoglobulins during nephrotic relapses characterized by depressed IgG, and elevated IgM and IgE [51, 52].

Although it is still unclear how an altered immune system may cause proteinuria in idiopathic nephrotic syndrome, there is strong evidence suggesting that the proteinuria in idiopathic nephrotic syndrome could be mediated by circulating factor(s) such as cytokines summarized in Table 2 [9, 53]. Persistent massive proteinuria, in turn, contributes to the phenomenon of glomerular hyperfiltration and ultimately progressive glomerulosclerosis, through the mediation of other cytokines like transforming growth factor-β (TGF-β), produced by the resident glomerular cells such as the mesangial cells [54].

Table 2: Cytokine profile in MCNS.

Cytokines	Upregulation	Downregulation	No Change
Th1-related			
IL-12	[55]		[56]
IFN-γ	[57]	[56]	[58, 59]
Th2-related			
IL-4	[60, 61]	[59]	[57, 58, 62]
IL-13	[58, 62]		
Th17-related			
IL-23	[63]		
IL-17	[63]		
Treg-related			
IL-10		[63, 64]	
TGF-β		[63]	
General activation			
IL-1	[65]	[66]	[57, 67]
IL-2	[57, 59, 65]		[58]
IL-6		[59]	[67]
TNF-α	[67]		[57]
Chemokines			
IL-8	[68]	[57]	

Numbers in brackets corresponds to the published journals as indexed in the reference.

1.2.2 Roles of Th2 cytokines in minimal change nephrotic syndrome

Studies on the role of cytokines in MCNS suggested MCNS is a result of primary immune disturbance, with a Th2 bias [53]. Th2 cytokines are anti-inflammatory and are associated with B-cells proliferation, class switching of B-cells to produce IgE and IgG4, and increased neutralizing antibody production [69, 70].

Our laboratory was the first to demonstrate that *IL-13* gene expression was upregulated in both $CD4^+$ and $CD8^+$ T-cells in children with steroid-sensitive nephrotic syndrome in relapse [58]. This was associated with increased intracytoplasmic IL-13 production by $CD3^+$ cells. We also demonstrated a

significant increase in serum IgE levels during nephrotic relapses compared to remission, and this correlated with the percentage of IL-13-producing $CD3^+$ cells suggesting the presence of polyclonal activation [51].

Our findings were consistent with Kimata's study where IL-13 was shown to be important for the spontaneous production of IgE and IgG4 by peripheral blood mononuclear cell (PBMC) from nephrotic patients [62]. Another Th2 cytokine, IL-4, was also found to be increased in PBMCs from patients with MCNS, and this was associated with increased B-cell expression of the type II IgE receptor and high IgE production [61], further supporting the association of atopy with nephrotic syndrome. In addition, Sahali *et al.* showed increased gene expression of *c-maf*, a Th2-specific transcription factor that binds to the IL-4 proximal promoter, while *IL-12R β2* gene expression was downregulated during relapses of MCNS through cDNA library differential screening [71].

Furthermore, we were able to demonstrate that genetic polymorphisms in the 3' untranslated region (3'UTR) of the *IL-13* gene correlated with long-term outcome of MCNS in Singapore Chinese children, rather than disease susceptibility [72]. Moreover, *IL-13* mRNA expression in PBMC of patients with the haplotype AAT, associated with continuing relapses 5 years from onset, was significantly higher than those with the haplotype GCC, associated with long-term remission. Unfortunately, the exact role of IL-13 in the pathogenesis of MCNS is not clear.

1.3. Role of podocytes in genesis of nephrotic syndrome

The ultrafiltration of plasma in the kidney occurs through the capillary wall of the glomerulus. The filtration barrier consists of three layers: (i) the glomerular endothelial cells (GECs), lining the interior side of the glomerular capillaries; (ii) the glomerular basement membrane (GBM); and (iii) the podocytes, lining the exterior of the glomerular capillary (Figure 2). Passage of plasma across this size-selective barrier results in water, small- and middle-sized molecules entering the urinary space; while serum albumin and macromolecules are retained in the capillary space. Our current understanding of the pathogenic

mechanism of nephrotic syndrome suggests that the podocyte is the main component of the glomerular filter and the crucial target in the development and progression of glomerulopathies. In fact, one of the hallmarks of MCNS is the effacement of podocyte foot processes (FP) and the degree of FP effacement has been shown to roughly correlate with the amount of proteinuria [73, 74].

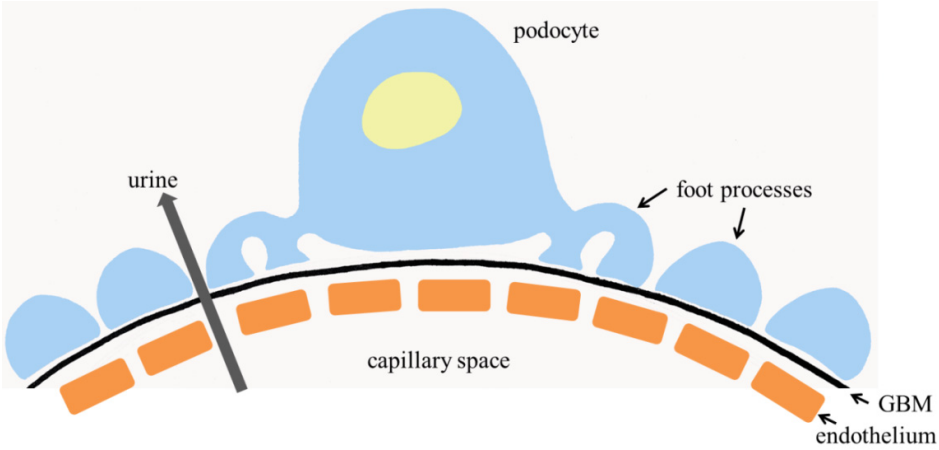

Figure 2: Glomerular filtration barrier.
The filtration barrier is composed of glomerular endothelial cells, the glomerular basement membrane (GBM), and the podocytes. Adopted and modified from reference [75].

Podocytes are terminally differentiated cells with a cell body and large cytoplasmic projections (major processes) that divide into long thin processes (foot processes). The FP are attached firmly to the underlying GBM and form a tight network of interdigitating pattern with FP of neighbouring podocytes, which are bridged by 'slit diaphragms' (SD) [76]. The SD thus divides the plasma membrane of FP to the apical, the lateral (slit diaphragm), and the basal domains. In the cytoplasm, these three surfaces are interconnected via the actin-based cytoskeleton (Figure 3) [77]. Disruption of any of the three domains or the underlying actin cytoskeleton can lead to FP effacement and hence proteinuria.

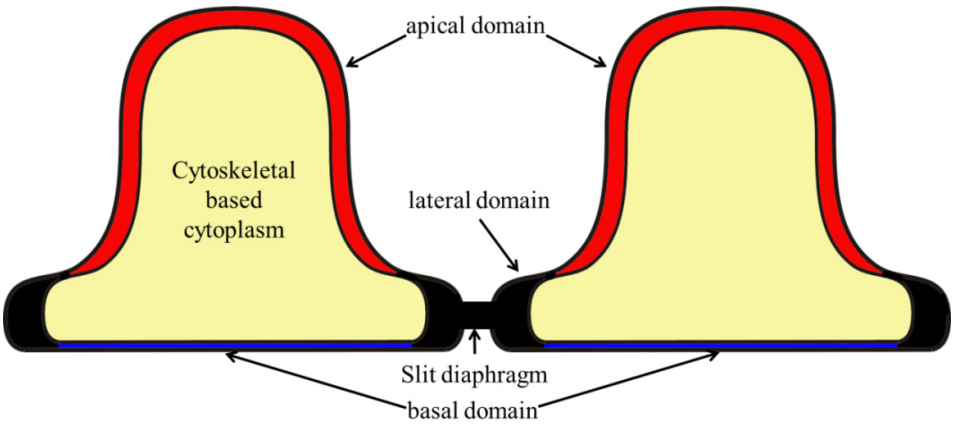

Figure 3: The three domains of the podocyte FP.
The FP interdigitates with FP of neighbouring podocytes, bridged by slit SD. The SD divides the plasma membrane of FP to the apical, the lateral, and the basal domains. These three surfaces are interconnected via the actin-based cytoskeleton in the cytoplasm. Adopted and modified from reference [77].

A wide range of proteins molecules are expressed on the podocytes FP (Figure 4), with diverse functions, such as structural support, adhesion, signaling and movement. The summation of the functions of these molecules forms the basis of the glomerular filtration barrier.

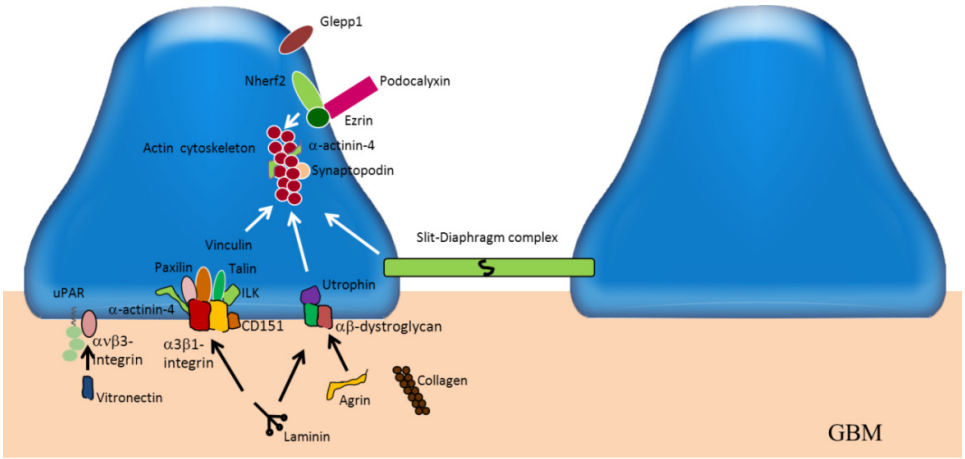

Figure 4: Molecules expressed in the podocytes.
Adopted and modified from reference [75].

1.3.1 Podocyte apical membrane domain

The apical surface of podocytes, which faces the urinary space, is covered by sialylated, O-glycosylated, and negatively charged transmembrane protein – podocalyxin [78]. Podocalyxin deficient mice failed to form FP and SD thus causing a block in urine production [79]. Podocalyxin is linked to the actin cytoskeleton in the cytoplasm through ezrin [80] and Na^+/H^+ exchanger

regulatory factor 2 (NHERF2) [81]. Disruption of the podocalyxin/ezrin/NHERF/actin interaction resulted in drastic loss of FP.

Another protein found at the apical surface of podocytes is glomerular epithelial protein 1 (GLEPP1). It is a podocyte-specific receptor tyrosine phosphatase. Structurally, it has a large ectodomain with multiple fibronectin type III repeats, a transmembrane domain, and a single cytoplasmic phosphatase active site sequence [82]. Podocytes of GLEPP1 deficient mice had an amoeboid instead of the typical octopoid structure. These mice showed reduced filtration surface area, reduced glomerular nephrin content and reduced glomerular filtration rate [83]. To date, cytoplasmic ligand of GLEPP1 has not been identified.

1.3.2 Podocyte slit diaphragm

The SD is characterized as modified adherens junction with rod-like proteins forming a zipper-like structure with a constant width of approximately 40 nm [84, 85]. The extracellular portion of the SD is composed of the extracellular domains of various transmembrane proteins such as nephrin [86-89], Neph1/2/3 [90-94], P-cadherin [84], VE-cadherin [84, 95] and FAT [96]. The cytoplasmic portion of the SD is composed of non-structural proteins like podocin [97, 98], TRPC5/6 [99, 100], CD2AP [101], Nck [102], Par3/Par6/aPKC [103], ZO-1 [104], dendrin [105], JAM4 [106], densin [107], MAGI-1/2 [108], CASK, IQGAP1, αII spectrin, and βII spectrin [109].

Nephrin was the first transmembrane protein identified in the SD through positional cloning. Mutation in nephrin gene, *NPHS1*, was found to be the cause of congenital nephrotic syndrome of the Finnish type [87] and reduction or altered distribution of nephrin expression was reported in patients with MCNS and IgAN [110, 111]. Nephrin has a short intracellular domain, a transmembrane domain, and an extracellular domain. The intracellular domain is connected to the actin cytoskeleton via CD2-associated protein (CD2AP) [101] and Nck proteins [102]. The extracellular domain of nephrin forms the "bridge" of the filtration slit through homophilic interaction of nephrin molecules from neighbouring FP [112]. Nephrin knockout mice showed

podocyte FP effacement, lack SD, massive proteinuria, edema and died within a day [113].

Neph1, Neph2, and Neph3 (also known as filtrin) proteins are structurally related to nephrin. Studies showed that nephrin can form heterodimers with Neph1 or Neph2, but that Neph1 and Neph2 do not interact with each other [114, 115]. Neph1 knockout mice had early postnatal death due to podocyte FP effacement and proteinuria [116]. In addition, interaction of Neph1 with nephrin caused tyrosine phosphorylation of Neph1 by Fyn and recruitment of Grb2, an event that is crucial in Neph1-induced actin polymerization [117]. However, functional significance of Neph2 or Neph3 is unknown.

P-cadherin, vascular endothelial cadherin (VE-cadherin or cadherin 5) and FAT1 are cadherin proteins which have been localized to the slit diaphragm. P-cadherin is not indispensable for the functional renal filtration barrier [118] and P-cadherin deficient mice showed no kidney abnormalities or function [119]. The role of VE-cadherin in the podocyte is still unknown [75]. Fat1 is a large protein with 34 tandem cadherin-like repeats and is an important regulator of actin dynamics via Ena/VASP interaction [120-122]. Fat1 knockout mice caused perinatal death, loss of SD, podocyte FP effacement and proteinuria [123].

Podocin was discovered through positional cloning of the gene mutated in early-onset steroid resistant nephrotic syndrome [97]. It is a member of stomatin family of protein containing a prohibitin homology domain for lipid recognition motif. It has a hairpin structure with both ends directed into the cytoplasmic side of SD. Studies showed that podocin served as the platform for recruitment of CD2AP, nephrin and Neph1 to SD [91, 124]. Podocin was also reported to cluster and regulate the ion channel TRPC6 thus enabling SD to act as the mechanosensor of the podocyte, to sense and respond to mechanical stimuli [125]. In addition to serving as a structural protein of the SD, podocin was reported to also serve as a platform that connects the tight junction proteins to the actin cytoskeleton via coxsackievirus and adenovirus receptor (CAR) [126].

Podocin knockout mice had podocyte FP effacement, lacked SD, and developed proteinuria and died a few days after birth [127].

TRPC5 or TRPC6 (transient receptor potential canonical type 5 or 6) are the two most extensively studied TRPC-channels in nephrotic syndrome. They belong to a member of a family of nonselective cation channels, regulating the intracellular calcium concentration in response to the activation of G-protein-coupled receptors and receptor tyrosine kinases. Gain-of-function mutations in the TRPC6 gene have been identified in familial FSGS [99, 128] while no mutation has yet been reported for TRPC5 in patients with nephrotic syndrome. In acquired forms of kidney disease, gene expression of TRPC6 in patients with MCNS and MN was found to be significantly higher as compared to control patients. *In vitro* studies suggested that increased TRPC6 expression resulted in reorganization of the podocyte actin cytoskeleton and dysregulation of calcium influx [129, 130]. In addition, overexpression of wild-type TRPC6 was shown to be sufficient to cause proteinuria in mice [129]. Recent studies of the AT1R-activated TRPC5 and TRPC6 channels delineated the antagonistic roles of TRPC5 and TRPC6 in the regulation of actin dynamics and cell motility in podocytes [100]. TRPC5 was shown to specifically activate Rac1; whereas TRPC6 specifically activates RhoA.

CD2-associated protein (CD2AP) is an adaptor protein which binds directly to nephrin and podocin [101, 124] and also interacts with actin [131], actin-binding proteins CapZ [132], cortactin [133], and the α-actinin-modulating protein synaptopodin [134], thus completing the signaling pathway from SD to actin cytoskeleton in the podocytes. CD2AP knockout mice died due to massive proteinuria and exhibited FP effacement [135].

The Nck proteins (Nck1 and Nck2) composed of an SH2 domain, which can interact with phosphotyrosines, and SH3 domains, which can recruit proteins involved in the regulation of actin assembly. In podocytes, SH2 domain of Nck has been shown to interact with tyrosine phosphorylated nephrin following phosphorylation through Fyn, while the SH3 domains of Nck bind to neuronal

Wiskott–Aldrich syndrome protein (N-WASP) [102, 136, 137]. N-WASP, in turn, activates the Arp2/3 complex, thus linking nephrin with the underlying actin. Inactivation of Nck proteins in adult mouse podocytes led to reduced phosphorylation of nephrin, proteinuria, glomerulosclerosis, and FP effacement [138].

Partitioning defective 3 (Par3), partitioning defective 6 (Par6) and atypical protein kinase C (aPKC) constitutes the cell polarity complex of the SD [103]. Binding of Par3 to nephrin and Neph1 resulting in recruitment of Par6/aPKC to the SD.

Dendrin interacts with nephrin and CD2AP [105] and relocalization of dendrin to the nucleus of podocytes enhanced TGF-β1-mediated apoptosis in an experimental proteinuric model [139].

ZO-1 is a tight and adherens junction protein of the MAGUK family shown to bind with Neph1/2/3 [140] and cortactin [141] thus connecting the membrane proteins at the SD complex to the actin cytoskeleton.

MAGI-1 and -2 serve as a platform for nephrin [108], α-actinin-4 [109] and synaptopodin [142]. In addition, MAGI-1 links the actin cytoskeleton to junctional adhesion molecule-4 (JAM4) [106, 108]. Densin, CASK, IQGAP1, αII- and βII-spectrin have also been reported to be associated with the SD [105, 107, 109, 143] but their role in podocytes remains to be elucidated.

1.3.3 Podocyte basal membrane domain

The podocytes are attached to the GBM through transmembrane cell receptors, such as integrins, tetraspanins and dystroglycans. The predominant integrin in podocytes is α3β1 integrin which interacts with the laminin in GBM [144]. Mice with α3-knockout died neonatally due to severe abnormalities in the lung and kidney epithelia in which the branching of glomerular capillary loops was reduced and the podocytes were unable to form mature FP [145]. Conditional knockout of α3-chain or the β1-chain in adult mice both resulted in massive

proteinuria within a week, extensive FP effacement and widespread lamination with protrusions of the GBM [146-148].

β3-chain binds to integrin-linked kinase (ILK) thus connecting the integrin to the cytoskeleton [149]. In addition, ILK also connects the GBM with the SD via interaction with nephrin, α-actinin, PINCH, and α-parvin [150, 151]. Podocyte specific inactivation of ILK in mice developed proteinuria, FP effacement, glomerulosclerosis, and died of renal failure [150, 152]. El-Aouni *et al.* observed thickening of the GBM in the mutant mice followed by abnormal distribution of α3-integrins [152]; while Dai *et al.* showed that ILK form a complex with nephrin and α-actinin-4, and mutation in mice resulted in redistribution of nephrin and α-actinin-4 [150]. Overexpression of ILK in podocytes induced Wnt signaling, decreased expression of CD2AP and P-cadherin, caused podocyte detachment, proliferation [153].

CD151 is a member of the tetraspanin family which interacts with α3β1 integrin [154, 155]. CD151 knockout mice developed proteinuria and also showed thickening and splitting of the GBM that preceded podocyte FP effacement [146].

In podocytes, dystroglycans are expressed specifically at the basal membrane of the FP [156, 157]. Dystroglycan is a heterodimeric transmembrane protein consisting of the α- and β-dystroglycan. The extracellular portion of dystroglycans binds to laminin and agrin of the GBM; whereas the cytoplasmic region of the dystroglycan is connected to the actin cytoskeleton of FP via utrophin. Expression of the α- and β-dystroglycan was shown to be significantly reduced in patients with MCNS, but normal in healthy kidneys and FSGS [156].

Recently, podocyte FP basal membrane expression of uPAR was reported in 3- and 12-month old diabetic rats [158]. Gene expression of *Plaur* mRNA which encodes uPAR was also shown to be higher in patients with FSGS and diabetic nephropathy. Plaur knockout mice were protected from lipopolysaccharide (LPS)-induced proteinuria and the protective effect was removed after the

reconstitution of *Plaur* gene in LPS injected *Plaur* knockout mice. uPAR has many ligands [159] which includes the urokinase-type plasminogen activator (uPA or urokinase) [160], vitronectin [161], and αvβ3-integrin [162]. In podocyte cultures and murine models, uPAR was shown to cause vitronectin dependent αvβ3-integrin activation, followed by integrin-mediated activation of Rac and Cdc42, resulting in reorganization of the actin cytoskeleton and caused proteinuria in mice [158]. Activation of αvβ3-integrin was sufficient to induce proteinuria and inhibition of αvβ3-integrin activation had an anti-proteinuric effect. Vitronectin was also induced during proteinuria, and vitronectin knockout mice were protected from LPS-induced proteinuria. Another study identified activated nuclear factor of activated T cells, cytoplasmic 1 (NFATc1) as a mediator of uPAR expression and β3-integrin activation in podocytes; and cyclosporine A (calcineurin inhibitors clinically used to reduce proteinuria in FSGS) interrupted NFATc1:uPAR:β3-integrin signaling and proteinuria [163].

1.3.4 Actin cytoskeleton of foot processes

In healthy FP, the actin cytoskeleton is bundled in an highly ordered manner that run parallel to the longitudinal axis of FP whereas in effaced FP, these parallel actin bundles reorganize to dense network of short, branched actin filaments [77]. Other than the cytoplasmic proteins mentioned above that connect the membrane proteins from the three domains to the cytoskeleton, α-actinin-4 and synaptopodin are two actin-associated proteins implicated to play an important role in regulating the actin cytoskeleton dynamics in podocytes FP.

Mutation in the α-actinin-4 coding gene *ACTN4* caused autosomal dominant FSGS [164]. Transgenic mice with podocyte specific mutation analogous to that affecting a human FSGS family developed proteinuria and had histologic features consistent with human ACTN4-associated FSGS [165]. The mutation was located to the actin-binding domain of α-actinin-4 which caused increased binding affinity to actin and abolished the Ca^{2+} regulation, resulting in FP effacement [166]. One study attributed the phenotype observed in the α-actinin-4 knockout mice to the reduced adhesion of the mutant podocytes to the GBM

which caused shedding of podocytes into the urine resulting in kidney failure [167].

Synaptopodin is a proline-rich, actin-associated protein found in dendritic spine apparatus of neurons and podocyte FP [168]. In podocytes, synaptopodin was shown to bind α-actinin-4 and regulate its actin-bundling activity in which synaptopodin knockout podocytes lacked stress fibers [169]. Other interacting partners for synaptopodin include CD2AP (found near SD) [134] and MAGI-1 (found near SD and also basal membrane domain) [142], connecting the signaling cascades of the SD and the basal membrane domain. In addition, synaptopodin was also shown to regulate RhoA signaling and cell migration in kidney podocytes [170]. Synaptopodin was able to compete with Smurf-1 for RhoA binding, thereby protecting RhoA from Smurf-1-mediated ubiquitination and subsequent proteasomic degradation, resulting in stress fibers formation and podocyte migration. Moreover, studies have shown that cyclosporine A seemed to have a direct anti-proteinuric effect on podocytes, by blocking the calcineurin-mediated dephosphorylation of synaptopodin thus protecting synaptopodin from cathepsin L mediated proteolysis and resulting in stabilization of the foot process cytoskeleton and resistance to proteinuria [171].

1.4. Role of IL-13 in nephrotic syndrome

IL-13 is an important immunoregulatory protein produced by T-cells and dendritic cells [172]. It is a 12kDa protein consisting of 132 amino acids. The human IL-13 gene is located on chromosome 5q31, in the same cluster of genes encoding IL-3, IL-4, IL-5, IL-9 and granulocyte-monocyte colony stimulating factor (GM-CSF) [173]. The receptor for IL-13 is a heterodimer of IL-13 receptor α1 chain (IL-13Rα1) and IL-4 receptor α chain (IL-4Rα). IL-13 first binds to IL-13Rα1 with moderate affinity, followed by subsequent recruitment of IL-4Rα which helps to increase the binding affinity for IL-13 and stabilize this high affinity interaction [174, 175]. IL-13 receptor α2 chain (IL-13Rα2) is another IL-13R which has a higher binding affinity for IL-13 compared to IL-13Rα1 [176]. IL-13Rα2 is traditionally considered a decoy receptor that regulates IL-13 response [177, 178]. However, recent studies suggested that IL-

13Rα2 may have a role in signaling. IL-13 was shown to upregulate TGF-β in macrophages in an IL-13Rα2-dependent manner. Gene silencing of IL-13Rα2 led to downregulation of TGF-β production [179]. Another study showed that IL-13Rα2 was involved in the immune evasion of tumour in mice [180].

IL-13 receptors are expressed on human B cells, basophils, eosinophils, mast cells, endothelial cells, fibroblasts, monocytes, macrophages, respiratory epithelial cells, and smooth muscle cells [181]. However, unlike IL-4, it fails to activate T cells since IL-13 receptors are virtually absent on T lymphocytes [182, 183]. IL-13 acts through its receptors on the cell surface, activating predominately the JAK/STAT pathway [181, 184, 185]. The cytoplasmic domains of IL-4Rα/IL-13Rα1 complex interact with tyrosine kinases (Tyk) of the Janus kinase (JAK) family. In non-hematopoietic cells, JAK2 is phosphorylated and activated instead of JAK3; while in hematopoietic cells, JAK3 is required for signal transducer and activator of transcription-6 (STAT6) [186]. Phosphorylation of Tyk leads to the recruitment and tyrosine phosphorylation of STAT6. Phosphorylated STAT6 migrates into the nucleus and binds to consensus sequences in the promoter regions of genes regulated by IL-4 and IL-13. Transcription factors c-fos, c-jun, and c-myc have been shown to be upregulated by IL-13 [187].

IL-13 exerts diverse functions on different cell types. It promotes B-cell proliferation and immunoglobulin isotype switching to IgE in combination with CD40/CD40 ligand costimulation [188]. It also promotes eosinophil survival, activation, and recruitment [189-191] activates mast cells and hence contributes to IgE priming of mast cells [192].

IL-13 also has important functions on non-hematopoietic cells. It induces vascular cell adhesion molecule 1 expression in endothelial cells [193]; enhances proliferation and cholinergic-induced contractions of smooth muscle cells [194]; induces chemokines expression in epithelial cells [195], changes mucociliary differentiation and decreases ciliary beat frequency of ciliated epithelial cells [196]; and causes goblet cell metaplasia [197-199].

1.4.1 IL-13 as a modulator of monocyte function

IL-13 is known to be an important modulator of monocyte function. It has been shown to induce significant changes in the phenotype and morphology of monocytes. It enhances the expression of CD11b, CD11c, CD18, CD29, MHC Class II and CD23 [183, 192], whereas it down-regulates the expression of CD64, CD16, CD32 and CD14 in a dose-dependent manner [200, 201]. IL-13 has also been shown to exert its anti-inflammatory activities by inhibiting the production of pro-inflammatory cytokines, like IL-12, IL-8, IL-6, TNF-α, IL-1α and IL-1β, by LPS-activated monocytes [192, 201] and upregulation of anti-inflammatory molecules like interleukin 1 receptor antagonist (IL-1RA) [202]. This may account for the observation that children in nephrotic relapse are more susceptible to bacterial infections.

Our laboratory has demonstrated that IL-13 downregulates proinflammatory cytokines, IL-8 and TNF-α in LPS-stimulated monocytes from patients with MCNS during nephrotic relapses as compared to remission and normal controls [203]. This was associated with decreased expression of CD14 and other monocyte surface markers, as well as soluble CD14. These results point to a major anti-inflammatory effect of IL-13 on monocytes which may place a crucial role in the pathogenesis of MCNS.

1.4.2 Role of monocyte/macrophage in nephrotic syndrome

The function of the monocyte-macrophage system in the pathogenesis of nephrotic syndrome has also been evaluated, considering that MCNS is a result of a primary immune disturbance, and the irrefutable role of monocytes in the host immune system.

Monocytes from SRNS patients with proteinuria were shown to have enhanced phagocytosis of opsonized particles and suppressed chemotaxis which might be due to the alteration of the monocyte surface receptors and lymphokines [204]. In addition, depressed function of Fc-receptors of monocytes and macrophages were observed in children with MCNS [205].

Garin *et al.* have identified a supernatant factor that caused a significant increase in sulfate uptake in rat GBM and they showed that both lymphocytes and monocytes were needed for the production of that supernatant factor [206].

Using reporter podocytes, Takano, Y, *et al.* showed that bystander macrophages and macrophage-derived cytokines IL-1β and TNF-α significantly suppressed activity of the nephrin gene promoter in podocytes. The reduced nephrin promoter activity was attributed to the activation of the phosphatidylinositol-3-kinase/Akt pathway [207].

Whether monocyte deficiency or activation found in MCNS is primary or secondary to the postulated T-cell defect in this disease remains to be elucidated.

1.5. Role of IL-13 on podocytes

As mentioned previously, MCNS is primarily caused by immune disturbance characterized by Th2 cytokine bias. However, the mechanism by which this observed cytokine imbalance in serum results in subsequent characteristic podocyte injury in MCNS is still unknown. Studies have shown that podocytes constitutively express functional receptors for cytokines IL-1 [208, 209], IL-4, IL-13 [210, 211], IL-10 [210] and TNF-α [212, 213], suggesting that cytokines could act directly on podocytes to cause injury. Studies have demonstrated that IL-4 and IL-13 increase transcellular ion transport in rat podocyte monolayer cultures [211]. Further work revealed that IL-4 and IL-13 induced H^+ transport in podocytes, thus lowering the pH and affecting the integrity of basal membrane matrix by activating the proteolytic enzyme, cathepsin L [214].

In our experimental rat model of Th2 cytokine-induced MCNS, we have demonstrated that overexpression of *IL-13* gene resulted in podocyte injury with downregulation of nephrin, podocin and dystroglycan and concurrent upregulation of B7-1 in the glomeruli [215, 216]. In this experimental model, we have demonstrated increased glomerular IL-4Rα and IL-13Rα2 gene expression, as well as increased fluorescent signal for IL-4Rα in most of the

glomeruli of nephrotic rats, suggesting that IL-13 may act directly on podocytes in the glomeruli. In addition, there was a significant correlation between serum IL-13 levels and B7-1 expression in the glomeruli of the *IL-13* overexpressed rats with nephrotic syndrome. The concomitant upregulation of B7-1 expression in the glomeruli following *IL-13* overexpression suggests a possible pathogenic link between IL-13 and podocyte dysfunction.

Studies have suggested a novel role for the costimulatory molecule B7-1 in podocytes as an inducible modifier of glomerular permselectivity and proteinuria [217, 218]. Podocyte-specific expression of B7-1 has been implicated as the final common pathway in the genesis of proteinuria in glomerulopathies. In genetic, drug-induced, autoimmune, and bacterial toxin-induced experimental kidney diseases with nephrotic syndrome, B7-1 expression in podocytes was upregulated. Following *in vitro* LPS stimulation, podocyte expression of B7-1 was increased with concurrent actin cytoskeleton reorganization. B7-1 knockout mice were protected from LPS-induced proteinuria, suggesting a functional link between podocyte B7-1 expression and proteinuria. Specific urinary CD80 (B7-1) excretion was reported in MCNS patients in relapse which was not observed in other glomerular diseases [219, 220]. In addition, renal biopsy results showed high expression of CD80 in glomeruli of MCNS patients in relapse but not MCNS patients in remission or FSGS patients. CD80 expression was shown to be co-localized with podocin expression in the glomeruli from an MCNS patient in relapse.

1.6. Gaps in current knowledge

Despite recent advances in our understanding of podocyte biology, we do not know the exact pathogenesis of MCNS or why some children require long term steroid therapy or even cytotoxic drugs while some do not. There is a large body of evidence that immunogenic stimuli interacting with immunoregulatory proteins, form the basis for the immunopathogenesis of MCNS. We have demonstrated increased T-cell production of IL-13 in MCNS patients in relapse [58] as well as downregulation of proinflammatory cytokines, IL-8 and TNF-α in LPS-stimulated monocytes from patients with MCNS during nephrotic

relapses compared to remission and normal controls [203]. This was associated with decreased expression of CD14 and other monocyte surface markers, as well as soluble CD14. These results point to a major anti-inflammatory effect of IL-13 on monocytes. Whether IL-13-induced monokines acts directly on the podocytes to cause foot process loss or activate another cascade of enzymes or cytokines to mediate proteinuria remains to be elucidated.

Current research by several groups worldwide has been focusing on the mechanism by which disruption in podocyte architecture results in podocyte FP effacement and proteinuria. As mentioned above, recent studies have suggested a novel role for the costimulatory molecule B7-1 in podocytes as an inducible modifier of glomerular permselectivity and proteinuria. Stimulation by LPS reorganized the podocyte actin cytoskeleton *in vitro*, and activation of B7-1 in cultured podocytes led to reorganization of vital slit diaphragm proteins [217, 218]. In fact, increased B7-1 expression on podocytes has been described in the different models of nephrotic syndrome, namely genetic (α3β1-integrin deficiency), toxic (puromycin and adriamycin-induced) and immunological (murine lupus nephritis). Therefore, our results from the *IL-13* overexpression rat model further strengthen the hypothesis that transient upregulation of B7-1 could occur in MCNS, resulting in nephrotic-range proteinuria [215, 216], and also provide an explanation for the possible link between Th2 cytokine bias and MCNS. However, the exact mechanism by which IL-13 interacts with the B7-1 danger signaling pathway remains an enigma.

1.7. Research hypothesis and scope of thesis

Our current understanding of the pathogenic mechanism of nephrotic syndrome suggests that the podocyte is the main component of the glomerular filter and the crucial target in the development and progression of glomerulopathies. In fact, the hallmark of nephrotic syndrome is effacement of podocyte foot processes (FP) seen on electron microscopy.

Studies attempting to elucidate the underlying pathogenesis of MCNS have suggested a Th2 cytokine bias. Our group has previously demonstrated that *IL-*

13 gene expression was upregulated in $CD4^+$ and $CD8^+$ T-cells of children with MCNS in relapse as well as downregulation of proinflammatory cytokines, IL-8 and TNF-α in LPS-stimulated monocytes from patients with MCNS during nephrotic relapses compared to remission and normal controls. We have, in addition, shown that *IL-13* overexpression in the rat resulted in podocyte injury with downregulation of the slit diaphragm proteins, namely nephrin and podocin, with upregulation of glomerular B7-1, inducing a minimal change-like nephropathy. In this model, we have also demonstrated increased glomerular IL-4Rα and IL-13Rα2 gene expression, as well as increased fluorescent signal for IL-4Rα in most of the glomerular podocytes of nephrotic rats, suggesting that IL-13 may act directly on podocytes in the glomeruli through a possible B7-1 mechanism. In our preliminary studies, we have also shown that glomerular gene expression of toll-like receptor-4 (TLR-4) was significantly elevated in the *IL-13* overexpressed rats, and also correlated significantly with glomerular B7-1 expression.

Therefore, we **hypothesize** that modulation of podocyte actin cytoskeleton in MCNS may possibly be a consequent summative effect of immune mediators on podocyte B7-1 expression (Figure 5), namely:

i) direct IL-13 stimulation;
ii) indirect signaling by other immune mediators through other ligands or receptors such as TLR-4.

As IL-13 is an important modulator of monocyte/macrophage function, it is plausible that the indirect action of IL-13 on podocytes may be mediated via monocyte/macrophage polarization with consequent secretion of monokine(s) acting on the TLR-4/B7-1 danger signaling, effecting podocyte actin cytoskeleton rearrangement.

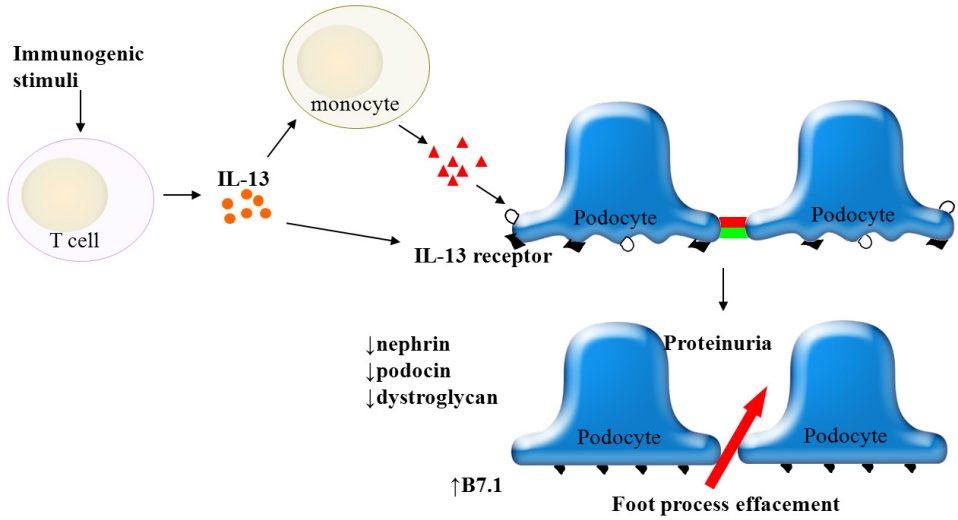

Figure 5: Hypothetical Th2 cytokine bias model of MCNS results from a primary immune disturbance.
IL-13 and/or other immune mediators may directly or indirectly act on podocytes and cause podocyte FP effacement, resulting in proteinuria and the nephrotic syndrome.

1.7.1 Objectives of the study

The primary aim of this project is to investigate the molecular mechanisms by which IL-13 downregulates the expression of podocyte-specific proteins resulting in proteinuria. The specific objectives are as follows:

A. *In vivo* rat model:

1 To characterize the molecular events in the glomeruli of the IL-13 rat model of MCNS using cDNA microarray and identifying differentially expressed genes (DEGs) induced by IL-13.

2 To determine the mechanistic link between IL-13 and B7-1 signaling in the rat model using pathway analysis tools.

3 To validate the microarray results both at the gene transcription level, using real-time PCR; and at the protein expression level, using immunohistochemistry staining.

B. *In vitro* human podocyte cell culture:

1 To set up a human podocyte cell culture system (gift by Professor Moin A. Saleem, University of Bristol) to validate the microarray glomerular gene expression results from the *in vivo* rat model.

2 To study the direct effect of IL-13 on podocytes. The specific objectives are:

a) Quantitate the expression levels of IL-13 receptor subunits, B7-1, CTLA-4, TLR-4 and SD proteins, in particular, nephrin, podocin and dystroglycan at both gene transcription (real-time PCR) and protein level (Western blotting);
b) Examine podocyte morphology, in particular, cytoskeletal changes associated with FP effacement using phalloidin staining and viewing with confocal microscopy.
c) Measure RhoA/Rac1 activity levels in association with IL-13 induced podocyte actin cytoskeleton rearrangement.

3 To perform functional study using podocytes transfected with siRNA specific to the selected DEGs, to delineate the mechanistic link of IL-13 mediated podocyte injury downstream of B7-1 activation. The markers for podocyte injury used in this functional assay are stated in 2a, b and c.

Knowledge of the signaling pathways involved in the pathogenesis of this disease may provide us more targeted treatment at the molecular level, allowing us to design new therapeutic strategies. Results of this proposed study should thus have an important impact on healthcare costs as nephrotic syndrome is one of the more important kidney disorders in childhood, as well as an important cause of end-stage kidney failure requiring dialysis and transplantation.

CHAPTER 2

MATERIALS & METHODS

2.1. *IL-13* overexpression rat model of MCNS

All animal studies were approved by the Institutional Animal Care and Use Committee of the National University of Singapore. Induction of frank nephrotic in rats has been reported before [216]. Six-week-old female Wistar rats weighing 150-180g were used in this study. Rats were put in metabolic cages 24 hours prior to the electroporation to collect 24-hour urine sample and the volume of urine was recorded. Before the electroporation, heparinized blood was collected from the ventral artery of the tail using a 23G needle. Rats were electroporated every 10 days over a period of 72 days with endotoxin-free, purified plasmid DNA injected into the quadriceps of rats. An electric current consisting 6 pulses of 20 milliseconds each at 160V was generated using the "Electro Square Porator ECM830" (BTX Technologies Inc, NY, USA) and delivered through the 10mm 2-Needle Array™ tip (BTX Technologies Inc, NY, USA) connected to a 2-Needle Array™ electrode (BTX Technologies Inc, NY, USA) [221]. Control rats received 200µg of the pCI (Promega, WI, USA) mammalian expression vector and test rats received 200µg of the pCI mammalian expression vector cloned with the rat *IL-13* gene. Once proteinuria develops, the rats were euthanised by overdose of anaesthetic (ketamine 75mg/kg and xylazine 10mg/kg) via intra-peritoneal injection. Heparinized blood was collected via cardiac puncture and kidney cortical tissue was harvested for isolation of glomeruli as well as snap-frozen and stored at –80°C for further use. Both blood and urine were centrifuged at 3,000rpm for 10 minutes to obtain plasma and remove sediment respectively. Plasma levels of albumin, cholesterol, creatinine and IL-13, and urine albumin concentration were measured serially to ensure successful induction of frank nephrosis in rats.

2.2. Plasma IL-13 ELISA

Plasma level of IL-13 was measured using commercially available Enzyme Linked Immuno Sorbent Assay (ELISA) kit (Invitrogen, CA, USA) according to the manufacturer's instructions. Briefly, 50µl of samples, IL-13 standards and positive controls were added to the wells, followed by 150µl of a biotinylated

secondary monoclonal antibody. Plasma from the *IL-13* overexpression rats was diluted five times, while the control plasma was used undiluted. After two hours incubation, the wells were washed with wash buffer provided to remove excess biotinylated antibody. Following 30 minutes incubation with 100µl of streptavidin-peroxidase, the wells were washed to remove unbound enzyme and 100µl of stabilized chromogen (substrate) was added to produce colour signal in proportion to the amount of IL-13 bound. The colour development was stopped by adding 100µl of stop solution and the intensity of the colour was measured using a microplate reader (Bio-Rad Laboratories, Inc, CA, USA) with wavelength set at 450 nm. The concentrations of IL-13 in the samples were determined from the standard curve, factoring in the dilution.

2.3. Plasma albumin quantification

Plasma albumin level was determined by bromocresol green (BCG) method using a commercial reagent kit (Randox Laboratories, Antrim, UK). Briefly, 5µl of samples and standard were added to 1.5ml of BCG reagent and incubated for 5 minutes at room temperature. Two hundred µl of the reaction mixture was transferred to the microtiter plate in duplicate and the absorbance of the reaction mixtures was read at 600nm using a microplate reader (Bio-Rad Laboratories, Inc, CA, USA) against the reagent blank consisting of 0.9% w/v NaCl in distilled water. Concentration of albumin in the sample was calculated by multiplying the absorbance ratio of the sample (A_{sample}) and the standard ($A_{standard}$) with the concentration of the standard provided by the manufacturer ($\frac{A_{sample}}{A_{standard}} \times$ concentration of standard).

2.4. Plasma cholesterol quantification

Plasma cholesterol level was determined by an enzymatic endpoint method [222] using a commercial reagent kit (Randox Laboratories, Antrim, UK). Briefly, 10µl of the samples and standard were added to 1ml of the reagent provided and incubated for 10 minutes at room temperature. Two hundred µl of the reaction mixture was transferred to the microtiter plate in duplicate and the absorbance of the reaction mixtures was read at 500nm using a microplate reader (Bio-Rad Laboratories, Inc, CA, USA) against the reagent blank

consisting of 0.9% w/v NaCl in distilled water. Concentration of cholesterol in the sample was calculated by multiplying the absorbance ratio of the sample (A_{sample}) and the standard ($A_{standard}$) with the concentration of the standard provided by the manufacturer ($\frac{A_{sample}}{A_{standard}} \times$ concentration of standard).

2.5. Plasma creatinine quantification

Plasma creatinine was determined by the alkaline picrate method [223]. Briefly, 100µl of samples and standards were added to a mixture containing 100µl of ddH_2O, 100µl of 5% w/v sodium tungstate in distilled water and 100µl of 2/3N sulphuric acid and incubated for 10 minutes at room temperature. The mixture was then centrifuged at 6,000rpm for 2 minutes. One hundred µl of the supernatant was transferred to the microtiter plate in duplicate. Following 20 minutes incubation with 20µl of saturated aqueous picric acid and 30µl of 1N NaOH for colour development, the absorbance of the reaction mixtures was read at 490nm using a microplate reader (Bio-Rad Laboratories, Inc, CA, USA). The concentrations of creatinine in the samples were determined from the standard curve.

2.6. Urine albumin ELISA

A direct sandwich ELISA was developed [224] to detect the concentration of rat albumin in 24-hour urine samples. One hundred µl of rabbit antiserum to rat albumin antibody (MP Biomedicals, CA, USA) diluted 1/2000 was used as the coating antibody and 50µl of horseradish peroxidase (HRP)-conjugated sheep polyclonal antibody to rat albumin secondary antibody (MP Biomedicals, CA, USA) diluted 1/20000 was used as the detecting antibody. o-Diphenylenediamine (OPD) (MP Biomedicals, CA, USA), in citrate buffer pH 5.0, was used as the substrate for colour development. Rat albumin standards (MP Biomedicals, CA, USA) of known concentrations were included in each assay. Endpoint absorbance was read at 490nm by a microplate reader (Bio-Rad Laboratories, Inc, CA, USA). The total amount of albumin excreted in 24-hour urine was calculated by multiplying the concentration of albumin (mg/ml) with the total volume (ml) of 24-hour urine sample. (Appendix 2.1)

2.7. Isolation of glomeruli by graded sieving technique

Glomeruli were isolated from kidney cortical tissue using graded sieving technique [225]. The cortical area of the kidney was cut into small pieces and pressed through a stainless steel sieve (W.S. TYLER Industrial Group, OH, USA) with a sieve diameter of 75µm with a spatula. The tissue was rinsed off with ice-cold 1x Hank's balanced salt solution (HBSS) (Gibco®, Invitrogen Life Technologies, CA, USA) to a petri dish placed underneath the sieve. The filtrate collected was then passed through a 70µm nylon sieve (Falcon™, BD Biosciences, CA, USA) and the filtrate was collected in a 50ml collection tube. Glomeruli and large tubular tissue fragments were retained on the nylon sieve while red blood cells (RBC) and smaller tissue fragments passed through. The 70µm nylon sieve was then inverted onto a new 50ml collection tube and the glomeruli washed down to the collection tube with 1x HBSS. Glomeruli obtained from the graded sieving technique were usually over 95% pure with minimal contamination from tubular epithelial cells.

2.8. RNA extraction using TRIzol® reagent

Total RNA was extracted by TRIzol® reagent (Invitrogen Life Technologies, CA, USA). Tissue or cells were lysed in 1ml of TRIzol® reagent and incubated for 5 minutes at room temperature for complete dissociation of nucleoprotein complexes. Two hundred µl of chloroform (Fisher Scientific, MA, USA) was then added per 1ml of TRIzol® reagent and the mixture was shaken vigorously for 15 seconds and incubated at room temperature for 3 minutes. The samples were then centrifuged at 12000*g* for 15 minutes at 4°C. Following centrifugation, the mixture separated into a lower red, phenol-chloroform phase, an interphase, and a colorless upper aqueous phase. RNA remained in the aqueous phase. The aqueous phase was transferred to a clean tube and 500µl of isopropanol (Fisher Scientific, MA, USA) was added per 1ml of initial TRIzol® reagent to precipitate the RNA. Samples were incubated at room temperature for 10 minutes and centrifuged at 12000*g* for 10 minutes at 4°C. The RNA pellet was then washed once with 1ml of 75% ethanol (Merck, NJ, USA) per 1ml of initial TRIzol® reagent and centrifuged at 7500*g* for 5 minutes at 4°C. The RNA pellet was then air dried briefly and dissolved with RNase-free water.

Concentration of RNA was measured using NanoDrop 1000 Spectrophotometer (NanoDrop products, Thermo Scientific, DE, USA).

2.9. RNA cleanup using RNeasy Mini-kit

Glomerular RNA for microarray was further purified using RNeasy Mini-kit (QIAGEN GmbH, Hilden, Germany) according to the manufacturer's instructions. (Appendix 2.2)

2.10. Quantification and quality analysis of RNA using Bioanalyzer 6000 Nano kit (for microarray)

The integrity of the total glomerular RNA was analysed by measuring the ratio of 28s/18s and the RIN number. The samples were processed using the Bioanalyzer 6000 Nano kit (Agilent Technologies, Inc, Waldbronn, Germany) and analysed using the Bioanalyzer 2100 (Agilent Technologies, Inc, Waldbronn, Germany). Briefly, RNA samples with concentration ranging from 25 to 500ng/µl were used. For gel preparation, 550µl of RNA 6000 Nano gel matrix was added into a spin filter and centrifuged at 1,500g for 10 minutes at room temperature. Sixty five µl of filtered gel was then aliquoted to 0.5ml RNase-free microcentrifuge tube. For gel-dye mix preparation, 1µl of the RNA 6000 Nano dye concentrated was added to the 65µl aliquot of filtered gel, mixed by vortexing and centrifuged at 13,000*g* for 10 minutes at room temperature. Loading of the gel-dye mixture was done on the chip priming station by adding 9µl of gel-dye mix in the well mark G, plunging the syringe in 1ml volume, waiting for exactly 30s before releasing the clip and pulling back the plunger back to the 1ml position. This is followed by adding 9µl of gel-dye mix in the well marked G. Five µl of RNA 6000 Nano marker was then added to all the sample wells as well as the ladder well marked . The reaction mix was completed by adding 1µl of prepared ladder in the well marked and 1µl of sample in the sample wells. The mixture was vortexed by placing the chip on the IKA vortexer for 1 minute at 2,400rpm and the chip was read using Agilent 2100 bioanalyzer within 5 minutes.

2.11. Reverse Transcription to Synthesize First Strand cDNA using Illumina® TotalPrep RNA Amplification Kit (for microarray)

Glomerular RNA sample was diluted to 300ng in final volume of 11ul with nuclease free water. Reverse Transcription Master Mix, consisting of 1µl of T7 Oligo (dT) primer, 2µl of 10x First Strand Buffer, 4µl of dNTP Mix, 1µl of RNase Inhibitor and 1µl of ArrayScript per reaction, was added to the RNA sample. The reactions were run at 42ºC for 2 hours followed by cooling at 4ºC.

2.12. Second strand cDNA sysnthesis using Illumina® TotalPrep RNA Amplification Kit (for microarray)

Second Strand Master Mix, consisting of 63µl of nuclease free water, 10µl of 10x Second Strand Buffer, 4µl of dNTP mix, 2µl of DNA polymerase and 1µl of RNase H per reaction, was added to the first strand cDNA sample. The reactions were run at 16ºC for 2 hours followed by cooling at 4ºC (for less than 1 hour). The reactions should proceed to cDNA purification immediately or store at -20ºC.

2.13. cDNA Purification using Illumina® TotalPrep RNA Amplification Kit (for microarray)

The cDNA was transferred into a 1.5ml microcentrifuge tube containing 250µl of cDNA binding buffer. The mixture was then transferred to a cDNA filter cartridge and centrifuged at 10,000*g* for 1 minute. This was followed by washing with 500µl of wash buffer and centrifuged at 10,000*g* for 1 minute. The filter cartridge was then transferred to a cDNA elution tube. The cDNA was eluted in two steps, first with 10µl of nuclease free water (pre-heated to 55ºC), incubated at room temperature for 2 minutes and centrifuged at 10,000*g* for 1.5 minutes, followed by another 9µl of nuclease free water (pre-heated to 55ºC), centrifuged at 10,000*g* for 2 minutes and collected in the same collection tube.

2.14. cRNA synthesis using Illumina® TotalPrep RNA Amplification Kit (for microarray)

In Vitro Transcription Master mix, consisting of 2.5µl of T7 10x Reaction buffer, 2.5µl of T7 Enzyme Mix and 2.5µl of Biotin-16-UTP per reaction, was

added to the cDNA sample. The reaction was run at 37°C for 14 hours and then stopped by adding 75µl of nuclease free water to bring to final volume of 100µl.

2.15. cRNA purification using Illumina® TotalPrep RNA Amplification Kit (for microarray)

The cRNA was transferred into a 1.5ml microcentrifuge tube containing 350µl of cRNA binding buffer followed by 250µl of absolute ethanol. The mixture was then transferred to a cRNA filter cartridge and centrifuged at 10,000*g* for 1 minute. This was followed by washing with 650µl of wash buffer and centrifuged at 10,000*g* for 1 minute. The filter cartridge was then transferred to a cRNA elution tube. The cRNA was eluted in two steps, first with 50µl of nuclease free water (pre-heated to 55°C), incubated at room temperature for 2 minutes and centrifuged at 10,000*g* for 1.5 minutes, followed by another 30µl of nuclease free water (pre-heated to 55°C), centrifuged at 10,000*g* for 1.5 minutes and collected in the same collection tube. The concentration of the cRNA was measured using NanoDrop 1000 Spectrophotometer (NanoDrop products, Thermo Scientific, DE, USA). Samples with concentration less than 150ng/µl was concentrated by vacuum centrifugation.

2.16. cRNA hybridization and array scanning

Hybridization of 750ng of cRNAs was carried out for 18.5 hours on Sentrix® BeadChip Array RatRef-12 v1 (Illumina®, CA, USA) according to the manufacturer's protocol. Array washing was performed followed by staining and scanning with BeadArray Reader (Illumina®, San Diego, CA, USA) using scan factor 1.5, PMT 531. (Appendix 2.3)

2.17. Microarray analysis

The raw intensity values of the array were extracted with background subtraction via BeadStudio (Illumina®, CA, USA) for analysis. The raw data was preprocessed to correct unreliable intensities for each array. The intensities with detection p-values greater than 0.05 were considered as unreliable and replaced by the intensity with detection p-value equal to 0.05. The preprocessed data was normalized by the Cross-Correlation method [226]. Differentially

expressed genes (DEGs) were selected based on the criteria of fold change greater than 1.6, coefficient of variance less than 0.7 and *t-test* $p<0.05$. Clustering of samples was generated with Cluster and TreeView software [227]. Gene ontology (GO) analysis was done using DAVID [228, 229] and pathway analysis were carried out using Ingenuity Pathway Analysis (Ingenuity, CA, USA) and MetaCore™ (GeneGo Inc, MI, USA).

2.18. Real-time PCR

Single-stranded cDNA was synthesized from 150ng of total RNA using the Superscript III First-Strand Synthesis System for RT-PCR (Invitrogen Life Technologies, CA, USA), according to the manufacturer's instructions (Appendix 2.4). Quantitative real-time PCR was performed using the LightCycler® 480 SYBR Green I Master (Roche, Germany). Briefly, the real-time PCR was performed in a final volume of 10µl reaction mixture containing 1µM each of the primers, 5µl of master mix, 1µl of PCR grade water and 2µl of cDNA. The thermal cycling conditions consisted of one cycle of 10 minutes at 95ºC, 45 cycles of 5 seconds at 95ºC, 10 seconds at 58ºC, and 20 seconds at 72ºC, followed by melting curve analysis and cooling to 40ºC. Standard curves were created for each PCR run using serial dilutions of plasmid standards that were cloned with the PCR products generated by their respective primers (Appendix 2.5). All samples were run in duplicates and copy number for each sample was determined from the respective standard curve. Results were expressed as an index of the housekeeping gene GAPDH.

2.19. Protein expression study using immunohistochemical technique

Formalin-fixed, paraffin-embedded kidney tissue was used for detection of vav1 in the glomeruli using LSAB2 system-HRP (DakoCytomation, Glostrup, Denmark). The tissue sections were dewaxed and rehydrated through alcohol by going through incubation with two changes of xylene (J.T. Baker® Chemicals, Avantor Performance Materials, PA, USA) for 10 minutes each, two changes of absolute ethanol (Merck, NJ, USA) for 2 minutes each, followed by 95% ethanol for 2 minutes and 70% ethanol for 2 minutes. The sections were then washed with tap water and incubated with peroxidase for 5 minutes.

Following avidin and biotin (DakoCytomation, Glostrup, Denmark) activity blocking for 10 minutes each, as well as antigen retrieval with proteinase K (DakoCytomation, Glostrup, Denmark) for 5 minutes, sections were sequentially incubated with rabbit anti-vav1 (1/50) (Bioworld Technology, Inc, MN, USA or Sigma-Aldrich, MO, USA), or mouse anti-synaptopodin (neat) (USBiological, MA, USA) primary antibody for 10 minutes, biotinylated goat anti-rabbit IgG for 10 minutes, and Streptavidin-HRP for 10 minutes. Staining was completed after incubation with 3-3' diaminobenzine (DAB) Substrate-Chromogen which produced brown colour precipitation at the antigen site. Nuclei were counterstained using Mayer's hemalum (Merck, NJ, USA) for 1 minute and blued in 0.05% aqueous ammonia solution (Merck, NJ, USA) for 1 minute. The sections were dehydrated and cleared by going through incubation with 70% ethanol for 1 minute, 95% ethanol for 1 minute, two changes of absolute ethanol for 1 minute each and two changes of xylene for 2 minutes each. The sections were then mounted with cover slip using DEPEX mounting medium (BDH Chemicals, VWR, PA, USA).

2.20. Protein expression study using Western blotting technique

Protein lysate of 40ug were separated using 12% sodium dodecyl sulfate (SDS)-polyacrylamide gel and transferred onto a polyvinylidene fluoride (PVDF) membrane. Membrane was blocked with 5% non-fat milk for 1 hour and probed with the following primary antibodies: rabbit anti-GAPDH (1/10,000) (Sigma-Aldrich, MO, USA); rabbit anti-vav1 (phospho Y174) (1/2,000) (Bioworld Technology, Inc, MN, USA); rabbit anti-vav1 (1/800) (Proteintech Group, Inc, IL, USA); rabbit anti-B7-1 (1/3,000) (Epitomics, Inc, CA, USA); and rabbit anti-IL-13Rα2 (1/1000) (Proteintech Group, Inc, IL, USA). Following incubation with donkey anti-rabbit IgG HRP-conjugated secondary antibodies (Santa Cruz Biotechnology, CA, USA), blots were developed using Lumina Forte Western HRP Substrate (Merck Millipore, MA, USA) and quantified using ImageJ software (National Institute of Health, MD, USA).

2.21. Culture of human podocytes

Conditionally immortalized human podocytes (kind gift from Dr. Moin Saleem, University of Bristol, UK) [230, 231] were cultured on 100mm type I collagen-coated petri dishes (Iwaki, Japan) in complete medium consisting of RPMI 1640 with L-glutamine (Gibco®, Invitrogen Life Technologies, CA, USA), 10% heat-inactivated Fetal Bovine Serum (Gibco®, Invitrogen Life Technologies, CA, USA), 100units/ml Penicillin/Streptomycin solution (Gibco®, Invitrogen Life Technologies, CA, USA), ITS cocktail (Sigma-Aldrich, MO, USA) of 10µg/ml insulin, 5.5µg/ml of transferrin and 5ng/ml of sodium selenium. The cells were grown at a permissive temperature of 33ºC with 5% CO_2. Complete medium was changed every two days and cells were observed everyday under the light microscope. Upon achieving 90% confluency, the cells were thermoshifted to 37ºC for differentiation.

Briefly, the culture medium was removed and the culture dishes were washed twice with 1xPBS. The cells were then incubated with 1ml of 0.25% of trypsin-ethylenediaminetetraacetic acid (trypsin-EDTA) solution at 37ºC for 3 minutes. Trypsin-EDTA activity was stopped by adding 10ml of complete medium. Cells were splited 1/5 and seeded to new petri dishes at a non-permissive temperature of 37ºC with 5% CO_2 for up to 14 days to allow for differentiation. Fully differentiated cells were stimulated with IL-13 (20ng/ml) (R&D Systems, MN, USA) for 1 to 48 hours. Unstimulated cells were included as the baseline control. Changes in gene expression were assessed using real-time PCR; changes in protein expression were analysed using Western blotting; and changes in the organization of the actin cytoskeleton were observed after phalloidin staining.

2.22. Transfection of human podocytes with sequence specific siRNA

Differentiated cells were transfected with siRNA specific for vav1 (target sequence: 5'-CAGGTGGAGTCAGCCAGCAAA-3'; sense strand: 5'-GGUGGAGUCAGCCAGCAAATT-3'; antisense strand: 5'-UUUGCUGGCUGACUCCACCTG-3') (QIAGEN GmbH, Hilden, Germany). Cells transfected negative control siRNA were included as negative control.

Briefly, conditionally immortalized human podocytes were cultured at 33ºC and shifted to 37ºC for differentiation for 10 to 14 days. Sequence specific siRNA was diluted in serum-free culture medium to final concentration of 6nM before adding 4% (v/v) transfection reagent (INTERFERin™, polyplus transfection, NY, USA). The transfection cocktail was incubated at room temperature for 10 minutes to allow complex formation and then added dropwise to fully differentiated cells. Cells were then incubated at 37ºC with 5% CO_2 for 24 hours before stimulation with 20ng/ml of IL-13 for 24 (for RNA analysis) or 48 hours (for protein analysis).

2.23. Immunofluorescence staining of podocytes

Cells were cultured on collagen-coated coverslips (Iwaki, Japan), fixed with 4% paraformaldehyde (Merck, NJ, USA) for 10 minutes, permeabilized with 0.3% w/v Triton-X100 (Bio-Rad Laboratories, Inc, CA, USA) in 1xPBS for 3 minutes, and blocked with 5% w/v BSA (Sigma-Aldrich, MO, USA) in 1xPBS for 30 minutes. Cells were stained with following antibodies: rabbit anti-vav1 (1/50) (Sigma-Aldrich, MO, USA or Abcam, Cambridge, UK) for 1 hour at room temperature and secondary antibody of goat polyclonal to rabbit IgG-FITC (1/200) (Abcam, Cambridge, UK) for 30 minutes at room temperature; or FITC-conjugated phalloidin (1/80) (Sigma-Aldrich, MO, USA) for 1 hour at room temperature and counterstained nucleus with 4'6-diamidino-2-phenylindole (DAPI) (1/1000) (Sigma-Aldrich, MO, USA) for 5 minutes. Images were taken at randomly selected fields using a confocal microscope (Olympus FluoView FV1000, Olympus, Tokyo, Japan).

2.24. Cortical F-actin score index

A cortical F-actin score index was derived as an indicator of the degree of cytoskelal rearrangement. Cortical F-actin score index was determined from at least three independent experiments [232]. In each experiment, at least three images were taken blindly from each culture condition. The F-actin cytoskeletal reorganization for each cell was scored on a scale ranging from 0 to 3 based on the degree of cortical F-actin ring formation (score = 0, no cortical F-actin,

normal stress fibers; score = 1, cortical F-actin deposits below half of the cell border; score = 2, cortical F-actin deposits exceeding half of the cell border; score = 3, complete cortical ring formatting and/or total absence of central stress fiber). A minimum of 15 cells were examined from each culture condition in each independent experiment, and the cortical F-actin score index for is the average score of the counted cells±SEM.

2.25. Podocyte cell culture treatment for RhoA and Rac1 assays

Differentiated podocytes were cultured on 100mm type I collagen coated dish (Iwaki, Japan) and serum starved for 24 hours to inactivate the endogenous RhoA activity. Serum starved cells were then incubated with IL-13 (20ng/ml) (R&D Systems, MN, USA) for 5, 10, 20 and 30 minutes. Unstimulated podocytes were used as baseline control. Each specific time point was first completed before proceeding to the next time point so as to allow rapid processing of each single time point and hence minimizing changes in signal over time. Following the stimulation, culture dishes were placed on ice and washed with 10ml of ice cold 1xPBS. Cells were then lysed in 250µl of G-LISA® Lysis Buffer and the lysate was clarified for 2 minutes at 14,000rpm, 4°C. Aliquots of lysate for protein quantification, G-LISA, total Rho and Rac1 assays were snap-frozen in liquid nitrogen and stored at -80°C for further experiments.

2.26. RhoA activation assay

Active RhoA was measured using G-LISA® RhoA Activation Assay Biochem Kit™ (Cytoskeleton, Inc, CO, USA) according to the manufacturer's instructions and normalized against total RhoA levels (refer to 2.27) (Cytoskeleton, Inc, CO, USA) in the cell lysate for accurate comparison of RhoA activity among samples. Protein lysate was equalized with Lysis Buffer and equal volume of Binding Buffer was added to the lysate. Fifty µl of equalized cell lysate samples, Lysis Buffer blank control and RhoA positive control were added separately to the wells coated with Rho-GTP-binding protein. The plate was placed on MicroMix 5 shaker (DPC Biermann GmbH, Bad Nauheim, Germany) at 390rpm, 4°C for 30 minutes. Active, GTP-bound

Rho in the cell lysates were bound to the wells. After incubation, the wells were washed twice with 200µl of Wash Buffer to remove the inactive GDP-bound Rho. Each well was incubated with 200µl of Antigen Presenting Buffer at room temperature for exactly 2 minutes and then washed thrice with 200µl of Wash Buffer. This was followed by sequential incubation of each well with 50µl of diluted anti-Rho primary antibody (1/250) and diluted HRP-conjugated secondary antibody (1/62.5) on MicroMix 5 shaker at room temperature for 45 minutes each. Each incubation was followed by three washes with 200µl of Wash Buffer. Fifty µl of HRP detection reagent was added for color development and stopped after 15 minutes by adding 50µl of HRP stop solution. The intensity of the colour was measured using a microplate reader (Bio-Rad Laboratories, Inc, CA, USA) with wavelength set at 490nm. The amount of active RhoA in the samples was determined from the Rho control protein which is at 1ng with linear OD from 0.05 to 2ng.

2.27. Total Rho assay

Total RhoA in the samples was measured using Total RhoA ELISA Kit™ (Cytoskeleton, Inc, CO, USA) according to the manufacturer's instructions. Briefly, 50µl of equalized cell lysate samples, RhoA standard and Lysis Buffer blank control were added separately to the wells coated with anti-Rho Igγ antibody which has high affinity to all Rho isotypes. The plate was incubated for 2 hours at room temperature, followed by washing with 200µl of Wash Buffer and incubation with 200µl of Antigen Presenting Buffer at room temperature for exactly 2 minutes. This was followed by sequential incubation of each well with 50µl of diluted anti-RhoA primary antibody (1/2000) and diluted HRP-conjugated secondary antibody (1/250) at room temperature for 1 hour each. Each incubation was followed by three washes with 200µl of Wash Buffer. Eighty µl of HRP detection reagent was added for color development and stopped after 20 minutes by adding 80µl of 1.8M sulfuric acid. The intensity of the colour was measured using a microplate reader (Bio-Rad Laboratories, Inc, CA, USA) with wavelength set at 490nm. The amount of RhoA in the samples was determined from the standard curve.

2.28. Rac1 activation assay

Active Rac1 was measured using G-LISA® Rac1 Activation Assay Biochem Kit™ (Cytoskeleton, Inc, CO, USA) according to the manufacturer's instructions and normalized against total protein concentration. Briefly, 50µl of equalized cell lysate samples, Lysis Buffer blank control and Rac1 positive control were added separately to the wells coated with Rac-GTP-binding protein. The plate was placed on MicroMix 5 shaker (DPC Biermann GmbH, Bad Nauheim, Germany) at 390rpm, 4°C for 30 minutes. Active, GTP-bound Rac1 in the cell lysates were bound to the wells. After incubation, the wells were washed twice with 200µl of Wash Buffer to remove the inactive GDP-bound Rac1. Each well was incubated with 200µl of Antigen Presenting Buffer at room temperature for exactly 2 minutes and then washed thrice with 200µl of Wash Buffer. This was followed by sequential incubation of each well with 50µl of diluted anti-Rac1 primary antibody (1/50) and diluted HRP-conjugated secondary antibody (1/100) on MicroMix 5 shaker at room temperature for 45 minutes each. Each incubation was followed by three washes with 200µl of Wash Buffer. Fifty µl of HRP detection reagent was added for color development and after 20 minutes by adding 50µl of HRP stop solution. The intensity of the colour was measured using a microplate reader (Bio-Rad Laboratories, Inc, CA, USA) with wavelength set at 490nm. The amount of active Rac1 in the samples was determined from the Rac1 control protein which is at 2ng with linear OD from 1 to 8ng.

2.29. Statistical analysis

Statistical analysis was performed using SPSS software (version 17.0 for Windows©, SPSS Inc, Ill, USA). Differences between groups were determined using the Mann-Whitney test, where $p < 0.05$ was considered significant. All values were expressed in mean ± SEM (standard error mean).

CHAPTER 3

DELINEATING THE MOLECULAR MECHANISM OF IL-13 INDUCED NEPHROTIC SYNDROME IN RAT MODEL OF MCNS

3.1. Introduction

MCNS is the most common cause of significant morbidity amongst the childhood glomerulonephritides. However, its pathogenesis is still unknown. Studies attempting to elucidate the underlying pathogenesis have suggested a Th2 cytokine bias. Our group has previously demonstrated that *IL-13* gene expression was upregulated in $CD4^+$ and $CD8^+$ T-cells of children with MCNS in relapse [58]. Moreover, *IL-13* overexpression in the rat resulted in podocyte injury with downregulation of the slit diaphragm proteins, namely nephrin and podocin, inducing a minimal change-like nephropathy [215, 216]. In this model, increased glomerular IL-4Rα and IL-13Rα2 gene expression, as well as increased fluorescent signal for IL-4Rα were demonstrated in most of the glomerular podocytes of nephrotic rats, suggesting that IL-13 may act directly on podocytes in the glomeruli.

Current understanding of the pathogenetic mechanism of nephrotic syndrome suggests that the podocyte is the main component of the glomerular filter and the crucial target in the development and progression of glomerulopathies [233-235]. In fact, one of the hallmarks of nephrotic syndrome is the effacement of podocyte FP [236]. Recent studies have suggested a novel role for the costimulatory molecule B7-1 in podocytes as an inducible modifier of glomerular permselectivity and proteinuria [217, 218]. In genetic, drug-induced, autoimmune, and bacterial toxin-induced experimental kidney diseases with nephrotic syndrome, B7-1 expression in podocytes was upregulated. In our *IL-13* overexpression rat model of MCNS, upregulation of B7-1 expression was also demonstrated in the glomeruli, and this correlated strongly with serum IL-13 levels.

We therefore hypothesized that IL-13 and/or other Th2 cytokines could act through IL-13-induced B7-1 danger signaling, thus causing podocyte effacement and proteinuria.

3.2. Aim of Chapter

In this chapter, we aimed to investigate the molecular mechanism by which IL-13 downregulates the expression of podocyte-specific proteins via B7-1-danger signaling, resulting in massive proteinuria. The specific objectives are to:

1. Characterize the molecular events in the glomeruli of the IL-13 rat model of MCNS using cDNA microarray and identifying differentially expressed genes (DEGs) induced by IL-13.
2. Determine the mechanistic link of IL-13 and B7-1 signaling in this rat model of MCNS using pathway analysis tools.
3. To validate the microarray results in the glomerular RNA using real-time PCR.

3.3. Results

3.3.1 Phenotype of rats used for microarray analysis

Serum IL-13 levels in *IL-13*-overexpressed rats were significantly higher than control rats (788±290 *vs.* 3.50±1.96 pg/ml, p=0.002). The *IL-13*-overexpressed rats compared to control rats, showed minimal change-like nephropathy characterized by increased proteinuria (10000±4800 *vs.* 286±44.8 ug/24hr, p=0.002), hypoalbuminemia (25.0±2.51 *vs.* 44.7±2.67 g/L, p=0.002), hypercholesterolemia (7.23±1.23 *vs.* 1.66±0.07mmol/L, p=0.002) (Figure 6). No significant difference was detected in the serum creatinine levels. (Appendix 3.1)

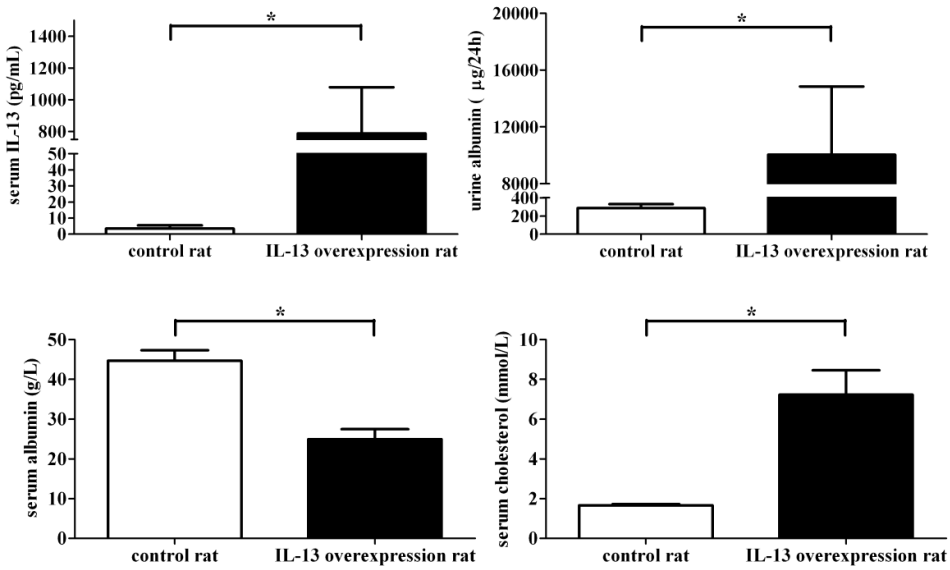

Figure 6: Biochemistry profile of rats used in microarray analysis.
Overexpression of *IL-13* in rats resulted in proteinuria, hypoalbuminemia and hypercholesterolemia. Asterisk indicates statistically significant differences (p<0.05).

3.3.2 Qualitative measurement of glomerular RNA

RNA samples used in this microarray study consisted of RNA Integrity Number (RIN) values of more than six (Figure 7). The RIN was developed by Agilent Technologies to standardize the interpretation of RNA integrity, taking into account the entire electrophoretic trace. It has a numbering system from 1 to 10, with 1 being the most degraded profile and 10 being the most intact profile.

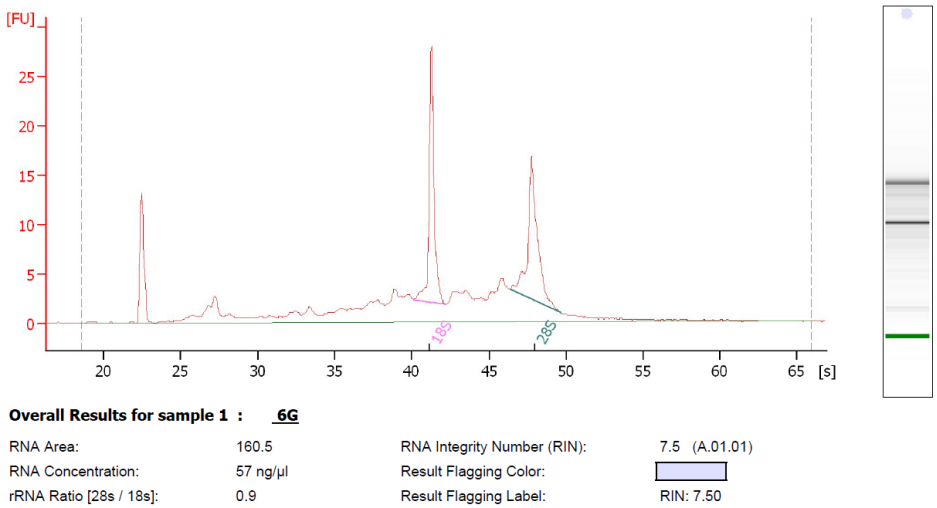

Figure 7: Electropherogram summary of a glomerular RNA sample.
Figure showed one of the electropherograms for the glomerular RNA used in the microarray. Ribosomal RNA ratio (28s/18s) and RIN were stated below the electropherogram.

3.3.3 Glomerular RNA transcriptional profile of *IL-13* overexpression rat model of MCNS

Transcriptional profile of the glomeruli in the *IL-13* overexpression rats showed a distinct regulation pattern. Of the 22,523 genes analyzed in the *IL-13*-transfected rats, 1322 genes showed differential regulation of at least 1.6-fold compared to control rats. These differentially expressed genes (DEGs) were hierarchically clustered into low (green) to high (red) expression level (Figure 8). Of the 1322 DEGs, 847 (64.1%) genes were down-regulated (with a maximum fold change of 6.88) and 475 (35.9%) genes were up-regulated (with a maximum fold change of 15.2).

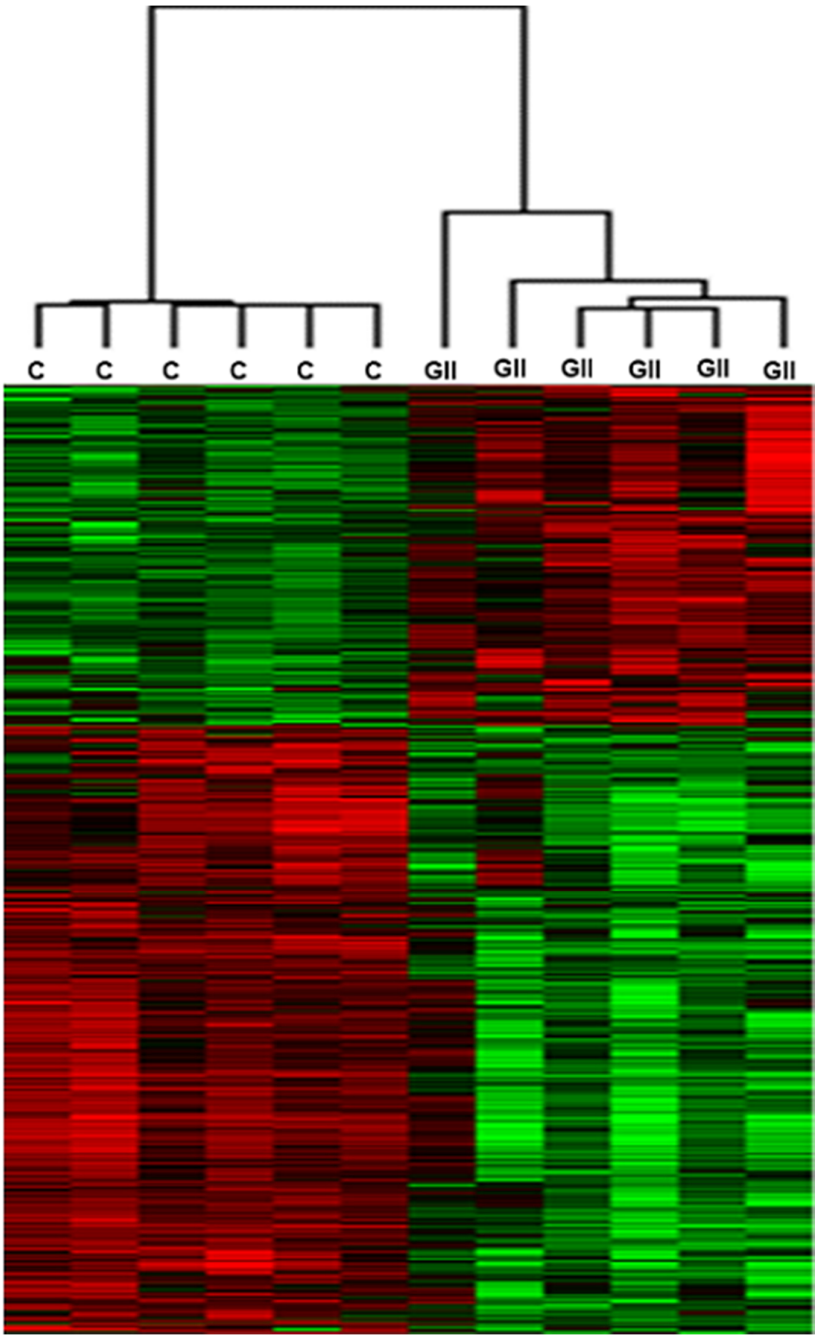

Figure 8: Hierarchy clustering of the 1322 DEGs.
The 1322 genes that were differentially regulated in the glomeruli of the *IL-13*-transfected rats compared to control rats were hierarchically clustered. Expression was indicated by a colour scale from low (green) to high (red). C indicates biological replicate for control rats, and GII indicates biological replicate for IL-13 overexpression rats.

Functional annotation clustering showed that these DEGs were principally related to vascular system development, cell adhesion/migration, cellular components, immune response, actin cytoskeleton, neuron development and protein binding (Table 3). The full list of DEGs is available at Appendix 3.2.

Table 3: DEGs were characterized according to their biological process classification using Gene Ontology analysis.

Functional Annotation Cluster	Enrichment score
Vascular system development	9.95
Cell adhesion	8.00
Cellular component	6.63
Cell migration	6.42
Extracellular matrix	6.31
Immune response	5.23
Contractile fibre component	5.20
Actin cytoskeleton	5.06
Neuron development	4.84
Protein binding (SH3 domain)	4.46

A list of podocyte related genes known to be important for the structure and function of podocytes was compiled from studies related to podocytes [77, 237-239] and 201 (15.2%) DEGs fell into this category (Appendix 3.3). Of the 201 DEGs, 173 (87.1%) genes were down-regulated 1.6-fold in comparison to control rats, with a profile carrying the characteristic signature of podocyte injury. Eleven genes were selected and analyzed using real-time PCR to confirm the microarray results. There was good agreement between the real-time PCR data and the microarray data, with confirmation of the up- or down-regulation of each gene and the fold change was also of a comparable magnitude (Figure 9).

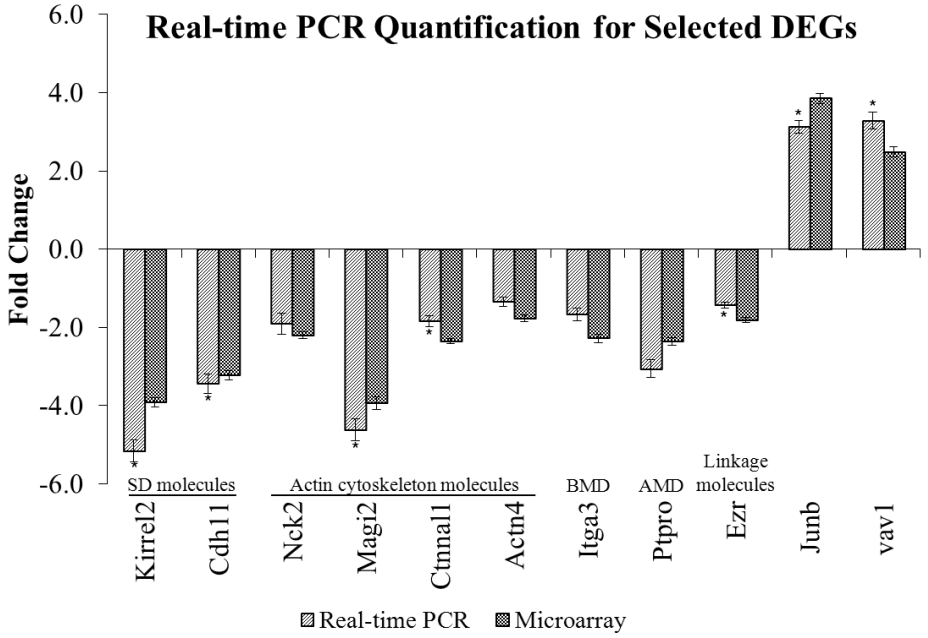

Figure 9: Microarray validation using real-time PCR quantification.
Eleven genes were selected and analyzed using real-time PCR to confirm the microarray results. Downregulated genes were arbitrarily assigned a negative value. For real-time PCR, gene expression levels were normalized using GAPDH and fold change was calculated using formula $2^{\Delta\Delta Ct}$ (where ΔΔCt was converted to an absolute value). Results were presented as fold change ± SEM. Asterisk (*) for real-time PCR data indicates significant difference with $p < 0.05$, between the ΔCt of control and *IL-13* overexpression rats. The pattern of transcript abundance detected for these genes in the array and in real-time PCR showed nearly identical expression profiles. BMD (basal membrane domain), AMD (apical membrane domain).

Decreased gene expression levels of podocyte slit diaphragm molecules namely kin of IRRE like 2 (*Kirrel2* or *NEPH2*) and cadherin 11 (*cdh11*) were seen in the *IL-13*-overexpressed rats, as well as actin cytoskeleton related molecules namely NCK adaptor protein 2 (*Nck2*), membrane associated guanylate kinase, WW and PDZ domain containing 2 (*Magi2*), α-catenin (*Ctnnal1*) and α-actinin-4 (*Actn4*). Additionally, downregulation of podocyte basal and apical membrane domain protein complex molecules, namely α3 integrin (*Itga3*) and protein tyrosine phosphatase, receptor type, O (*Ptpro* or *GLEPP1*) respectively, and linkage molecule Ezrin (*Ezr*), were demonstrated. However, the gene expression of *junb* was shown to be highly upregulated (3.85-fold) in the glomeruli of the *IL-13*-overexpressed rats.

The other highly upregulated gene (2.49-fold) was vav1 guanine nucleotide exchange factor (*vav1*) whose function in the kidney has not been previously

described. *Vav2* and *vav3* gene expression were not differentially regulated in the glomeruli of *IL-13* overexpressed nephrotic rats.

3.3.4 Pathway analysis of the differentially regulated genes in *IL-13* overexpressed rat model

MetaCore™ pathway analysis of the 1322 DEGs showed that the top pathway involved was cytoskeleton remodeling. The genes which were differentially regulated in this pathway were summarized in Table 4, in which *vav1* showed the greatest increase in gene expression (Figure 10).

Table 4: List of DEGs involved in cytoskeleton pathway.

GenBank Accession No.	Gene Symbol	Gene Description	Fold Change
NM_031836.1	Vegfa	vascular endothelial growth factor A	-3.67
XM_216679.4	Lamb1	laminin, beta 1	-2.84
NM_031520.1	Myh10	myosin, heavy chain 10, non-muscle	-2.47
NM_031005.2	Actn1	actinin, alpha 1	-2.30
XM_340884.2	Itga3	integrin alpha 3	-2.23
NM_017198.1	Pak1	p21 (CDKN1A)-activated kinase 1	-2.19
NM_012604.1	Myh3	myosin, heavy chain 3, skeletal muscle, embryonic	-2.18
NM_053356.1	Col1a2	collagen, type I, alpha 2	-2.08
NM_012606.1	Myl3	myosin, light polypeptide 3	-2.06
XM_343607.3	Col4a1	similar to procollagen, type IV, alpha 3	-1.99
XM_230950.4	Itgav	integrin alpha V	-1.97
XM_573030.2	Myh11	myosin, heavy polypeptide 11, smooth muscle	-1.75
NM_031675.2	Actn4	actinin alpha 4	-1.72
NM_013151.2	Plat	plasminogen activator, tissue	-1.66
XM_232064.4	Tcf3	transcription factor 3	-1.66
XM_236367.4	Tln2	similar to talin 2	-1.63
XM_001080622.1	Myh14	myosin, heavy polypeptide 14	-1.63
NM_012759.1	Vav1	vav 1 oncogene	2.40
NM_001012002.1	Zap70	zeta-chain (TCR) associated protein kinase	2.00
XM_232763.4	Lck	lymphocyte protein tyrosine kinase	1.99
NM_021835.3	Jun	Jun oncogene	1.88
XM_219517.3	Map3k11	mitogen-activated protein kinase kinase kinase 11	1.82
NM_053857.1	Eif4ebp1	eukaryotic translation initiation factor 4E binding protein 1	1.68

Each gene is given a representative GenBank accession number, gene symbol, gene description, and fold change (relative to control rats; negative values indicate down regulation). The list of genes was generated from MetaCore™ pathway analysis and arranged by fold change.

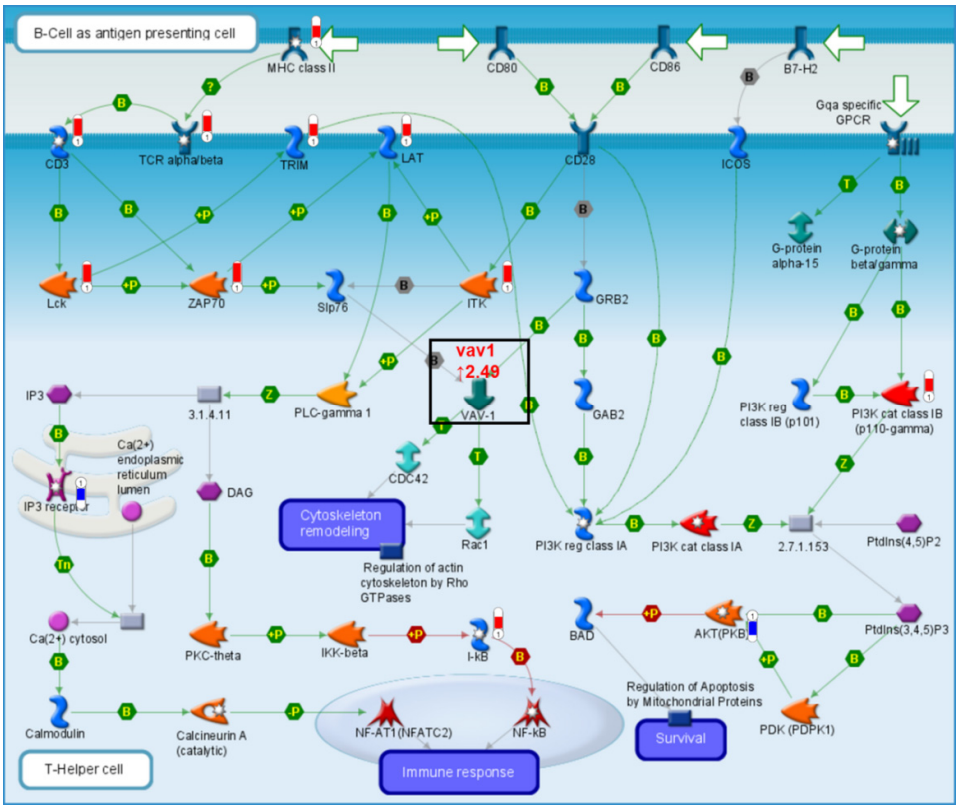

Figure 10: Cytoskeleton remodeling pathway involving vav1.
Figure was exported from MetaCore^{TM} during pathway analysis. Vav1 was boxed and the fold change was indicated in the diagram.

3.3.5. Glomerular gene expression levels of B7-1 interaction partners

Glomerular gene expression levels of three genes of interest known to interact with B7-1, namely *TLR4*, *CTLA4* and *CD28*, were examined. Gene expression levels of these three genes in the microarray analysis did not reach the DEGs selection criteria of fold change greater than 1.6, coefficient of variance less than 0.7 and *t-test* $p<0.05$ (Table 5).

Table 5: Gene expression of *TLR4*, *CTLA4* and *CD28* in the glomeruli of *IL-13* overexpression rats versus control rats.

GenBank Accession No.	Gene Symbol	Gene Description	Fold Change	cv	p-value
NM_019178.1	Tlr4	toll-like receptor 4	1.57	0.51	0.08
NM_031674.1	Ctla4	cytotoxic T-lymphocyte-associated protein 4	1.41	0.31	0.06
NM_013121.1	Cd28	Cd28 molecule	Not detected	N.A	N.A.

Each gene is given a representative GenBank accession number, gene symbol, gene description, fold change (relative to control rats), coefficient of variance (cv) and p-value. N.A., not applicable.

However, on further analysis of the expression levels of these three genes using quantitative real-time PCR, gene expression levels of *TLR4* ($11.5x10^{-4}$±$1.37x10^{-4}$ *vs.* $7.3x10^{-4}$±$0.61x10^{-4}$, p=0.02) and *CTLA4* ($3.04x10^{-4}$±$0.89x10^{-4}$ *vs.* $1.01x10^{-4}$ ± $0.36x10^{-4}$, p=0.04) were significantly upregulated in *IL-13* overexpressed rats as compared to control rats (Figure 11). No significant difference was detected in gene expression of CD28 in the *IL-13* overexpressed rats ($9.7x10^{-3}$±$2.6x10^{-3}$) in comparison to control rats ($6.3x10^{-3}$±$1.5x10^{-3}$) (p=0.38). (Appendix 3.4)

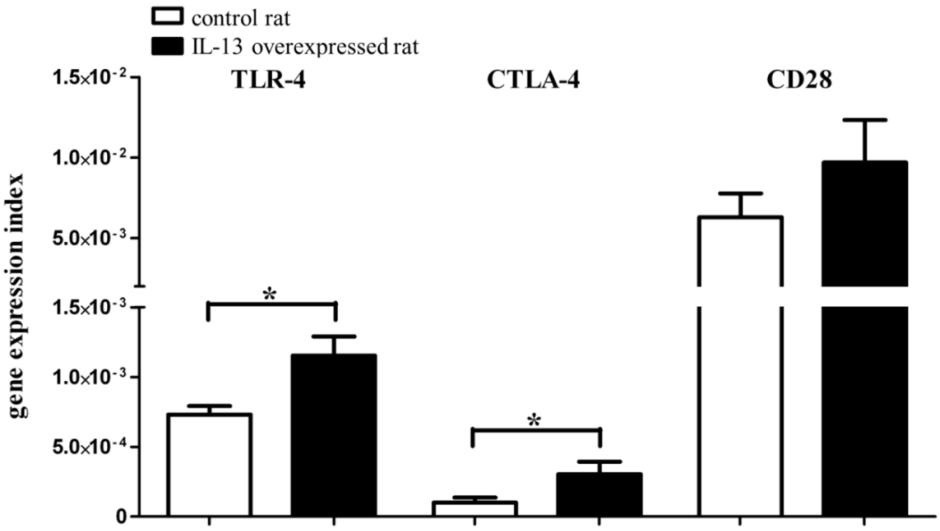

Figure 11: Increased gene expression of *TLR4* and *CTLA4* in IL-13 overexpressed rats. Gene expression index of *TLR4*, *CTLA4* and *CD28* in control and IL-13 overexpressed rats. Asterisk indicates statistically significant differences (p<0.05).

3.4. Discussion

Despite advances in the knowledge of podocyte biology, the etiology of MCNS remains unknown. We have recently reported that overexpression of *IL-13* gene could induce a minimal change-like nephropathy with podocyte FP effacement and proteinuria [215, 216]. This rat model provided a platform to study the molecular signaling pathways that were differentially regulated in the glomeruli, in order to better understand the pathogenesis of this intriguing disease.

MCNS represents a generalized disorder of the immune system resulting in renal manifestations. In this study, genes involved in immune response constituted one of the clusters highly enriched in the functional annotation analysis of the DEGs. IL-1b, IL-12a, IL-16, IL-18, receptors for interleukin (IL-1RII, IL-2Rα and IL-2Rγ), surface receptors (CD1d1, CD3δ, CD8b, CD24, CD36, CD37, CD38, CD52, CD69, CD83, CD97, CD200, CD247, and TLR6) and complement component (C4-2 and Cfb) were differentially regulated in the *IL-13* overexpressed rats, suggesting that IL-13 is a potent regulator of immune response genes in the glomeruli. As IL-13 is an important modulator of monocyte/macrophage function, it is also plausible that the glomerulopathy in our rat model may be a consequence of direct IL-13 stimulation and/or indirect signaling mediated by other immune mediators. Additionally, studies have suggested that the podocye itself may intensify immune glomerular injury through expression of receptors linked to pathways that induce proinflammatory molecules [240, 241]. However, the role of these receptor/surface molecules in podocytes remains to be elucidated.

The hallmark of MCNS is glomerular FP effacement, which is the only morphologic lesion identifiable on electron microscopy. This has been shown to be associated with conspicuous changes in the cytoskeleton of podocytes [77, 242, 243]. Microarray analysis of the glomeruli in our *IL-13* overexpression rat model of MCNS revealed that molecules responsible for the key architecture of podocytes, namely the SD, actin cytoskeleton, basal and apical membrane domain protein complexes and molecules that link to the apical membrane

domain, were dysregulated (Figure 12). Podocytes play a critical role in glomerular filtration, hence dysregulation of molecules important for the maintenance of the tertiary podocyte FP structure can conceivably result in albuminuria and development of frank nephrotic syndrome.

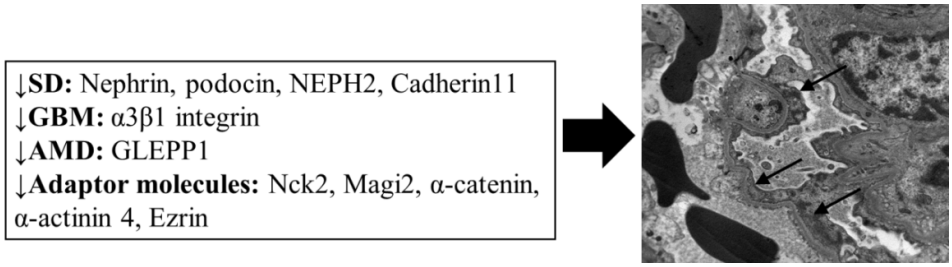

Figure 12: Downregulation of genes related to podocytes was associated with podocyte FP effacement in *IL-13* overexpression rat model of MCNS.
Electron microscopy (reproduced from our previous work [216]) showed podocyte foot process effacement (arrows) in the glomeruli of *IL-13* overexpressed rat.

In addition to the decreased expression of nephrin and podocin previously reported in our rat model of MCNS, gene expression of *NEPH2* was significantly downregulated in the glomeruli of the *IL-13* overexpressed rat. Neph2 protein is structurally related to nephrin which can form heterodimers with nephrin at the SD [114, 115]. Recent studies in Caenorhabditis elegans identified Neph2 as a critical regulator of glomerular function required for glomerular maintenance and development [244]. Knock down of Neph2 resulted in loss of SD and leakiness of the glomerular filtration barrier.

A number of DEGs identified in the glomeruli of our *IL-13* overexpressed rats were reported to be associated with nephrin. GLEPP1, though found at the apical surface of podocytes, was shown to cause reduced glomerular nephrin content in *GLEPP1*-deficient mice [83]. Another molecule, Nck adaptor protein, was shown to bind to the phosphorylated form of nephrin. SH2 domain of Nck interacts with tyrosine phosphorylated nephrin, while the SH3 domains of Nck bind to N-WASP and mediates interactions with downstream effectors of the actin cytoskeleton [102, 136, 245, 246]. Inactivation of Nck proteins in adult mouse podocytes reduced phosphorylation of nephrin, caused proteinuria, glomerulosclerosis, and FP effacement [138]. This was attributed to the role of Nck in facilitating signaling events at the SD by promoting Fyn-dependent

phosphorylation of nephrin, which may be important in the regulation of FP morphology and response to podocyte injury [247].

In a study examining the expression of nephrin, podocin and α-actinin-4, normal renal tissue showed linear and homogenous expression of these proteins along the glomerular capillary walls. In contrast, in renal tissue of patients with nephrotic proteinuria, immunostaining of these proteins showed a fine granular appearance. Moreover, among the 18 patients with nephrotic proteinuria, there was loss of at least one of these proteins in the glomeruli [248].

Decreased expression of ezrin has also been reported in children with nephrotic syndrome and the degree of reduced ezrin expression was correlated to severity of podocyte injury [249]. Ezrin expression has been noted to be lower in children with MCNS as compared to normal renal biopsy samples, and this was decreased even more in those with diffuse mesangial proliferation and those with FSGS respectively.

One of the DEGs that was highly upregulated in the glomeruli of *IL-13* overexpressed rats was *Junb*. *Junb* is a member of the jun family (jun, junb and jund) [250]. Structurally, it contains a JNK docking site, nuclear localization signal, basic domain for DNA binding and a leucine zipper domain for dimerization. *Junb* can form homodimers with one another, or dimerize with members of Fos and ATF families, to form AP-1 transcription factor. Although *Junb* was initially reported not to be phosphorylated by JNK [251], a later study showed that phosphorylation of *JunB* at Thr102 and 104 by JNK resulted in increased IL-4 expression in T-helper cells [252]. Studies have reported that *Junb* regulates human heme oxygenase 1 (*HO-1*) gene expression in renal epithelial cells [253]. *HO-1* mRNA expression within tubular, glomerular and Bowman's epithelial cells have been shown to be more intense with greater degrees of proteinuria [254], indicating its role in oxidative stress.

Interestingly, our microarray data showed that podocyte dysregulation in glomeruli from *IL-13* overexpressed rats with MCNS was also associated with

increased gene expression of *vav1*. The vav family of proteins consists of three isoforms – vav1, vav2 and vav3. Vav1 is a member of the Dbl family of Guanine nucleotide exchange factor (GEF) for the Rho family of GTPases [255-257]. Vav1 expression is generally restricted to the hematopoietic system [258, 259], whereas vav2 and vav3, are more widely expressed [258]. In fact, vav2 has also been described in podocytes [260], although both *vav2* and *vav3* gene expression were not differentially regulated in our *IL-13* overexpressed rats. Studies have shown that the HIV protein Nef interacts with DIP to increase Src-mediated phosphorylation of vav2, which is responsible for the loss of RhoA-mediated stress fiber formation and the increase in Rac1-mediated lamellipodia formation and membrane ruffling observed in HIV associated nephropathy [260]. Although vav1 has been classically associated with T-cell activation, the absence of inflammatory infiltrates in the glomeruli of our *IL-13* overexpression rat model of MCNS excludes T-cell expression as the source of increased *vav1* gene expression in our microarray data.

We have reported increased glomerular expression of B7-1 in our rat model of MCNS. Previous studies have suggested a novel role for the costimulatory molecule B7-1 in podocytes as an inducible modifier of glomerular permselectivity and proteinuria [217, 218]. Wild type and SCID mice exposed to LPS were shown to develop nephrotic-range proteinuria and upregulation of B7-1. These investigators demonstrated that podocytes constitutively expressed TLR-4 (a receptor for LPS in antigen presenting cells), as well as CD14 (a co-receptor of TLR-4) and suggested that podocytes detected LPS through TLR-4, resulting in reorganization of the kidney-filtration apparatus, podocyte FP effacement and proteinuria. In our current study, gene expression of *TLR4* was significantly upregulated in the glomeruli of the nephrotic rats, suggesting a possible role of TLR-4/B7-1 signaling in the pathogenesis of proteinuria. However, the role of this pathway in our rat model of MCNS remains to be elucidated.

Other molecules of interest in our model are CTLA-4 (Cytotoxic T-Lymphocyte Antigen 4), also known as CD152, and CD28. Both are members of the

immunoglobulin superfamily, and are ligands of B7-1 (CD80) as well as CD86. CTLA-4 is constitutively expressed on regulatory T cells [261, 262] as well as on activated T cells [263, 264], whereas CD28 is constitutively expressed on both resting and activated conventional T cells. CTLA-4 interacts with both ligands at a higher affinity and avidity than CD28, with the CTLA-4-CD80 interaction being the strongest [265]. Therefore, CTLA-4 acts as an antagonist of CD28-ligand interactions by competing for ligand binding and hence functions as a potent negative regulator of the T-cell response. On the other hand, CTLA-4 has been shown to be a potent activator of T cell polarization needed for motility [266]. Binding of T cell with anti-CTLA-4 and CD3/CTLA-4 induced rapid T cell polarization with increased formation of lamellipodia, filopodia, and uropods. Polarization required activation of PI3K, Vav1, Cdc42, and myosin L chain kinase. However, key downstream target of PI3K, protein kinase B, as well as Rho kinase and RhoA, were not required. Glomerular expression of CTLA-4 has been previously reported[267]. Injection of mice with polyIC, a TLR-3 ligand, resulted in significant increase in glomerular expression of B7-1 and IL-10 with a mild non-significant increase in CTLA-4, and significant decreased expression of synaptopodin. On the other hand, our study has demonstrated significantly increased glomerular CLTA-4 expression in our *IL-13* overexpression rat model of MCNS, suggesting a potential role for CTLA-4-B7-1 signaling in inducing podocyte injury.

In summary, we have demonstrated that the transcription profile of the glomeruli in our *IL-13* overexpressed rats displayed characteristic podocyte injury phenotype with significant decreased gene expression of podocyte SD molecules, actin cytoskeleton molecules, as well as podocyte basal and apical membrane domain protein complex molecules. In addition, the novel finding of increased gene expression of *vav1* associated with increased B7-1 expression in the glomeruli of *IL-13* overexpressed rats with MCNS suggest a possible downstream role in the regulation of glomerular filtration barrier. Increased *Junb* expression, on the other hand, could reflect its role in oxidative stress induced by glomerular proteinuria in this model of MCNS. Increased glomerular expression of TLR-4 and CTLA-4 in the *IL-13* overexpressed rats

suggests that these molecules could play a role in regulation of B7-1 expression. The next chapter will explore the significance of the glomerular molecular signature in the *IL-13* overexpressed rat model by studying the expression of these genes in IL-13 stimulated podocytes. In addition, we will address the role of vav1 in the kidneys and in particular whether it has a role in the regulation and maintenance of podocyte structure.

CHAPTER 4

NOVEL ROLE OF VAV1 IN PODOCYTES

4.1. Introduction

Our current understanding of the pathogenesis of nephrotic syndrome suggests that the podocyte is the main component of the glomerular filter and the crucial target in the development and progression of glomerulopathies. In MCNS, the major morphologic lesion is FP effacement, and the degree of FP effacement has been shown to roughly correlate with the amount of proteinuria [73, 74].

Several studies involving large scale identification of genes in podocytes have been carried out. Using cDNA libraries and cDNA microarrays constructed from isolated glomeruli of mice, Takemoto *et al*. identified podocyte enriched transcripts in mice [239]. Cultured podocytes were also used in cDNA and oligonucleotide microarrays to examine the changing global gene expression profiles in response to various conditions [268, 269]. Another study used highly purified podocytes isolated from transgenic mice to define podocyte gene expression at different developmental stages [237]. These studies enhanced our understanding of genes expressed in podocyte and hence facilitated molecular characterization of podocytes.

Our findings from the transcription profile of the glomeruli in our *IL-13*-overexpressed rats showed extensive downregulation of podocyte related genes, characteristic signature of podocyte FP effacement, with the decreased expression of key molecules important for the architecture of podocyte – SD, actin cytoskeleton, basal and apical membrane domain protein complexes and molecules that link to the AMD. Although both *Junb* and *vav1* were highly upregulated in the glomeruli of *IL-13* overexpressed rats, MetaCore^{TM} pathway analysis of the DEGs suggested only a possible role of vav1 in cytoskeleton remodeling.

4.2. Aim of chapter

The aim of this chapter is therefore to identify potential pathways important in podocyte injury in the *IL-13* overexpressed rat model of MCNS by studying the expression of the differentially expressed genes (DEGs) identified by the microarray studies as described in the previous chapter, in an *in-vitro* human podocyte culture stimulated by IL-13. In addition, we will address the role of vav1 in the kidneys and in particular whether it has a role in the regulation and maintenance of podocyte structure.

4.3. Results

4.3.1 Podocyte cell culture for microarray validation

Podocyte cell lines were developed by transfection of the human podocytes with temperature sensitive SV40-T gene and telomerase gene (kind gift from Dr. Moin Saleem, University of Bristol, UK). These cells proliferate at a permissive temperature of 33°C and enter growth arrest and differentiate at a non-permissive temperature of 37°C.

Cells were observed daily under a light microscope to check the morphology, distribution and absence of contamination. During proliferation, podocytes were polygonal in shape and displayed characteristic cobblestone morphology (Figure 13).

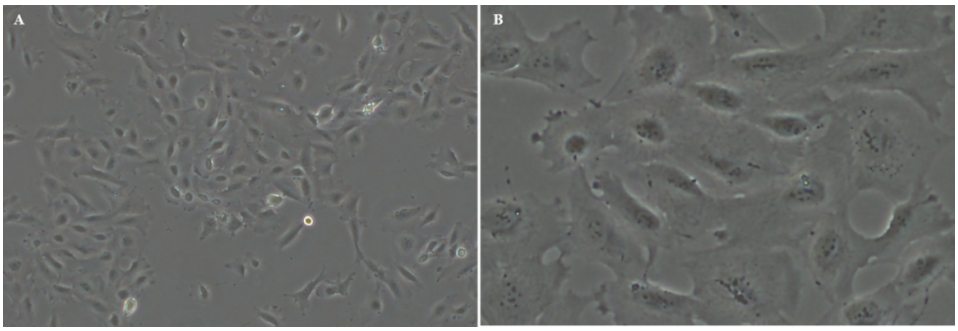

Figure 13: Morphology of podocytes at permissive temperature.
(A) Cells were grown at 33°C for proliferation until reaching 80-90% confluency before thermoshift (magnification, x40). (B) Undifferentiated podocytes were polygonal and display characteristic cobblestone appearance (magnification, x100).

Once the cells proliferated to 80% confluency, they were split 1:10 and cultured at 37°C for differentiation into mature podocytes. Cells were observed to continue replicating for the first 4 to 6 days after thermoshifting, following which the cells started to increase in size (decrease in nuclear-cytoplasmic ratio). The cells gradually changed from the cobblestone morphology into flat, irregular shape and arborized phenotype, with the formation of short and more rounded processes as well as long, spindle-like projections (Figure 14).

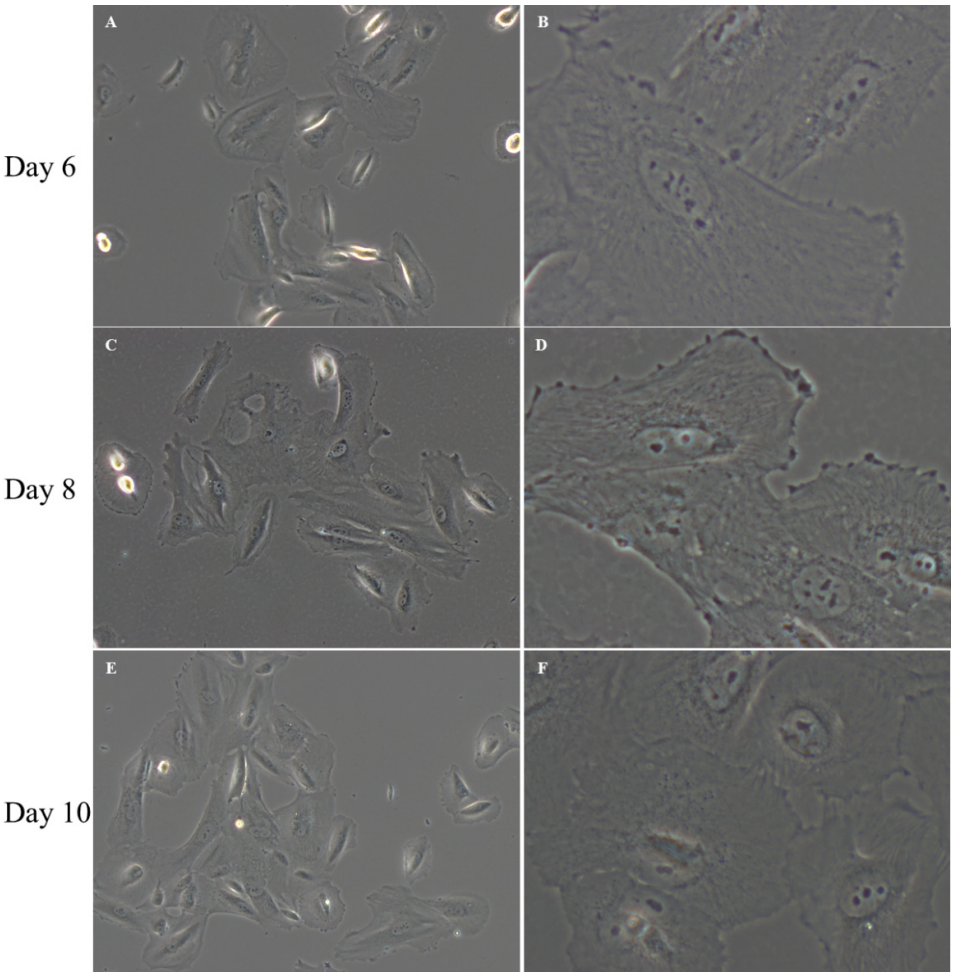

Figure 14: Morphology of podocytes at non-permissive temperature.
The left panel showed cells at x100 magnification; right panel showed cells at x400 magnification. (A-B) At day 6, podocytes were still replicating at a much slower rate than when they were at permissive temperature. (C-D) At day 8, cells ceased proliferation and started to form more short and rounded processes. (E-F) At day 10, majority of cells were fully differentiated. Cells were arborized with well developed cellular processes.

4.3.2 Microarray validation in IL-13 stimulated human podocytes

The 11 genes selected for real-time PCR validation in the rat glomeruli were further analysed in human podocyte cell culture system. To study the direct effect of these genes in IL-13 stimulated human podocytes, fully differentiated podocytes were incubated with IL-13 (20ng/ml) for 24 hours and the gene expression indices were compared to the respective unstimulated podocytes. *Vav1* was the only gene that showed the same expression pattern (1.52-fold increased expression in IL-13 stimulated podocytes, p=0.02) as the microarray profile (Figure 15). *Junb*, on the other hand was downregulated in IL-13 stimulated podocytes, unlike in the glomeruli of nephrotic rats.

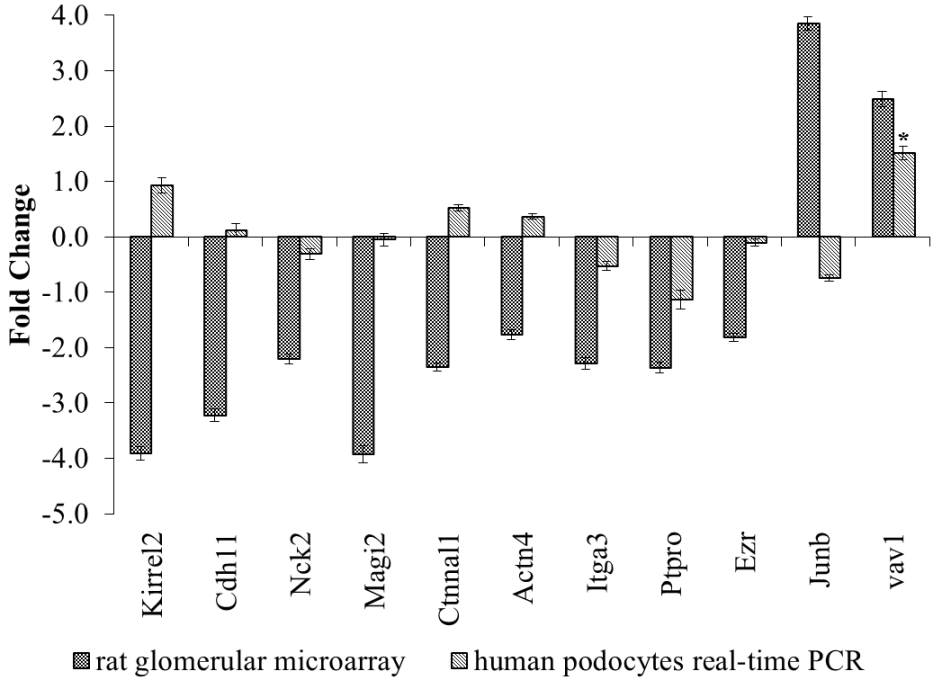

Figure 15: Expression profile for the selected DEGs from glomerular microarray in IL-13 stimulated podocytes.
Eleven DEGs selected from the microarray transcriptional profile of the glomeruli in the *IL-13* overexpression rats were analyzed in human podocyte cell culture using real-time PCR. Downregulated genes were arbitrarily assigned a negative value. For real-time PCR, gene expression levels were normalized using GAPDH and fold change was calculated using the formula $2^{\Delta\Delta Ct}$ (where ΔΔCt was converted to an absolute value). Results were presented as fold change ± SEM. Asterisk (*) for real-time PCR data indicates significant difference ($p<0.05$), between the ΔCt of unstimulated podocytes and IL-13 stimulated podocytes. *Vav1* was the only gene that showed the same expression pattern as the microarray profile.

4.3.3 Expression of vav1 in human podocytes

Gene expression of *vav1* in podocytes was demonstrated using PCR (Figure 16).

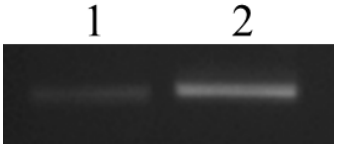

Figure 16: Gene expression of *vav1* in podocytes.
Representative agarose gel image of vav1 in 1) control unstimulated podocytes and 2) IL-13 stimulated podocytes.

Subsequently, protein expression of vav1 in podocytes was validated using Western blot (Figure 17). These results confirmed the presence of vav1 in the podocyte, a non-hematopoietic cell.

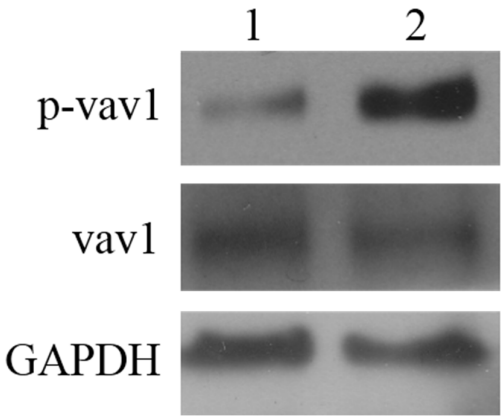

Figure 17: Protein expression of vav1 in podocytes.
Representative gel images of phosphorylated vav1 (p-vav1) and total vav1 in 1) control unstimulated podocytes and 2) IL-13 stimulated podocytes. Blots were first incubated with antibody against phosphorylated vav1 and then re-probed with antibody against total vav1. GAPDH was used as loading control.

The presence of vav1 in podocytes was further validated using immunofluorescence staining of vav1 in podocyte cell culture using antibodies from two different sources (SAB4503066 and Ab62622) (Figure 18).

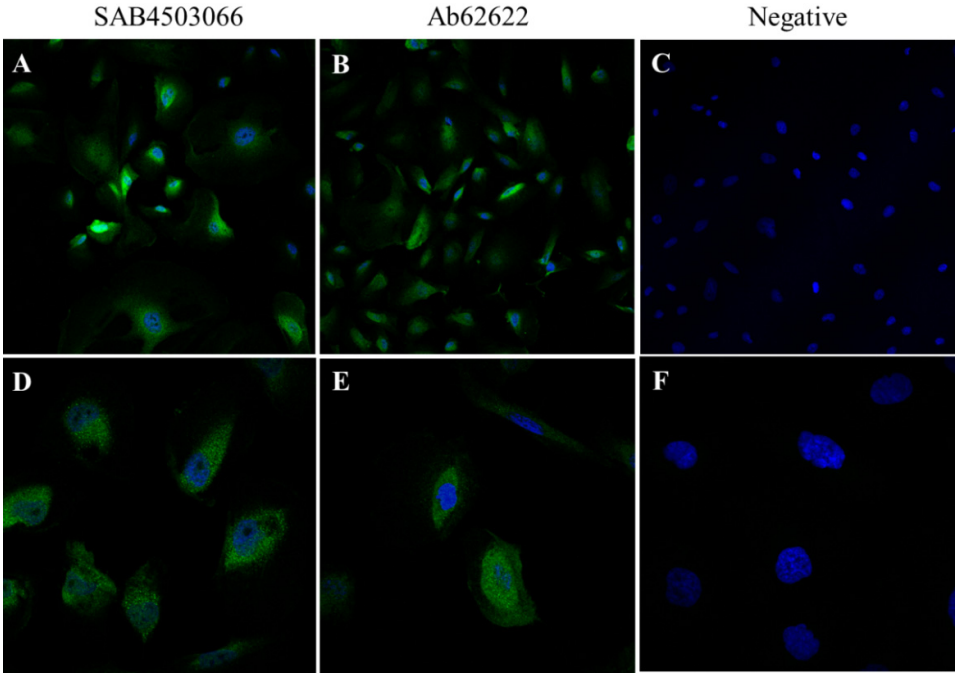

Figure 18: Podocytes expression of vav1.
Immunofluorescence staining of vav1 on podocytes using antibodies from (A, D) Sigma-Aldrich SAB4503066; and (B, E) Abcam Ab62622. (C, F) showed negative control for the immunofluorescence staining, without the primary antibody incubation. Images were taken at (A-C) x20 and (D-F) x60 magnification.

4.3.4 IL-13 induced B7-1 and vav1 expression in human podocytes

Following IL-13 stimulation, podocyte gene expression of *IL-13Rα2* ($1.45x10^{-3}$±$0.35x10^{-3}$ *vs.* $0.64x10^{-3}$±$0.10x10^{-3}$, p=0.001) and *IL-4Rα* ($1.51x10^{-2}$±$0.11x10^{-2}$ *vs.* $1.15x10^{-2}$±$0.14x10^{-2}$, p=0.02) were upregulated compared to controls. This was associated with significant higher gene expression of *B7-1* ($1.74x10^{-4}$±$0.25x10^{-4}$ *vs.* $1.00x10^{-4}$±$0.19x10^{-4}$, p=0.001) and *vav1* ($2.21x10^{-5}$±$0.26x10^{-5}$ *vs.* $1.32x10^{-5}$± $0.24\ x10^{-5}$, p=0.002) in IL-13 stimulated podocytes as compared to controls (Figure 19). No significant difference was detected in the gene expression of *TLR4*, *CTLA4*, *CD28*, *IL-13Rα1*, *nephrin*, *podocin* and *dystroglycan*. (Appendix 4.1)

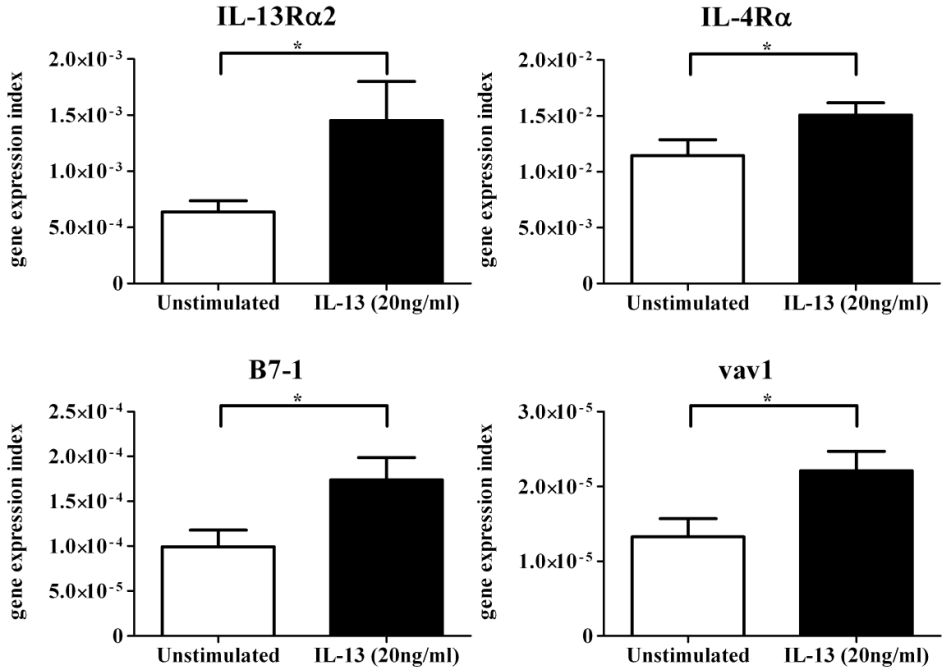

Figure 19: Increased gene expression of *IL-13Rα2*, *IL-4Rα*, *B7-1* and *vav1* in IL-13 stimulated podocytes.
Gene expression for IL-13Rα2, IL-4Rα, B7-1 and vav1 in control and IL-13 stimulated podocytes. Expression levels for the four genes were significantly higher in IL-13 stimulated podocytes compared to unstimulated podocytes. Asterisk indicates statistically significant differences (p<0.05).

Western blot analysis demonstrated increased protein expression of IL-13Rα2 (0.91±0.10 *vs.* 0.58±0.06, p=0.01) and B7-1 (0.97±0.12 *vs.* 0.63±0.11, p=0.04) in IL-13 stimulated podocytes compared to controls. No significant difference was detected for protein expression of vav1 in IL-13 stimulated podocytes (0.95±0.13) compared to controls (1.05±0.19) (p=0.82). However, activated phosphorylated form of vav1 was significantly increased in IL-13 stimulated

podocytes (3.45±0.63) compared to controls (1.97±0.47) (p=0.05) (Figure 20 and Figure 21). (Appendix 4.2)

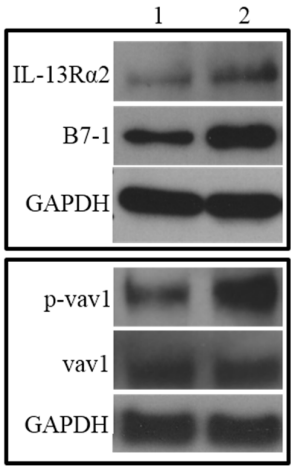

Figure 20: Protein expression of IL-13Rα2, B7-1, phosphorylated vav1, total vav1 in podocytes.
Representative gel images of IL-13Rα2, B7-1, phosphorylated vav1 and total vav1 in 1) control unstimulated podocytes and 2) IL-13 stimulated podocytes. GAPDH was used as loading control.

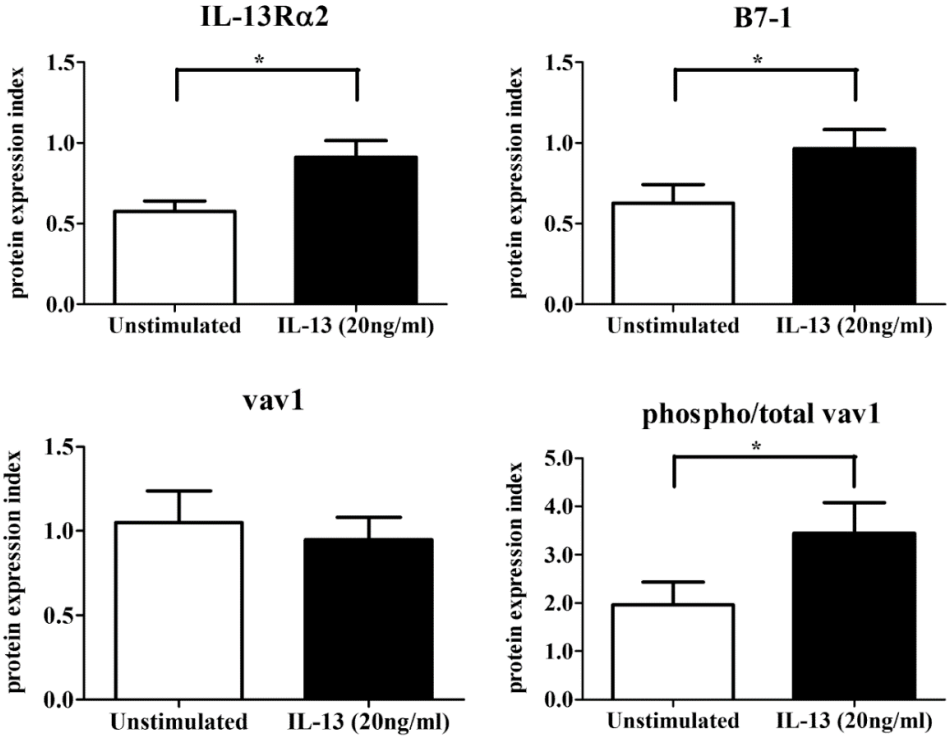

Figure 21: Densitometric analysis of IL-13Rα2, B7-1, phosphorylated vav1 and total vav1 in podocytes.
Protein expression was determined using Western blot analysis. The intensity of each band was quantitated and expressed as an index of the housekeeping gene GAPDH. Values represent the mean of ten independent experiments. Protein expression for IL-13Rα2 and B7-1 were significantly higher in IL-13 stimulated podocytes. In addition, IL-13 stimulation resulted in increased phosphorylation of vav1 in podocytes. Asterisk indicates statistically significant differences ($p<0.05$).

4.3.5 Identification and validation of vav1 gene and protein expression in the rat glomeruli

Microarray analysis of the glomeruli of *IL-13* overexpression nephrotic rats has identified the potential biological relevance of vav1, a molecule which has not been described in kidneys previously. In addition, our studies on human podocytes confirmed the presence of vav1 expression. To confirm glomerular expression of vav1, immunohistochemistry (IHC) staining of vav1 was performed on formalin-fixed, paraffin-embedded rat kidney tissue using antibodies from two different sources (BS1370 and SAB4503066). Glomeruli and tubular epithelial cells showed positive staining of vav1 (Figure 22). No different in vav1 signal intensity could be detected in the glomeruli of control and *IL-13* overexpressed rats using IHC staining (Figure 23).

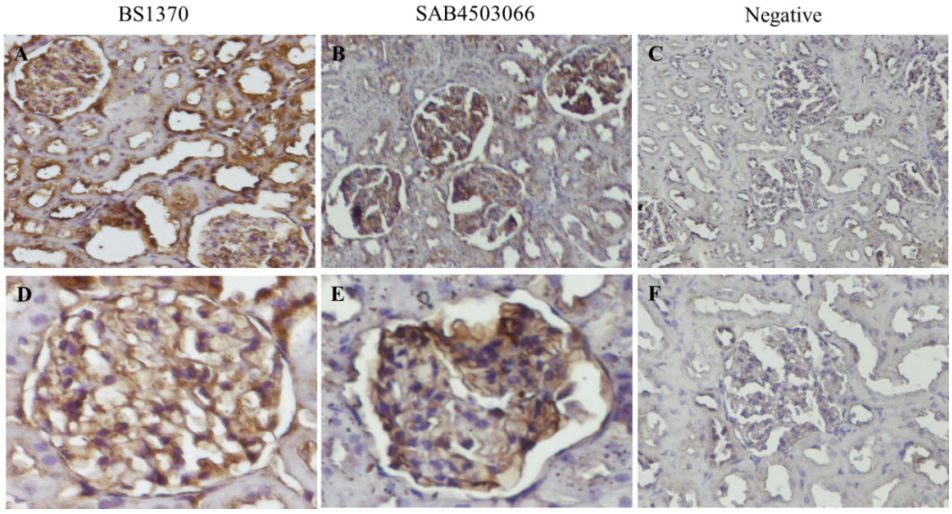

Figure 22: Glomerular expression of vav1.
Glomerular histology of vav1 expression in the glomeruli of *IL-13* overexpressed rat using antibody from (A, D) Bioworld, BS370; and (B, E) Sigma-Aldrich SAB4503066. Brown-colour developed at the glomeruli and tubular epithelium cells after incubation with DAB Substrate-Chromogen. (C, F) showed negative control for the immunohistochemical staining, without the primary antibody incubation. Images were taken at (A-C) x200 and (D-F) x400 magnification.

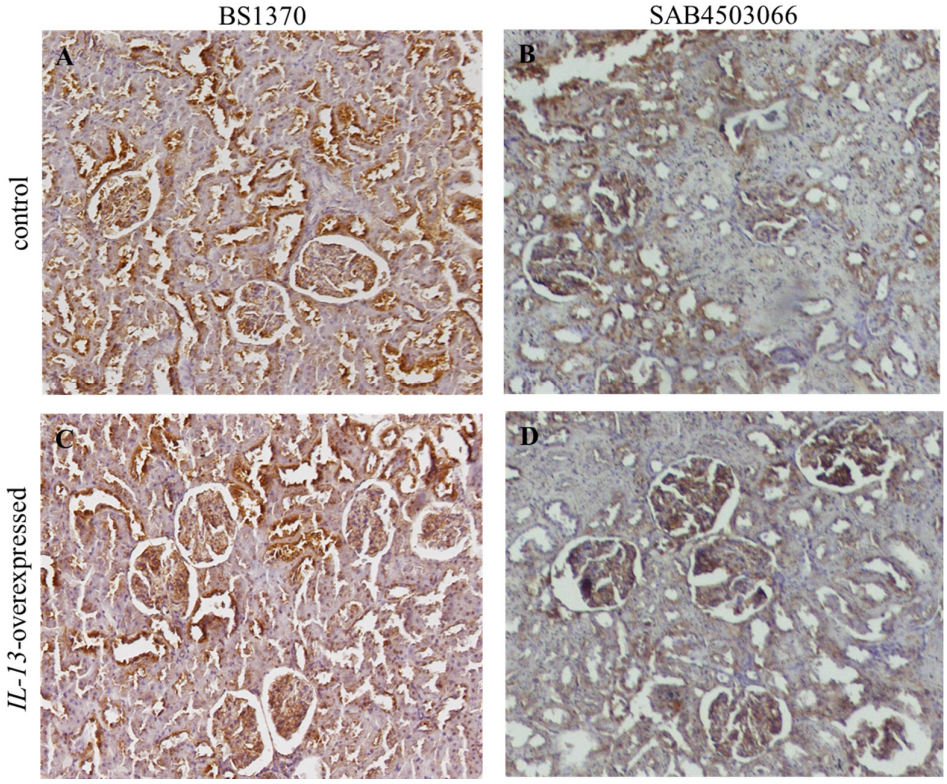

Figure 23: Glomerular expression of vav1 in control and *IL-13* overexpressed rats. Histology of vav1 expression in the glomeruli of (A, B) control or (C, D) *IL-13*-overexpressed rats using antibody from (A, C) Bioworld, BS370; and (B, D) Sigma-Aldrich SAB4503066. Brown-colour developed at the glomeruli and tubular epithelium cells after incubation with DAB Substrate-Chromogen. Images were taken at x200 magnification.

Rat kidney was sequentially sectioned, and the sections in series were stained with synaptopodin or vav1. Matching regions were identified to compare the staining pattern of synaptopodin (podocyte marker) and vav1. Regions staining positive for both synaptopodin and vav1 were indicated in Figure 24.

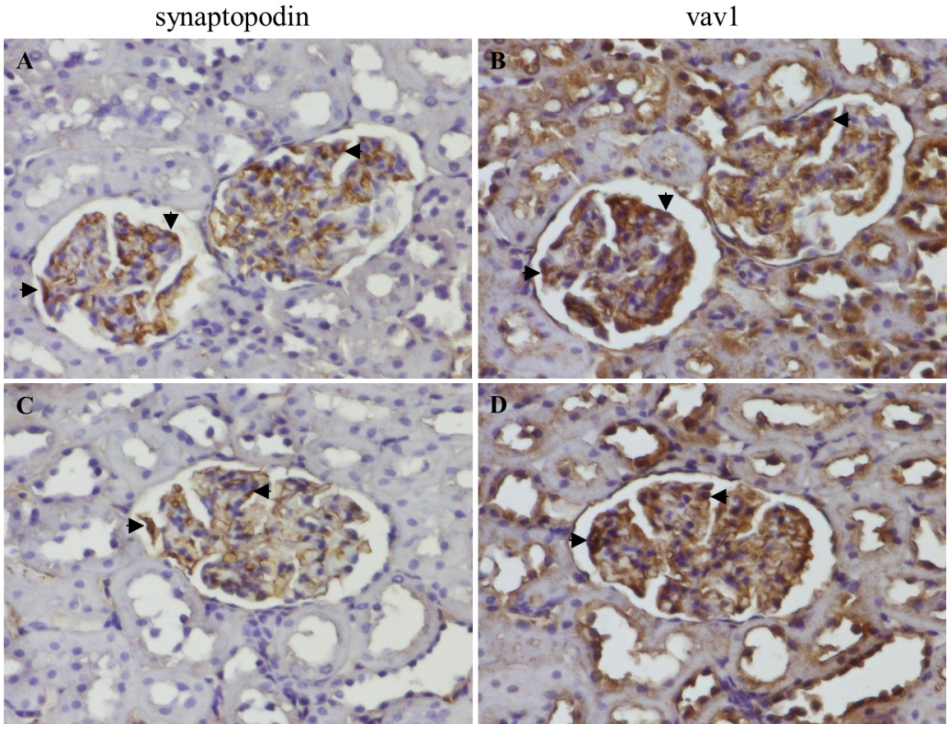

Figure 24: IHC analysis of synaptopodin and vav1 in paraffin-embedded renal cortex. Renal cortex sections in series from *IL-13* overexpressed rat were stained with synaptopodin (left column) or vav1 (right column). Matching regions were identified to compare the staining pattern of synaptopodin and vav1. Arrows indicated regions of the glomeruli staining positive for both synatopodin and vav1 (magnification, x600).

4.4. Discussion

Validation of the glomerular microarray studies in IL-13 stimulated human podocytes revealed that *vav1* was the only gene showing the same expression pattern (1.52-fold increase compared to unstimulated podocytes) as the microarray profile. *Junb*, on the other hand, was downregulated, though not statistically significant, in IL-13 stimulated podocytes, whereas it was upregulated in the glomeruli of nephrotic rats. Similarly, none of the other nine downregulated podocyte-specific DEGs in the glomerular microarray profile were significantly downregulated in IL-13 stimulated podocytes.

Junb was highly upregulated in the glomeruli of the *IL-13* overexpressed nephrotic rat. *JunB* is a transcription factor shown to be involved in the regulation of HO-1 gene expression in renal epithelial cells [253]. The HO-1 gene is upregulated in oxidative stress, and its expression in glomerular and Bowman's epithelial cells has been shown to be more intense with greater degrees of proteinuria [254]. HO-1 plays an important role in maintaining renal function by protecting renal epithelial cells from glomerular proteinuria which can become a cause of oxidative stress. It is interesting that our microarray data confirmed its marked upregulation in the glomeruli of *IL-13* overexpressed nephrotic rat. In contrast, IL-13 stimulated cultured podocytes showed a trend for downregulation of *Junb* gene expression compared to unstimulated podocytes. This suggests that IL-13 stimulation per se was not the triggering factor for increased *Junb* expression in the rat model.

We were able to demonstrate vav1 expression in both IL-13 stimulated and unstimulated podocytes, indicating the presence of this molecule in podocytes. In addition, phosphorylated vav1 was increased in IL-13 stimulated podocytes, suggesting that vav1 could have a functional role in podocytes. In T-cells, binding of CD28 to B7-1 results in phosphorylation of vav1 by tyrosine kinases, with subsequent activation of Rac1 and actin cytoskeleton remodeling [270, 271]. Vav1 activates Rac1 and Cdc24, which in turn activates JNK via MEKK1 and MKK4/7. Activated JNK phosphorylates transcription factors such as Jun, thereby activating AP1 complex, involved in regulation of cell proliferation.

Therefore, we postulate that vav1 could play a role in actin cytoskeleton remodeling or transcription regulation of genes in podocytes.

The ratio of phosphorylated vav1 to total vavl was 1.97±0.47 in unstimulated podocytes, which increased by approximately two-fold to 3.45±0.63 following IL-13 stimulation. Several studies had demonstrated presence of phosphorylated vav1 under basal states. In an early study of guanine nucleotide exchange activity of vav in T cells, Gulbins *et al.* demonstrated constitutive tyrosine phosphorylation of vav1 in resting Jurkat cells at the basal level (Figure 25A) and the phosphorylation level increased following stimulation with monoclonal antibody (mAbs) to CD3 [272]. Basal level of phosphorylated vav1 was also present in BALB/c splenic T cells (Figure 25B) and the phosphorylation level increased substantially following stimulation by anti-TCR, anti-TCR plus anti-CD4, anti-CD28, and anti-TCR plus anti-CD28 mAbs [270]. NIH 3T3 cell expressing wild-type vav showed presence of phosphorylated vav1 in unstimulated condition (Figure 25C) which was phosphorylated following epidermal growth factor stimulation [273]. Similar results were obtained using vav proteins obtained from transient transfections in COS-1 cells. $CD4^+$ T cells transduced with wild type vav1 was shown to express 20% to 30% phosphorylation of vav1 under basal state (Figure 25D) and stimulation with anti-CD3ε and anti-CD28 antibodies resulted four-fold increased of phosphorylated vav1 at 1 minute and two-fold increased of phosphorylated vav1 at 3 minutes [274].

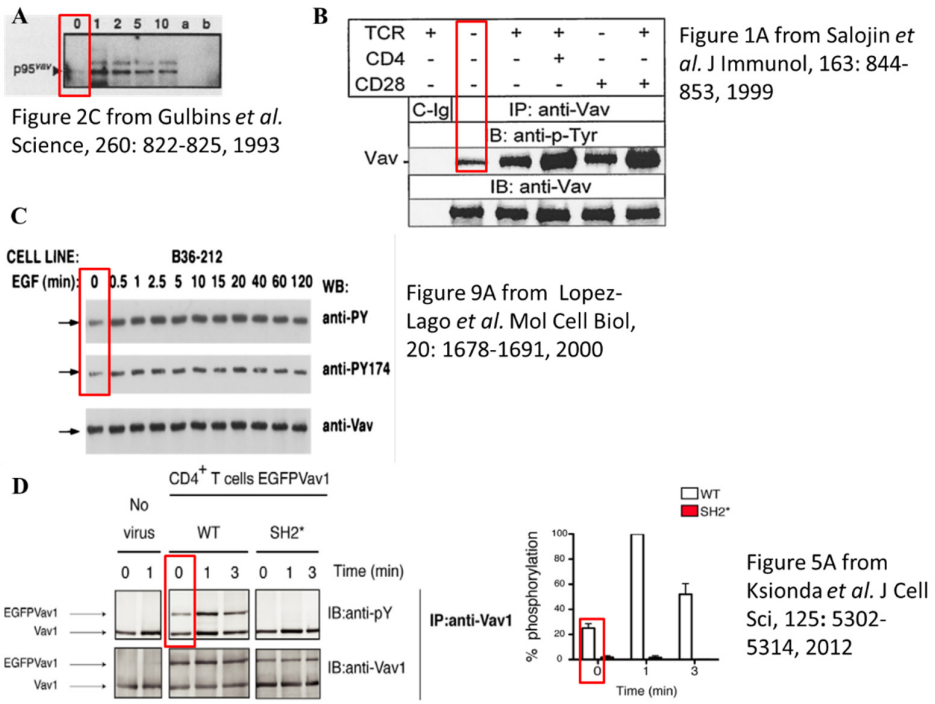

Figure 25: Basal level of Phosphorylated vav1.
Figure showed results from different studies. Basal levels of phosphorylated vav1 in these studies were highlighted with red box.

We have previously reported that *IL-13* overexpression in rats resulted in podocyte injury with upregulation of glomerular B7-1. In our *in vivo* rat model, we have shown increased glomerular IL-4Rα and IL-13Rα2 gene expression, as well as increased fluorescent signal for IL-4Rα in most of the glomerular podocytes of nephrotic rats, suggesting that IL-13 may act directly on podocytes in the glomeruli [215, 216]. Consistent with these findings, our *in-vitro* studies have demonstrated increased gene and protein expression of B7-1 on cultured human podocytes stimulated with IL-13. This further strengthens the hypothesis that transient upregulation of B7-1 could occur in MCNS, resulting in nephrotic-range proteinuria, and also provide an explanation for the possible link between Th2 cytokine bias and MCNS.

We have demonstrated that gene expression of *TLR4* and *CTLA4* in the IL-13 stimulated podocytes was not significantly different compared to unstimulated podocytes, indicating that upregulation of B7-1 expression in IL-13 stimulated podocytes was independent of these two known modulators of B7-1 expression. In contrast, increased glomerular expression of these two molecules was seen

in the *IL-13* overexpression rat model suggesting that the increased glomerular B7-1 could also occur via a second signal such as TLR-4. This gives credence to the hypothesis that B7-1 upregulation following IL-13 stimulation in this rat model could be sustained by a 'second-hit' occurring via another signaling receptor, such as TLR-4. Conceivably, IL-13 stimulation of other immune cells such as monocytes could produce mediators that can activate TLR-4 resulting in an additional signal for B7-1 upregulation. As CTLA-4 is a known negative regulator of B7-1, the increased glomerular gene expression of CTLA-4 in the *IL-13* overexpression rat model could be explained by positive feedback following increased B7-1 expression.

Reiser *et al.* have suggested a novel role for the costimulatory molecule B7-1 in podocytes as an inducible modifier of glomerular permselectivity and proteinuria [217, 218]. They showed that induction of B7-1 on the podocytes resulted in an alteration in shape with actin rearrangement that altered glomerular permeability and caused proteinuria. In patients with MCNS, urinary CD80 (B7-1) excretion has been reported, a finding not observed in other glomerular diseases [219, 220]. Renal biopsy also showed increased CD80 expression in glomeruli of MCNS patients in relapse, and this co-localized with podocin expression in the glomeruli. However, the mechanistic link between B7-1 and actin cytoskeleton remodeling remains to be elucidated.

Using two different sources of primary antibody which detects endogenous levels of total vav1 protein, we were able to demonstrate vav1 staining of glomerular and tubular epithelial cells in rat kidney. We further showed that vav1 co-localized with synaptopodin in serial sections of the kidney, confirming its location in podocytes. However, protein expression of vav1 was not restricted to podocytes as tubular cells also stained positive for vav1. Consistent with this finding in the *IL-13* overexpression rat model of MCNS, we were able to demonstrate significant increase in phosphorylated vav1 expression following IL-13 stimulation of cultured human podocytes, which was associated with upregulation of B7-1. Therefore it is conceivable that the effect of B7-1 on actin cytoskeleton rearrangement could be mediated via vav1 and its

downstream activation pathway mediated by Rac1 as has been described in activated T-cells [275].

In summary, we have confirmed the expression of vav1 in glomeruli and phosphorylated vav1 in IL-13 stimulated podocytes. The role of vav1 in regulation of actin cytoskeleton remodeling in podocytes will be further explored in the subsequent chapter.

CHAPTER 5

MECHANISM OF IL-13 INDUCED PODOCYTE INJURY

5.1. Introduction

In the previous chapter, we have demonstrated the presence of vav1 in rat glomeruli which co-localized with synaptopodin to the podocytes. We have also shown that podocyte injury in our rat model of MCNS was associated with increased gene expression of *vav1*. Vav1 is a member of the Dbl family of Guanine nucleotide exchange factor (GEF) for the Rho family of GTPases [255-257]. Rearrangement of the actin cytoskeleton is highly regulated by the activity of Rho family GTPases. Rho GTPases switch between a GTP-bound ‘‘active’’ state and a GDP-bound ‘‘inactive’’ state. GEFs facilitate the exchange of GDP for GTP, thus activating RhoGTPases.

The structure of vav proteins contains several domains which regulate the GEF activity (Figure 26). From the amino- to the carboxyl-terminal, it is lined with a calponin homology (CH) domain, an acidic (Ac) domain, Dbl homology (DH) domain, a pleckstrin homology (PH) domain, a C1 domain, ending with two SH3 domains and one SH2 domain [276]. The CH domain inhibits GEF activity by binding the cysteine-rich C1 domain; the Ac domain contains several sites of tyrosine phosphorylation; the DH domain has catalytic GEF activity for Rho-family GTPases; the PH domain regulates GEF activity following binding of the phospholipids PIP2 and PIP3; the C1 domain contributes to GEF activity by binding to the GTPases; and the SH3 and SH2 domains are the binding sites for several proteins, e.g. Grb2, SLP-76, ZAP70, Syk, Nef, Zyxin, Ku-70, hnRNP-K, hnRNP-C, Dynamin2 and VIK-1 [277-280].

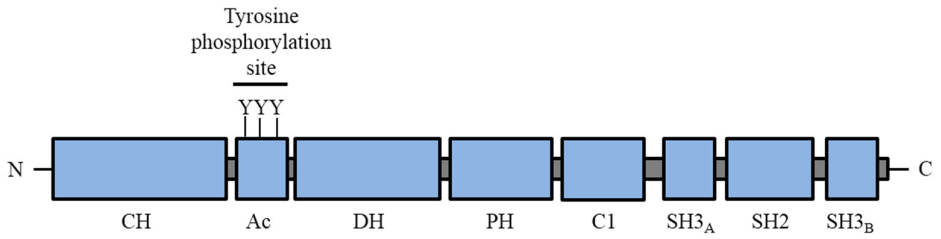

Figure 26: Domain structure of vav1.
The domain structure of vav1 showing from the amino (N)- to the carboxyl (C)-terminal: a calponin homology (CH) domain, an acidic (Ac) domain, Dbl homology (DH) domain, a pleckstrin homology (PH) domain, a C1 domain, ending with two SH3 domains and one SH2

domain. Ac domain contains several sites of tyrosine phosphorylation. Adopted and modified from reference [276].

In mammals, there are three members in the vav family of proteins – vav1, vav2 and vav3. Vav1 expression is generally restricted to the hematopoietic system [258, 259], whereas vav2 and vav3, are more widely expressed [258]. Each vav protein is thought to activate specific GTPases. Vav1 is a GEF for Rac1, Rac2 and RhoG; vav2 is a GEF for RhoA, RhoB and RhoG; whereas vav3 preferentially activates RhoA, RhoG and, to a lesser extent, Rac1 [281-283]. However, vav1 has also been shown to activate RhoA and Cdc42 [284]. Moreover, vav1 was able to stimulate Rac1 and RhoA in αvβ3 integrin-mediated adhesion of hematopoietic cells [285].

Activation of its GEF activity is mediated via tyrosine phosphorylation of vav1 [282, 284]. Many pathways are implicated in the vav-mediated reorganization of the cytoskeleton in T cells as summarized in Figure 27 [275]. In T-cells, binding of CD28 to B7-1 results in tyrosine phosphorylation of vav1 by kinases, and the subsequent activation of Rac1 and actin cytoskeleton remodeling [270, 271].

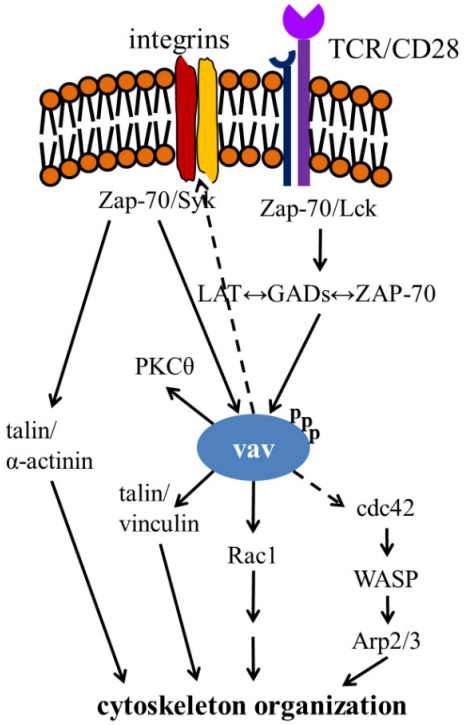

Figure 27: Vav-mediated regulation of cytoskeleton organization.
Adopted and modified from reference [275]

Our finding of B7-1 upregulation following IL-13 stimulation of podocytes, which was associated with increased phosphorylation of vav1 has led to the hypothesis that IL-13 induced podocyte injury with actin cytoskeleton rearrangement could be mediated via B7-1 induced activation of vav1. This would be analogous to the induction of podocyte FP effacement in the IL-13 overexpressed rat model of MCNS via B7-1 upregulation.

5.2. Aim of chapter

The aim of this chapter is therefore to investigate the biological relevance of vav1 and Rho/Rac1 signaling pathway in inducing podocyte injury using an *in-vitro* human podocyte culture system. The specific objectives are as follows:

1. To study the direct effect of IL-13 on podocyte morphology, in particular, cytoskeletal changes associated with FP effacement, using phalloidin staining and viewing with confocal microscopy.
2. To study the role of Rho/Rac1 in IL-13 induced podocyte actin cytoskeleton rearrangement.
3. To validate the role of *vav1* in the *B7-1-vav1* pathway in actin cytoskeleton rearrangement by using podocytes transfected with siRNA specific for *vav1*.

5.3. Results

5.3.1 Effect of IL-13 on podocyte actin cytoskeleton

As shown in Figure 28, the actin cytoskeleton in the unstimulated podocytes was evenly distributed with strong transcellular stress fibers. IL-13 stimulation resulted in actin cytoskeleton rearrangement with weak F-actin signal in the cell center and accumulation of F-actin at the cell peripheral, forming a cortical ring-like structure, suggesting that IL-13 could act directly on podocytes, causing podocyte injury. The cortical F-actin score index, a measure of the degree of cytoskelal rearrangement, was significantly increased in IL-13 stimulated podocytes (2.31±0.14) as compared to unstimulated podocytes (1.59±0.15) (p=0.02) (Figure 29). (Appendix 5.1)

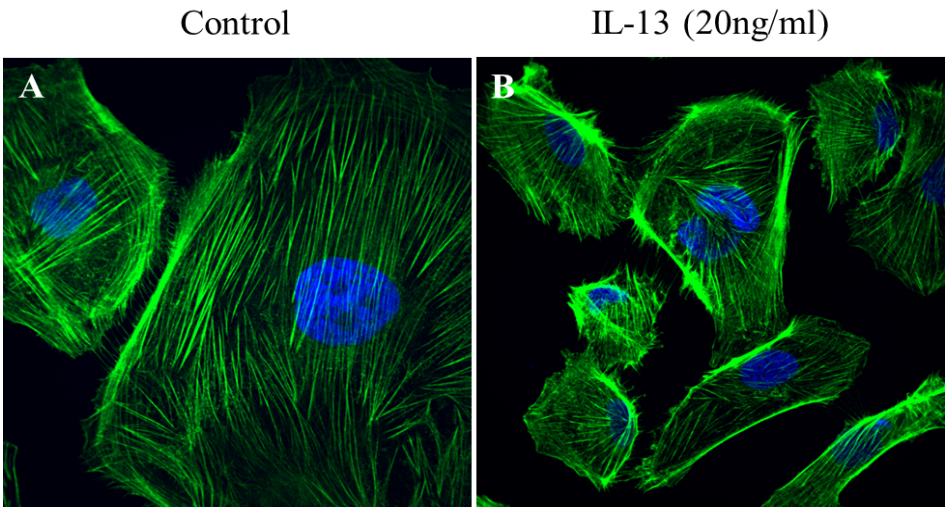

Figure 28: IL-13 induced actin cytoskeleton rearrangement in podocytes.
Human podocytes were stimulated with IL-13 for one hour and stained with phalloidin for F-actin (magnification, x60). A) Unstimulated podocytes showed features of larger size and strong transcellular stress fibers; B) IL-13 stimulation in podocytes resulted in smaller size and weak F-actin signal in the cell center and accumulation of F-actin at the cell peripheral.

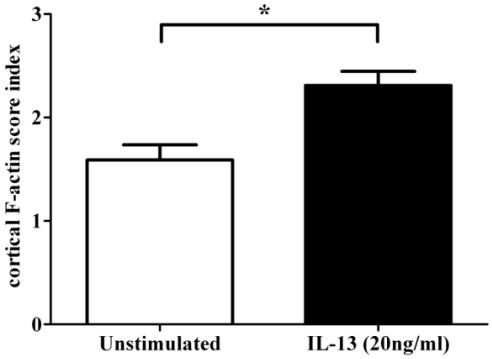

Figure 29: Increased cortical F-actin score index in IL-13 stimulated podocytes.
Cortical F-actin score was determined from at least three independent experiments and the cortical F-actin score index was calculated from the ratio of the score of the counted cells to the total number of cells counted. Asterisk indicates statistically significant differences ($p<0.05$).

5.3.2 Effect of IL-13 on RhoA and Rac1 activity

The activity levels of RhoA and Rac1 in IL-13 stimulated podocytes were measured using ELISA. Fold change of activated RhoA and Rac1 was expressed as ratio of activated RhoA or Rac1 in IL-13 stimulated podocytes versus unstimulated podocytes. RhoA activity in IL-13 stimulated podocytes remained largely unchanged at 5, 10, 20 and 30 minutes. In contrast, Rac1 activity in IL-13 stimulated podocytes increased 1.37-fold at 5 minutes to 1.59-fold at 20 minutes and returned to basal level at 30 minutes (Figure 30). Following 20 minutes stimulation of podocytes with IL-13, the Rac1 activity level (1.58±0.18) was significantly increased as compared to unstimulated podocytes (0.99±0.10) (p=0.01) (Figure 31). (Appendix 5.2)

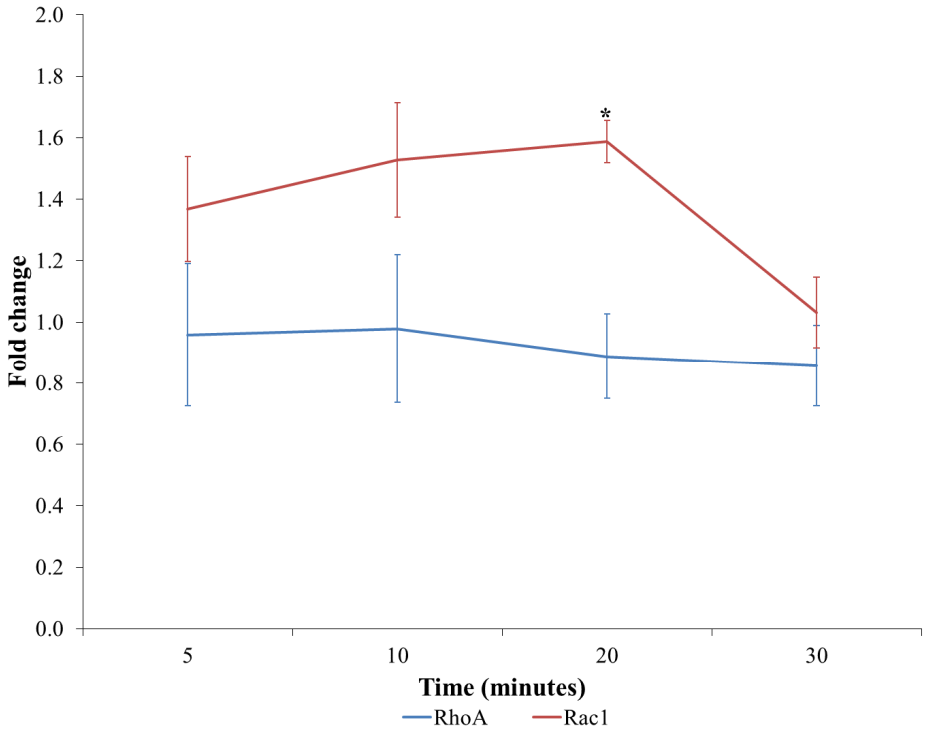

Figure 30: Time course of RhoA and Rac1 activity following IL-13 stimulation of human podocytes.
Podocytes were stimulated with IL-13 (20ng/ml) and RhoA and Rac1 activity were measured at 5, 10, 20 and 30 minutes. The activity levels of RhoA and Rac1 were expressed as mean fold change (ratio of IL-13 stimulated:unstimulated podocytes). Asterisk indicates statistically significant differences ($p<0.05$).

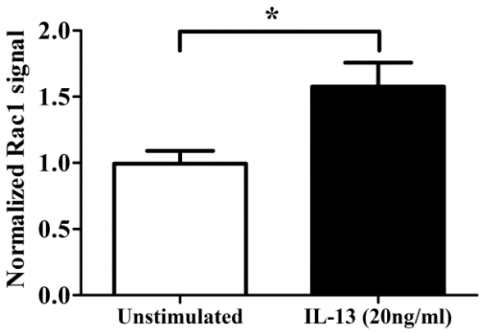

Figure 31: Increased Rac1 activity in podocytes incubated with IL-13 for 20 minutes.
Active Rac1 level was measured and normalized against total protein concentration. Asterisk indicates statistically significant differences ($p<0.05$).

5.3.3 Effect of IL-13 on podocytes transfected with *vav1* siRNA

Following IL-13 stimulation in podocytes transfected with control siRNA, gene expression levels of *IL-13Rα2* ($6.19x10^{-3}$±$2.38x10^{-3}$ *vs.* $1.28x10^{-3}$±$0.19x10^{-3}$, $p<0.001$), *B7-1* ($4.36x10^{-4}$±$1.36x10^{-4}$ *vs.* $1.28x10^{-4}$±$0.27x10^{-4}$, $p=0.03$) and *vav1* ($2.48x10^{-4}$±$0.70x10^{-4}$ *vs.* $0.71x10^{-4}$±$0.16x10^{-4}$, $p=0.04$) were significantly increased as compared to unstimulated podocytes transfected with control siRNA (negative control) (Figure 32). (Appendix 5.3)

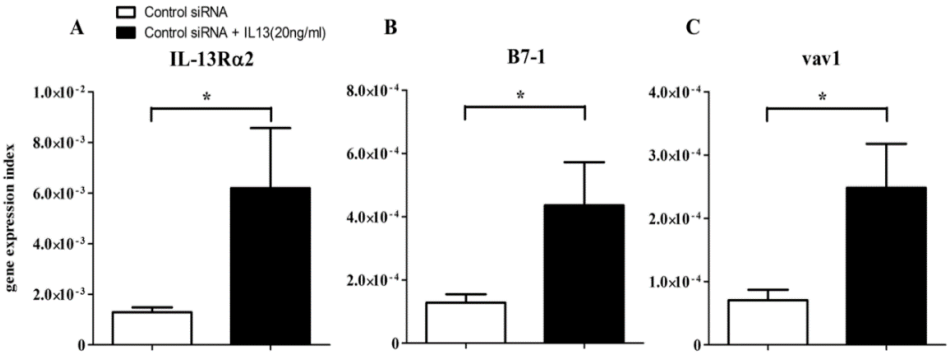

Figure 32: Increased gene expression of *IL-13Rα2*, *B7-1* and *vav1* in podocytes transfected with control siRNA following IL-13 stimulation.
Gene expression of A) *IL-13Rα2*, B) *B7-1*, and C) *vav1* in unstimulated podocytes transfected with control siRNA, and IL-13 stimulated podocytes with control siRNA transfection. Asterisk indicates statistically significant differences ($p<0.05$).

Western blot analysis showed that following incubation with IL-13, protein expression of IL-13Rα2 (1.39±0.20 *vs.* 0.65±0.07, $p=0.009$), B7-1 (0.92±0.15 *vs.* 0.50±0.08, $p=0.02$) and phosphorylated vav1 (1.32±0.16 *vs.* 0.79±0.15, $p=0.003$) were significantly increased in IL-13 stimulated podocytes with control siRNA transfection as compared to negative control (Figure 33 and Figure 34). Protein expression of vav1 in IL-13 stimulated podocytes with

control siRNA transfection remained unchanged as compared to negative control (Figure 35). (Appendix 5.4)

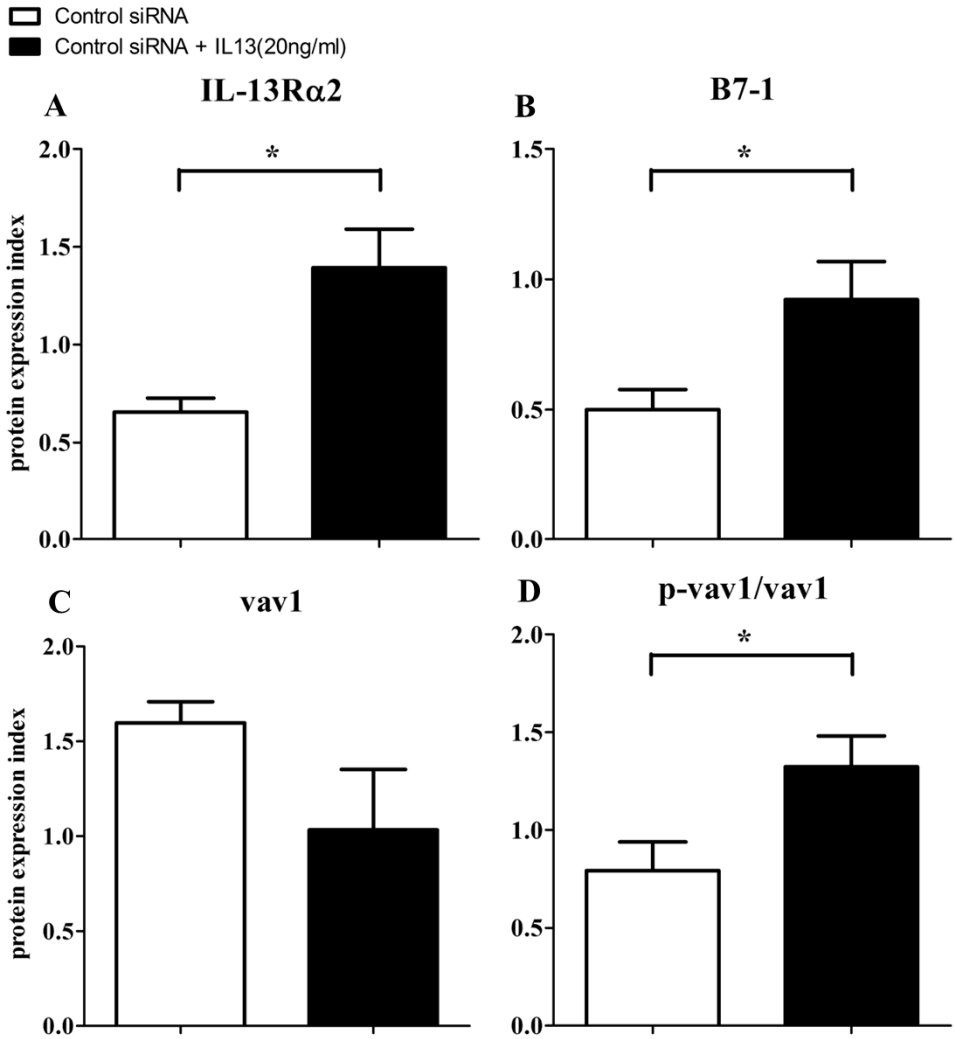

Figure 33: Increased protein expression of IL-13Rα2, B7-1 and phosphorylated vav1 in podocytes transfected with control siRNA following IL-13 stimulation.
Protein expression of A) IL-13Rα2, B) B7-1, C) vav1, and D) p-vav1/vav1 in unstimulated podocytes transfected with control siRNA, and IL-13 stimulated podocytes with control siRNA transfection. Asterisk indicates statistically significant differences ($p<0.05$).

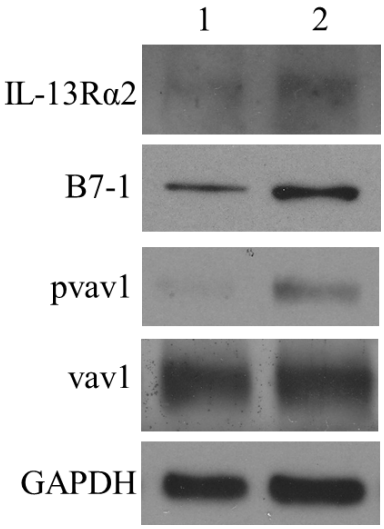

Figure 34: Protein expression of IL-13Rα2, B7-1, phosphorylated vav1, total vav1 in podocytes.
Representative gel images of IL-13Rα2, B7-1, phosphorylated vav1 and total vav1 in 1) unstimulated podocytes transfected with control siRNA and 2) IL-13 stimulated podocytes with control siRNA transfection. GAPDH was used as loading control.

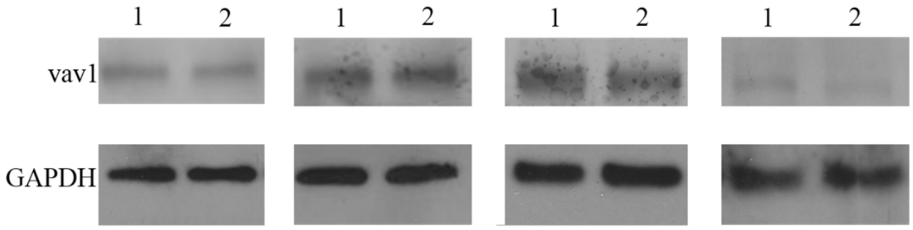

Figure 35: Vav1 and respective GAPDH blot images from four independent experiments.
Representative gel images of total vav1 in 1) unstimulated podocytes transfected with control siRNA and 2) IL-13 stimulated podocytes with control siRNA transfection. GAPDH was used as loading control.

Transfection of podocytes with siRNA specific for *vav1* resulted in 84.2% reduction in gene expression level of *vav1* which translated to reduction in vav1 protein expression by 42.8% (Figure 36).

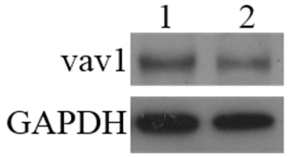

Figure 36: Protein expression of vav1 in podocytes.
Representative gel images of vav1 in podocytes transfected with 1) control siRNA and 2) vav1 siRNA. GAPDH was used as loading control.

Following IL-13 stimulation, gene expression levels of *IL-13Rα2* ($3.66 \times 10^{-3} \pm 1.19 \times 10^{-3}$ *vs.* $1.28 \times 10^{-3} \pm 0.19 \times 10^{-3}$, p=0.04) and *B7-1* ($3.33 \times 10^{-4} \pm 0.71 \times 10^{-4}$ *vs.*

$1.28x10^{-4}$±$0.27x10^{-4}$, p=0.01) were significantly increased in *vav1* knock down podocytes as compared to negative control (Figure 37).

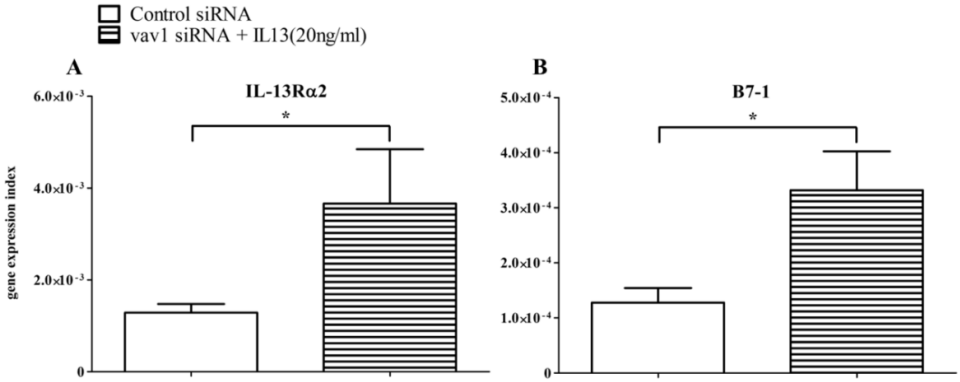

Figure 37: Increased gene expression of *IL-13Rα2* and *B7-1* in IL-13 stimulated podocytes transfected with vav1 siRNA.
Gene expression of A) *IL-13Rα2* and B) *B7-1* in unstimulated podocytes transfected with control siRNA, and IL-13 stimulated podocytes with vav1 siRNA transfection. Asterisk indicates statistically significant differences (p<0.05).

Similarly, increased protein expression levels of IL-13Rα2 (1.23±0.18 *vs.* 0.65±0.07, p=0.01) and B7-1 (1.30±0.44 *vs.* 0.50±0.08, p=0.03) were also demonstrated in IL-13 stimulated podocytes transfected with vav1 siRNA in comparison to negative control (Figure 38 and Figure 39).

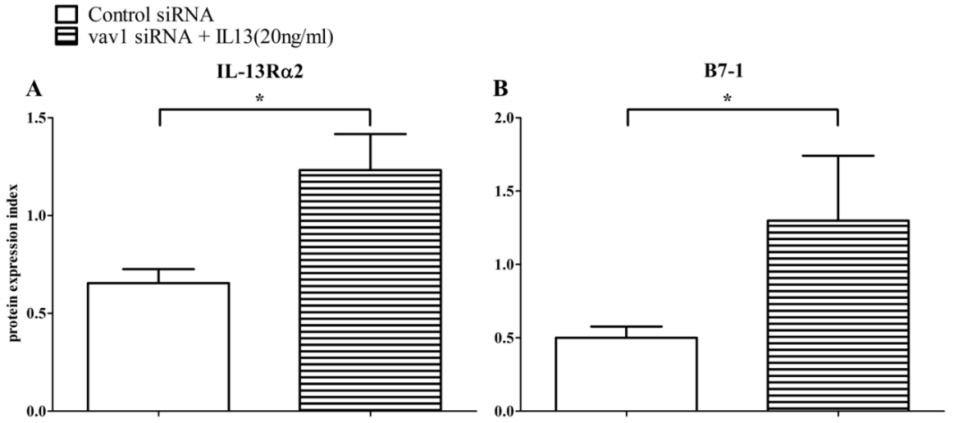

Figure 38: Increased protein expression of IL-13Rα2 and B7-1 in IL-13 stimulated podocytes transfected with vav1 siRNA.
Protein expression of A) *IL-13Rα2* and B) *B7-1* in unstimulated podocytes transfected with control siRNA, and IL-13 stimulated podocytes with vav1 siRNA transfection. Asterisk indicates statistically significant differences (p<0.05).

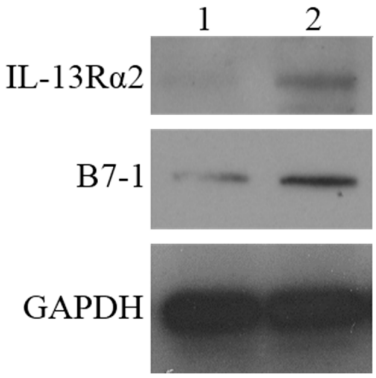

Figure 39: Protein expression of IL-13Rα2 and B7-1 in IL-13 stimulated podocytes transfected with *vav1* siRNA.
Representative gel images of IL-13Rα2 and B7-1 in 1) unstimulated podocytes transfected with control siRNA and 2) IL-13 stimulated podocytes with *vav1* siRNA transfection. GAPDH was used as loading control.

5.3.4 Effect of IL-13 on actin cytoskeleton in podocytes transfected with *vav1* siRNA

As shown in Figure 40, transfection of podocytes with control siRNA did not change the arrangement of actin cytoskeleton, with bright actin staining in the center of the cells. Following stimulation with IL-13 in podocytes transfected with control siRNA, less stress fibers were formed at the center of the cells. Podocytes transfected with *vav1* siRNA showed similar features as that of podocytes transfected with control siRNA. However, IL-13 stimulation in podocytes transfected with *vav1* siRNA showed strong stress fibers content at the center of the cells indicating that *vav1* siRNA transfection had prevented the action of IL-13 on actin cytoskeleton rearrangement.

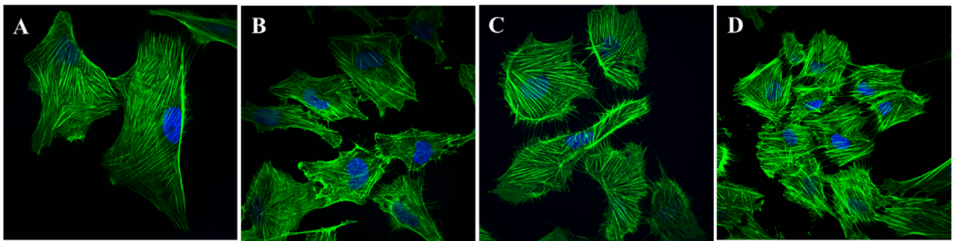

Figure 40: *Vav1* knock down podocytes were protected from IL-13 induced actin cytoskeleton rearrangement.
Human podocytes were stained with phalloidin for F-actin (magnification, x60). A) Podocytes tranfected with control siRNA showed features of larger size and strong transcellular stress fibers; B) IL-13 stimulation in podocytes transfected with control siRNA resulted in smaller size and weak F-actin signal in the cell center and accumulation of F-actin at the cell peripheral; C) Podocytes transfected with *vav1* siRNA showed similar features as that of podocytes transfected with control siRNA; D) IL-13 stimulation in podocytes transfected with *vav1* siRNA showed high stress fibers signal at the cell center.

Similarly, cortical F-actin score index was significantly increased in IL-13 stimulated podocytes with control siRNA transfection (2.41±0.10) as compared to unstimulated podocytes with control siRNA transfection (1.48±0.05) (p=0.05). Transfection of podocytes with *vav1* siRNA did not affect the cortical F-actin score index compared to that of negative controls. No significant difference in cortical F-actin score index was detected in IL-13 stimulated *vav1* knock down podocytes (1.57±0.10) as compared to the unstimulated podocytes with control siRNA transfection (1.48±0.05) (p=0.28) (Figure 41). (Appendix 5.5)

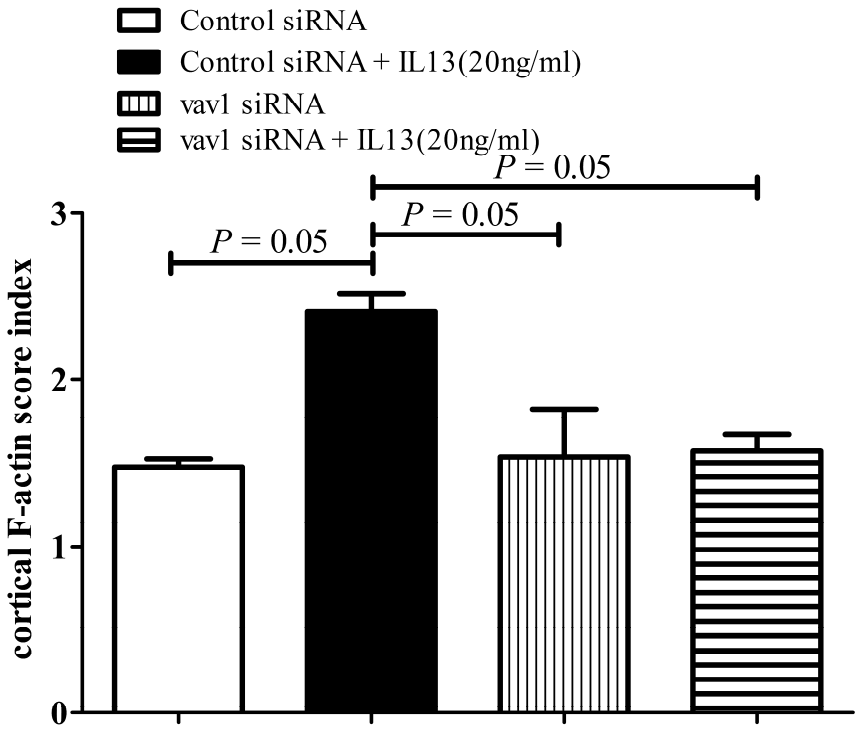

Figure 41: Cortical F-actin index in podocytes transfected with control siRNA or vav1 siRNA.
Graph showing cortical F-actin index in podocytes transfected with control siRNA (negative control), IL-13 stimulated podocytes with control siRNA transfection, podocytes transfected with *vav1* siRNA; and IL-13 stimulated *vav1* knock down podocytes.

5.3.5 Effect of IL-13 on RhoA and Rac1 activity in podocytes transfected with *vav1* siRNA

Rac1 activity level was significantly increased in podocytes transfected with control siRNA following IL-13 stimulation (1.17±0.15) as compared to negative control (0.71±0.10) (p=0.05) (Figure 42B); while no statistical difference in the RhoA activity level was detected (Figure 42A). Following IL-13 stimulation of

podocytes transfected with *vav1* siRNA, no significant change in both Rac1 and RhoA activity levels were detected. (Appendix 5.6)

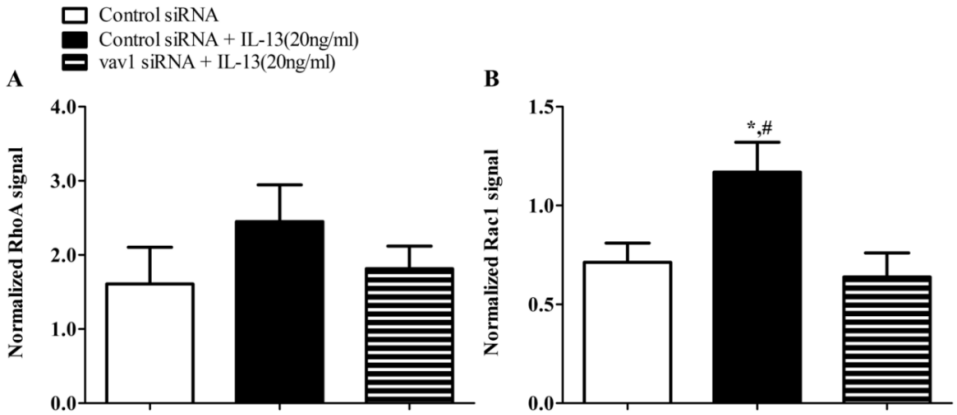

Figure 42: RhoA and Rac1 activity levels in podocytes transfected with control siRNA or *vav1* siRNA.

Activity levels of A) RhoA and B) Rac1 in podocytes transfected with control siRNA (negative control), IL-13 stimulated podocytes with siRNA transfection, and IL-13 stimulated vav1 knock down podocytes. $^{*}p<0.05$, compared to negative control; and $^{\#}p<0.05$, compared to IL-13 stimulated podocytes with siRNA transfection.

5.4. Discussion

The hallmark of nephrotic syndrome in the glomerulus is podocyte FP effacement, the corollary of which in the *in-vitro* podocyte culture system is that of actin cytoskeleton rearrangement [77]. In healthy podocytes, distinct bundles of actin filament are characteristically seen to traverse the cells from one end to the other. On the other hand following podocyte injury, a cortical ring of F-actin is formed. Our *in vitro* IL-13 stimulated podocytes displayed this characteristic feature of weak F-actin signal in the cell center with accumulation of F-actin at the cell periphery (Figure 28B), which was also reflected by the significantly increased cortical F-actin score index (Figure 29), suggesting that IL-13 could induce podocyte injury.

This change in actin cytoskeleton arrangement was associated with increased Rac1 activity in the IL-13 stimulated podocytes. Rho family small GTPases, namely RhoA, Rac1 and CDC42, are known regulators of the actin cytoskeleton. Activation of RhoA induces the assembly of contractile actin and stress fibres [286, 287]. Activation of Rac1 induces actin polymerization to form lamellipodia [287, 288], whereas activation of CDC42 stimulates the polymerization of actin to filopodia [287, 289]. Healthy, stationary podocytes with intact FP are generally thought to have predomoninat RhoA activity, whereas in injured, motile podocytes with retracted FP, Cdc42 or Rac1 activity is more prevalent [77].

Several studies have implicated the role of RhoA and Rac1 in podocyte FP effacement. Rho GDI$\alpha^{-/-}$ mice developed massive proteinuria resembling nephrotic syndrome and died due to renal failure [290]. This was associated with increased Rac1 (but not RhoA) and mineralocorticoid receptor signaling in the kidney [291]. Pharmacological intervention with a Rac1-specific small-molecule inhibitor diminished mineralocorticoid receptor hyperactivity and reduced proteinuria and renal damage in this mouse model of proteinuria.

Tian, D., *et al.* have shown that TRPC5 and TRPC6 channels were antagonistic regulators of actin dynamics and cell motility in podocytes through the

regulation of Rac1 and RhoA, respectively [100]. TRPC5-mediated Ca^{2+} influx was shown to activate Rac1, promoting cell migration; whereas TRPC6-mediated Ca^{2+} influx induced RhoA activity, inhibiting cell migration.

Rac1 has either beneficial or deleterious effects depending on the context of podocyte injury. Using the protamine sulfate model of acute podocyte injury, podocyte-specific deletion of Rac1 prevented podocyte FP effacement. In a long-term model of chronic hypertensive glomerular damage, however, loss of Rac1 led to worsening of albuminuria and glomerulosclerosis [292].

To date, there have been no reports of the role of vav1 in actin cytoskeleton reorganization in podocytes. However, in T-cells, reorganization of the cytoskeleton is needed for T cell activation and function [293-296] upon binding with co-receptors such as CD28, ICOS and CTLA-4 [297-299]. The full co-stimulatory effect of CD28 on T-cells involves the vav1-MEKK1-JNK pathway, whereas the ICOS signaling pathway is less understood and probably involves the PI3K-PDK-PKB pathway [299]. The polarization of T-cells by CTLA-4 requires PI3K, vav1, Cdc42, and myosin L chain kinase, but protein kinase B, Rho kinase and RhoA are not required [266]. Regulation of the actin cytoskeleton is subsequently mediated via vav1 activation of Rac1 and Cdc42 [275, 300].

The classical hematopoietic markers, CD80 (B7-1) [217, 218] and CTLA-4 [267, 301], have also been shown to be expressed in podocytes. Podocyte-specific expression of B7-1 has been implicated as the final common pathway in the genesis of proteinuria in glomerulopathies [211, 212]. Following *in vitro* LPS stimulation, podocyte expression of B7-1 was shown to be increased with concurrent actin cytoskeleton reorganization. B7-1 knockout mice were protected from LPS-induced proteinuria, suggesting a functional link between podocyte B7-1 expression and proteinuria. Our *in vitro* IL-13-stimulated podocytes showed increased B7-1 expression as well as actin cytoskeleton rearrangement, suggesting that IL-13 could induce podocyte injury possibly through B7-1 upregulation, correlating with the findings of increased B7-1

glomerular expression and FP effacement in our IL-13 overexpression rat model of MCNS.

In this chapter, we have demonstrated increased expression of IL-13Rα2, B7-1 and phosphorylated vav1 following IL-13 stimulation of podocytes transfected with control siRNA. This was associated with activation of Rac1 and actin cytoskeleton rearrangement. On the other hand, podocytes with vav1 siRNA transfection was protected from this IL-13 induced actin cytoskeleton rearrangement and Rac1 activation. In our vav1 knock-down studies, B7-1 expression remained upregulated following IL-13 stimulation, but no significant changes were seen in the actin-cytoskeleton, suggesting that B7-1 activation could be the upstream event of vav1 activation in podocytes. B7-1 has been shown in previous knock-down studies to be responsible for involvement in actin cytoskeleton rearrangement [217, 218].

In summary, we have demonstrated that vav1 plays a role in the IL-13 induced podocyte injury which could be mediated via Rac1 (Figure 43). These findings are consistent with the hypothesis that the podocyte FP effacement seen in our IL-13 overexpression rat model of MCNS involves the activation of B7-1 and subsequent phosphorylation of vav1 and activation of Rac1 resulting in actin cytoskeleton rearrangement in podocytes.

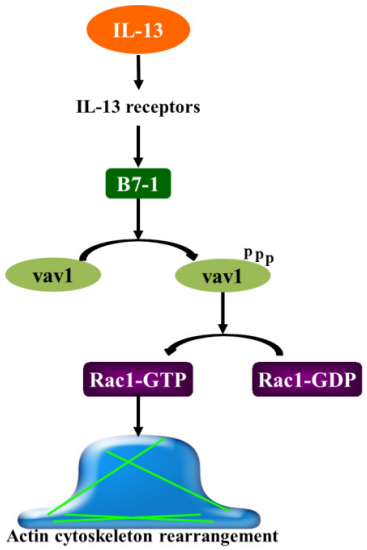

Figure 43: Proposed mechanism of IL-13 induced podocyte injury.
IL-13-induced actin cytoskeleton rearrangement in podocytes through activation of B7-1, phosphorylation of vav1 and activation of Rac1.

Knowledge of the signaling pathways involved in the pathogenesis of this disease may provide us more targeted treatment at the molecular level, allowing us to design new therapeutic strategies. Therapeutic strategies could either target the source, or stabilize the end point. In our case of increase IL-13 levels in the plasma of MCNS patient in relapse which then acts on the IL-13 receptors on the podocytes when blood pass through kidney, drugs could be designed to sequester IL-13, increasing the level of the IL-13Rα2, or blocking the IL-13Rα1 on the podocytes. The subsequent activation of B7-1 and vav1-Rac1 signaling pathway, could conceivably use Abatacept (CTLA-4-Ig) to block B7-1 activation or Azathioprine which was shown to have antagonistic effect in the vav-Rac signaling pathway in T cells [302, 303]. The challenge, however, will be to selectively target these effects to the podocytes (i.e. not affecting the T cells). In addition, targeting IL-13 might not be effective if there is a "second hit" which, by itself, may cause podocytes FP effacement.

CHAPTER 6

CONCLUSION AND FUTURE DIRECTIONS

6.1. Conclusion

In this study, we have delineated the molecular signature of the glomerulopathy associated with our *IL-13* overexpressed rat model of MCNS. This was defined by differential regulation of genes involved in immune responses, transcription regulation and actin cytoskeleton remodeling. In addition, more than 87% of genes known to be related to podocytes were significantly downregulated, suggesting extensive podocyte injury at the molecular level, whose phenotypic expression in this rat model translates to podocyte FP effacement and proteinuria. Moreover, we have identified a possible role of vav1 in the regulation of actin cytoskeleton rearrangement seen in podocyte FP effacement. This role of vav1 in the regulation of podocyte actin cytoskeleton rearrangement is novel, and has not been previously described in kidneys. We have further demonstrated protein expression of vav1 in the glomeruli and tubular epithelial cells of rat kidney and showed that vav1 co-localized with synaptopodin, confirming its location in podocytes.

Using *in vitro* human podocyte cell culture, we showed that gene expression of vav1 was upregulated by IL-13. We have also demonstrated gene and protein expression of vav1 as well as the phosphorylated form of vav1 in pure podocyte cell culture systems. Following IL-13 stimulation, expression levels of IL-13Rα2, B7-1 and phosphorylated vav1 were significantly increased from the basal level, indicating the possible roles of B7-1 and vav1 in IL-13 mediated podocyte injury.

IL-13 stimulated podocytes displayed the characteristic feature of actin cytoskeleton rearrangement consisting of weak central F-actin, but strong peripheral F-actin signal. This was associated with activation of Rac1, indicative of motile podocytes with retracted FP. *Vav1* knock-down podocytes were protected from IL-13 induced actin cytoskeleton changes and Rac1 activity, suggesting that the podocyte injury caused by IL-13 via B7-1 involved phosphorylation of vav1 and subsequent Rac1 activation.

In conclusion, the mechanism of IL-13 induced podocyte FP effacement seen in our rat model of MCNS was partly due to the direct action of IL-13 on podocytes through activation of B7-1-vav1-Rac1 mediated actin cytoskeleton rearrangement (Figure 44).

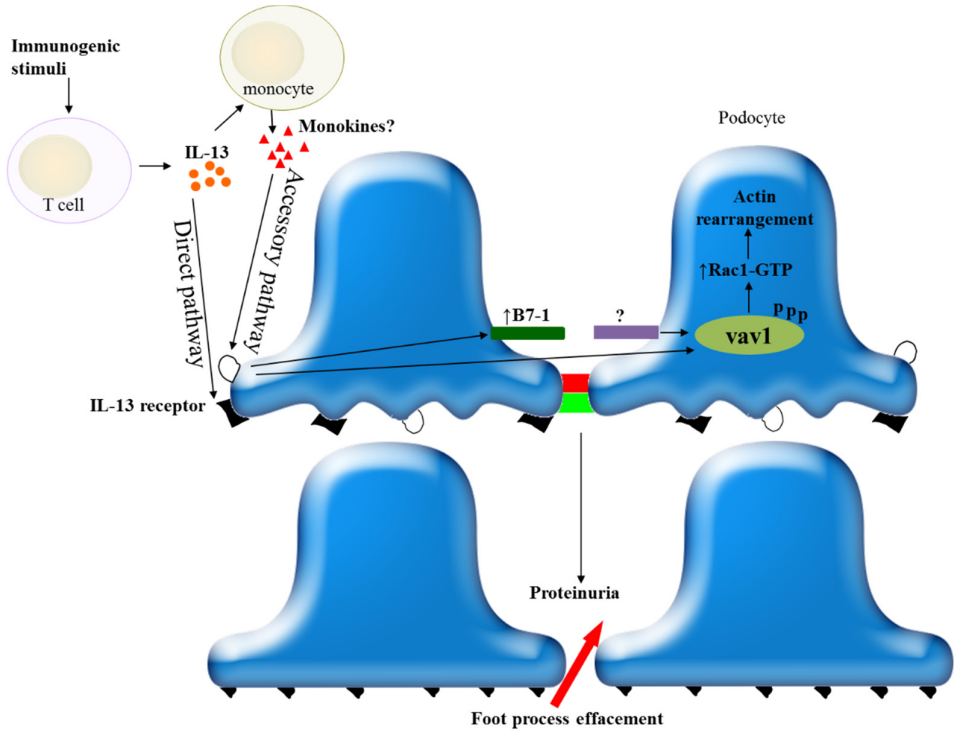

Figure 44: Mechanism of IL-13 induced podocyte foot process effacement in the rat model of MCNS.
IL-13 could act directly on podocytes, resulting in activation of B7-1 and phosphorylation of vav1, switching the Rac1 to the GTP-bound active state, resulting in actin cytoskeleton rearrangement. The podocyte FP effacement in the rat model of MCNS thus could be the result of this direct effect of IL-13 induced podocyte injury (direct pathway) or the indirect effect of IL-13 on other immune mediators which caused the dysregulation of other podocytes proteins not seen in the direct effect of IL-13 on podocytes (accessory pathway).

6.2. Future directions

We have demonstrated that IL-13 stimulation in cultured human podocytes resulted in upregulation of B7-1 gene expression, leading to increased phosphorylation of vav1. This was associated with increased level of activated Rac1, and subsequent actin cytoskeleton rearrangement. Though IL-13 was able to upregulate B7-1 gene expression in the podocyte cell cultures, the degree of upregulation was not as marked as that seen in the glomeruli of the IL-13 overexpressed rats. Therefore it is conceivable that a second signal could result in perpetuation of the glomerular B7-1 expression. We have shown that

glomerular gene expression of TLR-4 was also significantly elevated in the *IL-13* overexpressed rats, however, this was not seen in IL-13 stimulated human podocyte cell cultures. Stimulation of TLR-4 by specific ligands is a known potent inducer of B7-1 expression. Therefore, we hypothesized that the IL-13 induced podocyte FP effacement and subsequent proteinuria in our rat model could, in part, be due to the presence of an accessory pathway which augments and perpetuates the increased B7-1 expression with consequent actin cytoskeleton rearrangement.

This is in contrast to the 'Two-Hit' hypothesis proposed by Garin *et al.* [301, 304]. Reiser *et al,* in 2004 [217, 218], hypothesized that the initial hit is induction of B7-1 on the podocyte, and that this results in change in shape of the podocyte with actin rearrangement, leading to increase in glomerular permeability and proteinuria. Induction of B7-1 may result from either direct binding of podocyte receptors by activated T-cell cytokines, such as IL-13, or by activation of podocyte TLR by viral products or allergens. Garin *et al.* further hypothesized that under normal circumstances, B7-1 expression is only transiently expressed and proteinuria is minimal due to rapid autoregulatory response resulting in downregulation of B7-1 response. The second 'hit' in MCNS therefore consists of abnormal censoring of podocyte B7-1 expression due to a defective autoregulatory response by Tregs or by defective upregulation of podocyte CTLA4, a negative regulator of B7-1, resulting in persistent podocyte expression of B7-1 and hence proteinuria [304]. Our current study could not demonstrate defective upregulation of podocyte CTLA4 in the IL-13 overexpressed rat, instead, we showed significant upregulation of glomerular CTLA4, suggesting that this could be a positive feedback following upregulation of B7-1 in this model.

In our model, we are proposing that perpetuation of B7-1 expression occurred due to a consequent summative effect of direct IL-13 stimulation as well as indirect signaling through TLR-4 mediated by other immune mediators, on B7-1 (Figure 45). The identity of the mediator(s) which, via the accessory pathway,

augments B7-1 expression with consequent actin cytoskeleton rearrangement is, however, unclear.

As IL-13 is an important modulator of monocyte/macrophage function, it is plausible that the indirect action of IL-13 on podocyte may be mediated via monocyte polarization with consequent secretion of monokine(s) acting on the TLR-4/B7-1 danger signaling, resulting in podocyte actin cytoskeleton rearrangement. Therefore, we will be studying the monocyte transcription profile as well as cytokines/chemokines profile in our population of children with MCNS in order to identify the molecules which may be the crucial mediator(s) providing the "second hit" in the pathogenesis of MCNS in both humans and *IL-13* overexpressed rats.

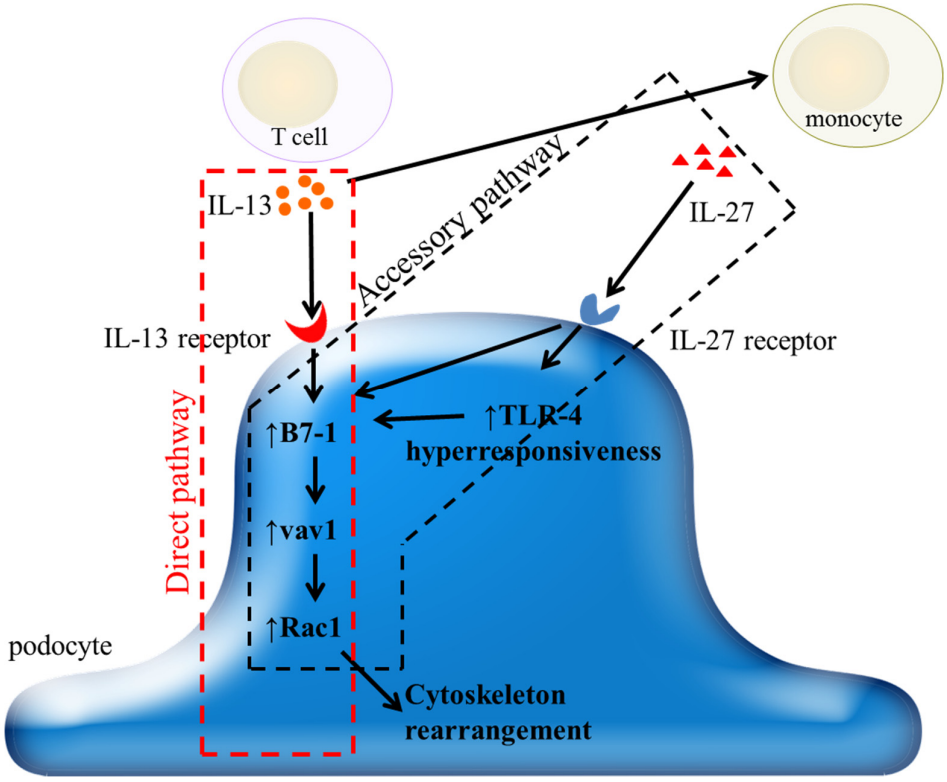

Figure 45: Direct and accessory pathways in the pathogenesis of MCNS ('Two-Hit' Hypothesis).
Perpetuation of B7-1 expression occurred due to a consequent summative effect of direct IL-13 stimulation as well as indirect signaling through TLR-4 mediated by other immune mediators, on B7-1.

REFERENCE

1. Yap, H.K., et al., *Acute Glomerulonephritis - Changing Patterns in Singapore Children.* Pediatric Nephrology, 1990. **4**(5): p. 482-484.
2. Gbadegesin, R. and W.E. Smoyer, *Nephrotic Syndrome*, in *Comprehensive Pediatrics Nephrology*, D.F. Geray and F. Schaefer, Editors. 2008, Mosby Elsevier. p. 205-216.
3. Querfeld, U., et al., *Lipoprotein profiles at different stages of the nephrotic syndrome.* Eur J Pediatr, 1988. **147**(3): p. 233-8.
4. Gherardi, E., et al., *Relationship among the concentrations of serum lipoproteins and changes in their chemical composition in patients with untreated nephrotic syndrome.* Eur J Clin Invest, 1977. **7**(6): p. 563-70.
5. Querfeld, U., *Should hyperlipidemia in children with the nephrotic syndrome be treated?* Pediatr Nephrol, 1999. **13**(1): p. 77-84.
6. Johansson, A.C., et al., *Dyslipidemia in peritoneal dialysis--relation to dialytic variables.* Perit Dial Int, 2000. **20**(3): p. 306-14.
7. ISKDC, *The primary nephrotic syndrome in children. Identification of patients with minimal change nephrotic syndrome from initial response to prednisone: A report of the international study of kidney disease in children.* The Journal of pediatrics, 1981. **98**(4): p. 561-564.
8. Niaudet, P., *Steroid-resistant idiopathic nephrotic syndrome in children*, in *Pediatric nephrology*. 2004, Lippincott Williams & Wilkins: Pholadelphia.
9. Eddy, A.A. and J.M. Symons, *Nephrotic syndrome in childhood.* Lancet, 2003. **362**(9384): p. 629-639.
10. Gipson, D.S., et al., *Management of Childhood Onset Nephrotic Syndrome.* Pediatrics, 2009. **124**(2): p. 747-757.
11. Kyrieleis, H.A., et al., *Long-term outcome of biopsy-proven, frequently relapsing minimal-change nephrotic syndrome in children.* Clin J Am Soc Nephrol, 2009. **4**(10): p. 1593-600.
12. Hodson, E.M., N.S. Willis, and J.C. Craig, *Corticosteroid therapy for nephrotic syndrome in children.* Cochrane Database Syst Rev, 2007(4): p. CD001533.
13. Rüth, E.-M., et al., *Children with Steroid-sensitive Nephrotic Syndrome Come of Age: Long-term Outcome.* The Journal of pediatrics, 2005. **147**(2): p. 202-207.
14. Srivastava, T., S.D. Simon, and U.S. Alon, *High incidence of focal segmental glomerulosclerosis in nephrotic syndrome of childhood.* Pediatr Nephrol, 1999. **13**(1): p. 13-8.
15. Hogg, R.J., et al., *Evaluation and management of proteinuria and nephrotic syndrome in children: recommendations from a pediatric nephrology panel established at the National Kidney Foundation conference on proteinuria, albuminuria, risk, assessment, detection, and elimination (PARADE).* Pediatrics, 2000. **105**(6): p. 1242-9.
16. McEnery, P.T. and C.F. Strife, *Nephrotic syndrome in childhood. Management and treatment in patients with minimal change disease, mesangial proliferation, or focal glomerulosclerosis.* Pediatr Clin North Am, 1982. **29**(4): p. 875-94.

17. Sharples, P.M., J. Poulton, and R.H. White, *Steroid responsive nephrotic syndrome is more common in Asians.* Archives of Disease in Childhood, 1985. **60**(11): p. 1014-1017.
18. Yap, H.K. *Nephrotic Syndrome Presenting in the Teens*. 2005 23 January, 2005 [cited 2012 9 March, 2012]; Available from: http://www.med.nus.edu.sg/paed/academic/NEPH_NS_in_teens.htm.
19. Chang, J.W., et al., *Clinicopathological features and prognosis of Chinese children with idiopathic nephrotic syndrome between different age groups.* Eur J Pediatr, 2009. **168**(10): p. 1189-94.
20. Mathieson, P.W., *Minimal change nephropathy and focal segmental glomerulosclerosis.* Semin Immunopathol, 2007. **29**(4): p. 415-26.
21. Shalhoub, R.J., *Pathogenesis of lipoid nephrosis: a disorder of T-cell function.* Lancet, 1974. **2**(7880): p. 556-60.
22. Cuoghi, D., P. Venturi, and E. Cheli, *Bee Sting and Relapse of Nephrotic Syndrome.* Child Nephrology and Urology, 1989. **9**(1-2): p. 82-83.
23. Tareyeva, I.E., A.J. Nikolaev, and T.N. Janushkevitch, *Nephrotic Syndrome Induced by Insect Sting.* Lancet, 1982. **2**(8302): p. 825-825.
24. Kuzemko, J.A., *Measles vaccination and the nephrotic syndrome.* Br Med J, 1972. **4**(5841): p. 665-6.
25. Macario, F., et al., *Nephrotic syndrome after recombinant hepatitis B vaccine.* Clin Nephrol, 1995. **43**(5): p. 349.
26. Reeves, W.G., J.S. Cameron, and C.S. Ogg, *IgE and the nephrotic syndrome.* Lancet, 1971. **1**(7712): p. 1299-300.
27. Florido, J.F., et al., *Nephrotic syndrome and respiratory allergy in childhood.* J Investig Allergol Clin Immunol, 1992. **2**(3): p. 136-40.
28. Williamson, D.A., *Nephrotic syndrome associated with inhaled allergens.* Lancet, 1970. **1**(7650): p. 778.
29. Reeves, W.G., et al., *Seasonal nephrotic syndrome. Description and immunological findings.* Clin Allergy, 1975. **5**(2): p. 121-37.
30. Couser, W., et al., *Hodgkin's disease and lipoid nephrosis.* Lancet, 1977. **1**(8017): p. 912-3.
31. Sherman, R.L., et al., *Lipoid nephrosis in Hodgkin's disease.* Am J Med, 1972. **52**(5): p. 699-706.
32. Peces, R., et al., *Minimal change nephrotic syndrome associated with Hodgkin's lymphoma.* Nephrol Dial Transplant, 1991. **6**(3): p. 155-8.
33. Orman, S.V., et al., *Nephrotic syndrome associated with a clonal T-cell leukemia of large granular lymphocytes with cytotoxic function.* Arch Intern Med, 1986. **146**(9): p. 1827-9.
34. Belghiti, D., et al., *Nephrotic syndrome associated with T-cell lymphoma.* Cancer, 1981. **47**(7): p. 1878-82.
35. Long, Q., et al., *Minimal change nephrotic syndrome associated with invasive thymoma: a case report with literature review.* Clin Nephrol, 2012.
36. Lee, H.C., et al., *Minimal change nephrotic syndrome associated with malignant thymoma: case report and literature review.* Chang Gung Med J, 2001. **24**(9): p. 576-81.
37. Zinger, C., et al., *Minimal-change nephropathy and malignant thymoma.* Am J Nephrol, 1998. **18**(1): p. 61-3.

38. McDonald, P., P.A. Kalra, and R.A. Coward, *Thymoma and minimal-change glomerulonephritis.* Nephrol Dial Transplant, 1992. **7**(4): p. 357-9.
39. Varsano, S., et al., *Minimal-change nephropathy and malignant thymoma.* Chest, 1980. **77**(5): p. 695-7.
40. Karras, A., et al., *Renal and thymic pathology in thymoma-associated nephropathy: report of 21 cases and review of the literature.* Nephrol Dial Transplant, 2005. **20**(6): p. 1075-82.
41. Cameron, J.S., et al., *Long-term stability of remission in nephrotic syndrome after treatment with cyclophosphamide.* Br Med J, 1974. **4**(5935): p. 7-11.
42. Kapp, U., et al., *Interleukin 13 is secreted by and stimulates the growth of Hodgkin and Reed-Sternberg cells.* J Exp Med, 1999. **189**(12): p. 1939-46.
43. Skinnider, B.F., et al., *Interleukin 13 and interleukin 13 receptor are frequently expressed by Hodgkin and Reed-Sternberg cells of Hodgkin lymphoma.* Blood, 2001. **97**(1): p. 250-5.
44. Skinnider, B.F., U. Kapp, and T.W. Mak, *The role of interleukin 13 in classical Hodgkin lymphoma.* Leuk Lymphoma, 2002. **43**(6): p. 1203-10.
45. Skinnider, B.F., et al., *Signal transducer and activator of transcription 6 is frequently activated in Hodgkin and Reed-Sternberg cells of Hodgkin lymphoma.* Blood, 2002. **99**(2): p. 618-26.
46. Trieu, Y., et al., *Soluble interleukin-13Ralpha2 decoy receptor inhibits Hodgkin's lymphoma growth in vitro and in vivo.* Cancer Res, 2004. **64**(9): p. 3271-5.
47. Neuhaus, T.J., et al., *T-lymphocyte activation in steroid-sensitive nephrotic syndrome in childhood.* Nephrol Dial Transplant, 1995. **10**(8): p. 1348-52.
48. Yan, K., et al., *The increase of memory T cell subsets in children with idiopathic nephrotic syndrome.* Nephron, 1998. **79**(3): p. 274-8.
49. Frank, C., et al., *Dominant T cells in idiopathic nephrotic syndrome of childhood.* Kidney Int, 2000. **57**(2): p. 510-7.
50. Sahali, D., et al., *Transcriptional and post-transcriptional alterations of IkappaBalpha in active minimal-change nephrotic syndrome.* J Am Soc Nephrol, 2001. **12**(8): p. 1648-58.
51. Cheung, W., et al., *Atopy, serum IgE, and interleukin-13 in steroid-responsive nephrotic syndrome.* Pediatr Nephrol, 2004. **19**(6): p. 627-32.
52. Yokoyama, H., et al., *Impaired Immunoglobulin-G Production in Minimal Change Nephrotic Syndrome in Adults.* Clinical and Experimental Immunology, 1987. **70**(1): p. 110-115.
53. Mathieson, P.W., *Immune dysregulation in minimal change nephropathy.* Nephrology Dialysis Transplantation, 2003. **18**: p. 26-29.
54. Schnaper, H.W., et al., *TGF-beta signal transduction and mesangial cell fibrogenesis.* Am J Physiol Renal Physiol, 2003. **284**(2): p. F243-52.
55. Matsumoto, K. and K. Kanmatsuse, *Increased IL-12 release by monocytes in nephrotic patients.* Clin Exp Immunol, 1999. **117**(2): p. 361-7.

56. Stefanovic, V., et al., *Interleukin-12 and interferon-gamma production in childhood idiopathic nephrotic syndrome.* Pediatr Nephrol, 1998. **12**(6): p. 463-6.
57. Daniel, V., et al., *T-lymphocyte populations, cytokines and other growth factors in serum and urine of children with idiopathic nephrotic syndrome.* Clin Nephrol, 1997. **47**(5): p. 289-97.
58. Yap, H.K., et al., *Th1 and Th2 cytokine mRNA profiles in childhood nephrotic syndrome: evidence for increased IL-13 mRNA expression in relapse.* J Am Soc Nephrol, 1999. **10**(3): p. 529-37.
59. Zachwieja, J., et al., *Intracellular cytokines of peripheral blood lymphocytes in nephrotic syndrome.* Pediatr Nephrol, 2002. **17**(9): p. 733-40.
60. Kang, J., et al., *Increased production of interleukin 4 in children with simple idiopathic nephrotic syndrome.* Chin Med J (Engl), 1994. **107**(5): p. 347-50.
61. Cho, B.-S., et al., *Up-regulation of interleukin-4 and CD23/FceRII in minimal change nephrotic syndrome.* Pediatric Nephrology, 1999. **13**(3): p. 199-204.
62. Kimata, H., M. Fujimoto, and K. Furusho, *Involvement of interleukin (IL)-13, but not IL-4, in spontaneous IgE and IgG4 production in nephrotic syndrome.* Eur J Immunol, 1995. **25**(6): p. 1497-501.
63. Liu, L.-l., et al., *Th17/Treg imbalance in adult patients with minimal change nephrotic syndrome.* Clinical Immunology, 2011. **139**(3): p. 314-320.
64. Matsumoto, K., *Decreased release of IL-10 by monocytes from patients with lipoid nephrosis.* Clin Exp Immunol, 1995. **102**(3): p. 603-7.
65. Saxena, S., A. Mittal, and A. Andal, *Pattern of interleukins in minimal-change nephrotic syndrome of childhood.* Nephron, 1993. **65**(1): p. 56-61.
66. Matsumoto, K., *Decreased production of interleukin-1 by monocytes from patients with lipoid nephrosis.* Clin Nephrol, 1989. **31**(6): p. 292-6.
67. Bustos, C., et al., *Increase of tumour necrosis factor alpha synthesis and gene expression in peripheral blood mononuclear cells of children with idiopathic nephrotic syndrome.* Eur J Clin Invest, 1994. **24**(12): p. 799-805.
68. Garin, E.H., et al., *IL-8 production by peripheral blood mononuclear cells in nephrotic patients.* Kidney Int, 1994. **45**(5): p. 1311-7.
69. Mosmann, T.R. and R.L. Coffman, *TH1 and TH2 cells: different patterns of lymphokine secretion lead to different functional properties.* Annu Rev Immunol, 1989. **7**: p. 145-73.
70. Romagnani, S., *T-cell subsets (Th1 versus Th2).* Ann Allergy Asthma Immunol, 2000. **85**(1): p. 9-18; quiz 18, 21.
71. Sahali, D., et al., *A Novel Approach to Investigation of the Pathogenesis of Active Minimal-Change Nephrotic Syndrome Using Subtracted cDNA Library Screening.* J Am Soc Nephrol, 2002. **13**(5): p. 1238-1247.
72. Wei, C.L., et al., *Interleukin-13 genetic polymorphisms in Singapore Chinese children correlate with long-term outcome of minimal-change disease.* Nephrology Dialysis Transplantation, 2005. **20**(4): p. 728-734.

73. Mundel, P. and S.J. Shankland, *Podocyte biology and response to injury.* J Am Soc Nephrol, 2002. **13**(12): p. 3005-15.
74. Seefeldt, T., et al., *Quantitative relationship between glomerular foot process width and proteinuria in glomerulonephritis.* Lab Invest, 1981. **6**(44): p. 541-6.
75. Patrakka, J. and K. Tryggvason, *Molecular make-up of the glomerular filtration barrier.* Biochem Biophys Res Commun, 2010. **396**(1): p. 164-9.
76. Pavenstadt, H., W. Kriz, and M. Kretzler, *Cell Biology of the Glomerular Podocyte.* Physiol. Rev., 2003. **83**(1): p. 253-307.
77. Faul, C., et al., *Actin up: regulation of podocyte structure and function by components of the actin cytoskeleton.* Trends Cell Biol, 2007. **17**(9): p. 428-37.
78. Nielsen, J.S. and K.M. McNagny, *The role of podocalyxin in health and disease.* J Am Soc Nephrol, 2009. **20**(8): p. 1669-76.
79. Doyonnas, R., et al., *Anuria, omphalocele, and perinatal lethality in mice lacking the CD34-related protein podocalyxin.* J Exp Med, 2001. **194**(1): p. 13-27.
80. ORLANDO, R.A., et al., *The Glomerular Epithelial Cell Anti-Adhesin Podocalyxin Associates with the Actin Cytoskeleton through Interactions with Ezrin.* Journal of the American Society of Nephrology, 2001. **12**(8): p. 1589-1598.
81. Takeda, T., et al., *Loss of glomerular foot processes is associated with uncoupling of podocalyxin from the actin cytoskeleton.* J Clin Invest, 2001. **108**(2): p. 289-301.
82. Thomas, P.E., et al., *GLEPP1, a renal glomerular epithelial cell (podocyte) membrane protein-tyrosine phosphatase. Identification, molecular cloning, and characterization in rabbit.* J Biol Chem, 1994. **269**(31): p. 19953-62.
83. Wharram, B.L., et al., *Altered podocyte structure in GLEPP1 (Ptpro)-deficient mice associated with hypertension and low glomerular filtration rate.* J Clin Invest, 2000. **106**(10): p. 1281-90.
84. Reiser, J., et al., *The glomerular slit diaphragm is a modified adherens junction.* J Am Soc Nephrol, 2000. **11**(1): p. 1-8.
85. Wartiovaara, J., et al., *Nephrin strands contribute to a porous slit diaphragm scaffold as revealed by electron tomography.* J Clin Invest, 2004. **114**(10): p. 1475-83.
86. Ruotsalainen, V., et al., *Nephrin is specifically located at the slit diaphragm of glomerular podocytes.* Proceedings of the National Academy of Sciences, 1999. **96**(14): p. 7962-7967.
87. Kestila, M., et al., *Positionally cloned gene for a novel glomerular protein--nephrin--is mutated in congenital nephrotic syndrome.* Mol Cell, 1998. **1**(4): p. 575-82.
88. Holthofer, H., et al., *Nephrin localizes at the podocyte filtration slit area and is characteristically spliced in the human kidney.* Am J Pathol, 1999. **155**(5): p. 1681-7.
89. Holzman, L.B., et al., *Nephrin localizes to the slit pore of the glomerular epithelial cell.* Kidney Int, 1999. **56**(4): p. 1481-91.

90. Liu, G., et al., *Neph1 and nephrin interaction in the slit diaphragm is an important determinant of glomerular permeability.* J Clin Invest, 2003. **112**(2): p. 209-21.
91. Sellin, L., et al., *NEPH1 defines a novel family of podocin interacting proteins.* Faseb J, 2003. **17**(1): p. 115-7.
92. Patrakka, J. and K. Tryggvason, *New insights into the role of podocytes in proteinuria.* Nat Rev Nephrol, 2009. **5**(8): p. 463-8.
93. Gerke, P., et al., *NEPH2 is located at the glomerular slit diaphragm, interacts with nephrin and is cleaved from podocytes by metalloproteinases.* J Am Soc Nephrol, 2005. **16**(6): p. 1693-702.
94. Ihalmo, P., et al., *Filtrin is a novel member of nephrin-like proteins.* Biochem Biophys Res Commun, 2003. **300**(2): p. 364-70.
95. Cohen, C.D., et al., *Comparative promoter analysis allows de novo identification of specialized cell junction-associated proteins.* Proc Natl Acad Sci U S A, 2006. **103**(15): p. 5682-7.
96. Inoue, T., et al., *FAT is a component of glomerular slit diaphragms.* Kidney Int, 2001. **59**(3): p. 1003-12.
97. Boute, N., et al., *NPHS2, encoding the glomerular protein podocin, is mutated in autosomal recessive steroid-resistant nephrotic syndrome.* Nat Genet, 2000. **24**(4): p. 349-54.
98. Roselli, S., et al., *Podocin localizes in the kidney to the slit diaphragm area.* Am J Pathol, 2002. **160**(1): p. 131-9.
99. Reiser, J., et al., *TRPC6 is a glomerular slit diaphragm-associated channel required for normal renal function.* Nat Genet, 2005. **37**(7): p. 739-44.
100. Tian, D., et al., *Antagonistic regulation of actin dynamics and cell motility by TRPC5 and TRPC6 channels.* Sci Signal, 2010. **3**(145): p. ra77.
101. Shih, N.Y., et al., *CD2AP localizes to the slit diaphragm and binds to nephrin via a novel C-terminal domain.* Am J Pathol, 2001. **159**(6): p. 2303-8.
102. Jones, N., et al., *Nck adaptor proteins link nephrin to the actin cytoskeleton of kidney podocytes.* Nature, 2006. **440**(7085): p. 818-23.
103. Simons, M., B. Hartleben, and T.B. Huber, *Podocyte polarity signalling.* Curr Opin Nephrol Hypertens, 2009. **18**(4): p. 324-30.
104. Schnabel, E., J.M. Anderson, and M.G. Farquhar, *The tight junction protein ZO-1 is concentrated along slit diaphragms of the glomerular epithelium.* J Cell Biol, 1990. **111**(3): p. 1255-63.
105. Patrakka, J., et al., *Expression and subcellular distribution of novel glomerulus-associated proteins dendrin, ehd3, sh2d4a, plekhh2, and 2310066E14Rik.* J Am Soc Nephrol, 2007. **18**(3): p. 689-97.
106. Hirabayashi, S., et al., *JAM4, a junctional cell adhesion molecule interacting with a tight junction protein, MAGI-1.* Mol Cell Biol, 2003. **23**(12): p. 4267-82.
107. Ahola, H., et al., *A novel protein, densin, expressed by glomerular podocytes.* J Am Soc Nephrol, 2003. **14**(7): p. 1731-7.
108. Hirabayashi, S., et al., *MAGI-1 is a component of the glomerular slit diaphragm that is tightly associated with nephrin.* Lab Invest, 2005. **85**(12): p. 1528-43.

109. Lehtonen, S., et al., *Cell junction-associated proteins IQGAP1, MAGI-2, CASK, spectrins, and alpha-actinin are components of the nephrin multiprotein complex.* Proc Natl Acad Sci U S A, 2005. **102**(28): p. 9814-9.
110. Mao, J., et al., *Expression profile of nephrin, podocin, and CD2AP in Chinese children with MCNS and IgA nephropathy.* Pediatr Nephrol, 2006. **21**(11): p. 1666-75.
111. Wernerson, A., et al., *Altered ultrastructural distribution of nephrin in minimal change nephrotic syndrome.* Nephrol Dial Transplant, 2003. **18**(1): p. 70-6.
112. Khoshnoodi, J., et al., *Nephrin promotes cell-cell adhesion through homophilic interactions.* Am J Pathol, 2003. **163**(6): p. 2337-46.
113. Putaala, H., et al., *The murine nephrin gene is specifically expressed in kidney, brain and pancreas: inactivation of the gene leads to massive proteinuria and neonatal death.* Hum Mol Genet, 2001. **10**(1): p. 1-8.
114. Gerke, P., et al., *Homodimerization and heterodimerization of the glomerular podocyte proteins nephrin and NEPH1.* J Am Soc Nephrol, 2003. **14**(4): p. 918-26.
115. Barletta, G.M., et al., *Nephrin and Neph1 co-localize at the podocyte foot process intercellular junction and form cis hetero-oligomers.* J Biol Chem, 2003. **278**(21): p. 19266-71.
116. Donoviel, D.B., et al., *Proteinuria and perinatal lethality in mice lacking NEPH1, a novel protein with homology to NEPHRIN.* Mol Cell Biol, 2001. **21**(14): p. 4829-36.
117. Garg, P., et al., *Neph1 cooperates with nephrin to transduce a signal that induces actin polymerization.* Mol Cell Biol, 2007. **27**(24): p. 8698-712.
118. Ruotsalainen, V., et al., *Role of nephrin in cell junction formation in human nephrogenesis.* Am J Pathol, 2000. **157**(6): p. 1905-16.
119. Radice, G.L., et al., *Precocious mammary gland development in P-cadherin-deficient mice.* J Cell Biol, 1997. **139**(4): p. 1025-32.
120. Tanoue, T. and M. Takeichi, *New insights into Fat cadherins.* J Cell Sci, 2005. **118**(Pt 11): p. 2347-53.
121. Moeller, M.J., et al., *Protocadherin FAT1 binds Ena/VASP proteins and is necessary for actin dynamics and cell polarization.* EMBO J, 2004. **23**(19): p. 3769-79.
122. Tanoue, T. and M. Takeichi, *Mammalian Fat1 cadherin regulates actin dynamics and cell-cell contact.* J Cell Biol, 2004. **165**(4): p. 517-28.
123. Ciani, L., et al., *Mice lacking the giant protocadherin mFAT1 exhibit renal slit junction abnormalities and a partially penetrant cyclopia and anophthalmia phenotype.* Mol Cell Biol, 2003. **23**(10): p. 3575-82.
124. Schwarz, K., et al., *Podocin, a raft-associated component of the glomerular slit diaphragm, interacts with CD2AP and nephrin.* J Clin Invest, 2001. **108**(11): p. 1621-9.
125. Huber, T.B., B. Schermer, and T. Benzing, *Podocin organizes ion channel-lipid supercomplexes: implications for mechanosensation at the slit diaphragm.* Nephron Exp Nephrol, 2007. **106**(2): p. e27-31.
126. Shono, A., et al., *Podocin participates in the assembly of tight junctions between foot processes in nephrotic podocytes.* J Am Soc Nephrol, 2007. **18**(9): p. 2525-33.

127. Roselli, S., et al., *Early glomerular filtration defect and severe renal disease in podocin-deficient mice.* Mol Cell Biol, 2004. **24**(2): p. 550-60.
128. Winn, M.P., et al., *A mutation in the TRPC6 cation channel causes familial focal segmental glomerulosclerosis.* Science, 2005. **308**(5729): p. 1801-4.
129. Moller, C.C., et al., *Induction of TRPC6 channel in acquired forms of proteinuric kidney disease.* J Am Soc Nephrol, 2007. **18**(1): p. 29-36.
130. Jiang, L., et al., *Over-expressing transient receptor potential cation channel 6 in podocytes induces cytoskeleton rearrangement through increases of intracellular Ca2+ and RhoA activation.* Experimental Biology and Medicine, 2011. **236**(2): p. 184-193.
131. Lehtonen, S., F. Zhao, and E. Lehtonen, *CD2-associated protein directly interacts with the actin cytoskeleton.* Am J Physiol Renal Physiol, 2002. **283**(4): p. F734-43.
132. Hutchings, N.J., et al., *Linking the T cell surface protein CD2 to the actin-capping protein CAPZ via CMS and CIN85.* J Biol Chem, 2003. **278**(25): p. 22396-403.
133. Lynch, D.K., et al., *A Cortactin-CD2-associated protein (CD2AP) complex provides a novel link between epidermal growth factor receptor endocytosis and the actin cytoskeleton.* J Biol Chem, 2003. **278**(24): p. 21805-13.
134. Huber, T.B., et al., *Bigenic mouse models of focal segmental glomerulosclerosis involving pairwise interaction of CD2AP, Fyn, and synaptopodin.* J Clin Invest, 2006. **116**(5): p. 1337-45.
135. Shih, N.Y., et al., *Congenital nephrotic syndrome in mice lacking CD2-associated protein.* Science, 1999. **286**(5438): p. 312-5.
136. Verma, R., et al., *Nephrin ectodomain engagement results in Src kinase activation, nephrin phosphorylation, Nck recruitment, and actin polymerization.* J Clin Invest, 2006. **116**(5): p. 1346-59.
137. Verma, R., et al., *Fyn binds to and phosphorylates the kidney slit diaphragm component Nephrin.* J Biol Chem, 2003. **278**(23): p. 20716-23.
138. Jones, N., et al., *Nck proteins maintain the adult glomerular filtration barrier.* J Am Soc Nephrol, 2009. **20**(7): p. 1533-43.
139. Asanuma, K., et al., *Nuclear relocation of the nephrin and CD2AP-binding protein dendrin promotes apoptosis of podocytes.* Proc Natl Acad Sci U S A, 2007. **104**(24): p. 10134-9.
140. Huber, T.B., et al., *The carboxyl terminus of Neph family members binds to the PDZ domain protein zonula occludens-1.* J Biol Chem, 2003. **278**(15): p. 13417-21.
141. Katsube, T., et al., *Cortactin associates with the cell-cell junction protein ZO-1 in both Drosophila and mouse.* J Biol Chem, 1998. **273**(45): p. 29672-7.
142. Patrie, K.M., et al., *Interaction of two actin-binding proteins, synaptopodin and alpha-actinin-4, with the tight junction protein MAGI-1.* J Biol Chem, 2002. **277**(33): p. 30183-90.
143. Johnstone, D.B. and L.B. Holzman, *Clinical impact of research on the podocyte slit diaphragm.* Nature Clinical Practice Nephrology, 2006. **2**(5): p. 271-282.

144. Doi, M., et al., *Recombinant human laminin-10 (alpha5beta1gamma1). Production, purification, and migration-promoting activity on vascular endothelial cells.* J Biol Chem, 2002. **277**(15): p. 12741-8.
145. Kreidberg, J.A., et al., *Alpha 3 beta 1 integrin has a crucial role in kidney and lung organogenesis.* Development, 1996. **122**(11): p. 3537-47.
146. Sachs, N., et al., *Kidney failure in mice lacking the tetraspanin CD151.* J Cell Biol, 2006. **175**(1): p. 33-9.
147. Pozzi, A., et al., *Beta1 integrin expression by podocytes is required to maintain glomerular structural integrity.* Dev Biol, 2008. **316**(2): p. 288-301.
148. Kanasaki, K., et al., *Integrin beta1-mediated matrix assembly and signaling are critical for the normal development and function of the kidney glomerulus.* Dev Biol, 2008. **313**(2): p. 584-93.
149. Blattner, S.M. and M. Kretzler, *Integrin-linked kinase in renal disease: connecting cell-matrix interaction to the cytoskeleton.* Curr Opin Nephrol Hypertens, 2005. **14**(4): p. 404-10.
150. Dai, C., et al., *Essential role of integrin-linked kinase in podocyte biology: Bridging the integrin and slit diaphragm signaling.* J Am Soc Nephrol, 2006. **17**(8): p. 2164-75.
151. Yang, Y., et al., *Formation and phosphorylation of the PINCH-1-integrin linked kinase-alpha-parvin complex are important for regulation of renal glomerular podocyte adhesion, architecture, and survival.* J Am Soc Nephrol, 2005. **16**(7): p. 1966-76.
152. El-Aouni, C., et al., *Podocyte-specific deletion of integrin-linked kinase results in severe glomerular basement membrane alterations and progressive glomerulosclerosis.* J Am Soc Nephrol, 2006. **17**(5): p. 1334-44.
153. Teixeira Vde, P., et al., *Functional consequences of integrin-linked kinase activation in podocyte damage.* Kidney Int, 2005. **67**(2): p. 514-23.
154. Sterk, L.M., et al., *Association of the tetraspanin CD151 with the laminin-binding integrins alpha3beta1, alpha6beta1, alpha6beta4 and alpha7beta1 in cells in culture and in vivo.* J Cell Sci, 2002. **115**(Pt 6): p. 1161-73.
155. Yauch, R.L., et al., *Highly stoichiometric, stable, and specific association of integrin alpha3beta1 with CD151 provides a major link to phosphatidylinositol 4-kinase, and may regulate cell migration.* Mol Biol Cell, 1998. **9**(10): p. 2751-65.
156. Regele, H.M., et al., *Glomerular expression of dystroglycans is reduced in minimal change nephrosis but not in focal segmental glomerulosclerosis.* J Am Soc Nephrol, 2000. **11**(3): p. 403-12.
157. Raats, C.J., et al., *Expression of agrin, dystroglycan, and utrophin in normal renal tissue and in experimental glomerulopathies.* Am J Pathol, 2000. **156**(5): p. 1749-65.
158. Wei, C., et al., *Modification of kidney barrier function by the urokinase receptor.* Nat Med, 2008. **14**(1): p. 55-63.
159. Eden, G., et al., *The urokinase receptor interactome.* Curr Pharm Des, 2011. **17**(19): p. 1874-89.

160. Ploug, M., et al., *Cellular receptor for urokinase plasminogen activator. Carboxyl-terminal processing and membrane anchoring by glycosyl-phosphatidylinositol.* J Biol Chem, 1991. **266**(3): p. 1926-33.
161. Wei, Y., et al., *Identification of the urokinase receptor as an adhesion receptor for vitronectin.* J Biol Chem, 1994. **269**(51): p. 32380-8.
162. Degryse, B., et al., *Domain 2 of the urokinase receptor contains an integrin-interacting epitope with intrinsic signaling activity: generation of a new integrin inhibitor.* J Biol Chem, 2005. **280**(26): p. 24792-803.
163. Zhang, B., et al., *The calcineurin-NFAT pathway allows for urokinase receptor-mediated beta3 integrin signaling to cause podocyte injury.* J Mol Med (Berl), 2012. **90**(12): p. 1407-20.
164. Kaplan, J.M., et al., *Mutations in ACTN4, encoding alpha-actinin-4, cause familial focal segmental glomerulosclerosis.* Nat Genet, 2000. **24**(3): p. 251-6.
165. Michaud, J.L., et al., *Focal and segmental glomerulosclerosis in mice with podocyte-specific expression of mutant alpha-actinin-4.* J Am Soc Nephrol, 2003. **14**(5): p. 1200-11.
166. Weins, A., et al., *Disease-associated mutant alpha-actinin-4 reveals a mechanism for regulating its F-actin-binding affinity.* Proc Natl Acad Sci U S A, 2007. **104**(41): p. 16080-5.
167. Dandapani, S.V., et al., *Alpha-actinin-4 is required for normal podocyte adhesion.* J Biol Chem, 2007. **282**(1): p. 467-77.
168. Mundel, P., et al., *Synaptopodin: an actin-associated protein in telencephalic dendrites and renal podocytes.* J Cell Biol, 1997. **139**(1): p. 193-204.
169. Asanuma, K., et al., *Synaptopodin regulates the actin-bundling activity of alpha-actinin in an isoform-specific manner.* J Clin Invest, 2005. **115**(5): p. 1188-98.
170. Asanuma, K., et al., *Synaptopodin orchestrates actin organization and cell motility via regulation of RhoA signalling.* Nat Cell Biol, 2006. **8**(5): p. 485-91.
171. Faul, C., et al., *The actin cytoskeleton of kidney podocytes is a direct target of the antiproteinuric effect of cyclosporine A.* Nat Med, 2008. **14**(9): p. 931-8.
172. de Vries, J.E., *The role of IL-13 and its receptor in allergy and inflammatory responses.* Journal of Allergy and Clinical Immunology, 1998. **102**(2): p. 165-169.
173. McKenzie, A.N., et al., *Structural comparison and chromosomal localization of the human and mouse IL-13 genes.* J Immunol, 1993. **150**(12): p. 5436-44.
174. Hilton, D.J., et al., *Cloning and characterization of a binding subunit of the interleukin 13 receptor that is also a component of the interleukin 4 receptor.* Proc Natl Acad Sci U S A, 1996. **93**(1): p. 497-501.
175. Andrews, A.L., et al., *Kinetic analysis of the interleukin-13 receptor complex.* J Biol Chem, 2002. **277**(48): p. 46073-8.
176. Donaldson, D.D., et al., *The murine IL-13 receptor alpha 2: molecular cloning, characterization, and comparison with murine IL-13 receptor alpha 1.* J Immunol, 1998. **161**(5): p. 2317-24.

177. Yasunaga, S., et al., *The negative-feedback regulation of the IL-13 signal by the IL-13 receptor alpha2 chain in bronchial epithelial cells.* Cytokine, 2003. **24**(6): p. 293-303.
178. Ohkuri, T., et al., *Expression of human IL-13 receptor [alpha]2 extracellular domain in Pichia pastoris.* Protein Expression and Purification, 2007. **56**(1): p. 48-53.
179. Fichtner-Feigl, S., et al., *IL-13 signaling through the IL-13alpha2 receptor is involved in induction of TGF-beta1 production and fibrosis.* Nat Med, 2006. **12**(1): p. 99-106.
180. Fichtner-Feigl, S., et al., *Restoration of tumor immunosurveillance via targeting of interleukin-13 receptor-alpha 2.* Cancer Res, 2008. **68**(9): p. 3467-75.
181. Hershey, G.K.K., *IL-13 receptors and signaling pathways: An evolving web.* Journal of Allergy and Clinical Immunology, 2003. **111**(4): p. 677-690.
182. Malefyt, R.d.W., et al., *Differential regulation of IL-13 and IL-4 production by human CD8+ and CD4+ Th0, Th1 and Th2 T cell clones and EBV-transformed B cells.* Int. Immunol., 1995. **7**(9): p. 1405-1416.
183. Zurawski, G. and J.E. de Vries, *Interleukin 13, an interleukin 4-like cytokine that acts on monocytes and B cells but not on T cells.* Immunol. Today, 1994. **15**: p. 19-26.
184. Orchansky, P.L., et al., *Characterization of the cytoplasmic domain of interleukin-13 receptor-alpha.* J Biol Chem, 1999. **274**(30): p. 20818-25.
185. Lin, J.X., et al., *The role of shared receptor motifs and common Stat proteins in the generation of cytokine pleiotropy and redundancy by IL-2, IL-4, IL-7, IL-13, and IL-15.* Immunity, 1995. **2**(4): p. 331-9.
186. Murata, T., et al., *Sharing of receptor subunits and signal transduction pathway between the IL-4 and IL-13 receptor system.* Int J Hematol, 1999. **69**(1): p. 13-20.
187. Doucet, C., et al., *IL-4 and IL-13 specifically increase adhesion molecule and inflammatory cytokine expression in human lung fibroblasts.* Int Immunol, 1998. **10**(10): p. 1421-33.
188. Oettgen, H.C. and R.S. Geha, *IgE regulation and roles in asthma pathogenesis.* J Allergy Clin Immunol, 2001. **107**(3): p. 429-40.
189. Horie, S., et al., *Interleukin-13 but not interleukin-4 prolongs eosinophil survival and induces eosinophil chemotaxis.* Intern Med, 1997. **36**(3): p. 179-85.
190. Luttmann, W., et al., *Activation of human eosinophils by IL-13. Induction of CD69 surface antigen, its relationship to messenger RNA expression, and promotion of cellular viability.* J Immunol, 1996. **157**(4): p. 1678-83.
191. Pope, S.M., et al., *IL-13 induces eosinophil recruitment into the lung by an IL-5- and eotaxin-dependent mechanism.* J Allergy Clin Immunol, 2001. **108**(4): p. 594-601.
192. de Vries, J.E., *The role of IL-13 and its receptor in allergy and inflammatory responses.* J Allergy Clin Immunol, 1998. **102**(2): p. 165-9.

193. Bochner, B.S., et al., *IL-13 selectively induces vascular cell adhesion molecule-1 expression in human endothelial cells.* J Immunol, 1995. **154**(2): p. 799-803.
194. Wills-Karp, M., *IL-12/IL-13 axis in allergic asthma.* J Allergy Clin Immunol, 2001. **107**(1): p. 9-18.
195. Li, L., et al., *Effects of Th2 cytokines on chemokine expression in the lung: IL-13 potently induces eotaxin expression by airway epithelial cells.* J Immunol, 1999. **162**(5): p. 2477-87.
196. Laoukili, J., et al., *IL-13 alters mucociliary differentiation and ciliary beating of human respiratory epithelial cells.* J Clin Invest, 2001. **108**(12): p. 1817-24.
197. Wills-Karp, M., et al., *Interleukin-13: central mediator of allergic asthma.* Science, 1998. **282**(5397): p. 2258-61.
198. Zhu, Z., et al., *Pulmonary expression of interleukin-13 causes inflammation, mucus hypersecretion, subepithelial fibrosis, physiologic abnormalities, and eotaxin production.* J Clin Invest, 1999. **103**(6): p. 779-88.
199. Grunig, G., et al., *Requirement for IL-13 independently of IL-4 in experimental asthma.* Science, 1998. **282**(5397): p. 2261-3.
200. Malefyt, R.D., et al., *Effects of IL-13 on Phenotype, Cytokine Production, and Cytotoxic Function of Human Monocytes - Comparison with IL-4 and Modulation by IFN-Gamma or IL-10.* Journal of Immunology, 1993. **151**(11): p. 6370-6381.
201. Cosentino, G., et al., *IL-13 Down-Regulates CD14 Expression and TNF-Alpha Secretion in Normal Human Monocytes.* Journal of Immunology, 1995. **155**(6): p. 3145-3151.
202. Scotton, C.J., et al., *Transcriptional profiling reveals complex regulation of the monocyte IL-1 beta system by IL-13.* Journal of Immunology, 2005. **174**(2): p. 834-845.
203. Chen, S.P., et al., *Childhood nephrotic syndrome in relapse is associated with down-regulation of monocyte CD14 expression and lipopolysaccharide-induced tumour necrosis factor-alpha production.* Clin Exp Immunol, 2003. **134**(1): p. 111-9.
204. Waga, S., et al., *Monocyte function in idiopathic nephrotic syndrome in childhood.* Tohoku J Exp Med, 1983. **141**(3): p. 295-303.
205. Davin, J.C., J.B. Foidart, and P.R. Mahieu, *Fc-receptor function in minimal change nephrotic syndrome of childhood.* Clin Nephrol, 1983. **20**(6): p. 280-4.
206. Garin, E.H. and K.P. Boggs, *Synergy of monocytes and lymphocytes from idiopathic minimal lesion nephrotic patients in relapse in the production of the supernatant factor that increases rat glomerular basement membrane sulfate uptake.* Int J Pediatr Nephrol, 1987. **8**(4): p. 187-92.
207. Takano, Y., et al., *Transcriptional suppression of nephrin in podocytes by macrophages: Roles of inflammatory cytokines and involvement of the PI3K/Akt pathway.* FEBS Letters, 2007. **581**(3): p. 421-426.
208. Huwiler, A., et al., *Inflammatory cytokines upregulate nephrin expression in human embryonic kidney epithelial cells and podocytes.* Biochem Biophys Res Commun, 2003. **305**(1): p. 136-42.

209. Niemir, Z.I., et al., *Podocytes are the major source of IL-1 alpha and IL-1 beta in human glomerulonephritides.* Kidney Int, 1997. **52**(2): p. 393-403.
210. Parry, R.G., K.M. Gillespie, and P.W. Mathieson, *Effects of type 2 cytokines on glomerular epithelial cells.* Exp Nephrol, 2001. **9**(4): p. 275-83.
211. Van Den Berg, J.G., et al., *Interleukin-4 and interleukin-13 act on glomerular visceral epithelial cells.* J Am Soc Nephrol, 2000. **11**(3): p. 413-22.
212. Aten, J., et al., *Strong and selective glomerular localization of CD134 ligand and TNF receptor-1 in proliferative lupus nephritis.* J Am Soc Nephrol, 2000. **11**(8): p. 1426-38.
213. Bruggeman, L.A., et al., *TNFR2 interposes the proliferative and NF-kappaB-mediated inflammatory response by podocytes to TNF-alpha.* Lab Invest. **91**(3): p. 413-25.
214. Van Den Berg, J.G., et al., *Interleukin-4 and -13 promote basolateral secretion of H(+) and cathepsin L by glomerular epithelial cells.* Am J Physiol Renal Physiol, 2002. **282**(1): p. F26-33.
215. Lai, K.W., et al., *Overexpression of interleukin-13 induces minimal change-like nephropathy in rats and is associated with increased B7-1 expression in the glomeruli.* Journal of Investigative Medicine, 2006. **54**(1): p. S139-S139.
216. Lai, K.-W., et al., *Overexpression of Interleukin-13 Induces Minimal-Change-Like Nephropathy in Rats.* J Am Soc Nephrol, 2007. **18**(5): p. 1476-1485.
217. Reiser, J. and P. Mundel, *Danger signaling by glomerular podocytes defines a novel function of inducible B7-1 in the pathogenesis of nephrotic syndrome.* J Am Soc Nephrol, 2004. **15**(9): p. 2246-8.
218. Reiser, J., et al., *Induction of B7-1 in podocytes is associated with nephrotic syndrome.* J. Clin. Invest., 2004. **113**(10): p. 1390-1397.
219. Garin, E.H., et al., *Urinary CD80 Excretion Increases in Idiopathic Minimal-Change Disease.* J Am Soc Nephrol, 2009. **20**(2): p. 260-266.
220. Garin, E.H., et al., *Urinary CD80 is elevated in minimal change disease but not in focal segmental glomerulosclerosis.* Kidney Int, 2010. **78**(3): p. 296-302.
221. Nickoloff, J.A., *Animal cell electroporation and electrofusion protocols*. Methods in molecular biology. 1995, Totowa, N.J.: Humana Press. xx, 369 p.
222. Allain, C.C., et al., *Enzymatic determination of total serum cholesterol.* Clin Chem, 1974. **20**(4): p. 470-5.
223. Archibald, R.M., *Reactions of creatinine with alkaline picrate.* J Biol Chem, 1962. **237**: p. 612.
224. Crowther, J., *Stages in ELISA*, in *The Elisa Guidebook*. 2000, Humana Press. p. 45-82.
225. Kreisberg, J.I., R.L. Hoover, and M.J. Karnovsky, *Isolation and characterization of rat glomerular epithelial cells in vitro.* Kidney Int, 1978. **14**(1): p. 21-30.
226. Chua, S.W., et al., *A novel normalization method for effective removal of systematic variation in microarray data.* Nucleic Acids Res, 2006. **34**(5): p. e38.

227. Eisen, M.B., et al., *Cluster analysis and display of genome-wide expression patterns.* Proc Natl Acad Sci U S A, 1998. **95**(25): p. 14863-8.
228. Huang da, W., B.T. Sherman, and R.A. Lempicki, *Systematic and integrative analysis of large gene lists using DAVID bioinformatics resources.* Nat Protoc, 2009. **4**(1): p. 44-57.
229. Huang da, W., B.T. Sherman, and R.A. Lempicki, *Bioinformatics enrichment tools: paths toward the comprehensive functional analysis of large gene lists.* Nucleic Acids Res, 2009. **37**(1): p. 1-13.
230. Saleem, M.A., et al., *A conditionally immortalized human podocyte cell line demonstrating nephrin and podocin expression.* J Am Soc Nephrol, 2002. **13**(3): p. 630-8.
231. O'Hare, M.J., et al., *Conditional immortalization of freshly isolated human mammary fibroblasts and endothelial cells.* Proc Natl Acad Sci U S A, 2001. **98**(2): p. 646-51.
232. Hsu, H.H., et al., *Mechanisms of angiotensin II signaling on cytoskeleton of podocytes.* J Mol Med, 2008. **86**(12): p. 1379-94.
233. Somlo, S. and P. Mundel, *Getting a foothold in nephrotic syndrome.* Nat Genet, 2000. **24**(4): p. 333-5.
234. Kerjaschki, D., *Caught flat-footed: podocyte damage and the molecular bases of focal glomerulosclerosis.* J Clin Invest, 2001. **108**(11): p. 1583-7.
235. Greka, A. and P. Mundel, *Cell biology and pathology of podocytes.* Annu Rev Physiol, 2012. **74**: p. 299-323.
236. Farquhar, M.G., R.L. Vernier, and R.A. Good, *An electron microscope study of the glomerulus in nephrosis, glomerulonephritis, and lupus erythematosus.* J Exp Med, 1957. **106**(5): p. 649-60.
237. Brunskill, E.W., et al., *Defining the molecular character of the developing and adult kidney podocyte.* PLoS One. **6**(9): p. e24640.
238. Kabgani, N., et al., *Primary cultures of glomerular parietal epithelial cells or podocytes with proven origin.* PLoS One. **7**(4): p. e34907.
239. Takemoto, M., et al., *Large-scale identification of genes implicated in kidney glomerulus development and function.* EMBO J, 2006. **25**(5): p. 1160-74.
240. Tipping, P.G., *Are podocytes passive or provocative in proteinuric glomerular pathology?* J Am Soc Nephrol, 2008. **19**(4): p. 651-3.
241. Banas, M.C., et al., *TLR4 Links Podocytes with the Innate Immune System to Mediate Glomerular Injury.* J Am Soc Nephrol, 2008. **19**(4): p. 704-713.
242. Kriz, W., et al., *Stability and leakiness: opposing challenges to the glomerulus.* Kidney Int, 1996. **49**(6): p. 1570-4.
243. Kriz, W., et al., *Structure-stabilizing forces in the glomerular tuft.* J Am Soc Nephrol, 1995. **5**(10): p. 1731-9.
244. Neumann-Haefelin, E., et al., *A model organism approach: defining the role of Neph proteins as regulators of neuron and kidney morphogenesis.* Hum Mol Genet, 2010. **19**(12): p. 2347-59.
245. Blasutig, I.M., et al., *Phosphorylated YDXV motifs and Nck SH2/SH3 adaptors act cooperatively to induce actin reorganization.* Mol Cell Biol, 2008. **28**(6): p. 2035-46.

246. Li, H., et al., *Rat nephrin modulates cell morphology via the adaptor protein Nck.* Biochem Biophys Res Commun, 2006. **349**(1): p. 310-6.
247. New, L.A., A. Keyvani Chahi, and N. Jones, *Direct regulation of nephrin tyrosine phosphorylation by Nck adaptor proteins.* J Biol Chem, 2013. **288**(3): p. 1500-10.
248. Arias, L.F., B.E. Vieco, and A.A. Arteta, *[Expression of nephrin, podocin and a-actinine-4 in renal tissue of patients with proteinuria].* Nefrologia, 2009. **29**(6): p. 569-75.
249. Ostalska-Nowicka, D., et al., *Ezrin--a useful factor in the prognosis of nephrotic syndrome in children: an immunohistochemical approach.* J Clin Pathol, 2006. **59**(9): p. 916-20.
250. Chen, F., *JUNB (jun B proto-oncogene)*, in *Atlas Genet Cytogenet Oncol Haematol.*, J.-L. Huret, Editor. 2003, INIST-CNRS.
251. Kallunki, T., et al., *c-Jun can recruit JNK to phosphorylate dimerization partners via specific docking interactions.* Cell, 1996. **87**(5): p. 929-39.
252. Li, B., et al., *Regulation of IL-4 expression by the transcription factor JunB during T helper cell differentiation.* EMBO J, 1999. **18**(2): p. 420-32.
253. Hock, T.D., et al., *JunB and JunD regulate human heme oxygenase-1 gene expression in renal epithelial cells.* J Biol Chem, 2007. **282**(9): p. 6875-86.
254. Shimizu, M., et al., *Glomerular proteinuria induces heme oxygenase-1 gene expression within renal epithelial cells.* Pediatr Res, 2005. **58**(4): p. 666-71.
255. Etienne-Manneville, S. and A. Hall, *Rho GTPases in cell biology.* Nature, 2002. **420**(6916): p. 629-635.
256. Hall, A. and C.D. Nobes, *Rho GTPases: molecular switches that control the organization and dynamics of the actin cytoskeleton.* Philos Trans R Soc Lond B Biol Sci, 2000. **355**(1399): p. 965-70.
257. Hall, A., *Rho GTPases and the Actin Cytoskeleton.* Science, 1998. **279**(5350): p. 509-514.
258. Bustelo, X.R., *Regulatory and signaling properties of the Vav family.* Mol Cell Biol, 2000. **20**(5): p. 1461-77.
259. Katzav, S., *Vav: Captain Hook for signal transduction?* Crit Rev Oncog, 1995. **6**(2): p. 87-97.
260. Lu, T.C., et al., *HIV-1 Nef disrupts the podocyte actin cytoskeleton by interacting with diaphanous interacting protein.* J Biol Chem, 2008. **283**(13): p. 8173-82.
261. Read, S., V. Malmstrom, and F. Powrie, *Cytotoxic T lymphocyte-associated antigen 4 plays an essential role in the function of CD25(+)CD4(+) regulatory cells that control intestinal inflammation.* J Exp Med, 2000. **192**(2): p. 295-302.
262. Takahashi, T., et al., *Immunologic self-tolerance maintained by CD25(+)CD4(+) regulatory T cells constitutively expressing cytotoxic T lymphocyte-associated antigen 4.* J Exp Med, 2000. **192**(2): p. 303-10.
263. Linsley, P.S., et al., *Coexpression and functional cooperation of CTLA-4 and CD28 on activated T lymphocytes.* J Exp Med, 1992. **176**(6): p. 1595-604.

264. Manzotti, C.N., et al., *Integration of CD28 and CTLA-4 function results in differential responses of T cells to CD80 and CD86.* Eur J Immunol, 2006. **36**(6): p. 1413-22.
265. Collins, A.V., et al., *The interaction properties of costimulatory molecules revisited.* Immunity, 2002. **17**(2): p. 201-10.
266. Wei, B., et al., *CTL-associated antigen-4 ligation induces rapid T cell polarization that depends on phosphatidylinositol 3-kinase, Vav-1, Cdc42, and myosin light chain kinase.* J Immunol, 2007. **179**(1): p. 400-8.
267. Ishimoto, T., et al., *Toll-like receptor 3 ligand, polyIC, induces proteinuria and glomerular CD80, and increases urinary CD80 in mice.* Nephrol Dial Transplant, 2013. **28**(6): p. 1439-46.
268. Endlich, N., et al., *Analysis of differential gene expression in stretched podocytes: osteopontin enhances adaptation of podocytes to mechanical stress.* Faseb J, 2002. **16**(13): p. 1850-2.
269. Han, S.H., et al., *Gene expression patterns in glucose-stimulated podocytes.* Biochem Biophys Res Commun, 2008. **370**(3): p. 514-8.
270. Salojin, K.V., J. Zhang, and T.L. Delovitch, *TCR and CD28 are coupled via ZAP-70 to the activation of the Vav/Rac-1-/PAK-1/p38 MAPK signaling pathway.* J Immunol, 1999. **163**(2): p. 844-53.
271. Nunes, J.A., et al., *The role of p21ras in CD28 signal transduction: triggering of CD28 with antibodies, but not the ligand B7-1, activates p21ras.* J Exp Med, 1994. **180**(3): p. 1067-76.
272. Gulbins, E., et al., *Tyrosine kinase-stimulated guanine nucleotide exchange activity of Vav in T cell activation.* Science, 1993. **260**(5109): p. 822-5.
273. Lopez-Lago, M., et al., *Tyrosine phosphorylation mediates both activation and downmodulation of the biological activity of Vav.* Mol Cell Biol, 2000. **20**(5): p. 1678-91.
274. Ksionda, O., et al., *Mechanism and function of Vav1 localisation in TCR signalling.* J Cell Sci, 2012. **125**(Pt 22): p. 5302-14.
275. Hornstein, I., A. Alcover, and S. Katzav, *Vav proteins, masters of the world of cytoskeleton organization.* Cell Signal, 2004. **16**(1): p. 1-11.
276. Tybulewicz, V.L., *Vav-family proteins in T-cell signalling.* Curr Opin Immunol, 2005. **17**(3): p. 267-74.
277. Gomez, T.S., et al., *Dynamin 2 regulates T cell activation by controlling actin polymerization at the immunological synapse.* Nat Immunol, 2005. **6**(3): p. 261-70.
278. Houlard, M., et al., *Characterization of VIK-1: a new Vav-interacting Kruppel-like protein.* Oncogene, 2005. **24**(1): p. 28-38.
279. Tybulewicz, V.L., et al., *Vav1: a key signal transducer downstream of the TCR.* Immunol Rev, 2003. **192**: p. 42-52.
280. Miller, S.L., et al., *Novel association of Vav2 and Nek3 modulates signaling through the human prolactin receptor.* Mol Endocrinol, 2005. **19**(4): p. 939-49.
281. Movilla, N. and X.R. Bustelo, *Biological and regulatory properties of Vav-3, a new member of the Vav family of oncoproteins.* Mol Cell Biol, 1999. **19**(11): p. 7870-85.

282. Crespo, P., et al., *Phosphotyrosine-dependent activation of Rac-1 GDP/GTP exchange by the vav proto-oncogene product.* Nature, 1997. **385**(6612): p. 169-72.
283. Schuebel, K.E., et al., *Phosphorylation-dependent and constitutive activation of Rho proteins by wild-type and oncogenic Vav-2.* EMBO J, 1998. **17**(22): p. 6608-21.
284. Han, J., et al., *Lck regulates Vav activation of members of the Rho family of GTPases.* Mol Cell Biol, 1997. **17**(3): p. 1346-53.
285. Gao, C., et al., *Beta3 tyrosine phosphorylation and alphavbeta3-mediated adhesion are required for Vav1 association and Rho activation in leukocytes.* J Biol Chem, 2005. **280**(15): p. 15422-9.
286. Ridley, A.J. and A. Hall, *The small GTP-binding protein rho regulates the assembly of focal adhesions and actin stress fibers in response to growth factors.* Cell, 1992. **70**(3): p. 389-99.
287. Nobes, C.D. and A. Hall, *Rho, rac, and cdc42 GTPases regulate the assembly of multimolecular focal complexes associated with actin stress fibers, lamellipodia, and filopodia.* Cell, 1995. **81**(1): p. 53-62.
288. Ridley, A.J., et al., *The small GTP-binding protein rac regulates growth factor-induced membrane ruffling.* Cell, 1992. **70**(3): p. 401-10.
289. Kozma, R., et al., *The Ras-related protein Cdc42Hs and bradykinin promote formation of peripheral actin microspikes and filopodia in Swiss 3T3 fibroblasts.* Mol Cell Biol, 1995. **15**(4): p. 1942-52.
290. Togawa, A., et al., *Progressive impairment of kidneys and reproductive organs in mice lacking Rho GDIalpha.* Oncogene, 1999. **18**(39): p. 5373-80.
291. Shibata, S., et al., *Modification of mineralocorticoid receptor function by Rac1 GTPase: implication in proteinuric kidney disease.* Nat Med, 2008. **14**(12): p. 1370-6.
292. Blattner, S.M., et al., *Divergent functions of the Rho GTPases Rac1 and Cdc42 in podocyte injury.* Kidney Int, 2013.
293. Kupfer, A., G. Dennert, and S.J. Singer, *Polarization of the Golgi apparatus and the microtubule-organizing center within cloned natural killer cells bound to their targets.* Proc Natl Acad Sci U S A, 1983. **80**(23): p. 7224-8.
294. Dustin, M.L. and J.A. Cooper, *The immunological synapse and the actin cytoskeleton: molecular hardware for T cell signaling.* Nat Immunol, 2000. **1**(1): p. 23-9.
295. Kupfer, A. and G. Dennert, *Reorientation of the microtubule-organizing center and the Golgi apparatus in cloned cytotoxic lymphocytes triggered by binding to lysable target cells.* J Immunol, 1984. **133**(5): p. 2762-6.
296. Lowin-Kropf, B., V.S. Shapiro, and A. Weiss, *Cytoskeletal polarization of T cells is regulated by an immunoreceptor tyrosine-based activation motif-dependent mechanism.* J Cell Biol, 1998. **140**(4): p. 861-71.
297. Chambers, C.A., T.J. Sullivan, and J.P. Allison, *Lymphoproliferation in CTLA-4-deficient mice is mediated by costimulation-dependent activation of CD4+ T cells.* Immunity, 1997. **7**(6): p. 885-95.
298. Alegre, M.L., K.A. Frauwirth, and C.B. Thompson, *T-cell regulation by CD28 and CTLA-4.* Nat Rev Immunol, 2001. **1**(3): p. 220-8.

299. Rudd, C.E. and H. Schneider, *Unifying concepts in CD28, ICOS and CTLA4 co-receptor signalling.* Nat Rev Immunol, 2003. **3**(7): p. 544-56.
300. Turner, M. and D.D. Billadeau, *VAV proteins as signal integrators for multi-subunit immune-recognition receptors.* Nat Rev Immunol, 2002. **2**(7): p. 476-86.
301. Shimada, M., et al., *Minimal change disease: a "two-hit" podocyte immune disorder?* Pediatr Nephrol, 2011. **26**(4): p. 645-9.
302. Marinkovic, G., et al., *Immunosuppressive drug azathioprine reduces aneurysm progression through inhibition of Rac1 and c-Jun-terminal-N-kinase in endothelial cells.* Arterioscler Thromb Vasc Biol, 2013. **33**(10): p. 2380-8.
303. Poppe, D., et al., *Azathioprine suppresses ezrin-radixin-moesin-dependent T cell-APC conjugation through inhibition of Vav guanosine exchange activity on Rac proteins.* J Immunol, 2006. **176**(1): p. 640-51.
304. Ishimoto, T., et al., *Minimal change disease: a CD80 podocytopathy?* Semin Nephrol, 2011. **31**(4): p. 320-5.

APPENDICES

Appendix 2.1: Protocol for rat urine albumin ELISA

1. Coat 96 well microtiter plate (Corning, MA, USA) with 100µl of rabbit antiserum to rat albumin antibody (MP Biomedicals, CA, USA) diluted 1/2000 in 0.1M carbonate buffer, 4°C, overnight.
2. Thoroughly aspirate and discard the coating antibody and wash with 3 changes of 400µl of 1X PBS.
3. Blocking with 100µl of 1% BSA in 1X PBS with 0.05% Tween 20 for 45 minutes, room temperature.
4. Thoroughly aspirate and discard the blocking solution. Do not wash.
5. Add 50µl of standards, diluted urine samples and diluent, as blank, to each well in triplicate. Incubate for 2 hours, 37°C.
6. Thoroughly aspirate and discard the liquid and wash with 3 changes of 400µl of 1X PBS.
7. Incubate with 50µl of HRP-conjugated sheep polyclonal antibody to rat albumin (MP Biomedicals, CA, USA), diluted 1/20000 in 1% BSA in 1X PBS with 0.05% Tween 20, for 1 hour at 37°C.
8. Thoroughly aspirate and discard the detecting antibody and wash with 4 changes of 400µl of 1X PBS.
9. Add 50µl of 0.05% OPD substrate (MP Biomedicals, CA, USA) in each well and incubate for 10 minutes at room temperature in dark.
10. Stop reaction with 60µl of 4.5 N sulphuric acid. Gently mix and incubate for 5 minutes.
11. Read the absorbance at 490 nm using a microplate reader.

Preparation of standards:

- Rat albumin (MP Biomedicals, CA, USA) stock solution = 20mg/ml
- Diluent = 0.05% Tween 20 in 1X PBS
- Dilute the 20 mg/ml stock solution 1/100 to final concentration of 200µg/ml: 10µl of stock solution + 990µl of diluent
- Dilute the 200µg/ml rat albumin solution 1/100 to 2µg/ml: 50µl of 200µg/ml rat albumin solution + 4950µl of diluent

- Make a 2X standard serial dilutions from the 2µg/ml rat albumin solution
- Concentration of standards: 2000, 1000, 500, 250, 125, 62.5, 31.25, 15.625 ng/ml

Dilution of urine samples:

- Dilute the urine samples 1/10: 50µl of urine sample + 450µl of diluent.
- Further serial dilute the urine samples ranging from 1/10 to 1/100 as shown in the table below.

Dilution factor (Final dilution)	Volume from first dilution/ µl	Volume of diluent/ µl
1/10 (1/100)	20	180
1/20 (1/200)	15	285
1/30 (1/300)	15	435
1/40 (1/400)	15	585
1/50 (1/500)	15	735
1/60 (1/600)	15	885
1/70 (1/700)	15	1035
1/80 (1/800)	15	1185
1/90 (1/900)	15	1335
1/100 (1/1000)	15	1485

Reagent preparation:

<u>0.1M Sodium carbonate buffer, pH 9.6:</u>

0.2M Sodium carbonate (Na_2CO_3)	8ml
0.2M Sodium bicarbonate ($NaHCO_3$)	17ml
ddH_2O	25ml

<u>0.2M Sodium carbonate (Na_2CO_3):</u>

Sodium carbonate (Na_2CO_3)	21.2g
ddH_2O	1000ml

<u>0.2M Sodium bicarbonate ($NaHCO_3$):</u>

Sodium bicarbonate ($NaHCO_3$)	16.8g
ddH_2O	1000ml

Blocking solution:

1X PBS	50ml
BSA	0.5g
Tween 20	25µl

Diluent for standards and urine samples:

1X PBS	500ml
Tween 20	250µl

OPD substrate:

Phosphate-citrate buffer, pH 5.0	6ml
OPD (o-Diphenylenediamine)	300µl
30% H_2O_2*	3µl

*Add the H_2O_2 just before use.

Phosphate-Citrate buffer pH 5.0 for OPD substrate:

0.1M Citrate buffer	24.3ml
0.2M Phosphate buffer	25.7ml
ddH_2O	50ml

0.1M Citrate buffer:

Citric acid	3.84g
ddH_2O	200ml

0.2M Phosphate buffer:

Na_2HPO_4 (anhydrous)	5.68g
ddH_2O	200ml

Appendix 2.2: Protocol for RNA cleanup using RNeasy® Kit (RNeasy® Mini Handbook, 4th Edition, 09/2010)

1. Adjust the sample to final volume of 100µl with RNase-free water.
2. Add 350µl Buffer RLT, and mix well.
3. Add 250µl absolute ethanol to the mixture and mix well by pipetting.
4. Transfer all the sample to an RNeasy Mini spin column placed in a 2 ml collection tube supplied. Close the lid, and centrifuge for 15s at 13,000rpm. Discard the flow-through.
5. Add 350µl of Buffer RW1 to the RNeasy spin column. Close the lid, and centrifuge for 15s at 13,000rpm. Discard the flow-through.
6. Add 10µl of DNase I stock solution to 70µl Buffer RDD. Mix by gently inverting the tube, and centrifuge briefly to collect residual liquid from the sides of the tube.
7. Add the DNase I incubation mix (80µl) directly to the RNeasy spin column membrane, and incubate at room temperature for 15 minutes.
8. Add 350µl of Buffer RW1 to the RNeasy spin column. Close the lid, and centrifuge for 15s at 13,000rpm. Discard the flow-through.
9. Add 500µl of Buffer RPE to the RNeasy spin column. Close the lid, and centrifuge for 15s at 13,000rpm. Discard the flow-through.
10. Add 500µl of Buffer RPE to the RNeasy spin column. Close the lid, and centrifuge for 2 minutes at 13,000rpm. Discard the flow-through.
11. Place the RNeasy spin column in a new 2ml collection tube (supplied) and discard the old collection tube with the flow-through. Close the lid gently, and centrifuge at 13,000rpm for 1 minute.
12. Place the RNeasy spin column in a new 1.5ml collection tube (supplied). Add 30µl of RNase-free water directly to the spin column membrane. Close the lid gently, and centrifuge for 1 minute at 13,000rpm to elute the RNA.
13. Repeat step 12 using the eluate from step 12 for high RNA concentration. Reuse the collection tube from step 12.

Reagent preparation:

Buffer RPE working solution:

Buffer RPE is supplied as a concentrate. Before using for the first time, add 4 volumes of absolute ethanol as indicated on the bottle to obtain a working solution.

DNase I stock solution:

Prepare DNase I stock solution before using the RNase-Free DNase Set for the first time. Dissolve the lyophilized DNase I (1500 Kunitz units) by injecting 550µl of the RNase free water provided using RNase-free needle and syringe. Mix gently by inverting the vial. Do not vortex. Aliquot the stock solution into single-use volume and store at –20°C.

Appendix 2.3: Protocol for cRNA hybridization and array scanning (Illumina® Whole-Genome Expression for BeadStation)

Hybridization:

Preheat the oven (with rocking platform) to 58°C.

Mix with Hyb Reagents:

1. Add up to 5µl of RNase free water to 750ng cRNA, and mix.
2. Incubate at room temperature for 10 minutes to resuspend cRNA.
3. Place the HYB and HCB bottles in the 58°C oven for 10 minutes to dissolve any salt precipitation. Cool to room temperature and mix thoroughly before use.
4. Add 10µl of HYB to each cRNA sample.

Set up Hybridization:

1. Place Illumina Hyb Chamber Gaskets into BeadChip Hyb Chamber.
2. Dispense 200µl of HCB into each of the two humidifying buffer reservoirs in each Hyb Chamber. Only add buffer to chambers that will be used.
3. Seal Hyb Chamber with lid and keep on bench at room temperature until ready to load BeadChips into Hyb Chamber.
4. Remove all BeadChips from their packages. (3 fingers at the notches to release)
5. Holding BeadChip by coverseal tab with tweezers using powder-free gloved hands, slide BeadChip into Hyb Chamber Insert such that the barcode lines up with barcode symbol on the Insert.
6. Preheat the assay sample at 65°C for 5 minutes.
7. Briefly vortex, then briefly centrifuge to collect the liquid in the bottom of the tube. Allow sample to cool to room temperature before using. Pipet sample immediately after cooling to room temperature.
8. Dispense 15µl of assay sample onto the large sample port of each array, ensuring pipet tip does not touch array.
9. Load Hyb Chamber Inserts containing BeadChips into the Hyb Chamber with rocker speed at 5.

10. Seal lid onto the Hyb Chamber by applying the back of the lid first and then bringing it down to the front to avoid dislodging the Hyb Chamber Insert(s).
11. Incubate for 18.5 hours at 58°C.

Prepare for High-Temp Wash & Overnight Incubation:

1. Prepare 1X High-Temp Wash buffer by adding 50ml of 10X stock to 450ml of RNAse free water.
2. Place waterbath insert into heat block, and add 500ml of 1X High-Temp Wash buffer.
3. Set heat block temperature to 55°C and pre-warm High-Temp Wash buffer to that temperature overnight.

Prepare Reagents:

1. The next day, prepare Wash E1BC solution by adding 3ml of E1BC buffer to 1L of RNase free water.
2. Pre-warm Block E1 buffer (4ml/chip) to room temperature.

Room-Temperature Incubation:

1. Remove Hyb Chamber from oven and disassemble. (Observe for bubbles, if any, and locate them on the tracking sheet).
2. Remove coverseal in a zig-zag manner in a container with 1L of Wash E1BC solution. Using tweezers or powder-free gloved hands, place the BeadChip into the slide rack submerged in the staining dish containing 250ml of Wash E1BC solution.
3. Using the slide rack handle, transfer the rack into the Hybex Waterbath insert containing High-Temp Wash buffer.

High-Temp Wash:

Incubate static for 10 minutes with the Hybex lid closed.

1st Room-Temp Wash:

1. During the 10 minutes High-Temp Wash buffer incubation, add fresh 250ml of Wash E1BC solution to a clean staining dish.
2. After the 10 minutes High-Temp Wash buffer incubation is complete, immediately transfer the slide rack into the above prepared staining dish.
3. Briefly agitate using rack, then shake on orbital shaker for 5 minutes at 110rpm.

Ethanol Wash:

Transfer rack to a clean staining dish containing 250ml of absolute ethanol. Briefly agitate using rack handle, then shake on orbital shaker for 10 minutes at 110rpm.

2nd Room-Temp Wash:

Transfer rack to a clean staining dish containing fresh 250ml of Wash E1BC solution. Briefly agitate using rack handle, then shake on orbital shaker for 2 minutes at 110rpm.

Block:

1. Pipette 4ml of Block E1 buffer into the Wash Tray(s).
2. Transfer the BeadChip, face up into BeadChip Wash Tray(s) on rocker.
3. Rock at medium speed for 10 minutes.
4. Prepare Block E1 buffer (cloudy looking, normal) (2 ml/chip) with streptavidin-Cy3 (2µl of 1mg/ml stock per chip). Use a single conical tube for all BeadChips. Store in dark until detection step.

Detect:

1. Pipette 2ml of Block E1 buffer + streptavidin-Cy3 into fresh Wash Tray(s).
2. Transfer the BeadChip, face up into Wash Tray(s) on rocker.
3. Place cover on tray and rock at medium speed for 10 minutes.

3rd Room-Temp Wash:

1. Add 250ml of Wash E1BC solution to a clean staining dish.

2. Transfer the BeadChip to the slide rack submerged in the staining dish.
3. Briefly agitate using rack, and then shake at room temperature on orbital shaker for 5 minutes.

Dry:

1. Prepare centrifuge with plateholders, paper towels and balance rack. Set speed to 270rcf.
2. Transfer rack of BeadChips from staining dish to centrifuge and spin at room temperature for 4 minutes.
3. Store dry chips in slide box until scanned.

Scanning:

Scan the arrays with scan factor 1.5, PMT 551 using Illumina® BeadArray Reader. Ensure the signal is strong enough, i.e. green colour on the slot instead of red. Check that all the housekeeping genes and other parameters are normal.

Appendix 2.4: Protocol for single-stranded cDNA synthesis using Superscript III First-Strand Synthesis System for RT-PCR

Single-stranded cDNA was synthesized from 150ng of total RNA using the Superscript III First-Strand Synthesis System for RT-PCR (Invitrogen Life Technologies, CA, USA), according to the manufacturer's instructions. The initial reaction mixture for cDNA conversion was prepared as shown below.

Reagent	Volume for 1 reaction
50pmol Oligo(dT)	1µl
10mM dNTP	1µl
150ng total RNA	Variable
DEPC-treated water	Top up to 13µl
Final Volume	13 µl

The mixture was incubated at 65 ºC for 5 minutes followed by incubation at 4ºC for at least 1 minute. A second reaction mixture was prepared as shown in the table below and added to each tube and mixed by gentle pipetting. All tubes were incubated at 50ºC for 1 hour, followed by inactivation at 70 ºC for 15 minutes and cooling at 4ºC.

Reagent	Volume for 1 reaction
5X First Strand Buffer	4µl
0.1M DTT	1µl
RNaseOUT recombinant RNase Inhibitor (40U/µl)	1µl
Superscript III Reverse Transcriptase (200U/µl)	1µl
Final Volume	7 µl

Appendix 2.5: Protocol for plasmid standard curve generation

Polymerase chain reaction (PCR) was carried out using podocyte cDNA and specific primer sequences as shown in the table below to obtain the genes of interest. The reactions were run at 95°C for 5 minutes, followed by 40 amplification cycles of 95°C for 30 seconds, annealing temperature of 58°C for 30 seconds and 72°C for 30 seconds. A final 9 minutes of extension at 72°C was performed after the last amplification cycle, followed by cooling at 4°C.

Nucleotide sequence of primers for the respective genes of interest in rat glomeruli.

Gene Accession no.	Primers	Nucleotide sequence 5' - 3'	bp
Rat vav1	Forward	5'- GGGTGAAAGATACAGCGGAA -3'	234
NM_012759	Reverse	5'- GCTTGTTGATGGCTCTCCTC -3'	
Rat Kirrel2	Forward	5'- TCTGTGTCTCTGGTTGCTGG -3'	169
XM_218486	Reverse	5'- AGGTGTTTTCAACTGTCCCG -3'	
Rat Cdh11	Forward	5'- CTTTGCAGCAGAAATCCACA -3'	299
XM_001059464	Reverse	5'- CACGTCGGGCATATACTCCT -3'	
Rat Nck2	Forward	5'- TCCACAGATCAGCTACACCG -3'	184
NM_001108216	Reverse	5'- TGATGCTTTGAGAGACACGG -3'	
Rat Magi2	Forward	5'- CGAGAGTGTCATTGGCAGAA -3'	228
NM_053621	Reverse	5'- GGGTCCTTGCAGTGTTTGAT -3'	
Rat Actn4	Forward	5'- AGTGGGATAACCTGGGCTCT -3'	227
NM_031675	Reverse	5'- GGTGGACTTGAACTGGTCGT -3'	
Rat Ctnnal1	Forward	5'- GTGTGGAGGACTTCACCGAT -3'	253
NM_001106649	Reverse	5'- TGGAATTTTAACAGGTCGGC -3'	
Rat Itga3	Forward	5'- AGGGACCTTAGGGCACATCT -3'	179
NM_001108292	Reverse	5'- TTCACAGTCTTCATGGCAGC -3'	
Rat Ptpro	Forward	5'- CTTGGAGAGGGAAGGGAAA -3'	281
NM_017336	Reverse	5'- GATCTGCAGCAAAGTGTGGA -3'	
Rat Ezr	Forward	5'- AAGATGACAAGTTGACCCCG -3'	187
NM_019357	Reverse	5'- ATGTACAGCTCGTGGTTCCC -3'	
Rat Junb	Forward	5'- GCAGCTACTTTTCGGGTCAG -3'	247
NM_021836	Reverse	5'- TGGTTCATCTTGTGCAGGTC -3'	
Rat GAPDH	Forward	5'- GGTGATGCTGGTGCTGAGTA-3'	273
NM_017008	Reverse	5'- GACTGTGGTCATGAGCCCTT-3'	

Nucleotide sequence of primers for the respective genes of interest in human podocytes.

Gene Accession No.	Primers	Nucleotide sequence 5' - 3'	bp
GAPDH NM_002046.3	Forward	5' – CTGGCATGGCCTTCCGTGTC – 3'	194
	Reverse	5' – GGAGGAGTGGGTGTCGCTGT – 3'	
B7.1 NM_005191.3	Forward	5' – CACGGAGGCAGGGAACATCA – 3'	183
	Reverse	5' – AGATGCGAGTTTGTGCCAGC – 3'	
Nephrin NM_004646.3	Forward	5' – GAGCACCCCACTCCCCTAAC – 3'	212
	Reverse	5' – GCAGACACGTTGGCAATGGT – 3'	
Podocin NM_014625.2	Forward	5' – CAGGACTCCGCACAAGGAGA – 3'	159
	Reverse	5' – ACCTCATCCACGTCCACCAC – 3'	
dystroglycan NM_004393.4	Forward	5' – AGGATGTCTGTGGGCCTCTC – 3'	240
	Reverse	5' – GGTCACTCGAAATGAGCGCC – 3'	
IL-4R NM_000418.2	Forward	5' – CCTGGAGCCAAGTCCTCCTG – 3'	200
	Reverse	5' – CACAGGGCATCTCGGGTTCT – 3'	
IL-13Rα1 NM_001560.2	Forward	5' – GCTCCGGAAACTCGTCGTTC – 3'	187
	Reverse	5' – AGCTCAGGTTGTGCCAAATGC – 3'	
IL-13Rα2 NM_000640.2	Forward	5' – CAATGGCAACCCCCACTGTC – 3'	186
	Reverse	5' – GCATTGCCATGGTAAAAGCGTG – 3'	
Vav1 NM_005428.2	Forward	5' – CCCTGTCTGCTCTGTCCTGG – 3'	241
	Reverse	5' – TCTGTCATCTTGGGCGGCAT – 3'	
ACTN4 (NM_004924.4)	Forward	5' – CAGCTTCTACCATGCCTTTT – 3'	195
	Reverse	5' – TCCTGGATAGTCTTTTGGGG – 3'	
CDH11 (NM_001797.2)	Forward	5' – TTGTACCTTCTGCCCATAGT – 3'	200
	Reverse	5' – ATGACCAGGAGAATGACGAT – 3'	
CTNNAL1 (NM_003798.2)	Forward	5' – AGCTCTTCGGGAGAATCTTT – 3'	193
	Reverse	5' – TTGAGCTTGAATCCACACAG – 3'	
EZR (NM_003379.4)	Forward	5' – ATGCCGAAACCAATCAATGT – 3'	192
	Reverse	5' – CTTCTTATCCAGCTTCAGCC – 3'	
ITGA3 (NM_002204.2)	Forward	5' – GCCAAGCTAATGAGACCATC – 3'	197
	Reverse	5' – TGTATAGTCCACCAGCAGAG – 3'	
JUNB (NM_002229.2)	Forward	5' – ACACGACTACAAACTCCTGA – 3'	200
	Reverse	5' – TGCTGTTGGGGACAATCA – 3'	
KIRREL2 (NM_199179.2)	Forward	5' – TCTCTGTGCTACACATTTCG – 3'	188
	Reverse	5' – CCCAGTGATGACCATAAGGA – 3'	
MAGI2 (NM_012301.3)	Forward	5' – CGAAAAAGGCTAAACCTCCA – 3'	192
	Reverse	5' – TTGTTCCAAGTTCTGTGTGG – 3'	
NCK2 (NM_003581.4)	Forward	5' – GACCAGAGGCAGCTCTTGGT – 3'	198
	Reverse	5' – GCAGCCAGCAAGAAGCATCA – 3'	
PTPRO (NM_030667.2)	Forward	5' – ACGGACAGGAACATTCATTG – 3'	187
	Reverse	5' – GAACTGCTGCTTCTTCTTCA – 3'	

The PCR products were cloned into pCR 2.1-TOPO vector using the TOPO® TA cloning kit (Invitrogen Life Technologies, CA, USA). The TA cloning reaction was set up as shown in the table below.

Reagent	Volume for 1 reaction
Fresh PCR product	3µl
Water	1µl
Salt Solution	1µl
TOPO vector	1µl
Final Volume	6µl

The reaction mixture for each gene was mixed gently and incubated at room temperature for 15 minutes. Two µl of the reaction mixture was then added to a vial of OneShot® TOP10 Chemically Competent *E. coli* cells and incubated for 15 minutes on ice before being subjected to heat shock for 30 seconds at 42ºC without shaking. The vial was placed on ice for 2 minutes before adding 250µl of S.O.C. medium to each vial and incubated for 1 hour at 37ºC with shaking at 250rpm.

One hundred µl of the incubation mixture was spread onto a pre-warmed Luria-Bertani (LB) agar plate containing 100µg/ml ampicillin and 40µg/ml 5-bromo-4-chloro-3-indolyl-beta-D-galactopyranoside (X-Gal) (Promega, WI, USA) for blue-white selection. Plates were incubated overnight at 37ºC. Isolated white colonies were picked for sub-culturing. Each colony was grown in 3ml of LB broth containing 100µg/ml ampicillin at 37ºC with shaking at 250rpm. After 8 hours, the bacterial culture was diluted by topping up the LB broth to 10ml and was incubated overnight under the same conditions but not more than 16 hours. Cells were then centrifuged at 6000*g* and 4ºC for 15 minutes. The supernatant was discarded and plasmids were extracted using the QIAprep Spin Miniprep Kit (QIAGEN GmbH, Hilden, Germany) according to the manufacturer's protocol. Concentration of the plasmid DNA stock was measured using NanoDrop 1000 Spectrophotometer (NanoDrop products, Thermo Scientific, DE, USA). Presence of gene inserts was confirmed by EcoRI restriction and agarose gel electrophoresis. Serial dilutions were done to get a series of plasmid standards, ranging from 10^9 copy number to 10^1 copy number. Plasmid

standards were run in triplicates in real-time PCR using LightCycler® 480 SYBR Green I Master reagent (Roche, Germany). Good standard curves should have efficiency of 2 and gradient of -3.3 in the curve of Cp value against copy number.

Appendix 3.1: Biochemistry data of control and *IL-13* overexpressed rats

Biochemistry profile of rats used for the microarray analysis.

Code	Sample	Serum IL-13 (pg/ml)	Serum albumin (g/L)	Serum cholesterol (mmol/L)	Serum creatinine (µmol/L)	urine albumin excretion (µg/24hr)
(3)C2	C2	0	41	1.94	88.2	218
(3)C3	C3	0	42.4	1.53	65.2	303
(3)C4	C4	0	56.9	1.63	67.2	194
(3)C5	C5	2	38.6	1.81	84.9	231
(6)C3	C15	11	42.4	1.5	82.2	495
(6)C5	C17	8	46.7	1.55	82.2	275
(3)J2	J2	1578	27.9	7.8	69.7	2331
(3)J4	J4	376	29.3	5.83	89.5	3098
(4)J5	J11	28	29	4.3	70.5	2996
(4)J9	J15	336	29.3	4.45	67.6	6846
(4)J13	J19	1753	18.9	8.78	79.3	12087
(4)J16	J22	657	15.5	12.2	56.8	32845

Sample starts with C represent control rat; sample starts with J represent *IL-13*-overexpressed rat.

Appendix 3.2: Full list of DEGs

List of genes differentially expressed in the glomeruli of *IL-13* overexpression rats versus control rats.

GenBank Accession No.	Gene Symbol	Gene Description	Fold Change
Vasculature development			
NM_053394.2	Klf5	Kruppel-like factor 5	-4.09
NM_031836.1	Vegfa	vascular endothelial growth factor A	-3.67
XM_241275.4	Sema5a	sema domain, seven thrombospondin repeats (type 1 and type 1-like), transmembrane domain (TM) and short cytoplasmic domain, (semaphorin) 5A	-3.01
NM_022950.1	C1galt1	core 1 synthase, glycoprotein-N-acetylgalactosamine 3-beta-galactosyltransferase, 1	-2.38
XM_344806.3	Hey2	hairy/enhancer-of-split related with YRPW motif 2	-2.36
NM_016991.2	Adra1b	adrenergic, alpha-1B-, receptor	-2.19
XM_001070551.1	Reck	reversion-inducing-cysteine-rich protein with kazal motifs	-2.09
NM_053356.1	Col1a2	collagen, type I, alpha 2	-2.08
NM_133386.2	Sphk1	sphingosine kinase 1	-2.01
XM_001079521.1	Fgfr2	fibroblast growth factor receptor 2	-1.97
XM_001060648.1	Tiparp	TCDD-inducible poly(ADP-ribose) polymerase	-1.69
NM_013151.2	Plat	plasminogen activator, tissue	-1.66
NM_001024781.1	Sox18	SRY (sex determining region Y)-box 18	1.90
NM_019386.2	Tgm2	transglutaminase 2, C polypeptide	1.77
NM_022277.1	Casp8	caspase 8	1.64
Cell adhesion			
XM_579693.1	Spon1	spondin 1, extracellular matrix protein	-6.88
NM_021682.1	Negr1	neuronal growth regulator 1	-4.93
XM_229775.4	LOC317070	similar to nidogen 2	-4.28
XM_342325.3	Col11a1	collagen, type XI, alpha 1	-3.62
NM_013137.1	Ddr1	discoidin domain receptor tyrosine kinase 1	-3.08
NM_138525.1	Mucdhl	mucin and cadherin like	-3.02
NM_031753.1	Alcam	activated leukocyte cell adhesion molecule	-2.93
NM_053848.1	Opcml	opioid binding protein/cell adhesion molecule-like	-2.92
NM_031716.1	Wisp1	WNT1 inducible signaling pathway protein 1	-2.77
XM_213902.4	Lamc2	laminin, gamma 2	-2.76
XM_213560.4	Pkp2	plakophilin 2	-2.76
NM_019358.1	Pdpn	podoplanin	-2.72
NM_019140.2	Ptprd	protein tyrosine phosphatase, receptor type, D	-2.59
XM_241632.4	Col18a1	collagen, type XVIII, alpha 1	-2.53

XM_221337.3	LOC288010	LIM domain containing preferred translocation partner in lipoma	-2.38
XM_001076220.1	Celsr2	cadherin, EGF LAG seven-pass G-type receptor 2 (flamingo homolog, Drosophila)	-2.38
XM_223583.4	Aebp1	AE binding protein 1	-2.28
NM_031521.1	Ncam1	neural cell adhesion molecule 1	-2.19
XM_001072297.1	RGD1564327	similar to integrin alpha 8	-2.00
XM_230950.4	Itgav	integrin alpha V	-1.97
XM_235308.4	Col14a1	collagen, type XIV, alpha 1	-1.97
XM_345584.3	Col16a1	collagen, type XVI, alpha 1	-1.96
XM_227117.4	Pcdh18	protocadherin 18	-1.93
NM_022944.1	Inppl1	inositol polyphosphate phosphatase-like 1	-1.91
NM_013016.2	Sirpa	signal-regulatory protein alpha	-1.88
NM_198747.1	Col27a1	collagen, type XXVII, alpha 1	-1.74
XM_001076634.1	LOC686988	discoidin domain receptor tyrosine kinase 2	-1.73
NM_030842.1	Itga7	integrin alpha 7	-1.70
NM_001004090.2	Tspan5	tetraspanin 5	-1.67
XM_575373.2	RGD1564980	ribosomal protein L29; similar to 60S ribosomal protein L29 (P23); ribosomal protein L29, pseudogene 1; similar to 60S ribosomal protein L29	3.26
NM_001025750.1	Plek	pleckstrin	2.43
XM_579351.1	LOC497761	Cd2 molecule	2.23
XM_575338.2	RGD1562323	similar to CD36 antigen; similar to fatty acid translocase/CD36; CD36 molecule (thrombospondin receptor)	2.19
NM_020308.1	Adam15	a disintegrin and metallopeptidase domain 15 (metargidin)	2.07
NM_019177.1	Sell	selectin, lymphocyte	2.05
NM_024360.2	Hes1	hairy and enhancer of split 1 (Drosophila)	2.01
XM_575339.1	LOC499985	similar to fatty acid translocase/CD36	2.01
NM_133306.1	Olr1	oxidized low density lipoprotein (lectin-like) receptor 1	2.00
NM_031691.1	Itgad	integrin, alpha D	1.91
XM_001067562.1	Itgb7	integrin, beta 7	1.88
XM_342930.2	Ptpru	protein tyrosine phosphatase, receptor type, U	1.69
XM_219001.4	Xlkd1	lymphatic vessel endothelial hyaluronan receptor 1	1.63
XM_001055526.1	Pcdhb10	protocadherin beta 10	1.61
Intrinsic to plasma membrane			
XM_001055768.1	Tmeff1	transmembrane protein with EGF-like and two follistatin-like domains 1	-6.67
NM_031739.1	Kcnd3	potassium voltage gated channel, Shal-related family, member 3	-5.64
NM_019214.1	Slc26a4	solute carrier family 26, member 4	-4.26
NM_019276.2	Ugt8	UDP glycosyltransferase 8	-4.19
NM_024376.1	Gja3	gap junction protein, alpha 3	-3.70
NM_145881.1	Rims2	regulating synaptic membrane exocytosis 2	-3.69

NM_012813.1	St8sia1	ST8 alpha-N-acetyl-neuraminide alpha-2,8-sialyltransferase 1	-3.68
NM_173103.1	Clcnkb	chloride channel Kb	-3.48
XM_234108.4	Prkcm	protein kinase D1	-3.21
XM_001075775.1	Mpv17l	Mpv17 transgene, kidney disease mutant-like	-3.09
NM_173293.1	Olr59	olfactory receptor 59	-2.96
NM_152938.1	Slc4a9	solute carrier family 4, sodium bicarbonate cotransporter, member 9	-2.88
NM_012799.1	Nmbr	neuromedin B receptor	-2.87
NM_001014171.1	Veph1	ventricular zone expressed PH domain homolog 1 (zebrafish)	-2.86
NM_053981.1	Kcnj12	potassium inwardly-rectifying channel, subfamily J, member 12	-2.80
NM_001025413.1	Tmem184a	transmembrane protein 184A	-2.71
NM_053445.1	Fads1	fatty acid desaturase 1	-2.67
NM_019243.1	Ptgfrn	prostaglandin F2 receptor negative regulator	-2.63
XM_217033.4	LOC300191	solute carrier family 48 (heme transporter), member 1	-2.62
NM_001034014.1	Accn1	amiloride-sensitive cation channel 1, neuronal	-2.57
XM_001057885.1	Atp2b3	ATPase, Ca++ transporting, plasma membrane 3	-2.56
NM_031007.1	Adcy2	adenylate cyclase 2 (brain)	-2.47
NM_021688.2	Kcnk1	potassium channel, subfamily K, member 1	-2.46
NM_053570.1	Cxadr	coxsackie virus and adenovirus receptor	-2.45
NM_022590.2	Slc5a2	solute carrier family 5 (sodium/glucose cotransporter), member 2	-2.45
NM_198786.2	Mal2	mal, T-cell differentiation protein 2	-2.45
NM_031841.1	Scd	stearoyl-CoA desaturase (delta-9-desaturase)	-2.44
NM_021266.2	Fzd1	frizzled homolog 1 (Drosophila)	-2.41
NM_001004282.1	Tmem178	transmembrane protein 178	-2.41
NM_031034.1	Gna12	guanine nucleotide binding protein, alpha 12	-2.40
XM_225718.3	Kcng2	potassium voltage-gated channel, subfamily G, member 2	-2.38
NM_031795.1	Ugcg	UDP-glucose ceramide glucosyltransferase	-2.34
NM_053571.1	Sec16b	SEC16 homolog B (S. cerevisiae)	-2.33
XM_344661.3	Reep5	receptor accessory protein 5	-2.31
NM_031344.2	Fads2	fatty acid desaturase 2	-2.30
NM_001005562.1	Creb3l1	cAMP responsive element binding protein 3-like 1	-2.24
NM_017060.1	Hrasls3	phospholipase A2, group XVI	-2.19
NM_017049.1	Slc4a3	solute carrier family 4 (anion exchanger), member 3	-2.18
NM_001013185.1	Cabc1	presenilin 2; chaperone, ABC1 activity of bc1 complex homolog (S. pombe)	-2.16
NM_172091.1	Gcgr	glucagon receptor	-2.15
XM_342986.2	Tas1r1	taste receptor, type 1, member 1	-2.12

NM_001005558.1	Fam151a	family with sequence similarity 151, member A	-2.11
NM_012507.2	Atp1b2	ATPase, Na+/K+ transporting, beta 2 polypeptide	-2.08
NM_199105.1	MGC72614	hypothetical LOC310540	-2.08
NM_130822.1	Lphn3	latrophilin 3	-2.07
NM_053735.1	Pi4k2a	phosphatidylinositol 4-kinase type 2 alpha	-2.06
NM_001010958.1	Slc25a29	solute carrier family 25, member 29	-2.06
NM_001007672.1	Tmem98	transmembrane protein 98	-2.05
NM_031648.1	Fxyd1	FXYD domain-containing ion transport regulator 1	-2.04
NM_181639.3	Slc29a3	solute carrier family 29 (nucleoside transporters), member 3	-1.99
NM_001003705.1	LOC291840	solute carrier family 38, member 7	-1.99
NM_017136.1	Sqle	squalene epoxidase	-1.97
NM_184050.2	Ermp1	endoplasmic reticulum metallopeptidase 1	-1.97
NM_017206.1	Slc6a6	solute carrier family 6 (neurotransmitter transporter, taurine), member 6	-1.95
NM_139325.1	Eno2	enolase 2, gamma, neuronal	-1.94
NM_017299.1	Slc19a1	solute carrier family 19 (folate transporter), member 1	-1.93
NM_053485.2	S100a6	S100 calcium binding protein A6	-1.90
NM_173145.1	Dlgap4	discs, large homolog-associated protein 4 (Drosophila)	-1.88
NM_139082.2	Bambi	BMP and activin membrane-bound inhibitor, homolog (Xenopus laevis)	-1.88
NM_022219.2	Fut4	fucosyltransferase 4 (alpha (1,3) fucosyltransferase, myeloid-specific)	-1.87
NM_022862.1	Unc13b	unc-13 homolog B (C. elegans)	-1.87
NM_183332.1	Myadm	myeloid-associated differentiation marker	-1.87
NM_012919.2	Cacna2d1	calcium channel, voltage-dependent, alpha2/delta subunit 1	-1.87
NM_001031652.1	St6galnac2	ST6 (alpha-N-acetyl-neuraminyl-2,3-beta-galactosyl-1,3)-N-acetylgalactosaminide alpha-2,6-sialyltransferase 2	-1.85
XM_001054081.1	Galnt2	UDP-N-acetyl-alpha-D-galactosamine:polypeptide N-acetylgalactosaminyltransferase 2 (GalNAc-T2)	-1.83
NM_001007679.1	Tmem206	transmembrane protein 206	-1.82
NM_001012345.1	Dgat2	diacylglycerol O-acyltransferase homolog 2 (mouse)	-1.82
NM_001014209.1	LOC363060	similar to RIKEN cDNA 1600029D21	-1.81
XM_574680.1	Cnnm2	cyclin M2	-1.81
NM_001013903.1	Tmem171	transmembrane protein 171; proline rich protein 2	-1.77
NM_080582.1	Abcb6	ATP-binding cassette, sub-family B (MDR/TAP), member 6	-1.77
NM_001013126.1	Cyb5r1	cytochrome b5 reductase 1	-1.75
NM_176861.1	Kcnmb2	potassium large conductance calcium-activated channel, subfamily M, beta member 2	-1.75

NM_012716.1	Slc16a1	solute carrier family 16, member 1 (monocarboxylic acid transporter 1)	-1.74
NM_134363.1	Slc12a5	solute carrier family 12 (potassium-chloride transporter), member 5	-1.73
NM_033352.1	Abcd2	ATP-binding cassette, sub-family D (ALD), member 2	-1.72
NM_001012018.1	B4galt4	UDP-Gal:betaGlcNAc beta 1,4-galactosyltransferase, polypeptide 4	-1.71
NM_001008358.1	Tmem106c	transmembrane protein 106C	-1.69
NM_001007002.1	Mxra8	matrix-remodelling associated 8	-1.68
XM_001080929.1	RGD1565432	similar to hypothetical protein	-1.66
NM_001004204.2	MGC94190	similar to 0610007L01Rik protein	-1.66
NM_080480.1	Pip5k2c	phosphatidylinositol-5-phosphate 4-kinase, type II, gamma	-1.66
XM_220982.3	Ptrf	polymerase I and transcript release factor	-1.66
NM_031559.1	Cpt1a	carnitine palmitoyltransferase 1a, liver	-1.64
NM_012661.1	Sts	steroid sulfatase	-1.64
NM_017223.2	Slc20a2	solute carrier family 20 (phosphate transporter), member 2	-1.62
NM_001024897.1	Ehd2	similar to hypothetical protein; hypothetical gene supported by X51706; similar to ribosomal protein L9; similar to 60S ribosomal protein L9; ribosomal protein L9; EH-domain containing 2	-1.61
NM_017037.1	Pmp22	peripheral myelin protein 22	2.85
XM_001064152.1	Loc266761	cytochrome P450, family 4, subfamily v, polypeptide 3; family with sequence similarity 149, member A	2.51
NM_030848.1	Bst1	bone marrow stromal cell antigen 1	2.45
NM_031664.1	Slc28a2	similar to solute carrier family 28, member 2; solute carrier family 28 (sodium-coupled nucleoside transporter), member 2	2.24
NM_020100.2	Ramp3	receptor (G protein-coupled) activity modifying protein 3	2.21
XM_001071501.1	St8sia4	similar to CMP-N-acetylneuraminate-poly-alpha-2,8-sialyltransferase (Alpha-2,8-sialyltransferase 8D) (ST8Sia IV) (Polysialyltransferase-1); ST8 alpha-N-acetyl-neuraminide alpha-2,8-sialyltransferase 4	2.15
XM_001077664.1	LOC691312	cytochrome P450 4F5; cytochrome P450, family 4, subfamily f, polypeptide 37	2.11
NM_001008843.1	RT1-CE5	RT1 class I, CE5	2.07
NM_017054.1	Tbxa2r	thromboxane A2 receptor	2.03
NM_012800.1	P2ry1	purinergic receptor P2Y, G-protein coupled 1	1.96
NM_019354.1	Ucp2	uncoupling protein 2 (mitochondrial, proton carrier)	1.96
NM_053822.1	S100a8	S100 calcium binding protein A8	1.92
NM_001024995.1	Lrrc33	leucine rich repeat containing 33	1.91
NM_031684.2	Slc29a1	solute carrier family 29 (nucleoside transporters), member 1	1.91
NM_031349.2	Aplnr	apelin receptor	1.90
NM_001005384.1	Osmr	oncostatin M receptor	1.90

NM_001025415.1	Ch25h	cholesterol 25-hydroxylase	1.90
NM_173124.1	Cyp4f5	cytochrome P450 4F5; cytochrome P450, family 4, subfamily f, polypeptide 37	1.88
NM_001024968.1	Slc46a3	solute carrier family 46, member 3	1.88
XM_001069340.1	Prr7	proline rich 7 (synaptic)	1.88
NM_001008306.1	Calhm2	calcium homeostasis modulator 2	1.87
NM_139341.1	Slc15a3	solute carrier family 15, member 3	1.86
NM_144758.1	Slc15a4	solute carrier family 15, member 4	1.85
NM_001010964.1	Klrb1a	killer cell lectin-like receptor subfamily B, member 1A	1.81
NM_053607.1	Acsl5	acyl-CoA synthetase long-chain family member 5	1.80
NM_023021.1	Kcnn4	potassium intermediate/small conductance calcium-activated channel, subfamily N, member 4	1.78
NM_053596.1	Ece1	endothelin converting enzyme 1	1.77
NM_023099.1	Gpr27	G protein-coupled receptor 27	1.77
NM_053951.1	Mcf2l	MCF.2 cell line derived transforming sequence-like	1.77
NM_198754.2	Cmtm8	CKLF-like MARVEL transmembrane domain containing 8	1.77
NM_053827.1	Plod1	procollagen-lysine 1, 2-oxoglutarate 5-dioxygenase 1	1.76
NM_001002802.1	Bace2	beta-site APP-cleaving enzyme 2	1.75
NM_031740.1	B4galt6	UDP-Gal:betaGlcNAc beta 1,4-galactosyltransferase, polypeptide 6	1.75
NM_031322.1	Lrp4	low density lipoprotein receptor-related protein 4	1.74
NM_001013895.1	Prkd2	protein kinase D2	1.71
NM_031079.1	Pde2a	phosphodiesterase 2A, cGMP-stimulated	1.71
XM_001078922.1	Gprc5b	G protein-coupled receptor, family C, group 5, member B	1.71
NM_020543.3	Cnr2	cannabinoid receptor 2 (macrophage)	1.70
NM_173310.2	GalNAc4S6ST	B cell RAG associated protein	1.70
NM_013091.1	Tnfrsf1a	tumor necrosis factor receptor superfamily, member 1a	1.68
NM_139110.1	Gpr116	G protein-coupled receptor 116	1.68
NM_001008845.1	RT1-CE7	similar to RT1 class I, CE11; RT1 class I, CE11; RT1 class I, CE7	1.67
XM_342524.3	Plcb1	phospholipase C, beta 1 (phosphoinositide-specific)	1.66
NM_053821.2	Ralb	v-ral simian leukemia viral oncogene homolog B (ras related; GTP binding protein)	1.66
NM_001004269.1	Jam3	junctional adhesion molecule 3	1.66
NM_145679.1	Lrrc3	leucine rich repeat containing 3	1.65
NM_030844.1	Ica1	islet cell autoantigen 1	1.65
NM_017292.1	Gabrr2	gamma-aminobutyric acid (GABA) receptor, rho 2	1.65
NM_172040.1	Hyal2	hyaluronoglucosaminidase 2	1.65
NM_173135.1	Accn3	amiloride-sensitive cation channel 3	1.64
XM_344616.3	MGC112790	frizzled homolog 8 (Drosophila)	1.64

NM_001008834.1	RT1-CE11	similar to RT1 class I, CE11; RT1 class I, CE11; RT1 class I, CE7	1.63
NM_053492.2	Cdw92	CDW92 antigen	1.62
NM_001008840.1	RT1-CE2	RT1 class I, CE2	1.62
NM_017071.1	Insr	insulin receptor	1.62
NM_031649.1	Klrg1	killer cell lectin-like receptor subfamily G, member 1	1.62
NM_001007728.1	Mpzl1	myelin protein zero-like 1	1.62
NM_001014059.1	RGD1304952	similar to RIKEN cDNA C530028O21 gene	1.61
XM_235609.4	Prickle1	prickle homolog 1 (Drosophila)	1.61
NM_020086.1	Plvap	plasmalemma vesicle associated protein	1.61
NM_053321.2	Ptafr	platelet-activating factor receptor	1.60
NM_057201.1	Gpr37	G protein-coupled receptor 37	1.60
Cell motion			
XM_217250.3	Ephb1	Eph receptor B1	-6.40
NM_012648.1	Scnn1b	sodium channel, nonvoltage-gated 1 beta	-4.12
NM_080778.1	Nr2f2	nuclear receptor subfamily 2, group F, member 2	-3.64
NM_012807.1	Smo	smoothened homolog (Drosophila)	-3.27
XM_222785.4	Astn1	astrotactin 1	-3.00
XM_001070296.1	Plxna2	plexin A2	-2.73
NM_012934.1	Dpysl3	dihydropyrimidinase-like 3	-2.57
NM_031520.1	Myh10	myosin, heavy chain 10, non-muscle	-2.47
NM_053503.1	Jub	jub, ajuba homolog (Xenopus laevis)	-2.35
NM_017003.2	Erbb2	v-erb-b2 erythroblastic leukemia viral oncogene homolog 2, neuro/glioblastoma derived oncogene homolog (avian)	-2.30
NM_017195.1	Gap43	growth associated protein 43	-2.10
NM_013040.2	Abcc9	ATP-binding cassette, sub-family C (CFTR/MRP), member 9	-2.09
NM_001033701.1	Zeb2	zinc finger E-box binding homeobox 2	-2.01
XM_573530.1	Enah	enabled homolog (Drosophila)	-2.01
NM_031022.1	Cspg4	chondroitin sulfate proteoglycan 4	-1.87
NM_031321.1	Slit3	slit homolog 3 (Drosophila)	-1.72
NM_031056.1	Mmp14	matrix metallopeptidase 14 (membrane-inserted)	-1.62
XM_215451.4	Cspg2	versican	2.28
NM_013114.1	Selp	selectin, platelet	2.20
NM_017076.1	PVR	poliovirus receptor	2.14
NM_130411.2	Coro1a	coronin, actin binding protein 1A	2.12
NM_021759.1	Lypd3	Ly6/Plaur domain containing 3	2.09
XM_227600.4	RGD1565941	vav 3 guanine nucleotide exchange factor	1.98
NM_022206.1	Unc5a	unc-5 homolog A (C. elegans)	1.75
NM_201272.1	Plekhg5	pleckstrin homology domain containing, family G (with RhoGef domain) member 5	1.72
NM_175756.1	Fcgr2b	Fc fragment of IgG, low affinity IIb, receptor (CD32); Fc fragment of IgG, low affinity IIa, receptor (CD32)	1.71

NM_012945.1	Hbegf	heparin-binding EGF-like growth factor	1.69
NM_012967.1	Icam1	intercellular adhesion molecule 1	1.64
XM_001057564.1	Csf3r	colony stimulating factor 3 receptor (granulocyte)	1.62
NM_001007729.1	Pf4	platelet factor 4	1.62
Extracellular region			
NM_001012039.1	Efemp1	epidermal growth factor-containing fibulin-like extracellular matrix protein 1	-4.76
NM_020071.1	Fgb	fibrinogen beta chain	-4.33
XM_001060132.1	C1qtnf7	C1q and tumor necrosis factor related protein 7	-4.16
NM_021586.1	Ltbp2	latent transforming growth factor beta binding protein 2	-3.52
XM_001066152.1	Egfl6	EGF-like-domain, multiple 6	-3.47
NM_001012225.1	Mgat4a	mannoside acetylglucosaminyltransferase 4, isoenzyme A	-3.28
NM_053385.1	Prelp	proline arginine-rich end leucine-rich repeat protein	-3.10
NM_012559.2	Fgg	fibrinogen gamma chain	-2.92
NM_031810.1	Defb1	defensin beta 1	-2.74
NM_053856.1	Scg3	secretogranin III	-2.64
NM_032616.1	Lsr	lipolysis stimulated lipoprotein receptor	-2.64
NM_017061.1	Lox	lysyl oxidase	-2.58
XM_001064272.1	Crim1	cysteine rich transmembrane BMP regulator 1 (chordin like)	-2.57
NM_031609.1	Nbl1	neuroblastoma, suppression of tumorigenicity 1	-2.54
NM_130741.1	Lcn2	lipocalin 2	-2.54
XM_001056704.1	RGD1560408	similar to Mannoside acetylglucosaminyltransferase 4, isoenzyme A; mannosyl (alpha-1,3-)-glycoprotein beta-1,4-N-acetylglucosaminyltransferase, isozyme A	-2.52
NM_053606.1	Mmp23	matrix metallopeptidase 23	-2.43
NM_013122.1	Igfbp2	insulin-like growth factor binding protein 2	-2.41
NM_019237.1	Pcolce	procollagen C-endopeptidase enhancer protein	-2.35
NM_001014104.1	Metrnl	meteorin, glial cell differentiation regulator-like	-2.31
NM_080698.1	Fmod	fibromodulin	-2.26
NM_031826.1	Fbn2	fibrillin 2	-2.25
NM_001007710.1	Acpl2	acid phosphatase-like 2	-2.24
XM_001076441.1	Cilp	cartilage intermediate layer protein, nucleotide pyrophosphohydrolase	-2.22
NM_013144.1	Igfbp1	insulin-like growth factor binding protein 1	-2.20
NM_001014140.1	RGD1309676	similar to RIKEN cDNA 5730469M10	-2.13
NM_012880.1	Sod3	superoxide dismutase 3, extracellular	-2.12
NM_001006979.1	Matn1	matrilin 1, cartilage matrix protein	-2.09
XM_343607.3	Col4a3	collagen, type IV, alpha 3	-1.99
NM_012590.1	Inha	inhibin alpha	-1.98

NM_133557.1	Cda08	integrin alpha FG-GAP repeat containing 1	-1.94
XM_001077795.1	Ltbp4	latent transforming growth factor beta binding protein 4	-1.89
NM_172030.1	Entpd2	ectonucleoside triphosphate diphosphohydrolase 2	-1.87
NM_023967.1	Gfra4	GDNF family receptor alpha 4	-1.83
NM_053629.2	Fstl3	follistatin-like 3	-1.82
NM_031697.1	St3gal3	ST3 beta-galactoside alpha-2,3-sialyltransferase 3	-1.79
NM_031640.1	Pgcp	plasma glutamate carboxypeptidase	-1.76
XM_001070303.1	Gpld1	glycosylphosphatidylinositol specific phospholipase D1	-1.75
NM_203493.2	Dmp1	dentin matrix acidic phosphoprotein 1	-1.72
NM_021989.2	Timp2	tissue inhibitor of metalloproteinase 2	-1.71
XM_001058647.1	Pappa	pregnancy-associated plasma protein A	-1.68
XM_001060614.1	Olfml2a	olfactomedin-like 2A	-1.68
NM_001004218.1	Fuca2	fucosidase, alpha-L- 2, plasma	-1.61
NM_031766.1	Cpz	carboxypeptidase Z	-1.60
XM_001061784.1	Chit1	chitinase 1 (chitotriosidase)	3.18
NM_022221.1	Mmp8	matrix metallopeptidase 8	3.07
NM_001024240.1	RGD1310251	similar to RIKEN cDNA 2010001M09	2.59
NM_031645.1	Ramp1	receptor (G protein-coupled) activity modifying protein 1	2.57
NM_053373.1	Pglyrp1	peptidoglycan recognition protein 1	2.36
NM_172328.2	Tac4	tachykinin 4	2.30
NM_012908.1	Faslg	Fas ligand (TNF superfamily, member 6)	2.24
XM_001058441.1	RGD1565970	mast cell protease 8-like 2; similar to mast cell protease 8; mast cell protease 8	2.21
NM_134361.1	Xcl1	chemokine (C motif) ligand 1	2.11
NM_012636.1	Pthlh	parathyroid hormone-like hormone	2.09
NM_012548.1	Edn1	endothelin 1	2.08
NM_001003403.1	Apold1	apolipoprotein L domain containing 1	2.02
XM_239260.4	Sez6	seizure related 6 homolog (mouse)	2.00
NM_012859.1	Lipe	lipase, hormone sensitive	1.99
NM_021664.1	Dnase2b	deoxyribonuclease II beta	1.96
NM_013092.1	Cma1	chymase 1, mast cell	1.94
NM_017066.2	Ptn	pleiotrophin	1.94
XM_001074055.1	LOC690312	Fc receptor-like A; similar to Fc receptor-like and mucin-like 1	1.89
NM_017330.2	Prf1	perforin 1 (pore forming protein)	1.89
NM_153721.1	Ppbp	pro-platelet basic protein (chemokine (C-X-C motif) ligand 7)	1.88
NM_212507.2	Ltb	lymphotoxin beta (TNF superfamily, member 3)	1.87
NM_020074.2	Srgn	serglycin	1.86
NM_012762.2	Casp1	caspase 1	1.86
NM_001012467.1	Rnase10	ribonuclease, RNase A family, 10 (non-active)	1.85
XM_001067964.1	Tgfbi	transforming growth factor, beta induced	1.82
NM_153294.1	Npw	neuropeptide W	1.81

XM_001061982.1	Col5a2	collagen, type V, alpha 2	1.79
NM_022534.1	Tcn2	transcobalamin 2	1.77
NM_139104.1	Egfl7	EGF-like-domain, multiple 7	1.76
NM_020082.2	Rnase4	ribonuclease, RNase A family 4	1.76
XM_235461.3	Apol3	similar to apolipoprotein L, 3; apolipoprotein L, 3	1.71
XM_001063886.1	LOC685462	EMI domain containing 1	1.71
XM_236642.3	Camp	cathelicidin antimicrobial peptide	1.66
NM_030988.1	Tg	thyroglobulin	1.66
NM_021587.1	Ltbp1	latent transforming growth factor beta binding protein 1	1.64
NM_138882.1	Pla1a	phospholipase A1 member A	1.62
Immune response			
NM_013163.1	Il2ra	interleukin 2 receptor, alpha	-2.83
NM_012752.2	Cd24	CD24 molecule	-2.51
NM_052807.1	Igf1r	insulin-like growth factor 1 receptor	-2.48
NM_181086.2	Tnfrsf12a	tumor necrosis factor receptor superfamily, member 12a	-2.45
NM_001002805.1	C4-2	complement component 4, gene 2	-2.43
NM_019165.1	Il18	interleukin 18	-2.42
NM_145765.1	Tnfsf15	tumor necrosis factor (ligand) superfamily, member 15	-2.03
NM_012671.1	Tgfa	transforming growth factor alpha	-1.82
NM_012895.3	Adk	adenosine kinase	-1.69
NM_053858.1	Ccl4	chemokine (C-C motif) ligand 4	3.12
XM_001059278.1	LOC301133	tumor necrosis factor (ligand) superfamily, member 14	2.93
NM_031539.1	Cd8b	CD8b molecule	2.71
NM_053953.1	Il1r2	interleukin 1 receptor, type II	2.67
NM_053647.1	Cxcl2	chemokine (C-X-C motif) ligand 2	2.63
NM_017124.1	Cd37	CD37 molecule	2.57
NM_031512.1	Il1b	interleukin 1 beta	2.39
NM_022205.3	Cxcr4	chemokine (C-X-C motif) receptor 4	2.37
NM_017079.1	Cd1d1	CD1d1 molecule	2.22
NM_053983.1	Cd52	CD52 antigen	2.17
NM_134327.1	Cd69	Cd69 molecule	2.17
NM_053634.1	Fcnb	ficolin B	2.14
NM_013169.1	Cd3d	CD3 molecule delta polypeptide	2.14
NM_013127.1	Cd38	CD38 molecule	2.12
NM_019311.1	Inpp5d	inositol polyphosphate-5-phosphatase D	2.12
NM_030845.1	Cxcl1	chemokine (C-X-C motif) ligand 1 (melanoma growth stimulating activity, alpha)	2.09
XM_001059172.1	RGD1562408	SH2 domain protein 1A	2.07
NM_130399.2	Ada	adenosine deaminase	2.04
XM_218851.4	Il16_mapped	interleukin 16	2.01
NM_053390.1	Il12a	interleukin 12a	2.00
NM_001012002.1	Zap70	zeta-chain (TCR) associated protein kinase	2.00

NM_031561.2	Cd36	similar to CD36 antigen; similar to fatty acid translocase/CD36; CD36 molecule (thrombospondin receptor)	1.99
NM_212466.2	Cfb	complement factor B	1.99
NM_031116.2	Ccl5	chemokine (C-C motif) ligand 5	1.96
NM_145672.3	Cxcl9	chemokine (C-X-C motif) ligand 9	1.95
NM_031518.1	Cd200	Cd200 molecule	1.95
NM_145680.3	Gimap5	GTPase, IMAP family member 1; GTPase, IMAP family member 5	1.92
NM_012745.2	Klrd1	killer cell lectin-like receptor, subfamily D, member 1; killer cell lectin-like receptor, family E, member 1	1.92
NM_170789.1	Cd247	Cd247 molecule	1.91
NM_133534.1	Cx3cr1	chemokine (C-X3-C motif) receptor 1	1.85
NM_022303.1	Card9	caspase recruitment domain family, member 9	1.84
XM_343800.2	Il2rg	interleukin 2 receptor, gamma	1.83
NM_001008839.1	RT1-CE16	RT1 class I, CE14; RT1 class I, CE16; RT1 class Ia, locus A2; RT1 class Ib, locus Cl; RT1 class Ia, locus A1; RT1 class I, A3	1.83
NM_138880.2	Ifng	interferon gamma	1.72
NM_001012164.1	Cd97	CD97 molecule	1.70
NM_001017478.1	Cxcl16	chemokine (C-X-C motif) ligand 16	1.66
XM_344184.3	Hlx1	H2.0-like homeobox	1.65
NM_207604.1	Tlr6	toll-like receptor 6	1.63
XM_341509.3	Cd83	CD83 molecule	1.60
Cytoskeletal component/process			
XM_001054365.1	Arhgap28	Rho GTPase activating protein 28	-4.83
XM_215469.4	Map1b	microtubule-associated protein 1B	-3.55
NM_031613.1	Tmod2	tropomodulin 2	-3.46
XM_225259.4	Dsp	desmoplakin	-3.33
XM_214338.3	LOC290704	similar to palladin	-3.18
NM_053309.1	Homer2	homer homolog 2 (Drosophila)	-3.16
XM_223229.4	Shroom3	shroom family member 3	-3.02
NM_001009645.1	Kif22	kinesin family member 22	-2.97
XM_230774.4	Myh7b	myosin, heavy chain 7B, cardiac muscle, beta	-2.96
NM_001034105.1	Tnnc1	troponin C type 1 (slow)	-2.74
NM_024396.1	Abca2	ATP-binding cassette, sub-family A (ABC1), member 2	-2.72
NM_024127.2	Gadd45a	growth arrest and DNA-damage-inducible 45 alpha	-2.67
NM_133545.1	Ptpn21	protein tyrosine phosphatase, non-receptor type 21	-2.67
NM_001034075.1	Tpm1	tropomyosin 1, alpha	-2.55
XM_342179.3	Rgnef	Rho-guanine nucleotide exchange factor	-2.47
NM_013082.2	Sdc2	syndecan 2	-2.46
XM_216688.4	Arhgap5	Rho GTPase activating protein 5	-2.43
NM_145682.1	Filip1	filamin A interacting protein 1	-2.41
XM_237042.4	Dst	dystonin	-2.39

XM_220031.4	Myof	myoferlin	-2.38
XM_001064622.1	Itgb5	integrin beta 5	-2.37
XM_001065955.1	Ttn	titin	-2.34
XM_238004.3	RGD1309427	tubulin, beta 2b	-2.32
XM_238004.3	Tubb2b	tubulin, beta 2B	-2.32
NM_032071.1	Synj2	synaptojanin 2	-2.28
XM_574117.2	RGD1561153	myosin VIIb	-2.26
NM_183054.1	Rhbg	Rh family, B glycoprotein	-2.25
NM_001013246.1	Arhgef12	Rho guanine nucleotide exchange factor (GEF) 12	-2.21
NM_012909.2	Aqp2	aquaporin 2 (collecting duct)	-2.19
NM_017327.1	Gnao1	guanine nucleotide binding protein (G protein), alpha activating activity polypeptide O	-2.19
NM_022178.1	Myo5a	myosin Va	-2.18
NM_138921.1	Eml2	echinoderm microtubule associated protein like 2	-2.18
NM_012604.1	Myh3	myosin, heavy chain 3, skeletal muscle, embryonic	-2.18
XM_235213.3	Srgap1	SLIT-ROBO Rho GTPase activating protein 1	-2.17
NM_017137.1	Clcn2	chloride channel 2	-2.16
NM_017032.1	Pde4d	phosphodiesterase 4D, cAMP-specific (phosphodiesterase E3 dunce homolog, Drosophila)	-2.14
XM_240464.3	Ank1	ankyrin 1, erythrocytic	-2.13
NM_017083.1	Myo5b	myosin Vb	-2.08
NM_017180.1	Phlda1	pleckstrin homology-like domain, family A, member 1	-2.06
XM_001058944.1	RGD1565118	actin binding LIM protein family, member 3	-2.06
NM_012606.1	Myl3	myosin, light chain 3, alkali; ventricular, skeletal, slow	-2.06
NM_001007150.1	Stau2	staufen, RNA binding protein, homolog 2 (Drosophila)	-2.05
XM_227658.3	Fnbp1l	formin binding protein 1-like	-2.03
XM_217035.4	Krt7	keratin 7	-2.01
NM_001002798.1	Top1mt	DNA topoisomerase 1, mitochondrial	-2.01
XM_001078859.1	Farp1	FERM, RhoGEF (Arhgef) and pleckstrin domain protein 1 (chondrocyte-derived)	-2.00
NM_019167.1	Sptbn2	spectrin, beta, non-erythrocytic 2	-1.98
NM_053326.1	Pdlim5	PDZ and LIM domain 5	-1.91
NM_012935.2	Cryab	crystallin, alpha B	-1.90
XM_341538.2	Kif5b	kinesin family member 5B	-1.87
NM_031552.1	Add3	adducin 3 (gamma)	-1.85
NM_080689.3	Dnm1	dynamin 1	-1.81
NM_012676.1	Tnnt2	troponin T type 2 (cardiac)	-1.81
XM_001080795.1	LOC366669	similar to mKIAA1011 protein	-1.80
XM_001074984.1	Bbs4	Bardet-Biedl syndrome 4 homolog (human)	-1.77
XM_573030.2	Myh11	myosin, heavy chain 11, smooth muscle	-1.75

XM_345195.3	Tbl1xr1	transducin (beta)-like 1 X-linked receptor 1	-1.75
NM_001024341.1	Fam110b	family with sequence similarity 110, member B	-1.74
XM_001072750.1	RGD1308350	similar to hypothetical protein MGC13251	-1.72
XM_001061392.1	Myo6	myosin VI	-1.72
NM_139231.1	Nexn	nexilin (F actin binding protein)	-1.72
NM_017155.1	Adora1	adenosine A1 receptor	-1.72
XM_573863.2	RGD1564875	LIM domain binding 3	-1.71
XM_343248.3	Mtss1	metastasis suppressor 1	-1.71
NM_001009966.2	Pacsin3	protein kinase C and casein kinase substrate in neurons 3	-1.69
NM_001014070.1	LOC313672	kazrin	-1.68
XM_218858.4	Cpeb1	cytoplasmic polyadenylation element binding protein 1	-1.68
NM_024368.1	Frk	fyn-related kinase	-1.66
NM_001033987.1	Map2k5	mitogen activated protein kinase kinase 5	-1.65
XM_001066467.1	RGD1310722	ubinuclein 2	-1.65
XM_001081714.1	Evpl	envoplakin	-1.63
XM_236367.4	RGD1565416	similar to talin 2	-1.63
XM_001080622.1	Myh14	myosin, heavy chain 14	-1.63
NM_053603.1	Clic5	chloride intracellular channel 5	-1.62
XM_576473.1	LOC367171	microtubule-associated protein 4	-1.61
XM_226175.4	Mib1	mindbomb homolog 1 (Drosophila)	-1.61
NM_130894.2	Mfn2	mitofusin 2	-1.60
NM_001008384.1	Rac2	ras-related C3 botulinum toxin substrate 2 (rho family, small GTP binding protein Rac2)	2.52
NM_012759.1	Vav1	vav 1 guanine nucleotide exchange factor	2.40
NM_019169.2	Snca	synuclein, alpha (non A4 component of amyloid precursor)	2.28
NM_021909.1	Fxyd5	FXYD domain-containing ion transport regulator 5	2.12
XM_232763.4	Lck_mapped	similar to lymphocyte protein tyrosine kinase; lymphocyte-specific protein tyrosine kinase	1.99
NM_001012044.1	Lcp1	lymphocyte cytosolic protein 1	1.98
NM_001013430.1	Rhoh	ras homolog gene family, member H	1.97
NM_022542.1	Rhob	ras homolog gene family, member B	1.86
XM_219517.3	Map3k11	mitogen-activated protein kinase kinase kinase 11	1.82
NM_017317.2	Rab27a	RAB27A, member RAS oncogene family	1.80
NM_030857.1	Lyn	v-yes-1 Yamaguchi sarcoma viral related oncogene homolog	1.80
XM_001059351.1	Hist1h2bc	histone cluster 1, H2bc	1.77
NM_030863.1	Msn	moesin	1.76
XM_217152.3	Pstpip1	proline-serine-threonine phosphatase-interacting protein 1	1.75
XM_219540.4	RGD1310168	fermitin family homolog 3 (Drosophila)	1.75
NM_001037195.1	Rhog	ras homolog gene family, member G (rho G)	1.75

NM_001025680.1	Gpr4	G protein-coupled receptor 4	1.74
NM_133392.1	Stk17b	serine/threonine kinase 17b	1.74
XM_001070203.1	Itga5_mapped	integrin alpha 5 (fibronectin receptor alpha)	1.72
NM_138520.1	Klc3	kinesin light chain 3	1.71
XM_221956.3	LOC288515	MICAL-like 2	1.71
NM_017280.2	Psma3	proteasome (prosome, macropain) subunit, alpha type 3; proteasome subunit alpha type 3-like; similar to Proteasome subunit alpha type 3 (Proteasome component C8) (Macropain subunit C8) (Multicatalytic endopeptidase complex subunit C8) (Proteasome subunit K)	1.68
XM_001054737.1	Adam10	ADAM metallopeptidase domain 10	1.67
NM_001025733.2	Procr	protein C receptor, endothelial	1.67
NM_198787.1	Sgsm3	small G protein signaling modulator 3	1.66
XM_001060919.1	Dapk1	death associated protein kinase 1	1.64
NM_053484.1	Gas7	growth arrest specific 7	1.63
NM_001011965.1	Stom	stomatin; ABO-family member 5	1.61
NM_053783.1	Ifngr1	interferon gamma receptor 1	1.61
NM_053920.1	Trip10	thyroid hormone receptor interactor 10	1.60
NM_001039207.1	Narf	nuclear prelamin A recognition factor	1.60
Neuron development			
XM_001062426.1	Sema3g	sema domain, immunoglobulin domain (Ig), short basic domain, secreted, (semaphorin) 3G	-3.98
NM_001033757.1	Cdkn1c	cyclin-dependent kinase inhibitor 1C (P57)	-3.26
XM_231354.4	Sema3e	sema domain, immunoglobulin domain (Ig), short basic domain, secreted, (semaphorin) 3E	-3.24
XM_236640.4	Plxnb1	plexin B1	-2.78
NM_022589.1	Tspan2	tetraspanin 2	-2.74
XM_001063804.1	Hoxd10	homeo box D10	-2.72
NM_012827.1	Bmp4	bone morphogenetic protein 4	-2.41
NM_013088.1	Ptpn11	protein tyrosine phosphatase, non-receptor type 11	-2.26
XM_001056831.1	LOC681886	acyl-CoA synthetase short-chain family member 1; visual system homeobox 1	-2.05
XM_001068573.1	Hoxc10	homeo box C10	-2.00
NM_053896.1	Aldh1a2	aldehyde dehydrogenase 1 family, member A2	-1.88
NM_017129.1	Ctf1	cardiotrophin 1	-1.83
NM_052803.1	Atp7a	ATPase, Cu++ transporting, alpha polypeptide	-1.79
NM_019284.1	Cspg5	chondroitin sulfate proteoglycan 5	-1.71
NM_017259.1	Btg2	B-cell translocation gene 2, anti-proliferative	2.91
NM_012566.1	Gfi1	growth factor independent 1 transcription repressor	2.34
XM_001069879.1	Bcl11b	B-cell CLL/lymphoma 11B (zinc finger protein)	1.90
NM_013058.2	Id3	inhibitor of DNA binding 3	1.90

NM_053594.1	Ptprr	protein tyrosine phosphatase, receptor type, R	1.79
XM_220712.4	Scarf1	scavenger receptor class F, member 1	1.67
NM_022673.1	Mecp2	methyl CpG binding protein 2	1.64
Motif/Domain			
XM_222763.4	Tdrd5	tudor domain containing 5	-3.84
XM_001073627.1	Plekha5	pleckstrin homology domain containing, family A member 5	-3.79
XM_001055725.1	Kank1	KN motif and ankyrin repeat domains 1	-2.88
XM_001069410.1	Hoxc6	homeobox C6	-2.87
XM_001058167.1	Sgip1	SH3-domain GRB2-like (endophilin) interacting protein 1	-2.78
NM_019316.1	Mafb	v-maf musculoaponeurotic fibrosarcoma oncogene family, protein B	-2.71
XM_001053668.1	Rc3h2	ring finger and CCCH-type zinc finger domains 2	-2.66
XM_001062112.1	Sh3bgrl2	SH3 domain binding glutamic acid-rich protein like 2	-2.44
XM_342682.3	Mpp6	membrane protein, palmitoylated 6 (MAGUK p55 subfamily member 6)	-2.39
NM_001012048.1	Sh2d4a	SH2 domain containing 4A	-2.28
NM_001014268.1	Lrrc1	leucine rich repeat containing 1	-2.11
NM_001011922.1	Nedd9	neural precursor cell expressed, developmentally down-regulated gene 9	-1.84
NM_012828.1	Cacnb3	calcium channel, voltage-dependent, beta 3 subunit	-1.76
NM_001007148.1	Btrc	beta-transducin repeat containing protein	-1.73
NM_001002277.1	Ahi1	Abelson helper integration site 1	-1.66
XM_233830.4	Plekhh2	pleckstrin homology domain containing, family H (with MyTH4 domain) member 2	-1.65
XM_001081287.1	Ankrd40	ankyrin repeat domain 40	-1.61
NM_130821.1	Samsn1	SAM domain, SH3 domain and nuclear localization signals, 1	2.75
XM_576306.2	LOC500904	neutrophil cytosolic factor 4	2.52
NM_001013118.1	Abi3	ABI family, member 3	2.23
NM_017168.1	Plcg2	phospholipase C, gamma 2	1.98
NM_031238.1	Sh3gl3	SH3-domain GRB2-like 3	1.96
NM_001024260.1	Nostrin	nitric oxide synthase trafficker	1.92
NM_001024255.1	Txk	TXK tyrosine kinase	1.92
NM_053851.1	Cacnb2	calcium channel, voltage-dependent, beta 2 subunit	1.86
NM_001011961.1	Srms	src-related kinase lacking C-terminal regulatory tyrosine and N-terminal myristylation sites	1.83
XM_340911.3	Mpp3	membrane protein, palmitoylated 3 (MAGUK p55 subfamily member 3)	1.77
NM_130413.1	Skap2	src family associated phosphoprotein 2	1.75
AMD protein complexes			
NM_017336.1	Ptpro	protein tyrosine phosphatase, receptor type, O	-2.42
NM_019357.1	Ezr	ezrin	-1.82
BMD protein complexes			

XM_342410.3	Aif1l	allograft inflammatory factor 1-like	-3.43
NM_012649.1	Sdc4	syndecan 4	-2.79
NM_001012032.1	Arhgap24	Rho GTPase activating protein 24	-2.48
NM_012983.2	Myo1d	myosin ID	-2.28
XM_340884.2	Itga3	integrin alpha 3	-2.23
XM_343483.3	Dag1	dystroglycan 1	-2.07
XM_001066264.1	Tenc1	tensin like C1 domain-containing phosphatase	-2.00
NM_012904.1	Anxa1	annexin A1	-1.91
XM_001078155.1	Parvb	parvin, beta	1.65
SD protein complexes			
NM_053621.1	Magi2	membrane associated guanylate kinase, WW and PDZ domain containing 2	-3.93
NM_021695.1	Synpo	synaptopodin	-3.62
XM_218486.3	Kirrel2	kin of IRRE like 2 (Drosophila)	-3.47
XM_001059464.1	Cdh11	cadherin 11	-3.16
NM_022628.1	Nphs1	nephrosis 1 homolog, nephrin	-3.06
NM_130828.2	Nphs2	nephrosis 2 homolog, podocin	-3.02
NM_001012055.1	Cdh16	cadherin 16	-2.73
XM_001059679.1	Ctnnal1	catenin (cadherin associated protein), alpha-like 1	-2.42
NM_031005.2	Actn1	actinin, alpha 1	-2.30
XM_001059817.1	Nck2	NCK adaptor protein 2	-2.10
XM_237115.1	Nck2	NCK adaptor protein 2	-1.62
XM_226213.4	Cdh5	cadherin 5	1.88
Cell junction			
XM_236385.4	Cgnl1	cingulin-like 1	-2.54
NM_012528.1	Chrnb1	cholinergic receptor, nicotinic, beta polypeptide 1 (muscle)	-2.40
NM_017198.1	Pak1	p21 protein (Cdc42/Rac)-activated kinase 1	-2.19
NM_012663.2	Vamp2	vesicle-associated membrane protein 2	-1.60
Tight junction			
NM_031699.1	Cldn1	claudin 1	-3.19
XM_001080868.1	Mpp5	membrane protein, palmitoylated 5 (MAGUK p55 subfamily member 5)	-2.33
NM_031675.2	Actn4	actinin alpha 4	-1.72
NM_017093.1	Akt2	thymoma viral proto-oncogene 2	-1.68
XM_342223.3	Prkci	protein kinase C, iota	-1.61
Cell morphogenesis			
XM_216679.4	Lamb1	laminin, beta 1	-2.84
NM_031235.1	Pard3	par-3 (partitioning defective 3) homolog (C. elegans)	-2.64
NM_012715.1	Adm	adrenomedullin	-2.10
XM_242297.4	Ntng2	netrin G2	-1.93
NM_024159.1	Dab2	disabled homolog 2	-1.74
NM_017089.2	Efnb1	ephrin B1	-1.65
Ion transport			
NM_001033693.1	Slc31a2	solute carrier family 31, member 2	-2.15

NM_022269.1	Cd55	CD55 antigen	-1.95
NM_139332.3	Tpcn1	two pore channel 1	-1.81
Kidney development			
XM_213677.3	Robo2	roundabout homolog 2	-4.77
NM_031534.1	Wt1	Wilms tumor 1 homolog	-4.05
NM_001032397.1	Tcf21	transcription factor 21	-3.54
NM_053758.1	Plce1	phospholipase C, epsilon 1	-3.29
XM_001053727.1	Bmp7	bone morphogenetic protein 7	-2.68
NM_012774.1	Gpc3	glypican 3	-2.37
NM_030849.1	Bmpr1a	bone morphogenetic protein receptor, type 1A	-2.13
XM_213954.4	Nid1	nidogen 1	-2.12
NM_173101.1	Myo1e	myosin IE	-2.03
NM_053566.1	Ptch1	patched homolog 1	-1.99
NM_053698.2	Cited2	Cbp/p300-interacting transactivator, with Glu/Asp-rich carboxy-terminal domain, 2	-1.68
XM_001070482.1	Cutl1	similar to CCAAT displacement protein isoform b; cut-like homeobox 1	-1.67
XM_340765.2	Pkd1	polycystic kidney disease 1 homolog (human)	-1.65
NM_001002827.1	Notch4	Notch homolog 4 (Drosophila)	1.76
XM_001054314.1	Tek	TEK tyrosine kinase, endothelial	1.71
Protein modification			
XM_001057269.1	Mgat5	mannoside acetylglucosaminyltransferase 5	-3.21
XM_219805.4	Prkg1	protein kinase, cGMP-dependent, type I	-3.02
XM_001076056.1	Uck2	uridine-cytidine kinase 2	-2.70
XM_001080770.1	Cpd	carboxypeptidase D	-2.30
XM_236687.4	Oxsr1	oxidative-stress responsive 1	-1.89
XM_227618.4	Cdc14a	CDC14 cell division cycle 14 homolog A	-1.66
Regulation of transcription			
NM_012760.1	Plagl1	pleiomorphic adenoma gene-like 1	-3.08
XR_007660.1	Zfp462	zinc finger protein 462	-2.29
NM_133560.2	Trak2	trafficking protein, kinesin binding 2	-2.26
NM_031346.1	Rod1	ROD1 regulator of differentiation 1	-2.04
NM_053583.1	Zfp423	zinc finger protein 423	-1.72
NM_021597.1	Eif2c2	eukaryotic translation initiation factor 2C, 2	-1.67
NM_021836.2	Junb	jun B proto-oncogene	3.85
XM_001076072.1	Lmcd1	LIM and cysteine-rich domains 1	1.96
NM_021835.3	Jun	Jun	1.88
NM_012855.1	Jak3	Janus kinase 3	1.63
Signal transduction			
NM_001002829.1	Rasl11a	RAS-like, family 11, member A	-2.31
XM_001073244.1	Plxdc2	plexin domain containing 2	-2.31
NM_080904.2	Arf3	ADP-ribosylation factor 3	-1.92
NM_032076.2	Ptger4	prostaglandin E receptor 4 (subtype EP4)	-1.78
NM_001009405.1	Arhgap29	Rho GTPase activating protein 29	-1.61

Vesicle			
NM_022251.1	Enpep	glutamyl aminopeptidase	-2.92
NM_145081.3	Optn	optineurin	-2.84
XM_341428.2	Clcn3	chloride channel 3	-2.14
XM_342271.3	Lrba	LPS-responsive beige-like anchor	-1.83
Miscellaneous (podocyte related)			
NM_022943.1	Mertk	c-mer proto-oncogene tyrosine kinase	-3.12
XM_217192.4	Rora	RAR-related orphan receptor alpha	-2.70
XM_236376.4	Fam81a	family with sequence similarity 81, member A	-2.65
NM_017031.2	Pde4b	phosphodiesterase 4B, cAMP specific	-2.49
NM_133569.1	Angptl2	angiopoietin-like 2	-2.45
XM_221276.3	Arvcf	armadillo repeat gene deleted in velo-cardio-facial syndrome	-2.39
XM_575387.2	Thsd7a	thrombospondin, type I, domain containing 7A	-2.38
XM_219201.4	Ppfibp2	PTPRF interacting protein, binding protein 2 (liprin beta 2)	-2.37
XM_001053270.1	Ccpg1	cell cycle progression 1	-2.34
NM_013220.1	Ankrd1	ankyrin repeat domain 1	-2.32
XM_226988.4	Fndc3b	fibronectin type III domain containing 3B	-2.30
XM_001061817.1	Erlin2	ER lipid raft associated 2	-2.26
XM_001075785.1	Fam65a	family with sequence similarity 65, member A	-2.26
XM_340875.3	Rnft1	ring finger protein, transmembrane 1	-2.04
XM_340886.3	Nfe2l1	nuclear factor, erythroid derived 2,-like 1	-2.01
NM_133601.1	Cblb	Casitas B-lineage lymphoma b	-1.94
NM_001013882.1	Dctd	dCMP deaminase	-1.92
NM_021850.2	Bcl2l2	Bcl2-like 2; poly(A) binding protein, nuclear 1	-1.89
NM_001005888.1	Galc	galactosylceramidase	-1.85
NM_001014102.1	Spats2l	spermatogenesis associated, serine-rich 2-like	-1.80
NM_001007654.1	Agtrap	angiotensin II receptor-associated protein	-1.80
NM_001025627.1	Leprel1	leprecan-like 1	-1.77
XM_343420.3	Fam63b	family with sequence similarity 63, member B	-1.75
XM_230036.4	Ssfa2	sperm specific antigen 2	-1.68
XM_001070133.1	Nbeal1	neurobeachin like 1	-1.65
NM_033485.2	Pawr	PRKC, apoptosis, WT1, regulator	-1.64
NM_012868.1	Npr3	natriuretic peptide receptor 3	-1.61
NM_199412.1	Cbara1	calcium binding atopy-related autoantigen 1	-1.61
NM_031970.1	Hspb1	heat shock protein 1	2.42
NM_053704.1	Bik	BCL2-interacting killer (apoptosis-inducing)	2.15
NM_173153.2	Gimap4	GTPase, IMAP family member 4	2.02
NM_012938.1	Ctse	cathepsin E	2.01
XM_001067588.1	Tm6sf1	transmembrane 6 superfamily member 1	1.83
NM_023962.2	Pdgfd	platelet-derived growth factor, D polypeptide	1.80

NM_057138.2	Cflar	CASP8 and FADD-like apoptosis regulator	1.80
XM_215117.4	Ifitm1	interferon induced transmembrane protein 1	1.74
XM_001059368.1	Ldb2	LIM domain binding 2	1.74
NM_001025141.1	Ccnb1ip1	cyclin B1 interacting protein 1	1.67
Miscellaneous (functional annotation enrichment scores <4.46)			
NM_145093.1	Aard	alanine and arginine rich domain containing protein	-6.02
XM_001056569.1	RGD1312005	similar to DD1	-5.88
XM_347233.3	LOC368066	indolethylamine N-methyltransferase	-5.10
NM_001012475.1	Rxfp2	relaxin/insulin-like family peptide receptor 2	-4.83
XM_573676.1	LOC498427	similar to ubiquitin specific protease 34	-4.81
XR_008037.1	RGD1561455	similar to Ras GTPase-activating-like protein IQGAP2	-4.53
NM_153300.1	Aldh1a3	aldehyde dehydrogenase 1 family, member A3	-4.26
NM_017081.1	Hsd11b2	hydroxysteroid 11-beta dehydrogenase 2	-4.17
XM_001081892.1	Ngfg	kallikrein 1-related peptidase b3	-4.14
XM_575542.1	LOC500190	similar to IgM kappa chain variable region	-4.14
XM_001072453.1	RGD1560652	RGD1560652; hypothetical protein LOC690830	-4.07
XM_575706.1	LOC500353	RGD1566261	-4.06
XM_576597.1	LOC501170	similar to adaptor-related protein complex AP-1, sigma 3	-3.95
XM_238042.4	RGD1564108	Hedgehog-interacting protein	-3.85
XM_001062343.1	Marveld2	MARVEL domain containing 2	-3.84
XM_001065454.1	Elovl7	ELOVL family member 7, elongation of long chain fatty acids (yeast)	-3.83
XM_344015.3	RGD1562717	similar to ABI gene family, member 3 (NESH) binding protein	-3.82
XM_001060350.1	Large	like-glycosyltransferase	-3.82
XM_342632.3	Pftk1	PFTAIRE protein kinase 1	-3.81
XM_001054726.1	RGD1561985	dystrobrevin alpha	-3.79
NM_001034160.1	Apeg3	antisense paternally expressed gene 3	-3.78
XM_001067936.1	RGD1561090	protein tyrosine phosphatase, receptor type, D	-3.75
XM_238275.3	LOC295976	RGD1560837	-3.73
XM_575380.2	RGD1563612	similar to testhymin	-3.67
XM_575721.2	RGD1559723	sarcospan	-3.64
NM_001014244.1	Cyb5r2	cytochrome b5 reductase 2	-3.64
XM_001063197.1	RGD1559717	RPE-spondin	-3.56
XM_574931.1	LOC499605	similar to LRRGT00057	-3.54
XM_219909.4	RGD1307524	similar to Friedreich ataxia region gene X123	-3.53
XM_001069399.1	LOC684205	similar to MIC2 like 1	-3.44
XM_001053430.1	RGD1559891	similar to synaptonemal complex protein 3	-3.40
XM_573889.1	LOC498611	similar to LRRGT00176	-3.38
NM_012593.1	Klk1l	kallikrein 1-like peptidase; kallikrein-related peptidase 7	-3.36

XM_001079138.1	RGD1563574	similar to Hypothetical protein MGC30332	-3.36
XM_001078963.1	Usp43	ubiquitin specific peptidase 43	-3.33
XM_213993.4	Abhd7	epoxide hydrolase 4	-3.33
XM_215016.3	Sox6	SRY (sex determining region Y)-box 6	-3.31
NM_001024297.1	Spz1	spermatogenic leucine zipper 1	-3.29
XM_001059530.1	RGD1305809	Na+/K+ transporting ATPase interacting 4	-3.28
XM_224841.4	Odz3	odz, odd Oz/ten-m homolog 3 (Drosophila)	-3.26
XM_001053329.1	RGD1311196	tudor and KH domain containing	-3.26
XM_577046.1	LOC501651	similar to LRRGT00057	-3.25
XM_573435.1	LOC498217	similar to LRRG00135	-3.19
XM_001070775.1	Sorcs1	sortilin-related VPS10 domain containing receptor 1	-3.19
NM_053352.1	Cxcr7	chemokine (C-X-C motif) receptor 7	-3.18
XM_575335.1	LOC499981	similar to lamin B3	-3.10
XM_574804.1	LOC499481	similar to LRRGT00057	-3.05
NM_175759.2	Klks3	kallikrein, submaxillary gland S3	-3.04
XM_574907.1	LOC499582	similar to LRRGT00176	-3.02
XM_001059696.1	LOC498331	protein tyrosine phosphatase, non-receptor type 13	-3.02
XM_575738.1	LOC500380	similar to LRRGT00008	-2.99
XM_575195.1	LOC499854	similar to putative RNA binding protein 1	-2.98
XM_575790.1	LOC500428	similar to putative RNA binding protein 1	-2.97
XM_577047.1	LOC501652	similar to LRRGT00194	-2.96
XM_574687.1	LOC499372	similar to ORF1	-2.96
XM_575071.1	LOC499737	similar to LRRGT00057	-2.95
XM_574880.1	LOC499555	similar to LRRGT00082	-2.94
XM_342147.2	LOC361853	family with sequence similarity 184, member A	-2.94
XM_575748.1	LOC500389	similar to LRRGT00176	-2.92
XM_233266.3	Ttc22	tetratricopeptide repeat domain 22	-2.92
XM_574484.1	LOC499197	similar to LRRGT00057	-2.90
XM_221497.4	Bbx	bobby sox homolog (Drosophila)	-2.89
NM_001004278.2	Tsga10ip	testis specific 10 interacting protein	-2.88
XM_576800.1	LOC501387	similar to LRRGT00173	-2.87
XM_001079607.1	RGD1560542	proline rich Gla (G-carboxyglutamic acid) 4 (transmembrane)	-2.87
XM_574888.1	LOC499564	similar to LRRGT00057	-2.86
XM_576360.1	LOC500949	similar to LRRGT00176	-2.85
XM_573538.2	RGD1564105	vasohibin 2	-2.85
XM_342182.2	LOC361885	similar to LRRGT00194	-2.83
XM_341843.2	Ankrd27	ankyrin repeat domain 27 (VPS9 domain)	-2.83
XM_576325.1	LOC500916	similar to LRRGT00176	-2.82
XR_009191.1	RGD1309847	similar to peptidylglycine alpha-amidating monooxygenase COOH-terminal interactor; peptidylglycine alpha-amidating monooxygenase COOH-terminal interactor protein-1	-2.82

XM_001062695.1	RGD1562954	aldo-keto reductase family 1, member C19	-2.81
XM_574855.1	LOC499531	similar to LRRGT00176	-2.81
NM_017058.1	Vdr	vitamin D (1,25- dihydroxyvitamin D3) receptor	-2.81
XM_575541.1	LOC500189	similar to Ig kappa chain	-2.79
NM_001002830.2	Rasl11b	RAS-like family 11 member B	-2.76
NM_001024265.1	RGD1311251	similar to RIKEN cDNA 4930550C14	-2.76
NM_001030024.1	Slc19a2	solute carrier family 19 (thiamine transporter), member 2	-2.76
XM_234454.4	Ston2	stonin 2	-2.76
XM_213964.4	Disp1	dispatched homolog 1 (Drosophila)	-2.75
XM_001059200.1	LOC681982	tuftelin 1	-2.75
XM_574260.1	LOC498973	similar to LRRGT00176	-2.74
XM_575869.1	LOC500507	similar to LRRGT00194	-2.74
XM_574084.1	LOC498799	similar to LRRGT00057	-2.74
XM_573613.1	LOC498378	similar to LRRGT00176	-2.74
XM_576530.1	LOC501112	similar to putative RNA binding protein 1 (LOC501112)	-2.73
NM_001024888.1	Gatad2b	GATA zinc finger domain containing 2B	-2.73
XM_001079075.1	Ppl	periplakin	-2.72
XM_573829.1	LOC498553	similar to putative RNA binding protein 1 (LOC498553)	-2.72
XM_574081.1	LOC498795	coiled-coil domain containing 3	-2.72
NM_001013863.1	Ydjc	YdjC homolog (bacterial)	-2.71
XM_574492.1	LOC499206	similar to LRRGT00057	-2.70
XM_573952.1	LOC498669	similar to LRRGT00176	-2.70
XM_576174.1	LOC500788	similar to LRRGT00176	-2.70
XM_575859.1	LOC500495	similar to LRRGT00176	-2.69
NM_019249.1	Ptprf	protein tyrosine phosphatase, receptor type, F	-2.69
NM_177426.1	Gstm2	glutathione S-transferase mu 2	-2.69
XM_579642.1	LOC497701	hypothetical gene supported by NM_134459	-2.69
XM_225733.4	Pard6g	par-6 partitioning defective 6 homolog gamma (C. elegans)	-2.68
XM_574023.1	LOC498745	similar to LRRGT00057	-2.68
XM_001067343.1	Arhgef17	Rho guanine nucleotide exchange factor (GEF) 17	-2.68
XM_001060502.1	RGD1566180	RGD1566180	-2.67
XM_576284.1	LOC500883	similar to LRRGT00082	-2.67
XM_340961.2	LOC360690	similar to LRRGT00194	-2.66
XM_579538.1	LOC497706	hypothetical gene supported by NM_031819	-2.66
XM_001056810.1	RGD1309701	family with sequence similarity 114, member A1; similar to RIKEN cDNA 9130005N14	-2.65
XM_575567.1	LOC500216	similar to LRRGT00194	-2.64
XM_001064705.1	RGD1564709	similar to ATP-binding cassette, sub-family G (WHITE), member 3	-2.63
XM_342428.2	LOC362127	similar to putative RNA binding protein 1	-2.63

NM_130738.1	Snurf	similar to small nuclear ribonucleoparticle-associated protein; SNRPN upstream reading frame	-2.62
XM_001054725.1	Ogn	osteoglycin	-2.62
XM_001069683.1	RGD1565408	SERTA domain containing 4	-2.61
XM_001069787.1	Snx12	sorting nexin 12	-2.61
XM_001070222.1	Dcdc2	doublecortin domain containing 2	-2.60
XM_573579.1	LOC498346	similar to putative RNA binding protein 1	-2.59
XR_009111.1	RGD1311309	similar to 2510002A14Rik protein	-2.58
XM_343130.2	LOC362803	similar to putative RNA binding protein 1	-2.56
NM_001007645.1	MGC95152	similar to B230212L03Rik protein	-2.56
XM_227030.4	Ttc14	tetratricopeptide repeat domain 14	-2.55
NM_053573.1	Olfm1	olfactomedin 1	-2.55
NM_031745.2	Clip1	CAP-GLY domain containing linker protein 1	-2.55
XM_574188.1	LOC498901	similar to LRRGT00176	-2.55
XM_343479.3	Sema3b	sema domain, immunoglobulin domain (Ig), short basic domain, secreted, (semaphorin) 3B	-2.53
XM_001061697.1	Susd1	sushi domain containing 1	-2.53
XM_345984.2	LOC501057	similar to Mtap4 protein	-2.51
XM_237064.4	RGD1310819	similar to putative protein (5S487)	-2.50
NM_001015017.1	Olfm2	olfactomedin 2	-2.50
XM_576950.1	LOC501548	similar to LRRG00135	-2.49
NM_133402.2	Nap1l3	nucleosome assembly protein 1-like 3	-2.49
XM_001074148.1	Piwil4	piwi-like 4 (Drosophila)	-2.49
XM_215728.4	Smarca3	helicase-like transcription factor	-2.49
XM_577034.1	LOC501637	similar to LRRG00135	-2.49
XM_573309.1	LOC498105	similar to LRRGT00176	-2.48
XM_342281.3	Muc1	mucin 1, cell surface associated	-2.47
NM_001024791.1	Epn3	epsin 3	-2.47
NM_001011984.1	Asb2	ankyrin repeat and SOCS box-containing 2	-2.46
XM_576904.1	LOC501503	nucleic acid binding protein; hypothetical protein LOC689117	-2.46
XM_218462.4	RGD1310942	similar to R27328_1	-2.45
XM_579778.1	LOC498061	RGD1564312	-2.45
XM_574001.2	Elovl2	elongation of very long chain fatty acids (FEN1/Elo2, SUR4/Elo3, yeast)-like 2; similar to Elongation of very long chain fatty acids protein 2	-2.44
XM_001071030.1	Kbtbd9	kelch-like 29 (Drosophila)	-2.44
XM_226397.2	RGD1308358	similar to 2210023G05Rik protein	-2.44
XM_001065428.1	Ccbe1	collagen and calcium binding EGF domains 1	-2.44
XM_579677.1	LOC497785	hypothetical gene supported by NM_147211	-2.43
XM_574960.1	LOC499638	similar to LRRGT00057	-2.43
XM_573611.1	LOC498376	similar to ORF4	-2.42
XM_341405.2	LOC361117	similar to Rb1-inducible coiled coil protein 1	-2.41

XM_001063544.1	LOC362564	BEN domain containing 5	-2.41
XM_232253.3	LOC312683	similar to KIAA0819 protein	-2.40
XM_576977.1	LOC501573	similar to LRRGT00194	-2.40
XM_001062086.1	RGD1564964	similar to WD repeat domain 11 protein	-2.40
XM_001067324.1	RGD1564560	similar to RCK	-2.40
XM_575756.1	LOC500397	similar to LRRGT00176	-2.40
XM_575955.1	LOC500586	similar to LRRGT00057	-2.40
XM_226455.4	Zfp612	zinc finger protein 23 (KOX 16)	-2.39
XM_217293.4	Ctdspl	CTD (carboxy-terminal domain, RNA polymerase II, polypeptide A) small phosphatase-like	-2.38
NM_001014095.1	Dzip1l	DAZ interacting protein 1-like	-2.38
XM_574268.1	LOC498979	similar to LRRGT00194	-2.37
XM_579762.2	RGD1562012	RGD1562012	-2.37
XM_345970.3	Chst2	carbohydrate sulfotransferase 2	-2.36
XR_005694.1	LOC680293	similar to developmental pluripotency associated 4 isoform 1	-2.35
XM_575695.1	LOC500343	similar to LRRGT00176	-2.35
XM_573278.1	LOC498076	similar to RIKEN cDNA 2410116I05	-2.35
NM_001008364.1	Snx24	sorting nexin 24	-2.35
XM_573468.1	LOC498245	similar to LRRGT00176	-2.34
XM_221263.4	Slc7a4	solute carrier family 7 (cationic amino acid transporter, y+ system), member 4	-2.34
XM_579843.1	LOC498652	RGD1562341	-2.34
XM_001059291.1	Klhdc8a	kelch domain containing 8A	-2.34
XM_578457.1	LOC502952	similar to alpha-2u globulin PGCL4	-2.32
XM_576350.1	LOC500940	similar to LRRGT00126	-2.31
XM_579720.1	LOC497836	hypothetical gene supported by NM_181475	-2.29
XM_001063318.1	Xpo4	exportin 4	-2.29
XM_001061729.1	RGD1565886	RGD1565886	-2.29
XM_001054590.1	LOC679075	similar to l(3)mbt-like 3	-2.29
XM_573902.1	LOC498623	similar to LRRGT00176	-2.28
XM_575635.1	LOC500285	similar to LRRGT00176	-2.28
XM_213921.3	Creg	cellular repressor of E1A-stimulated genes 1	-2.27
XM_001071978.1	RGD1306151	similar to hypothetical protein DKFZp761D0211	-2.27
NM_001025063.1	Scrn1	secernin 1	-2.26
XM_575503.1	LOC500151	similar to RIKEN cDNA 2410116I05	-2.26
XM_001076815.1	RGD1310958	similar to RIKEN cDNA C130090K23	-2.24
XM_578934.1	LOC503396	similar to Ac1147	-2.24
XM_342055.3	Sema4g	sema domain, immunoglobulin domain (Ig), transmembrane domain (TM) and short cytoplasmic domain, (semaphorin) 4G	-2.23
NM_001014199.1	Atp6v1c2	ATPase, H+ transporting, lysosomal V1 subunit C2	-2.23
XM_001056150.1	LOC362068	G protein-coupled receptor 98	-2.23

XM_001071508.1	Sema5b	sema domain, seven thrombospondin repeats (type 1 and type 1-like), transmembrane domain (TM) and short cytoplasmic domain, (semaphorin) 5B	-2.22
XM_576443.1	LOC501032	similar to LRRGT00176	-2.22
XM_344817.2	LOC365104	similar to hypothetical protein cgd4_1450	-2.21
XM_234584.3	LOC299356	similar to RIKEN cDNA 4831426I19	-2.18
XM_576580.1	LOC501156	similar to LRRGT00176	-2.17
XM_001078792.1	RGD1309576	transmembrane protein 220	-2.17
XM_577983.2	RGD1565105	small EDRK-rich factor 1	-2.16
XM_576265.1	LOC500867	similar to LRRG00116	-2.16
NM_172038.1	Gstm5	glutathione S-transferase, mu 5	-2.16
XM_577051.1	LOC501656	similar to LRRGT00057	-2.15
XM_573248.1	LOC498048	similar to ORF4	-2.15
NM_017303.2	Kcnab1	potassium voltage-gated channel, shaker-related subfamily, beta member 1	-2.14
XM_001078124.1	Arhgap8	proline rich 5 (renal)	-2.14
XM_223428.4	RGD1307468	RELT-like 1	-2.13
XM_001055013.1	RGD1561255	leucine-rich repeats and immunoglobulin-like domains 3	-2.13
XM_230024.4	RGD1562244	SEC14 and spectrin domains 1	-2.13
XM_001071349.1	Lrp6	low density lipoprotein receptor-related protein 6	-2.12
XM_001068317.1	RGD1563354	similar to hypothetical protein D630003M21	-2.12
XM_001068586.1	RGD1564808	ubiquitin specific peptidase 46	-2.12
NM_001014240.2	LOC364773	aldo-keto reductase family 1, member C13	-2.11
XM_001076292.1	RGD1565496	similar to Butyrate-induced transcript 1	-2.11
XM_001070748.1	Lrrc16	leucine rich repeat containing 16A	-2.11
XM_213633.4	Hoxd3_mapped	homeo box D3	-2.10
XM_573616.1	LOC498381	similar to ORF1	-2.10
XM_576615.1	LOC501187	hypothetical protein LOC501187	-2.10
XM_215524.4	Tpd52	tumor protein D52	-2.09
XM_345665.2	LOC366608	similar to mKIAA0716 protein	-2.09
XM_220693.4	RGD1307222	similar to mKIAA0664 protein	-2.09
XM_342631.2	LOC362315	similar to Retrovirus-related POL polyprotein	-2.09
XM_237794.3	LOC287564	transmembrane protein 132E	-2.08
XR_009616.1	LOC498759	hypothetical protein LOC685873; LRRGT00094	-2.08
XM_342241.2	LOC361942	similar to ORF4	-2.08
XM_342864.2	LOC362543	similar to LRRG00116	-2.08
NM_019363.2	Aox1	aldehyde oxidase 1	-2.08
XM_227657.4	Bcar3	breast cancer anti-estrogen resistance 3	-2.07
NM_177425.3	Csrp2	cysteine and glycine-rich protein 2	-2.07
XM_576501.1	LOC501087	similar to LRRGT00057	-2.07
XM_576860.1	LOC501449	similar to ORF2 consensus sequence encoding endonuclease and reverse transcriptase minus RNaseH	-2.06

NM_017226.1	Padi2	peptidyl arginine deiminase, type II	-2.06
XM_574702.1	LOC499388	similar to LRRGT00082	-2.05
XM_001063599.1	Odz4	odz, odd Oz/ten-m homolog 4 (Drosophila)	-2.05
XM_001059473.1	Lysmd2	LysM, putative peptidoglycan-binding, domain containing 2	-2.04
XM_001057514.1	Fcmd	fukutin	-2.04
XM_343815.2	LOC363492	similar to Ac1262	-2.04
NM_001031660.1	Msrb2	methionine sulfoxide reductase B2	-2.04
XM_575847.1	LOC500480	similar to ORF1	-2.04
XM_001058156.1	Lrpap1	low density lipoprotein receptor-related protein associated protein 1	-2.03
XM_001058239.1	Syngr3	synaptogyrin 3	-2.03
XM_575569.1	LOC500218	similar to LRRGT00173	-2.03
XM_001072062.1	Wdr35	WD repeat domain 35; WD repeat domain 35-like	-2.03
XM_001080610.1	Nxn	nucleoredoxin	-2.02
XM_224972.3	LOC306577	similar to expressed sequence BB049667	-2.02
NM_031117.1	Snrpn	small nuclear ribonucleoprotein polypeptide N; small nuclear ribonucleoprotein polypeptides B and B1	-2.02
NM_001025402.1	Umps	uridine monophosphate synthetase	-2.01
XM_342067.3	RGD1307158	similar to oocyte-testis gene 1	-2.01
XM_001054328.1	RGD1564930	similar to novel protein similar to Tensin Tns	-2.01
XM_238787.4	Rhpn2	rhophilin, Rho GTPase binding protein 2	-2.01
NM_001024978.1	RGD1305844	hypothetical LOC294883	-2.00
XM_222679.4	RGD1560834	zinc finger and BTB domain containing 41	-2.00
XM_573943.2	LOC498662	similar to RIKEN cDNA 2610019F03	-2.00
XM_574144.2	RGD1561942	coiled-coil domain containing 112	-2.00
XM_579646.1	LOC497726	hypothetical gene supported by NM_138518	-2.00
XM_343907.3	Gtlf3b	gene trap locus F3b	-2.00
XM_342331.3	Agl	amylo-1,6-glucosidase, 4-alpha-glucanotransferase	-1.99
XR_008124.1	RGD1565779	similar to hypothetical protein E230025N22	-1.98
NM_031141.2	Pax8	paired box 8	-1.98
XM_001074613.1	RGD1311980	family with sequence similarity 20, member C	-1.97
XM_225864.4	Spire1	spire homolog 1 (Drosophila)	-1.96
XM_227409.4	Ash1l	ash1 (absent, small, or homeotic)-like (Drosophila)	-1.96
XM_243652.4	Plxnb2	plexin B2	-1.95
NM_001012091.1	Foxs1	forkhead box S1	-1.94
XM_001073019.1	Zfp521	zinc finger protein 521	-1.94
XM_577516.1	LOC502081	similar to LRRGT00049	-1.94
XR_008228.1	RGD1566399	similar to MYST histone acetyltransferase monocytic leukemia 4; similar to Histone acetyltransferase MYST4 (MYST protein 4) (MOZ,	-1.94

		YBF2/SAS3, SAS2 and TIP60 protein 4) (Querkopf protein)	
XR_007788.1	RGD1309368	crumbs homolog 2 (Drosophila)	-1.93
NM_001004246.1	Ttc12	tetratricopeptide repeat domain 12	-1.93
XM_238219.2	RGD1562890	RGD1562890	-1.93
XM_001076726.1	RGD1561651	similar to zinc finger protein 609; zinc finger protein 609	-1.93
XM_234092.4	RGD1311444	patatin-like phospholipase domain containing 8	-1.93
XM_343313.3	RGD1308012	family with sequence similarity 116, member B	-1.91
XR_009418.1	LOC688018	similar to SH3-domain binding protein 3	-1.91
NM_134398.1	P34	p34 protein; similar to Alpha- and gamma-adaptin-binding protein p34	-1.91
XM_574161.2	Nedd4l	neural precursor cell expressed, developmentally down-regulated 4-like	-1.91
XM_233953.3	LOC313940	similar to Hypothetical protein KIAA1240	-1.91
XM_001060542.1	LOC681153	hypothetical protein LOC681153	-1.90
XM_579502.1	LOC497745	hypothetical gene supported by NM_031049	-1.90
NM_001013132.1	Fbxo16	F-box protein 16	-1.89
XM_342207.2	LOC361912	similar to LRRG00116	-1.89
XM_225526.4	Larp5	La ribonucleoprotein domain family, member 5	-1.89
NM_001013984.1	Npl	N-acetylneuraminate pyruvate lyase	-1.89
XM_575855.1	LOC500490	similar to Retrovirus-related POL polyprotein	-1.89
XM_341148.3	Pou2f1	POU domain, class 2, transcription factor 1	-1.88
NM_133586.1	Ces2	carboxylesterase 2 (intestine, liver)	-1.88
XM_347084.2	LOC362870	RGD1566301	-1.88
XM_001079241.1	LOC687582	outer dense fiber of sperm tails 2-like	-1.87
XM_215939.4	Pltp	phospholipid transfer protein	-1.87
XM_580203.1	LOC501498	LOC501498	-1.87
XM_001066967.1	Kctd3	potassium channel tetramerisation domain containing 3	-1.87
XM_341918.2	LOC361639	similar to CG14182-PA	-1.87
XM_579486.1	LOC497780	hypothetical gene supported by NM_024353	-1.87
NM_022400.1	Bcat2	branched chain aminotransferase 2, mitochondrial	-1.87
NM_001025772.1	MGC114440	similar to RIKEN cDNA 4930555I21	-1.86
XM_222190.3	LOC304500	similar to acetyl-coA dehydrogenase - related (111.6 kD) (5G231)	-1.86
NM_031347.1	Ppargc1a	peroxisome proliferator-activated receptor gamma, coactivator 1 alpha	-1.85
XM_236411.4	Myo5c	myosin VC	-1.85
XM_001072989.1	Sulf2	sulfatase 2	-1.85
XM_001074860.1	RGD1559432	RGD1559432	-1.84
XM_225941.4	Dmxl1	Dmx-like 1	-1.84
XM_001067729.1	Mll_mapped	myeloid/lymphoid or mixed-lineage leukemia 1	-1.84
XM_575799.1	LOC500437	similar to LRRGT00094	-1.84

NM_001007628.1	Cxxc5	CXXC finger 5	-1.84
XM_575015.2	RGD1560967	G-protein signaling modulator 2 (AGS3-like, C. elegans)	-1.83
XM_001061692.1	Pus7	pseudouridylate synthase 7 homolog (S. cerevisiae)	-1.83
XM_574879.1	LOC499554	similar to ORF2 consensus sequence encoding endonuclease and reverse transcriptase minus RNaseH	-1.83
NM_001013979.1	LOC304131	similar to C21ORF7	-1.82
XM_001067414.1	Phldb1	pleckstrin homology-like domain, family B, member 1	-1.82
NM_181362.1	Cand2	cullin-associated and neddylation-dissociated 2 (putative)	-1.82
XM_574477.1	LOC499184	similar to LRRGT00082	-1.82
NM_199376.1	Sil1	SIL1 homolog, endoplasmic reticulum chaperone (S. cerevisiae)	-1.81
XM_001081128.1	Zc3h6	zinc finger CCCH type containing 6	-1.80
XM_573393.1	LOC498177	zinc finger protein ZFOC1	-1.80
NM_001008861.2	Usp11	ubiquitin specific peptidase 11	-1.80
XM_001071113.1	RGD1562920	androgen-induced 1	-1.80
XM_579872.1	LOC498813	LOC498813	-1.79
XR_009136.1	LOC360932	ATPase, class V, type 10D	-1.79
XM_574910.1	LOC499585	similar to LRRG00135	-1.79
NM_001009537.1	MGC72997	zinc finger protein 799	-1.79
XM_221043.4	Tex2	testis expressed 2	-1.79
XM_236938.4	RGD1310693	radial spoke head 9 homolog (Chlamydomonas)	-1.78
XM_218816.4	Man2a2	mannosidase 2, alpha 2	-1.78
XM_576459.2	Ppp2r3a	protein phosphatase 2 (formerly 2A), regulatory subunit B", alpha	-1.78
XM_574735.1	Pcbp3	poly(rC) binding protein 3	-1.78
XM_001062225.1	Kctd1	potassium channel tetramerisation domain containing 1	-1.78
XM_222685.3	Hrpt2	cell division cycle 73, Paf1/RNA polymerase II complex component, homolog (S. cerevisiae)	-1.77
XM_222288.3	LOC304592	similar to olf186-F CG11430-PB, isoform B; ORAI calcium release-activated calcium modulator 2	-1.77
XM_235064.4	Eea1	early endosome antigen 1	-1.76
XM_579655.1	LOC497844	hypothetical gene supported by NM_138846	-1.76
NM_001005906.1	Chpf	chondroitin polymerizing factor	-1.76
XM_341029.3	RGD1307396	similar to RIKEN cDNA 6330406I15	-1.76
XM_001054836.1	LOC300472	vacuolar protein sorting 26 homolog B (S. pombe)	-1.76
NM_053642.2	Sc5dl	sterol-C5-desaturase (ERG3 delta-5-desaturase homolog, S. cerevisiae)-like	-1.76
NM_001008316.1	Plag1	pleiomorphic adenoma gene 1	-1.75
XM_573911.2	RGD1559427	WW and C2 domain containing 2	-1.75
XM_573735.1	LOC498477	similar to Spetex-2C protein	-1.75
XM_341877.3	Iqgap1	IQ motif containing GTPase activating protein 1	-1.75

NM_139330.1	Sipa1l1	signal-induced proliferation-associated 1 like 1	-1.75
XM_579393.1	LOC497757	guanylate cyclase 1, soluble, alpha 3	-1.75
NM_001007646.1	Fkbp9	FK506 binding protein 9, 63 kDa	-1.75
XM_573448.1	LOC498228	major facilitator superfamily domain containing 4	-1.75
XM_576133.1	LOC500755	similar to LRRGT00008	-1.75
XM_225213.4	Aof1	amine oxidase (flavin containing) domain 1	-1.75
NM_080899.1	Ikbkap	inhibitor of kappa light polypeptide gene enhancer in B-cells, kinase complex-associated protein	-1.74
XM_234923.4	RGD1304737	similar to KIAA1086 protein	-1.74
XM_001070228.1	Braf	v-raf murine sarcoma viral oncogene homolog B1	-1.74
XM_001055328.1	Fign	fidgetin	-1.74
XM_575991.1	LOC500617	similar to LRRGT00014	-1.74
XM_001071417.1	Gpr126	G protein-coupled receptor 126	-1.73
NM_032074.1	Irs3	insulin receptor substrate 3	-1.73
XM_001080455.1	Klk1c10	T-kininogenase	-1.73
NM_184046.1	Rtkn	rhotekin	-1.73
NM_001013071.1	Tm7sf2	transmembrane 7 superfamily member 2	-1.73
XM_001069309.1	RGD1562848	RGD1562848	-1.73
XM_238063.4	Ibrdc1	ring finger protein 217	-1.73
XM_228042.3	RGD1309887	potassium channel tetramerisation domain containing 20	-1.72
NM_001033656.1	Man1a	mannosidase, alpha, class 1A, member 1	-1.72
XM_232620.3	Mybl1	myeloblastosis oncogene-like 1	-1.72
XM_236192.2	Ddx6	DEAD (Asp-Glu-Ala-Asp) box polypeptide 6 (Ddx6)	-1.72
XM_001063707.1	Msc	musculin	-1.72
XM_573061.2	Rgs11	regulator of G-protein signaling 11	-1.72
NM_053456.1	Plcl1	phospholipase C-like 1	-1.72
XM_579620.1	LOC497747	hypothetical gene supported by NM_133395	-1.72
XM_580006.1	LOC499701	RGD1563244	-1.72
XM_001057150.1	Ptpdc1	protein tyrosine phosphatase domain containing 1	-1.72
XM_001060543.1	RGD1560335	phosphatidylinositol glycan anchor biosynthesis, class G	-1.71
XM_343376.2	Znf500	zinc finger protein 500	-1.71
XM_227769.2	LOC310926	hypothetical protein LOC310926	-1.71
NM_031503.1	Ascl2	achaete-scute complex homolog 2 (Drosophila)	-1.71
XM_577031.1	LOC501634	similar to LRRGT00176	-1.71
NM_001014165.1	RGD1310039	similar to hypothetical protein FLJ10058	-1.70
XM_001073363.1	Chst9	carbohydrate (N-acetylgalactosamine 4-0) sulfotransferase 9	-1.70
NM_017220.1	Pts	6-pyruvoyl-tetrahydropterin synthase	-1.70
XM_342286.3	Slc39a1	solute carrier family 39 (zinc transporter), member 1	-1.70
NM_001014131.1	RGD1309708	similar to RIKEN cDNA 4930455F23	-1.70

XM_001079385.1	Jmjd3	jumonji domain containing 3	-1.70
XM_001069011.1	RGD1566359	similar to RIKEN cDNA B230219D22	-1.70
NM_001024315.1	LOC499949	similar to hypothetical protein FLJ90166	-1.70
NM_012736.1	Gpd2	glycerol-3-phosphate dehydrogenase 2, mitochondrial	-1.70
XM_342731.2	Sumf1	sulfatase modifying factor 1	-1.70
XM_222315.4	Baz2a	bromodomain adjacent to zinc finger domain, 2A	-1.69
XM_576928.1	LOC501527	similar to LRRGT00057	-1.69
NM_133541.1	Gtf3c1	general transcription factor III C 1	-1.69
XM_575347.1	LOC499992	similar to Retrovirus-related POL polyprotein	-1.69
XM_001071807.1	RGD1566054	tetratricopeptide repeat domain 15	-1.69
XM_001070393.1	RGD1307696	fat storage-inducing transmembrane protein 2	-1.68
XM_001061189.1	RGD1306493	WD repeat domain 60	-1.68
XM_574587.2	RGD1562983	HCCA2 protein	-1.68
XM_001053950.1	RGD1566050	similar to hypothetical protein FLJ32745	-1.68
XM_001056091.1	LOC499337	dedicator of cytokinesis 8	-1.68
NM_022857.1	N5	DNA binding protein N5	-1.68
NM_133421.1	Lkap	hypothetical gene supported by AB012133; NM_133421; similar to limkain b1; limkain b1	-1.68
XM_578786.2	RGD1565095	similar to hypothetical protein MGC52110	-1.68
XM_001056385.1	Ptchd1	patched domain containing 1	-1.68
NM_001024975.1	Morn4	MORN repeat containing 4	-1.68
XM_575480.2	RGD1564419	similar to hypothetical gene supported by BC025338	-1.67
XM_342548.3	Snta1	syntrophin, acidic 1	-1.67
XM_001055537.1	LOC679271	rhomboid, veinlet-like 2 (Drosophila)	-1.67
XM_341106.3	Fvt1	3-ketodihydrosphingosine reductase	-1.67
XM_001071547.1	LOC689581	eukaryotic translation initiation factor 5B, pseudogene 1; eukaryotic translation initiation factor 5B	-1.67
XM_234373.4	Ttc8	tetratricopeptide repeat domain 8	-1.67
XM_579510.1	LOC497724	hypothetical gene supported by NM_031525	-1.67
XM_001060860.1	LOC685778	pyruvate dehydrogenase E1 alpha 1 pseudogene; pyruvate dehydrogenase (lipoamide) alpha 1	-1.66
XM_001058768.1	Thoc2	similar to THO complex subunit 2 (Tho2); THO complex 2	-1.66
XM_001072660.1	Chchd6	coiled-coil-helix-coiled-coil-helix domain containing 6	-1.66
XM_220933.3	Arf4l	ADP-ribosylation factor 4-like	-1.66
XM_001071249.1	Kcnq5	potassium voltage-gated channel, subfamily Q, member 5-like	-1.66
NM_001012075.1	Tspyl4	TSPY-like 4	-1.66
XM_232064.4	Tcf3	transcription factor 3	-1.66
XM_342683.3	RGD1564287	oxysterol binding protein-like 3	-1.66
XM_217443.3	Glb1l	galactosidase, beta 1-like	-1.66

XM_579478.2	Gucy1a2	guanylate cyclase 1, soluble, alpha 2	-1.66
NM_001015012.1	Rab30	RAB30, member RAS oncogene family	-1.66
NM_153302.1	Dcps	decapping enzyme, scavenger	-1.66
XM_001060916.1	RGD1308290	similar to RIKEN cDNA 5730454B08; similar to Zinc finger CCCH-type domain-containing protein 11A	-1.66
XM_345130.1	LOC365612	similar to putative aminopeptidase Fxna	-1.65
XM_347115.2	LOC363240	RGD1565696	-1.65
NM_012988.1	Nfia	nuclear factor I/A	-1.65
XM_001053119.1	LOC360728	hypothetical protein LOC678704; ATPase type 13A3	-1.64
XM_223592.3	Zfp278	zinc finger protein 278	-1.64
NM_147145.1	Dclre1c	DNA cross-link repair 1C, PSO2 homolog (S. cerevisiae)	-1.64
XM_224461.3	Klf12	Kruppel-like factor 12	-1.64
XM_576559.1	LOC501139	similar to Ormdl1 protein	-1.64
NM_021581.1	Sc65	synaptonemal complex protein SC65	-1.64
XR_009288.1	RGD1564206	synapse defective 1, Rho GTPase, homolog 2 (C. elegans)	-1.64
XM_223945.4	Samd4	sterile alpha motif domain containing 4A	-1.63
NM_001004095.1	S100a11	S100 calcium binding protein A11 (calizzarin)	-1.63
XM_214734.4	RGD1311558	similar to 4930506M07Rik protein	-1.63
NM_001003957.1	Dnmt3a	DNA (cytosine-5-)-methyltransferase 3 alpha	-1.63
NM_182672.1	Cbr4	carbonyl reductase 4	-1.63
XM_216149.3	LOC297099	homeobox A9-like	-1.63
NM_022268.1	Pygl	phosphorylase, glycogen, liver	-1.63
NM_001014065.1	Zcchc12	zinc finger, CCHC domain containing 12	-1.63
NM_053718.1	Mllt3	myeloid/lymphoid or mixed-lineage leukemia (trithorax homolog, Drosophila); translocated to, 3	-1.63
XM_001078585.1	RGD1564019	similar to GTPase activating RANGAP domain-like 3	-1.62
XM_340870.3	RGD1305547	integrator complex subunit 2	-1.62
XM_001075851.1	RGD1309779	similar to ENSANGP00000021391	-1.62
XM_236292.4	Npat	nuclear protein, ataxia-telangiectasia locus	-1.62
XM_579481.1	LOC497728	hypothetical gene supported by NM_024137	-1.62
XM_574868.1	Pip3ap	myotubularin related protein 12	-1.61
XM_343923.2	Kctd11	potassium channel tetramerisation domain containing 11	-1.61
XM_228708.4	RGD1563226	ubiquitin-conjugating enzyme E2Q family member 2-like	-1.61
XM_001055855.1	Mtf1	metal-regulatory transcription factor 1	-1.61
XM_575067.1	LOC499732	leucine-rich repeats and IQ motif containing 3	-1.61
XM_236739.4	Fyco1	FYVE and coiled-coil domain containing 1	-1.61
NM_001025755.1	MGC116197	similar to RIKEN cDNA 1700001E04	-1.60
XM_001060093.1	RGD1561059	methyltransferase like 8	-1.60
XM_579986.1	LOC499614	RGD1559718	-1.60

XM_214751.3	Mrpl18	mitochondrial ribosomal protein L18	15.19
XM_575546.1	LOC500194	similar to immunoglobulin kappa-chain	3.48
NM_001013063.1	Raet1l	retinoic acid early transcript 1L	3.36
XR_009489.1	Cd300le	CD300 molecule-like family member E	3.28
XM_575513.1	LOC500161	similar to Immunoglobulin kappa-chain VJ precursor	3.18
XM_578288.1	LOC502789	similar to Immunoglobulin kappa-chain VJ precursor	3.14
NM_001014132.1	Traf3ip3	TRAF3 interacting protein 3	3.09
XM_221094.3	LOC303666	similar to dendritic cell-derived immunoglobulin(Ig)-like receptor 1, DIgR1 - mouse	2.93
NM_001009541.1	Ier2	immediate early response 2	2.76
XM_234930.2	Edg6	sphingosine-1-phosphate receptor 4	2.74
XM_001072477.1	Sema7a	sema domain, immunoglobulin domain (Ig), and GPI membrane anchor, (semaphorin) 7A	2.73
XM_236646.2	Ngp	neutrophilic granule protein	2.72
XM_345752.2	LOC366765	similar to Ig H-chain	2.71
XM_001070786.1	Stfa2	stefin A2-like 2; stefin A2-like 3	2.70
XM_573293.1	RGD1560676	stefin A2-like 2; stefin A2-like 3	2.70
XM_341195.2	Igj	immunoglobulin joining chain	2.69
XM_217791.4	Tagap	T-cell activation GTPase activating protein	2.65
NM_138547.1	LOC191574	aldo-keto reductase family 1, member C14	2.61
XM_577145.1	LOC501744	similar to Immunoglobulin superfamily, member 7	2.59
XM_343664.2	LOC363326	hypothetical LOC363326	2.57
XM_575732.1	LOC500374	Ig kappa chain V region S211	2.57
XM_578343.1	LOC502843	similar to immunoglobulin kappa-chain	2.55
XM_341534.2	Tcrg	T cell receptor gamma locus	2.53
XM_001075162.1	LOC690672	similar to Discs large homolog 5 (Placenta and prostate DLG) (Discs large protein P-dlg)	2.52
XM_575512.1	LOC500160	similar to Immunoglobulin light chain	2.48
XM_576812.2	LOC501399	similar to Discs large homolog 5 (Placenta and prostate DLG) (Discs large protein P-dlg)	2.46
XM_575930.2	RGD1564994	glycine/arginine rich protein 1	2.43
XM_575544.1	LOC500192	similar to Ig kappa chain V-IV region precursor	2.42
XM_222692.4	Rgs18	regulator of G-protein signaling 18	2.42
XM_001061476.1	Tcf15	transcription factor 15	2.38
XM_575525.1	LOC500173	similar to immunoglobulin light chain precursor	2.38
XM_217546.3	LOC302210	similar to RIKEN cDNA 4930555G01	2.37
NM_001009681.1	Oasl	2'-5'-oligoadenylate synthetase-like	2.35
XM_579453.1	Gcnt1	glucosaminyl (N-acetyl) transferase 1, core 2	2.35
XM_236658.4	Ccrl2	chemokine (C-C motif) receptor-like 2	2.35
NM_001014125.1	Pdia5	protein disulfide isomerase family A, member 5	2.35

XM_575524.1	LOC500172	similar to immunoglobulin kappa-chain	2.35
XM_576305.1	LOC500903	similar to RIKEN cDNA 2210421G13	2.32
NM_001024289.1	Ptprcap	protein tyrosine phosphatase, receptor type, C-associated protein	2.31
XM_001061883.1	LOC363181	similar to RIKEN cDNA 1700001E04	2.31
NM_001025115.1	Stap1	signal transducing adaptor family member 1	2.31
NM_001014039.1	Tnfaip8l2	tumor necrosis factor, alpha-induced protein 8-like 2	2.30
XM_579388.1	LOC497767	hypothetical gene supported by BC081816; NM_017043	2.30
NM_053713.1	Klf4	Kruppel-like factor 4 (gut)	2.29
NM_181087.2	Cyp26b1	cytochrome P450, family 26, subfamily b, polypeptide 1	2.28
XM_575447.1	LOC500096	similar to T cell receptor variable region:SUBUNIT=beta:ISOTYPE=8.3	2.27
XM_225319.3	RGD1306939	similar to mKIAA0386 protein	2.27
XM_576504.1	LOC501089	similar to Discs large homolog 5 (Placenta and prostate DLG) (Discs large protein P-dlg)	2.26
XM_224344.3	Dok2	docking protein 2	2.25
XM_345803.3	Ankrd47	KN motif and ankyrin repeat domains 3	2.25
XM_580254.1	LOC502542	RGD1565497	2.25
XM_001059693.1	RGD1311960	transmembrane and coiled-coil domain family 2	2.25
NM_001009717.1	Lrg1	leucine-rich alpha-2-glycoprotein 1	2.21
XM_001059284.1	RGD1560455	similar to RIKEN cDNA A630033H20 gene	2.21
XM_579438.1	LOC497816	hypothetical gene supported by NM_019371	2.20
XM_228320.4	Prdm1	PR domain containing 1, with ZNF domain	2.19
NM_001012469.1	Il21r	interleukin 21 receptor	2.17
NM_001009489.1	Oas1k	2 ' -5 ' oligoadenylate synthetase 1K	2.17
NM_001008518.1	MGC105649	hypothetical LOC302884	2.16
XM_001073723.1	Kif23	kinesin family member 23	2.16
XM_001059303.1	RGD1560293	SAM and SH3 domain containing 3	2.15
XM_234747.2	LOC314521	similar to BWK3	2.15
XM_214825.3	Nova2	neuro-oncological ventral antigen 2	2.15
NM_133540.1	Nkg7	natural killer cell group 7 sequence	2.15
NM_001030043.1	RGD1311300	similar to T cell receptor V delta 6	2.13
XM_579551.1	LOC497748	hypothetical gene supported by NM_053313	2.13
XM_573856.2	RGD1561145	similar to novel protein	2.12
XM_574335.1	LOC499056	similar to KRAB-zinc finger protein; similar to 3110052M02Rik protein; zinc finger protein 53; zinc finger protein 51	2.11
XM_001078162.1	Dapp1	dual adaptor of phosphotyrosine and 3-phosphoinositides	2.11
XM_001062861.1	Akr1cl1	aldo-keto reductase family 1, member C-like 1	2.11
XR_009153.1	RGD1559899	similar to mannose receptor precursor-like isoform 4	2.10

XM_216745.3	Batf	basic leucine zipper transcription factor, ATF-like	2.10
XM_220513.4	Cias1	NLR family, pyrin domain containing 3	2.08
XM_222017.3	Hrbl	ArfGAP with FG repeats 2	2.07
NM_024356.1	Gch1	GTP cyclohydrolase 1	2.07
XM_001055834.1	LOC680128	similar to phospholipase C-like 2	2.05
XM_213490.4	RGD1307288	similar to Protein C21orf58	2.05
XM_234419.4	Rps6kl1	ribosomal protein S6 kinase-like 1	2.05
XM_578684.1	LOC503160	similar to Ly6-C antigen gene	2.03
NM_053847.1	Map3k8	mitogen-activated protein kinase kinase kinase 8	2.03
NM_001030025.1	Upp1	uridine phosphorylase 1	2.02
XM_001058249.1	LOC680665	Fc receptor-like 1	2.01
XM_001060043.1	Ptk9l	protein tyrosine kinase 9-like (A6-related protein)	2.01
XM_001058119.1	Mcpt10	mast cell protease 8-like 3; mast cell protease 10	2.00
XM_221216.4	Cd7	Cd7 molecule	2.00
NM_017016.1	Hdc	histidine decarboxylase	1.98
XM_213365.3	Centb1	ArfGAP with coiled-coil, ankyrin repeat and PH domains 1	1.98
NM_001012226.1	Stat4	signal transducer and activator of transcription 1; signal transducer and activator of transcription 4	1.96
NM_145683.1	Ptpn7	protein tyrosine phosphatase, non-receptor type 7	1.96
XR_008288.1	RGD1565895	kelch-like 35 (Drosophila)	1.95
XM_573119.2	RGD1560850	phosphoinositide-3-kinase, regulatory subunit 6	1.95
XM_219476.3	Ifitm6	interferon induced transmembrane protein 6	1.95
XM_001078275.1	RGD1563164	G-2 and S-phase expressed 1	1.95
XM_223423.4	Klf3_mapped	Kruppel-like factor 3 (basic)	1.94
XM_001067912.1	LOC684490	similar to methylenetetrahydrofolate dehydrogenase (NAD) (EC 1.5.1.15)/methenyltetrahydrofolate cyclohydrolase (EC 3.5.4.9) precursor; methylenetetrahydrofolate dehydrogenase (NADP+ dependent) 2, methenyltetrahydrofolate cyclohydrolase	1.94
XM_001055140.1	Dscr6	Down syndrome critical region homolog 6 (human)	1.93
XM_344042.2	LOC363828	similar to immunoglobulin light chain variable region	1.93
XM_342673.2	LOC362350	similar to T-cell receptor beta-2 chain C region	1.92
XM_228821.3	RGD1561019	G protein-coupled receptor associated sorting protein 2	1.92
XM_001068004.1	Ap1s2	adaptor-related protein complex 1, sigma 2 subunit	1.92
XM_343880.2	Itk	IL2-inducible T-cell kinase	1.92
NM_172044.1	Mcpt2	mast cell protease 2	1.91
NM_053769.2	Dusp1	dual specificity phosphatase 1	1.91

NM_199110.1	Mfng	MFNG O-fucosylpeptide 3-beta-N-acetylglucosaminyltransferase	1.90
NM_001024776.1	Hipk4	homeodomain interacting protein kinase 4	1.90
XM_230610.4	Hspa12b	heat shock protein 12B	1.89
XM_573745.2	RGD1565031	REST corepressor 2; similar to REST corepressor 2	1.89
XM_001063436.1	RGD1566325	similar to regulator of sex-limitation candidate 16	1.89
XM_001069146.1	RGD1311012	sterile alpha motif domain containing 5	1.89
XM_576127.1	LOC500748	similar to Rap guanine nucleotide exchange factor 5 (Guanine nucleotide exchange factor for Rap1) (M-Ras-regulated Rap GEF) (MR-GEF)	1.88
NM_053502.1	Abcg1	ATP-binding cassette, sub-family G (WHITE), member 1	1.88
XR_000311.1	LOC501207	similar to 2810022L02Rik protein	1.88
XM_224699.3	LOC306324	tetraspanin 14; SH2 domain containing 4B	1.87
XM_001071145.1	RGD1311490	TBC1 domain family, member 10C	1.87
XM_220639.3	Nek8	NIMA (never in mitosis gene a)- related kinase 8	1.87
XM_579446.1	LOC497690	hypothetical gene supported by NM_021684	1.87
XM_214592.4	Stard4	StAR-related lipid transfer (START) domain containing 4	1.86
NM_133290.2	Zfp36	zinc finger protein 36	1.86
XM_577148.2	RGD1562974	glutamine rich 2	1.86
XM_578296.1	LOC502797	similar to immunoglobulin kappa-chain	1.86
NM_001009662.1	Car8	carbonic anhydrase 8	1.86
XM_224403.4	RGD1304929	similar to chromosome 13 open reading frame 18	1.86
XM_001072042.1	RGD1311475	similar to FLJ00354 protein	1.85
XM_576264.2	RGD1564335	Golgi-localized protein	1.85
XM_235398.4	RGD1311559	DENN/MADD domain containing 3	1.85
XM_341876.3	RGD1564385	feline sarcoma oncogene	1.83
XM_579397.1	LOC497811	xanthine dehydrogenase	1.83
XM_580072.1	LOC500488	LOC500488	1.83
NM_031821.1	Plk2	polo-like kinase 2 (Drosophila)	1.83
XM_001072174.1	RGD1311132	exocyst complex component 3-like	1.82
XM_231388.4	RGD1305854	DBF4 homolog (S. cerevisiae)	1.82
XM_580016.1	LOC499785	RGD1564003	1.82
NM_001039204.1	LOC290071	similar to RIKEN cDNA A430107P09 gene	1.81
NM_053391.1	Hs3st1	heparan sulfate (glucosamine) 3-O-sulfotransferase 1	1.81
XM_001076779.1	LOC499828	copine VIII; similar to copine VIII isoform 1	1.81
XM_001078315.1	Def6	differentially expressed in FDCP 6 homolog (mouse)	1.80
XM_343579.2	Raph1	Ras association (RalGDS/AF-6) and pleckstrin homology domains 1	1.80
NM_001024316.1	Gata5	GATA binding protein 5	1.80
NM_001025693.1	Cdca7	cell division cycle associated 7	1.80

XM_001071550.1	Arrdc1	arrestin domain containing 1	1.79
NM_175761.2	Hsp90aa1	similar to heat shock protein 1, alpha; heat shock protein 90, alpha (cytosolic), class A member 1	1.79
XM_001054586.1	RGD1565985	tetratricopeptide repeat domain 9	1.79
XM_341832.2	LOC361546	similar to mKIAA0841 protein	1.79
XM_219594.3	LOC293746	membrane-spanning 4-domains, subfamily A, member 4C	1.79
XM_575036.1	LOC499708	similar to 60S ribosomal protein L7a	1.79
XM_001071725.1	RGD1560608	similar to novel protein	1.78
XM_217350.4	Mrpl14	mitochondrial ribosomal protein L14	1.78
NM_001025688.1	Palmd	palmdelphin	1.78
XM_342414.3	Sh2d3c	SH2 domain containing 3C	1.78
XM_001072688.1	Mmp17	matrix metallopeptidase 17	1.78
NM_012964.2	Hmmr	hyaluronan mediated motility receptor (RHAMM)	1.78
NM_001011968.1	Gimap6	GTPase, IMAP family member 6	1.77
XM_576214.1	LOC500824	FYVE, RhoGEF and PH domain containing 6	1.77
XM_340854.3	RGD1564005	similar to novel protein	1.77
XM_001068254.1	RGD1561783	StAR-related lipid transfer (START) domain containing 5	1.77
NM_207605.3	Sh2d2a	SH2 domain protein 2A	1.77
NM_001008398.2	Gimap9	GTPase, IMAP family member 9	1.76
XM_340836.3	RGD1308747	hypothetical protein LOC680565; family with sequence similarity 64, member A	1.76
XM_578149.1	LOC502655	similar to heat shock 90kDa protein 1, beta	1.76
XM_001055379.1	Arhgef3	Rho guanine nucleotide exchange factor (GEF) 3	1.76
XM_001067802.1	Pcdh19	protocadherin 19	1.76
NM_031085.2	Prkch	protein kinase C, eta	1.76
XM_001065725.1	RGD1565540	cytotoxic T lymphocyte-associated protein 2 alpha	1.76
XM_001079575.1	RGD1310788	similar to RIKEN cDNA 0610039P13	1.76
XM_233480.3	RGD1309802	defects in morphology 1 homolog (S. cerevisiae)	1.75
XM_001066862.1	Nalp12	NACHT, leucine rich repeat and PYD containing 12	1.75
NM_001007694.1	Ifit3	interferon-induced protein with tetratricopeptide repeats 3	1.75
NM_199491.1	Fut7	fucosyltransferase 7 (alpha (1,3) fucosyltransferase)	1.75
XM_573480.1	LOC498256	immediate early response 5	1.75
NM_001033963.1	Prkx	protein kinase, X-linked	1.75
NM_001025708.1	Ogfrl1	opioid growth factor receptor-like 1	1.75
XM_216334.3	Hspcal3	heat shock 90kDa protein 1, alpha-like 3	1.75
NM_153468.1	Gzma	granzyme A	1.74
XM_216310.4	Casc1	cancer susceptibility candidate 1	1.74
NM_001014050.1	Fam110a	family with sequence similarity 110, member A	1.73
XM_001079908.1	Ifi44	interferon-induced protein 44	1.73

XM_227546.3	LOC295340	similar to Acidic ribosomal phosphoprotein P0	1.73
NM_001007684.1	Klf2	Kruppel-like factor 2 (lung)	1.73
XM_216547.4	Sh3bgrl3	SH3 domain binding glutamic acid-rich protein-like 3	1.73
XM_001081251.1	RGD1561062	family with sequence similarity 117, member A	1.72
XM_001062502.1	RGD1564040	similar to methylenetetrahydrofolate dehydrogenase (NAD) (EC 1.5.1.15)/methenyltetrahydrofolate cyclohydrolase (EC 3.5.4.9) precursor; methylenetetrahydrofolate dehydrogenase (NADP+ dependent) 2, methenyltetrahydrofolate cyclohydrolase	1.72
NM_172021.2	Tbkbp1	TBK1 binding protein 1	1.72
XM_001061125.1	RGD1564160	solute carrier family 37 (glycerol-3-phosphate transporter), member 2	1.70
XM_235547.4	RGD1560783	family with sequence similarity 118, member A	1.70
XM_001053661.1	Stim2	stromal interaction molecule 2	1.69
XM_213896.2	LOC289084	similar to RIKEN cDNA 1700025G04 gene	1.69
XM_001065344.1	RGD1560731	G protein-coupled receptor 146	1.69
NM_001014236.1	Ssbp4	single stranded DNA binding protein 4	1.69
XM_001058176.1	RGD1563721	OTU domain containing 7A	1.69
NM_017119.1	Gzmk	granzyme K	1.69
XM_001068837.1	RGD1563517	C-type lectin domain family 1, member b	1.69
XM_230560.2	LOC311382	similar to ribosomal protein S2	1.68
XM_346339.2	LOC367874	similar to 60S ribosomal protein L29 (P23)	1.68
XM_343921.3	Sox15	SRY (sex determining region Y)-box 15	1.68
NM_053857.1	Eif4ebp1	eukaryotic translation initiation factor 4E binding protein 1	1.68
NM_001024299.1	Zfp458	zinc finger protein 458	1.68
XM_579288.1	Ly49s4	Ly49 stimulatory receptor 4; Ly-49 stimulatory receptor 3	1.68
NM_001006998.1	Aldh3b1	aldehyde dehydrogenase 3 family, member B1	1.68
NM_001024361.1	LOC501110	similar to Glutathione S-transferase A1 (GTH1) (HA subunit 1) (GST-epsilon) (GSTA1-1) (GST class-alpha)	1.68
XM_213626.4	Pvrl3	poliovirus receptor-related 3	1.67
XR_008282.1	RGD1565661	similar to RIKEN cDNA 3110001I22	1.67
NM_053826.2	Pdk1	pyruvate dehydrogenase kinase, isozyme 1	1.67
NM_053736.1	Casp11	caspase 4, apoptosis-related cysteine peptidase	1.67
XM_577892.1	LOC502411	similar to Mature alpha chain of major histocompatibility complex class I antigen	1.67
NM_213561.2	Tcf19	transcription factor 19	1.66
XM_234898.4	Hmha1	histocompatibility (minor) HA-1	1.66
XM_001053269.1	Asah3l	alkaline ceramidase 2	1.65
NM_206815.1	Rnase6	ribonuclease, RNase A family, 6	1.65

XM_575130.1	LOC499794	ribosomal protein L10; similar to ribosomal protein L10; ribosomal protein L10-like	1.65
NM_001007667.1	Sat1	spermidine/spermine N1-acetyl transferase 1	1.65
XM_212694.3	LOC288178	similar to extracellular signal-related kinase 1c	1.64
XM_001061731.1	Galntl2	UDP-N-acetyl-alpha-D-galactosamine:polypeptide N-acetylgalactosaminyltransferase-like 2	1.64
XR_009158.1	RGD1565520	similar to 60S ribosomal protein L7a	1.64
NM_001007144.1	Adfp	adipose differentiation related protein	1.64
XR_008840.1	RGD1564580	similar to ribosomal protein S10	1.64
XM_575291.1	LOC366258	similar to 60S ribosomal protein L7a	1.64
NM_001013880.1	Isyna1	inositol-3-phosphate synthase 1	1.64
XM_001054287.1	Rnpc1	RNA binding motif protein 38	1.64
XM_001072744.1	RGD1309543	similar to 2310014H01Rik protein	1.63
NM_001008876.1	Rsl1d1	ribosomal L1 domain containing 1	1.63
XM_001061369.1	Luzp5	leucine zipper protein 5	1.63
XM_234471.4	Rin3	Ras and Rab interactor 3	1.63
XM_001080759.1	Rasip1	Ras interacting protein 1	1.63
NM_001037775.1	Chst12	carbohydrate sulfotransferase 12	1.63
XR_009032.1	RGD1565356	similar to RIKEN cDNA 2210421G13	1.63
NM_199089.2	Tcirg1	T-cell, immune regulator 1, ATPase, H+ transporting, lysosomal V0 subunit A3	1.63
NM_020103.1	Ly6c	Ly6-C antigen	1.62
XM_574285.2	RGD1566426	nuclear receptor coactivator 7	1.62
XM_001081011.1	RGD1562705	Src homology 2 domain containing F	1.62
XM_341842.3	Cebpg	CCAAT/enhancer binding protein (C/EBP), gamma	1.62
XM_226529.3	LOC307907	similar to RIKEN cDNA 6430548M08	1.62
XR_007676.1	RGD1560557	similar to minichromosome maintenance protein 8 isoform 1	1.62
NM_019339.1	Rgs12	regulator of G-protein signaling 12	1.61
XM_578590.1	LOC503070	similar to immunoglobulin heavy chain variable region	1.61
XM_001064856.1	Thsd1	thrombospondin, type I, domain containing 1	1.61
XM_001060148.1	RGD1306498	zinc finger and SCAN domain containing 20; zinc finger protein 362	1.61
XM_342643.3	Mdfic	MyoD family inhibitor domain containing	1.61
XM_233741.2	Tyk2	tyrosine kinase 2	1.60
XM_001062249.1	LOC685088	Src homology 2 domain containing E	1.60
XR_008462.1	RGD1305138	similar to expressed sequence AW556797	1.60

Each gene is given a representative GenBank accession number, gene symbol, gene description, and fold change (relative to control rats; negative values indicate down regulation). Genes are grouped according to the functional annotation cluster analysed using DAVID and arranged by fold change.

Appendix 3.3: Differentially expressed podocyte related genes

List of podocyte related genes differentially expressed in *IL-13* overexpression rat versus control rat.

GenBank Accession No.	Gene Symbol	Gene Description	Fold Change
AMD protein complexes			
NM_017336.1	Ptpro	protein tyrosine phosphatase, receptor type, O	-2.42
NM_019357.1	Ezr	ezrin	-1.82
BMD protein complexes			
XM_342410.3	Aif1l	allograft inflammatory factor 1-like	-3.43
NM_012649.1	Sdc4	syndecan 4	-2.79
NM_001012032.1	Arhgap24	Rho GTPase activating protein 24	-2.48
NM_012983.2	Myo1d	myosin ID	-2.28
XM_340884.2	Itga3	integrin alpha 3	-2.23
XM_343483.3	Dag1	dystroglycan 1	-2.07
XM_001066264.1	Tenc1	tensin like C1 domain-containing phosphatase	-2.00
NM_012904.1	Anxa1	annexin A1	-1.91
XM_001078155.1	Parvb	parvin, beta	1.65
SD protein complexes			
NM_053621.1	Magi2	membrane associated guanylate kinase, WW and PDZ domain containing 2	-3.93
NM_021695.1	Synpo	synaptopodin	-3.62
XM_218486.3	Kirrel2	kin of IRRE like 2 (Drosophila)	-3.47
XM_001059464.1	Cdh11	cadherin 11	-3.16
NM_022628.1	Nphs1	nephrosis 1 homolog, nephrin	-3.06
NM_130828.2	Nphs2	nephrosis 2 homolog, podocin	-3.02
NM_001012055.1	Cdh16	cadherin 16	-2.73
XM_001059679.1	Ctnnal1	catenin (cadherin associated protein), alpha-like 1	-2.42
NM_031005.2	Actn1	actinin, alpha 1	-2.30
XM_001059817.1	Nck2	NCK adaptor protein 2	-2.10
XM_237115.1	Nck2	NCK adaptor protein 2	-1.62
XM_226213.4	Cdh5	cadherin 5	1.88
Cell junction			
XM_236385.4	Cgnl1	cingulin-like 1	-2.54
NM_012528.1	Chrnb1	cholinergic receptor, nicotinic, beta polypeptide 1 (muscle)	-2.40
NM_017198.1	Pak1	p21 protein (Cdc42/Rac)-activated kinase 1	-2.19
NM_012663.2	Vamp2	vesicle-associated membrane protein 2	-1.60
Tight junction			
NM_031699.1	Cldn1	claudin 1	-3.19
XM_001080868.1	Mpp5	membrane protein, palmitoylated 5 (MAGUK p55 subfamily member 5)	-2.33
NM_031675.2	Actn4	actinin alpha 4	-1.72
NM_017093.1	Akt2	thymoma viral proto-oncogene 2	-1.68
XM_342223.3	Prkci	protein kinase C, iota	-1.61
Extracellular region			

NM_001012039.1	Efemp1	epidermal growth factor-containing fibulin-like extracellular matrix protein 1	-4.76
XM_001060132.1	C1qtnf7	C1q and tumor necrosis factor related protein 7	-4.16
NM_001012225.1	Mgat4a	mannoside acetylglucosaminyltransferase 4, isoenzyme A	-3.28
XM_001064272.1	Crim1	cysteine rich transmembrane BMP regulator 1 (chordin like)	-2.57
NM_031609.1	Nbl1	neuroblastoma, suppression of tumorigenicity 1	-2.54
NM_053606.1	Mmp23	matrix metallopeptidase 23	-2.43
NM_019237.1	Pcolce	procollagen C-endopeptidase enhancer protein	-2.35
XM_343607.3	Col4a3	collagen, type IV, alpha 3	-1.99
NM_053629.2	Fstl3	follistatin-like 3	-1.82
NM_031697.1	St3gal3	ST3 beta-galactoside alpha-2,3-sialyltransferase 3	-1.79
NM_031640.1	Pgcp	plasma glutamate carboxypeptidase	-1.76
NM_021989.2	Timp2	tissue inhibitor of metalloproteinase 2	-1.71
NM_001004218.1	Fuca2	fucosidase, alpha-L- 2, plasma	-1.61
Intrinsic to plasma membrane			
NM_053570.1	Cxadr	coxsackie virus and adenovirus receptor	-2.45
NM_017206.1	Slc6a6	solute carrier family 6 (neurotransmitter transporter, taurine), member 6	-1.95
NM_183332.1	Myadm	myeloid-associated differentiation marker	-1.87
NM_001007002.1	Mxra8	matrix-remodelling associated 8	-1.68
NM_139110.1	Gpr116	G protein-coupled receptor 116	1.68
NM_173135.1	Accn3	amiloride-sensitive cation channel 3	1.64
Cell adhesion			
NM_031753.1	Alcam	activated leukocyte cell adhesion molecule	-2.93
NM_019358.1	Pdpn	podoplanin	-2.72
NM_019140.2	Ptprd	protein tyrosine phosphatase, receptor type, D	-2.59
XM_223583.4	Aebp1	AE binding protein 1	-2.28
XM_230950.4	Itgav	integrin alpha V	-1.97
NM_013016.2	Sirpa	signal-regulatory protein alpha	-1.88
NM_001004090.2	Tspan5	tetraspanin 5	-1.67
Cell morphogenesis			
XM_216679.4	Lamb1	laminin, beta 1	-2.84
NM_031235.1	Pard3	par-3 (partitioning defective 3) homolog (C. elegans)	-2.64
NM_012715.1	Adm	adrenomedullin	-2.10
XM_242297.4	Ntng2	netrin G2	-1.93
NM_024159.1	Dab2	disabled homolog 2	-1.74
NM_017089.2	Efnb1	ephrin B1	-1.65
Cytoskeletal component/process			
XM_214338.3	Palld	similar to palladin	-3.18
XM_001054365.1	Arhgap28	Rho GTPase activating protein 28	-4.83
XM_223229.4	Shroom3	shroom family member 3	-3.02
NM_024127.2	Gadd45a	growth arrest and DNA-damage-inducible 45 alpha	-2.67

NM_133545.1	Ptpn21	protein tyrosine phosphatase, non-receptor type 21	-2.67
NM_001034075.1	Tpm1	tropomyosin 1, alpha	-2.55
NM_013082.2	Sdc2	syndecan 2	-2.46
XM_216688.4	Arhgap5	Rho GTPase activating protein 5	-2.43
XM_237042.4	Dst	dystonin	-2.39
XM_220031.4	Myof	myoferlin	-2.38
XM_001064622.1	Itgb5	integrin beta 5	-2.37
XM_238004.3	Tubb2b	tubulin, beta 2B	-2.32
NM_001013246.1	Arhgef12	Rho guanine nucleotide exchange factor (GEF) 12	-2.21
XM_235213.3	Srgap1	SLIT-ROBO Rho GTPase activating protein 1	-2.17
NM_017180.1	Phlda1	pleckstrin homology-like domain, family A, member 1	-2.06
XM_227658.3	Fnbp1l	formin binding protein 1-like	-2.03
XM_217035.4	Krt7	keratin 7	-2.01
NM_001002798.1	Top1mt	DNA topoisomerase 1, mitochondrial	-2.01
NM_053326.1	Pdlim5	PDZ and LIM domain 5	-1.91
NM_012935.2	Cryab	crystallin, alpha B	-1.90
XM_341538.2	Kif5b	kinesin family member 5B	-1.87
NM_080689.3	Dnm1	dynamin 1	-1.81
XM_573030.2	Myh11	myosin, heavy chain 11, smooth muscle	-1.75
XM_001061392.1	Myo6	myosin VI	-1.72
XM_343248.3	Mtss1	metastasis suppressor 1	-1.71
NM_053603.1	Clic5	chloride intracellular channel 5	-1.62
XM_001059351.1	Hist1h2bc	histone cluster 1, H2bc	1.77
NM_030863.1	Msn	moesin	1.76
XM_001070203.1	Itga5	integrin alpha 5 (fibronectin receptor alpha)	1.72
NM_053783.1	Ifngr1	interferon gamma receptor 1	1.61
Ion transport			
NM_001033693.1	Slc31a2	solute carrier family 31, member 2	-2.15
NM_022269.1	Cd55	CD55 antigen	-1.95
NM_139332.3	Tpcn1	two pore channel 1	-1.81
Kidney development			
XM_213677.3	Robo2	roundabout homolog 2	-4.77
NM_031534.1	Wt1	Wilms tumor 1 homolog	-4.05
NM_001032397.1	Tcf21	transcription factor 21	-3.54
NM_053758.1	Plce1	phospholipase C, epsilon 1	-3.29
XM_001053727.1	Bmp7	bone morphogenetic protein 7	-2.68
NM_012774.1	Gpc3	glypican 3	-2.37
NM_030849.1	Bmpr1a	bone morphogenetic protein receptor, type 1A	-2.13
XM_213954.4	Nid1	nidogen 1	-2.12
NM_173101.1	Myo1e	myosin IE	-2.03
NM_053566.1	Ptch1	patched homolog 1	-1.99
NM_053698.2	Cited2	Cbp/p300-interacting transactivator, with Glu/Asp-rich carboxy-terminal domain, 2	-1.68
XM_001070482.1	Cutl1	similar to CCAAT displacement protein isoform b; cut-like homeobox 1	-1.67

XM_340765.2	Pkd1	polycystic kidney disease 1 homolog (human)	-1.65
NM_001002827.1	Notch4	Notch homolog 4 (Drosophila)	1.76
XM_001054314.1	Tek	TEK tyrosine kinase, endothelial	1.71
Neuron development			
XM_001062426.1	Sema3g	sema domain, immunoglobulin domain (Ig), short basic domain, secreted, (semaphorin) 3G	-3.98
NM_001033757.1	Cdkn1c	cyclin-dependent kinase inhibitor 1C (P57)	-3.26
XM_231354.4	Sema3e	sema domain, immunoglobulin domain (Ig), short basic domain, secreted, (semaphorin) 3E	-3.24
XM_236640.4	Plxnb1	plexin B1	-2.78
NM_022589.1	Tspan2	tetraspanin 2	-2.74
NM_017259.1	Btg2	B-cell translocation gene 2, anti-proliferative	2.91
Protein modification			
XM_001057269.1	Mgat5	mannoside acetylglucosaminyltransferase 5	-3.21
XM_219805.4	Prkg1	protein kinase, cGMP-dependent, type I	-3.02
XM_001076056.1	Uck2	uridine-cytidine kinase 2	-2.70
XM_001080770.1	Cpd	carboxypeptidase D	-2.30
XM_236687.4	Oxsr1	oxidative-stress responsive 1	-1.89
XM_227618.4	Cdc14a	CDC14 cell division cycle 14 homolog A	-1.66
Regulation of transcription			
NM_012760.1	Plagl1	pleiomorphic adenoma gene-like 1	-3.08
XR_007660.1	Zfp462	zinc finger protein 462	-2.29
NM_133560.2	Trak2	trafficking protein, kinesin binding 2	-2.26
NM_031346.1	Rod1	ROD1 regulator of differentiation 1	-2.04
NM_053583.1	Zfp423	zinc finger protein 423	-1.72
NM_021597.1	Eif2c2	eukaryotic translation initiation factor 2C, 2	-1.67
NM_021836.2	Junb	jun B proto-oncogene	3.85
XM_001076072.1	Lmcd1	LIM and cysteine-rich domains 1	1.96
NM_021835.3	Jun	Jun	1.88
NM_012855.1	Jak3	Janus kinase 3	1.63
Signal transduction			
NM_001002829.1	Rasl11a	RAS-like, family 11, member A	-2.31
XM_001073244.1	Plxdc2	plexin domain containing 2	-2.31
NM_080904.2	Arf3	ADP-ribosylation factor 3	-1.92
NM_032076.2	Ptger4	prostaglandin E receptor 4 (subtype EP4)	-1.78
NM_001009405.1	Arhgap29	Rho GTPase activating protein 29	-1.61
Vasculature development			
NM_031836.1	Vegfa	vascular endothelial growth factor A	-3.67
XM_241275.4	Sema5a	sema domain, seven thrombospondin repeats (type 1 and type 1-like), transmembrane domain (TM) and short cytoplasmic domain, (semaphorin) 5A	-3.01
XM_001070551.1	Reck	reversion-inducing-cysteine-rich protein with kazal motifs	-2.09
NM_053356.1	Col1a2	collagen, type I, alpha 2	-2.08
NM_013151.2	Plat	plasminogen activator, tissue	-1.66
Vesicle			
NM_022251.1	Enpep	glutamyl aminopeptidase	-2.92

NM_145081.3	Optn	optineurin	-2.84
XM_341428.2	Clcn3	chloride channel 3	-2.14
XM_342271.3	Lrba	LPS-responsive beige-like anchor	-1.83
Motif/Domain			
XM_222763.4	Tdrd5	tudor domain containing 5	-3.84
XM_001073627.1	Plekha5	pleckstrin homology domain containing, family A member 5	-3.79
XM_001055725.1	Kank1	KN motif and ankyrin repeat domains 1	-2.88
XM_001069410.1	Hoxc6	homeobox C6	-2.87
XM_001058167.1	Sgip1	SH3-domain GRB2-like (endophilin) interacting protein 1	-2.78
NM_019316.1	Mafb	v-maf musculoaponeurotic fibrosarcoma oncogene family, protein B	-2.71
XM_001053668.1	Rc3h2	ring finger and CCCH-type zinc finger domains 2	-2.66
XM_001062112.1	Sh3bgrl2	SH3 domain binding glutamic acid-rich protein like 2	-2.44
NM_001012048.1	Sh2d4a	SH2 domain containing 4A	-2.28
NM_001014268.1	Lrrc1	leucine rich repeat containing 1	-2.11
NM_001011922.1	Nedd9	neural precursor cell expressed, developmentally down-regulated gene 9	-1.84
NM_001007148.1	Btrc	beta-transducin repeat containing protein	-1.73
XM_233830.4	Plekhh2	pleckstrin homology domain containing, family H (with MyTH4 domain) member 2	-1.65
XM_001081287.1	Ankrd40	ankyrin repeat domain 40	-1.61
NM_130413.1	Skap2	src family associated phosphoprotein 2	1.75
Miscellaneous			
NM_022943.1	Mertk	c-mer proto-oncogene tyrosine kinase	-3.12
XM_217192.4	Rora	RAR-related orphan receptor alpha	-2.70
XM_236376.4	Fam81a	family with sequence similarity 81, member A	-2.65
NM_017031.2	Pde4b	phosphodiesterase 4B, cAMP specific	-2.49
NM_133569.1	Angptl2	angiopoietin-like 2	-2.45
XM_221276.3	Arvcf	armadillo repeat gene deleted in velo-cardio-facial syndrome	-2.39
XM_575387.2	Thsd7a	thrombospondin, type I, domain containing 7A	-2.38
XM_219201.4	Ppfibp2	PTPRF interacting protein, binding protein 2 (liprin beta 2)	-2.37
XM_001053270.1	Ccpg1	cell cycle progression 1	-2.34
NM_013220.1	Ankrd1	ankyrin repeat domain 1	-2.32
XM_226988.4	Fndc3b	fibronectin type III domain containing 3B	-2.30
XM_001061817.1	Erlin2	ER lipid raft associated 2	-2.26
XM_001075785.1	Fam65a	family with sequence similarity 65, member A	-2.26
XM_340875.3	Rnft1	ring finger protein, transmembrane 1	-2.04
XM_340886.3	Nfe2l1	nuclear factor, erythroid derived 2,-like 1	-2.01
NM_133601.1	Cblb	Casitas B-lineage lymphoma b	-1.94
NM_001013882.1	Dctd	dCMP deaminase	-1.92
NM_021850.2	Bcl2l2	Bcl2-like 2; poly(A) binding protein, nuclear 1	-1.89
NM_001005888.1	Galc	galactosylceramidase	-1.85
NM_001014102.1	Spats2l	spermatogenesis associated, serine-rich 2-like	-1.80

NM_001007654.1	Agtrap	angiotensin II receptor-associated protein	-1.80
NM_001025627.1	Leprel1	leprecan-like 1	-1.77
XM_343420.3	Fam63b	family with sequence similarity 63, member B	-1.75
XM_230036.4	Ssfa2	sperm specific antigen 2	-1.68
XM_001070133.1	Nbeal1	neurobeachin like 1	-1.65
NM_033485.2	Pawr	PRKC, apoptosis, WT1, regulator	-1.64
NM_012868.1	Npr3	natriuretic peptide receptor 3	-1.61
NM_199412.1	Cbara1	calcium binding atopy-related autoantigen 1	-1.61
NM_031970.1	Hspb1	heat shock protein 1	2.42
NM_053704.1	Bik	BCL2-interacting killer (apoptosis-inducing)	2.15
NM_173153.2	Gimap4	GTPase, IMAP family member 4	2.02
NM_012938.1	Ctse	cathepsin E	2.01
XM_001067588.1	Tm6sf1	transmembrane 6 superfamily member 1	1.83
NM_023962.2	Pdgfd	platelet-derived growth factor, D polypeptide	1.80
NM_057138.2	Cflar	CASP8 and FADD-like apoptosis regulator	1.80
XM_215117.4	Ifitm1	interferon induced transmembrane protein 1	1.74
XM_001059368.1	Ldb2	LIM domain binding 2	1.74
NM_001025141.1	Ccnb1ip1	cyclin B1 interacting protein 1	1.67

Each gene is given a representative GenBank accession number, gene symbol, gene description, and fold change (relative to control rats; negative values indicate down regulation). Genes are grouped according to the functional annotation cluster analysed using DAVID and arranged by fold change.

Appendix 3.4: Gene expression index of *TLR4*, *CTLA4* and *CD28* in control and IL-13 overexpression rats.

Glomerular gene expression index normalized against GAPDH.

Code	Sample	TLR-4	CTLA-4	CD28
(3)C1	C1	6.84E-04	3.16E-04	1.62E-02
(3)C2	C2	6.81E-04	1.94E-04	5.18E-03
(3)C3	C3	7.12E-04	7.16E-05	5.72E-03
(3)C4	C4	5.32E-04	4.79E-05	6.64E-03
(3)C5	C5	6.97E-04	5.27E-05	4.90E-03
(3)C6	C6	5.70E-04	2.19E-05	2.98E-03
(6)C4	C16	9.27E-04	6.47E-05	5.23E-03
(6)C5	C17	1.04E-03	3.72E-05	3.42E-03
(3)J1	J1	7.96E-04	3.62E-05	4.07E-03
(3)J2	J2	1.65E-03	6.50E-05	4.71E-03
(3)J3	J3	1.23E-03	9.51E-05	4.70E-03
(3)J4	J4	1.15E-03	4.73E-04	8.58E-03
(3)J5	J5	9.07E-04	5.87E-05	7.52E-03
(3)J6	J6	5.57E-04	8.97E-05	6.26E-03
(4)J1	J7	6.80E-04	2.84E-04	3.08E-02
(4)J2	J8	1.15E-03	1.90E-04	1.38E-02
(4)J3	J9	1.17E-03	2.02E-04	2.21E-02
(4)J4	J10	1.19E-03	4.66E-04	2.57E-02
(4)J5	J11	9.04E-04	5.45E-04	1.76E-02
(4)J6	J12	1.18E-03	1.86E-04	1.40E-02
(4)J7	J13	1.69E-03	2.64E-04	1.97E-02
(4)J8	J14	8.26E-04	1.92E-04	6.76E-03
(4)J9	J15	9.07E-04	2.46E-04	3.86E-03
(6)J1	J25	1.04E-03	2.91E-04	1.71E-02
(6)J2	J26	1.12E-03	1.62E-04	1.24E-02
(6)J6	J30	1.36E-03	9.93E-05	1.17E-02
(6)J7	J31	1.35E-03	1.78E-04	1.23E-02
(6)J8	J32	1.32E-03	1.83E-04	1.60E-02
(6)J9	J33	1.26E-03	2.67E-04	1.64E-02
(6)J13	J37	9.89E-04	2.42E-04	1.04E-02
(6)J16	J40	1.26E-03	1.02E-04	1.10E-02

Sample starts with C represent control rat; sample starts with J represent *IL-13*-overexpressed rat.

Appendix 4.1: Gene expression index of B7-1, IL-13 receptors, vav1, dystroglycan, nephrin and podocin in unstimulated and IL-13 stimulated podocytes.

Human podocytes gene expression index normalized against GAPDH (Part I).

Group	B7-1	IL13Rα2	IL13Rα1	IL4Rα	vav1	dystro	nephrin	podocin
1	1.27E-04	8.51E-04	7.96E-03	1.06E-02	6.54E-06	1.55E-02	2.36E-05	3.47E-05
1	2.00E-04	6.34E-04	1.05E-02	1.56E-02	2.03E-05	1.41E-02	1.30E-05	2.85E-05
1	5.26E-05	3.03E-04	8.56E-03	9.32E-03	1.42E-05	8.14E-03	2.74E-05	5.77E-05
1	1.77E-05	8.97E-04	4.14E-03	4.80E-03	2.29E-05	4.84E-03	2.57E-04	7.48E-06
1	2.30E-05	4.88E-04	3.34E-03	3.47E-03	5.20E-06	1.86E-03	7.20E-06	3.73E-05
1	9.21E-05	1.35E-03	1.27E-02	1.56E-02	7.69E-06	1.21E-02	6.43E-05	4.35E-05
1	3.47E-05	7.91E-04	1.09E-02	1.43E-02	1.06E-05	1.25E-02	2.05E-05	2.54E-05
1	1.89E-04	1.17E-03	1.55E-02	1.42E-02	2.95E-05	2.05E-02	5.26E-04	1.83E-04
1	1.70E-04	4.52E-04	1.73E-02	1.30E-02	4.77E-06	1.73E-02	1.89E-04	9.14E-05
1	1.74E-04	1.40E-04	3.95E-03	3.88E-03	1.68E-05	5.59E-03	3.93E-06	2.07E-06
1	1.10E-04	4.57E-04	1.57E-02	8.92E-03	4.31E-06	1.52E-02	2.32E-05	4.26E-05
1	6.94E-05	4.66E-04	1.26E-02	1.95E-02	2.46E-05	2.85E-02	3.01E-05	3.57E-05
1	3.44E-05	2.99E-04	1.76E-02	1.57E-02	4.76E-06	2.92E-02	8.83E-05	1.57E-05
2	1.46E-04	1.63E-03	1.03E-02	1.77E-02	9.50E-06	1.58E-02	1.31E-05	3.04E-05
2	2.47E-04	9.45E-04	1.13E-02	1.96E-02	1.83E-05	1.80E-02	1.38E-05	2.44E-05
2	1.37E-04	6.37E-04	1.43E-02	1.55E-02	1.95E-05	1.25E-02	2.41E-05	1.09E-04
2	4.45E-05	1.08E-03	5.63E-03	1.17E-02	2.61E-05	5.44E-03	1.34E-03	6.94E-06
2	1.08E-04	4.94E-03	1.45E-02	1.57E-02	1.89E-05	9.82E-03	7.93E-05	3.59E-05
2	2.77E-04	2.96E-03	1.43E-02	1.90E-02	2.72E-05	1.42E-02	1.01E-04	5.11E-05
2	6.27E-05	1.55E-03	1.22E-02	1.88E-02	2.00E-05	1.69E-02	1.70E-05	4.08E-05
2	3.52E-04	1.76E-03	1.53E-02	1.72E-02	3.54E-05	1.71E-02	5.46E-04	1.29E-04
2	2.52E-04	8.12E-04	2.06E-02	1.57E-02	8.25E-06	2.44E-02	4.39E-04	5.60E-06
2	1.83E-04	3.98E-04	5.44E-03	7.21E-03	3.06E-05	1.05E-02	6.88E-06	2.18E-06
2	1.80E-04	5.91E-04	1.68E-02	9.58E-03	9.13E-06	8.93E-03	2.05E-05	3.02E-05
2	9.01E-05	8.64E-04	1.02E-02	1.14E-02	3.05E-05	2.41E-02	7.69E-05	3.57E-05
2	1.80E-04	7.14E-04	1.32E-02	1.69E-02	3.39E-05	2.62E-02	1.72E-04	1.98E-05

Group 1 represents unstimulated podocytes; Group 2 represents IL-13 stimulated podocytes.

Human podocytes gene expression index normalized against GAPDH (Part II).

group	TLR4	CTLA4	CD28
1	1.60E-02	3.51E-03	2.49E-04
1	2.13E-02	4.38E-04	4.04E-04
1	1.86E-02	3.13E-04	2.81E-04
1	1.72E-02	9.54E-04	1.18E-03
1	2.04E-02	3.78E-03	3.07E-04
1	1.40E-02	5.39E-03	1.76E-03
1	2.04E-02	3.13E-04	5.51E-04
1	9.81E-03	2.18E-04	6.54E-04
1	1.35E-02	5.02E-04	9.01E-04
1	1.34E-02	1.54E-03	3.64E-04
1	1.46E-02	3.95E-04	1.25E-04
1	1.83E-02	6.39E-04	1.57E-04
1	ND	5.96E-04	ND
1	ND	3.28E-04	ND
2	1.27E-02	5.63E-04	1.91E-04
2	1.70E-02	2.56E-04	4.66E-04
2	1.79E-02	4.36E-04	3.40E-04
2	6.71E-03	7.98E-04	8.73E-04
2	2.55E-02	4.67E-03	2.27E-04
2	1.14E-02	5.12E-04	1.10E-03
2	1.39E-02	1.85E-04	2.28E-04
2	1.51E-02	3.39E-04	2.65E-04
2	1.20E-02	4.74E-04	9.68E-04
2	1.56E-02	1.07E-03	2.51E-04
2	1.06E-02	5.70E-04	1.57E-04
2	1.27E-02	3.35E-04	2.33E-04
2	ND	1.09E-04	ND
2	ND	1.38E-03	ND

Group 1 represents unstimulated podocytes; Group 2 represents IL-13 stimulated podocytes.
ND, not determined

Appendix 4.2: Protein expression index of B7-1, IL-13Rα2, vav1, phosphorylated vav1 and phosphor-vav1/vav1 in unstimulated and IL-13 stimulated podocytes.

Human podocytes protein expression index normalized against GAPDH.

Group	B7-1	IL-13Rα2	vav1	p-vav1	p-vav1/vav1
1	0.36	1.00	1.76	0.56	0.32
1	0.19	0.58	1.16	1.03	0.89
1	0.89	0.49	2.13	2.39	1.12
1	0.11	0.61	0.64	1.64	2.57
1	1.03	0.41	1.21	3.63	3.00
1	0.42	0.66	0.63	1.56	2.48
1	0.60	0.77	1.02	5.57	5.46
1	1.06	0.49	1.32	1.76	1.33
1	1.03	0.49	0.31	0.38	1.24
1	0.59	0.27	0.31	0.38	1.24
2	0.38	1.22	0.77	0.68	0.88
2	0.73	0.72	0.75	2.32	3.09
2	1.11	0.60	1.86	2.44	1.31
2	0.37	1.09	1.10	4.51	4.10
2	1.26	0.61	0.47	1.52	3.24
2	1.43	0.77	0.60	1.79	2.99
2	1.04	0.98	1.38	10.93	7.92
2	1.23	1.56	1.12	3.02	2.70
2	1.23	1.00	0.68	2.01	2.96
2	0.88	0.58	0.76	4.01	5.27

Group 1 represents unstimulated podocytes; Group 2 represents IL-13 stimulated podocytes.

Appendix 5.1: Cortical F-actin scores in unstimulated and IL-13 stimulated podocytes.

Cortical F-actin scores in podocytes.

Batch	Group	Total no. of cells	Number of cells				Scores				sum of score
			0	1	2	3	0	1	2	3	
H30	1	3	0	2	1	0	0	2	2	0	4
H30	1	10	0	6	2	2	0	6	4	6	16
H30	1	12	0	7	5	0	0	7	10	0	17
H30	1	6	1	5	0	0	0	5	0	0	5
H30	1	1	0	1	0	0	0	1	0	0	1
H30 Total		32	1	21	8	2	0	21	16	6	43
H29	1	7	1	6	0	0	0	6	0	0	6
H29	1	8	0	2	4	2	0	2	8	6	16
H29	1	1	0	1	0	0	0	1	0	0	1
H29 Total		16	1	9	4	2	0	9	8	6	23
H23	1	3	0	2	1	0	0	2	2	0	4
H23	1	2	1	0	0	1	0	0	0	3	3
H23	1	6	0	1	2	3	0	1	4	9	14
H23	1	5	0	0	4	1	0	0	8	3	11
H23	1	3	0	0	2	1	0	0	4	3	7
H23	1	3	0	1	0	2	0	1	0	6	7
H23	1	2	0	1	0	1	0	1	0	3	4
H23	1	2	0	0	2	0	0	0	4	0	4
H23	1	3	0	2	1	0	0	2	2	0	4
H23 Total		29	1	7	12	9	0	7	24	27	58
H22	1	5	0	4	1	0	0	4	2	0	6
H22	1	4	0	3	0	1	0	3	0	3	6
H22	1	1	0	1	0	0	0	1	0	0	1
H22	1	3	0	0	3	0	0	0	6	0	6
H22	1	2	0	1	1	0	0	1	2	0	3
H22	1	4	0	1	2	1	0	1	4	3	8
H22 Total		19	0	10	7	2	0	10	14	6	30
H30	2	2	0	1	0	1	0	1	0	3	4
H30	2	1	0	0	0	1	0	0	0	3	3
H30	2	2	0	0	2	0	0	0	4	0	4
H30	2	5	0	1	0	4	0	1	0	12	13
H30	2	3	0	0	2	1	0	0	4	3	7
H30	2	7	0	2	2	3	0	2	4	9	15
H30	2	9	0	1	3	5	0	1	6	15	22
H30	2	3	0	1	0	2	0	1	0	6	7
H30	2	12	0	1	8	3	0	1	16	9	26
H30 Total		44	0	7	17	20	0	7	34	60	101

H29	2	1	0	0	0	1	0	0	0	3	3
H29	2	1	0	0	0	1	0	0	0	3	3
H29	2	8	0	6	2	0	0	6	4	0	10
H29	2	8	0	0	3	5	0	0	6	15	21
H29 Total		18	0	6	5	7	0	6	10	21	37
H23	2	4	0	0	1	3	0	0	2	9	11
H23	2	6	0	1	0	5	0	1	0	15	16
H23	2	6	0	0	1	5	0	0	2	15	17
H23	2	1	0	0	0	1	0	0	0	3	3
H23	2	3	0	0	0	3	0	0	0	9	9
H23	2	2	0	0	0	2	0	0	0	6	6
H23	2	3	0	0	2	1	0	0	4	3	7
H23	2	3	0	0	3	0	0	0	6	0	6
H23	2	1	0	0	0	1	0	0	0	3	3
H23 Total		29	0	1	7	21	0	1	14	63	78
H22	2	4	0	0	4	0	0	0	8	0	8
H22	2	3	0	0	2	1	0	0	4	3	7
H22	2	7	0	1	6	0	0	1	12	0	13
H22	2	1	0	0	0	1	0	0	0	3	3
H22	2	1	0	0	1	0	0	0	2	0	2
H22	2	6	0	0	0	6	0	0	0	18	18
H22	2	10	0	1	9	0	0	1	18	0	19
H22 Total		32	0	2	22	8	0	2	44	24	70

Group 1 represents unstimulated podocytes; Group 2 represents IL-13 stimulated podocytes.

Appendix 5.2: RhoA and Rac1 activities in unstimulated and IL-13 stimulated podocytes.

Normalized RhoA and Rac1 activities in podocytes.

	Normalized RhoA				Normalized Rac1			
Group	**5 mins**	**10 mins**	**20 mins**	**30 mins**	**5 mins**	**10 mins**	**20 mins**	**30 mins**
1	3.99	3.76	0.98	1.63	0.31	0.88	0.72	0.59
1	3.58	3.99	1.66	1.44	1.37	1.08	1.18	1.15
1	4.23	4.53	1.81	2.57	0.72	0.58	0.74	0.53
1	1.23	4.02	1.14	1.34	2.43	2.16	0.85	2.31
1	3.81	1.99	2.41	1.88	1.22	1.08	1.17	1.15
1	4.79	5.50	3.61	3.06	0.28	0.32	0.78	0.71
1	1.94	2.71	2.32	3.23	0.16	0.30	1.51	1.11
1	0.97	1.36	2.03	1.62	0.26	0.29	1.00	
2	3.27	4.27	1.35	1.14	0.38	0.64	1.28	0.69
2	3.35	2.92	1.20	1.39	1.53	1.51	2.05	1.56
2	4.28	3.96	2.13	2.09	0.64	0.63	0.98	0.64
2	1.33	3.33	0.85	1.09	3.22	4.32	1.06	2.28
2	2.84	3.42	1.46	2.15	2.76	2.41	1.51	1.14
2	4.98	6.23	3.46	3.52	0.23	0.24	1.57	0.61
2	2.23	1.80	2.35	1.92	0.18	0.18	1.66	0.87
2	1.26	1.32	1.37	1.06	0.29	0.29	2.51	

Group 1 represents unstimulated podocytes; Group 2 represents IL-13 stimulated podocytes.

Appendix 5.3: Gene expression index of B7-1, IL-13 receptors, vav1, dystroglycan, nephrin and podocin in podocyte siRNA experiments.

Human podocytes gene expression index normalized against GAPDH.

Group	B7-1	IL-13Rα2	IL-13Rα1	IL-4Rα	dystro	nephrin	podocin	vav1
3	2.24E-04	8.21E-04	1.47E-02	1.19E-02	1.79E-02	2.63E-05	3.21E-05	1.62E-05
3	6.03E-05	1.10E-03	3.19E-02	4.15E-02	6.17E-02	4.62E-05	1.18E-04	3.86E-05
3	7.74E-05	7.45E-04	1.28E-02	1.73E-02	2.11E-02	3.67E-05	2.29E-05	1.57E-04
3	1.83E-04	6.44E-04	2.01E-02	2.87E-02	4.37E-02	1.16E-04	6.88E-05	6.72E-05
3	8.86E-05	2.24E-03	1.59E-02	2.50E-02	3.12E-02	2.28E-04	2.48E-05	5.66E-05
3	2.12E-04	8.76E-04	2.21E-02	2.71E-02	3.76E-02	2.67E-04	6.81E-05	4.57E-05
3	1.77E-05	1.92E-03	1.31E-02	2.40E-02	2.95E-02	3.97E-05	1.42E-05	2.78E-05
3	7.28E-05	1.50E-03	1.68E-02	2.58E-02	3.46E-02	5.27E-05	6.79E-05	8.73E-05
3	2.16E-04	1.71E-03	1.59E-02	3.33E-02	3.62E-02	8.36E-05	1.27E-05	1.40E-04
4	3.83E-04	2.44E-02	2.00E-02	5.23E-02	2.83E-02	2.53E-03	3.45E-05	6.65E-04
4	1.19E-03	2.77E-03	2.06E-02	3.37E-02	2.09E-02	5.91E-05	5.72E-05	1.96E-04
4	1.25E-04	3.22E-03	3.30E-02	3.53E-02	3.57E-02	6.42E-05	7.69E-05	4.71E-04
4	2.05E-04	6.50E-03	2.10E-02	2.96E-02	4.05E-02	5.20E-04	4.86E-05	3.16E-04
4	2.91E-04	2.68E-03	1.67E-02	2.83E-02	3.67E-02	8.14E-05	1.84E-05	2.00E-04
4	1.15E-04	8.13E-03	3.27E-02	4.85E-02	3.58E-02	2.31E-04	5.76E-05	1.16E-04
4	1.76E-04	2.11E-03	2.64E-02	2.95E-02	2.97E-02	2.92E-04	2.40E-05	2.14E-04
4	1.08E-03	2.60E-03	1.61E-02	3.05E-02	3.23E-02	3.27E-05	6.44E-05	3.30E-05
4	3.59E-04	3.29E-03	1.58E-02	3.04E-02	3.60E-02	1.23E-04	2.46E-05	2.39E-05
5	5.71E-04	1.18E-02	3.34E-02	8.24E-02	3.86E-02	5.39E-04	3.86E-05	1.30E-05
5	6.85E-04	1.05E-03	2.07E-02	3.60E-02	2.47E-02	2.17E-05	8.07E-05	0.00E+00
5	2.68E-04	1.33E-03	1.88E-02	1.02E-02	1.17E-02	4.63E-05	7.93E-05	3.46E-05
5	1.32E-04	6.25E-03	2.80E-02	3.22E-02	5.37E-02	4.88E-04	8.09E-05	3.68E-06
5	5.20E-04	1.46E-03	1.71E-02	2.62E-02	4.17E-02	1.71E-04	2.54E-05	0.00E+00
5	2.64E-04	5.09E-03	3.41E-02	3.15E-02	4.73E-02	2.75E-03	4.04E-05	2.70E-06
5	9.73E-05	2.27E-03	1.28E-02	3.24E-02	3.57E-02	3.72E-05	3.05E-05	3.78E-05
5	1.38E-04	1.24E-03	1.90E-02	3.24E-02	3.99E-02	3.66E-05	6.90E-05	6.22E-06
5	3.12E-04	2.46E-03	2.13E-02	3.30E-02	4.28E-02	6.06E-05	1.25E-05	2.70E-06

Group 3 represents podocytes transfected with control siRNA (negative control); Group 4 represents IL-13 stimulated podocytes with control siRNA transfection; Group 5 represents IL-13 stimulated podocytes with vav1 siRNA transfection.

Appendix 5.4: Protein expression index of B7-1, IL-13 receptors, vav1, dystroglycan, nephrin and podocin in podocyte siRNA experiments.

Human podocytes protein expression index normalized against GAPDH.

Group	B7-1	IL-13Rα2	vav1	p-vav1	p-vav1/vav1
3	0.34	0.82	1.34	1.69	1.26
3	0.71	0.64	1.78	0.27	0.15
3	0.11	0.37	1.04	1.07	1.03
3	0.59	0.45	1.68	0.97	0.58
3	0.63	0.91	1.7	1.96	1.15
3	0.56	0.67	1.82	1.20	0.66
3	0.56	0.72	1.82	1.31	0.72
4	0.79	1.94	0.95	1.56	1.64
4	0.91	1.51	1.61	1.13	0.7
4	0.59	0.8	2.62	3.69	1.41
4	0.66	1.01	0.99	0.78	0.79
4	0.62	2.05	0.41	0.73	1.77
4	1.61	1.63	0.42	0.63	1.5
4	1.28	0.81	0.23	0.34	1.46
5	1.25	1.9	0.74	0.57	0.77
5	0.69	0.95	1.15	0.63	0.55
5	0.95	1.81	1.08	0.60	0.56
5	3.89	1.14	1.04	0.36	0.35
5	1.13	0.68	1.07	0.58	0.54
5	0.63	1.38	0.82	0.16	0.2
5	0.55	0.77	0.49	0.45	0.92

Group 3 represents podocytes transfected with control siRNA (negative control); Group 4 represents IL-13 stimulated podocytes with control siRNA transfection; Group 5 represents IL-13 stimulated podocytes with vav1 siRNA transfection.

Appendix 5.5: Cortical F-actin scores in podocyte siRNA experiments.

Cortical F-actin scores in podocytes.

Batch	Group	Total no. of cells	Number of cells				Scores				sum of score
			0	1	2	3	0	1	2	3	
H30	3	6	0	4	2	0	0	4	4	0	8
H30	3	3	0	2	1	0	0	2	2	0	4
H30	3	1	0	1	0	0	0	1	0	0	1
H30	3	19	0	9	10	0	0	9	20	0	29
H30	3	21	0	7	13	1	0	7	26	3	36
H30	3	16	0	9	4	3	0	9	8	9	26
H30	3	2	0	2	0	0	0	2	0	0	2
H30	3	5	0	4	0	1	0	4	0	3	7
H30	3	4	0	2	2	0	0	2	4	0	6
H30	3	6	0	3	3	0	0	3	6	0	9
H30	3	1	0	1	0	0	0	1	0	0	1
H30 Total		84	0	44	35	5	0	44	70	15	129
H29	3	4	0	3	1	0	0	3	2	0	5
H29	3	5	0	3	2	0	0	3	4	0	7
H29	3	14	0	4	7	3	0	4	14	9	27
H29	3	9	0	5	3	1	0	5	6	3	14
H29	3	1	0	1	0	0	0	1	0	0	1
H29	3	19	0	11	7	1	0	11	14	3	28
H29	3	1	1	0	0	0	0	0	0	0	0
H29	3	14	0	9	3	2	0	9	6	6	21
H29	3	1	1	0	0	0	0	0	0	0	0
H29 Total		68	2	36	23	7	0	36	46	21	103
H31	3	3	0	3	0	0	0	3	0	0	3
H31	3	6	0	4	2	0	0	4	4	0	8
H31	3	13	0	10	3	0	0	10	6	0	16
H31	3	11	0	7	4	0	0	7	8	0	15
H31	3	6	0	4	2	0	0	4	4	0	8
H31	3	12	0	5	7	0	0	5	14	0	19
H31	3	9	0	5	4	0	0	5	8	0	13
H31	3	4	0	3	1	0	0	3	2	0	5
H31	3	6	0	4	2	0	0	4	4	0	8
H31	3	6	0	2	4	0	0	2	8	0	10
H31 Total		76	0	47	29	0	0	47	58	0	105
H30	4	2	0	0	0	2	0	0	0	6	6
H30	4	2	0	0	0	2	0	0	0	6	6
H30	4	5	0	0	3	2	0	0	6	6	12
H30	4	11	0	4	6	1	0	4	12	3	19
H30	4	13	0	0	12	1	0	0	24	3	27

H30	4	11	0	4	4	3	0	4	8	9	21
H30	4	1	0	0	1	0	0	0	2	0	2
H30	4	1	0	0	0	1	0	0	0	3	3
H30	4	8	0	0	3	5	0	0	6	15	21
H30	4	12	0	0	3	9	0	0	6	27	33
H30	4	7	0	1	2	4	0	1	4	12	17
H30 Total		73	0	9	34	30	0	9	68	90	167
H29	4	6	0	1	0	5	0	1	0	15	16
H29	4	1	0	0	0	1	0	0	0	3	3
H29	4	11	0	1	1	9	0	1	2	27	30
H29	4	11	0	1	8	2	0	1	16	6	23
H29	4	4	0	0	1	3	0	0	2	9	11
H29	4	22	0	3	5	14	0	3	10	42	55
H29	4	3	0	0	0	3	0	0	0	9	9
H29	4	32	0	10	10	12	0	10	20	36	66
H29	4	1	1	0	0	0	0	0	0	0	0
H29 Total		91	1	16	25	49	0	16	50	147	213
H31	4	5	0	0	0	5	0	0	0	15	15
H31	4	3	0	0	0	3	0	0	0	9	9
H31	4	9	0	0	2	7	0	0	4	21	25
H31	4	4	0	1	2	1	0	1	4	3	8
H31	4	4	0	0	3	1	0	0	6	3	9
H31	4	6	0	0	3	3	0	0	6	9	15
H31 Total		31	0	1	10	20	0	1	20	60	81
H30	5	11	0	6	4	1	0	6	8	3	17
H30	5	15	0	10	5	0	0	10	10	0	20
H30	5	18	0	10	8	0	0	10	16	0	26
H30	5	11	0	8	2	1	0	8	4	3	15
H30	5	1	0	1	0	0	0	1	0	0	1
H30 Total		56	0	35	19	2	0	35	38	6	79
H29	5	5	0	3	1	1	0	3	2	3	8
H29	5	1	0	0	0	1	0	0	0	3	3
H29	5	6	0	2	2	2	0	2	4	6	12
H29	5	5	0	3	2	0	0	3	4	0	7
H29	5	5	0	1	1	3	0	1	2	9	12
H29	5	4	1	2	1	0	0	2	2	0	4
H29	5	1	0	0	1	0	0	0	2	0	2
H29	5	5	1	2	0	2	0	2	0	6	8
H29 Total		32	2	13	8	9	0	13	16	27	56
H31	5	7	0	1	2	4	0	1	4	12	17
H31	5	1	0	1	0	0	0	1	0	0	1
H31	5	3	0	1	0	2	0	1	0	6	7
H31	5	11	0	5	6	0	0	5	12	0	17
H31	5	19	0	14	5	0	0	14	10	0	24
H31	5	13	0	8	4	1	0	8	8	3	19

H31	5	10	0	6	4	0	0	6	8	0	14
H31	5	6	0	2	4	0	0	2	8	0	10
H31 Total		70	0	38	25	7	0	38	50	21	109

Group 3 represents podocytes transfected with control siRNA (negative control); Group 4 represents IL-13 stimulated podocytes with control siRNA transfection; Group 5 represents IL-13 stimulated podocytes with vav1 siRNA transfection.

Appendix 5.6: RhoA and Rac1 activities in podocyte siRNA experiments.

Normalized RhoA and Rac1 activities in podocytes.

Group	RhoA	Rac1
3	3.23	0.97
3	2.63	0.86
3	2.97	0.96
3	1.23	0.73
3	0.29	0.31
3	0.08	0.42
3	0.82	0.74
4	3.86	0.87
4	3.46	1.6
4	4.12	1.8
4	1.23	0.92
4	1.03	0.71
4	1.64	1.03
4	1.81	1.25
5	2.88	0.71
5	1.68	0.47
5	2.77	1.02
5	0.77	1.04
5	2.1	0.19
5	1.33	0.35
5	1.17	0.69

Group 3 represents podocytes transfected with control siRNA (negative control); Group 4 represents IL-13 stimulated podocytes with control siRNA transfection; Group 5 represents IL-13 stimulated podocytes with vav1 siRNA transfection.